ATL

GPO PRICE $ _____

OTS PRICE(S) $ _____

Hard copy (HC) 5.00

Microfiche (MF) 1.00

ASTRONAUTICS
ELECTRONICS
MECHANICS
ATOMICS

ADVANCED TECHNOLOGY LABORATORIES

A DIVISION OF

AMERICAN-Standard

AMERICAN RADIATOR & STANDARD SANITARY CORPORATION

Final Report

HEAT-FLUX-TRANSDUCER DESIGNS AND EFFECT OF THERMAL DISTURBANCES ON TRANSDUCER PERFORMANCE

ATL Job 1230401

ATL-D-[illegible]271 26 October 1964

for
National Aeronautics and Space Administration
George C. Marshall Space Flight Center
Contract No. NAS8-5323
Covering work performed from
June 1963 through October 1964

Submitted by:
R. C. Bachmann

Approved by:
R. W. Towle
J. T. Chambers
W. H. Giedt (Consultant)

American Radiator & Standard Sanitary Corporation
Advanced Technology Laboratories Division
369 Whisman Road
Mountain View, California

American-Standard
Advanced Technology Laboratories Division

FOREWORD

This report was prepared by American Radiator & Standard Sanitary Corporation, Advanced Technology Laboratories (ATL) Division, Mountain View, California. The work was performed under Contract No. NAS8-5323, National Aeronautics and Space Administration (NASA), George C. Marshall Space Flight Center, Huntsville, Alabama. The technical representative for the NASA contracting officer was V. L. Glasgow, R-P&VE-PTF.

Principal investigators for ATL were E. C. Bachmann and D. R. Hornbaker. Dr. W. H. Giedt, Professor of Aeronautical Services at the University of California, Berkeley, acted as consultant.

CONTENTS

American-Standard
ADVANCED TECHNOLOGY LABORATORIES DIVISION

CONTENTS
(concl.)

LIST OF ILLUSTRATIONS

LIST OF ILLUSTRATIONS
(cont.)

LIST OF ILLUSTRATIONS
(cont.)

LIST OF ILLUSTRATIONS
(cont.)

LIST OF ILLUSTRATIONS
(cont.)

LIST OF ILLUSTRATIONS
(cont.)

LIST OF ILLUSTRATIONS
(concl.)

SUMMARY

Several types of heat-flux transducers now in use were evaluated experimentally to determine their applicability and accuracy under specific heating environments and installation conditions. The transducers are utilized to give, as nearly as possible, an accurate measurement of the fundamental heating environment to which the instrumented structure is exposed. Calibration and/or data-correction procedures were developed to account for the effect of thermal disturbances resulting from transducer-structure interaction.

It was found that the most serious problem faced in the use of a heat-flux transducer results from the possible changes in temperature distribution in the heated instrumented structure. These changes can cause cross conduction and, in the case of convective heating, surface-temperature-discontinuity effects. The magnitude of the difference between the heating rate to the undisturbed structure and that to the transducer depends on the heating environment, the type of transducer, and the installation. For example, nonisothermal-surface effects caused a transducer to indicate heating rates as much as 140% in error with respect to the heating rate to a thermally undisturbed structure.

Primarily because of the different perturbations resulting from thermally mismatched transducer-structure conditions, it has been determined that a single calibration procedure for heat-flux transducers used in a variety of environments is questionable. The desired output of the transducer is an indication of the heating environment of the instrumented structure in the absence of the transducer, but the calibration of the transducer may be strongly dependent upon the nature of the structure in which it is mounted and upon the type of heating. Consequently, a single calibration often does not apply to heating conditions significantly different from the calibrating conditions.

Experimental and analytical investigation of the above problems has led to the conclusion that it is possible and extremely beneficial to perform a thorough experimental evaluation of heat-flux transducers in addition to the general transducer calibration. The results presented show that if a heat-flux transducer can be evaluated for a number of mounting structures and under a variety of heating conditions, a prediction of the probable accuracy of the transducer in a given application can be made, provided a reasonable knowledge of the actual heating environment is known.

INTRODUCTION

The importance of measuring heat transfer to surfaces exposed to aerodynamic heating and rocket-engine exhaust gases has led to the development of a number of techniques and instruments for this purpose. The basic requirement is to install a sensing element in the heated surface in such a way that its output is proportional to the heating rate to the undisturbed structure. For comparatively high heating rates and thick structures, precisely located thermocouple junctions have been used successfully.[1,2] For lower heating rates, measurement of the average temperature change in a thin plate is satisfactory. A wide variety of heat-flux transducers (or calorimeters) have been designed based on this principle because of its simplicity and adaptability. Such slug-type calorimeters have been applied to the measurement of both radiant and convective heating, as well as to the combination of the two. In the latter case, the meter is called a "total calorimeter."

Another type of calorimeter design is based on the principle of heat input flowing radially in a thin metal skin (membrane) to a surrounding heat sink.[3] The temperature difference between the membrane center and the heat sink is a measure of the imposed heating rate.

Although both slug-type and membrane-type calorimeters are very adaptable, they introduce different types and varying degrees of thermal disturbances in the structure in which they are installed. Phase 1 of the program reported here was an analytical investigation of the accuracy and applicability of several of these meters, with emphasis on slug-type meters because of their convenience and widespread use. Experience has shown that results obtained with these meters were often not in full agreement with theoretical predictions. A study of the important parameters affecting the accuracy of the meter was therefore conducted.[4] Phase 2 was an experimental verification of the Phase 1 results and the evaluation, under various heating conditions, of slug-type meters.[5]

Work performed during these two phases led to the conclusion that, to be effective, any slug-type heat-flux meter must meet the following three design requirements:

---

1. See References, page 53.

1) The thermal isolation of the slug from the supporting structure must be sufficiently effective to make negligible the rate of heat exchange between the slug and the structure.

2) The method of insulation and isolation must be such that it does not excessively perturb the desired behavior of the meter by altering the heat-transfer characteristics from those of the surrounding structure.

3) Techniques must be developed to permit practical utilization of data gathered, recognizing that requirements 1 and 2 above cannot be fully met in most applications.

The current program, Phase 3, was aimed at further investigation of the above heat-flux-transducer design parameters. The primary tasks involved were to evaluate several meters currently used by NASA, to study the effect of thermal disturbances on transducer performance, to evaluate variations in heat-flux-meter design, and to study calibration and/or data-correction techniques. The results of the study and an analysis are presented in this report.

CALORIMETER-INDUCED DISTURBANCES

A. Necessity for Accurate Heat-Flux Measurements

Current missile and space boosters employing multiple engines cause complex flow patterns in the base region and around the exhaust nozzles. In certain cases, hot exhaust gases circulating into the base area cause excessive heating, which may result in damage to the missile. A heat shield is often required to prevent this damage. For missile-base configurations utilizing a heat shield, the weight of the shield imposes serious performance penalties and hence should be held to a minimum. Experience has shown, however, that present knowledge is often inadequate to permit theoretical predictions of heating rates with the accuracy required for optimum design work. Accurate structural heating-rate measurements for both ground and flight test environments are therefore necessary to eliminate the costly possibility of over design and to insure maximum performance.

B. Cross Conduction

The temperature variation in a heated structure may be influenced by installation of a calorimeter because of differences in the thermal characteristics and optical properties of the calorimeter and the surrounding material. These two factors can cause a temperature difference to occur between the instrumented panel and the meter. One result is that the meter and the structure will each receive different heat inputs and thus cross-conduction heat flow may occur through the meter-structure interface. This can obviously result in serious errors when slug-type meters are being used because these meters rely on a heat-storage principle. Cross-conduction effects can be basically represented by*

$$q = \frac{T_s - T_m}{\Sigma R} \quad . \tag{1}$$

The cross conduction is shown to depend on the temperature potential established, the thermal resistance of the meter and the surrounding structure, and the resistance at the meter-structure interface.

When slug-type meters are exposed to convective heating, cross conduction could be manifested simultaneously by both heat addition and heat loss. Such a situation might arise

---

* See Nomenclature, page 51.

if the meter were installed in a low-diffusivity structure (insulation material). During the convective-heating cycle, the high-diffusivity slug absorbs heat, which is distributed evenly throughout the slug. The structure also absorbs heat, but because of its low diffusivity, the heat is stored near the surface. The result is a large temperature difference between the slug and the insulation near the surface and a similar but reversed temperature difference between the insulation and the slug below the surface. Since the two resulting cross-conduction effects probably would not occur at identical rates, the net heat input to the meter could differ from the flux to the surface of the undisturbed structure. Thus a knowledge of the magnitude of the cross conduction is desirable for interpreting meter readings.

C. Surface-Temperature Discontinuities

Another prominent source of calorimeter error is surface-temperature discontinuities. Consider a structure subject to high-temperature gas-flow heating other than pure stagnation heating; i.e., parallel-flat-plate flow or axially symmetrical flow. The convective heat-transfer rate from the hot gases to the wall is given by[6]

$$q = k A (dT/dy)_w \quad , \tag{2}$$

where y is taken as zero at the wall.

Expressed in terms of a film heat-transfer coefficient, h, the heating rate is

$$q = h A (T_{aw} - T_w) \quad , \tag{3}$$

which is the form used in conventional heat-transfer work. In low-velocity flow, T_{aw} is the free-stream gas temperature; in supersonic flow, it is the recovery temperature of the fluid.

An expression for the film coefficient, h, is obtained by combining equations 2 and 3:

$$h = \frac{k}{(T_{aw} - T_w)} (dT/dy)_w \quad . \tag{4}$$

The requirements for surface-temperature simulation on a calorimeter surface can be seen from equation 4. Generally the adiabatic wall temperature of the gas is not changed by installation of a calorimeter in a structure. Although the gas conductivity is affected

by the wall temperature, the effect is minor, especially when the temperature change of the gas is small. Thus the heat transfer is basically identified by the wall temperature and the gas-temperature gradient at the wall. The wall temperature, of course, rises continually during a rocket firing.

If a calorimeter is installed in a structure and assumes a temperature significantly different from that of the surrounding material, the local convective heat transfer will be affected, as indicated by equation 4. As the gases pass over a temperature discontinuity, the temperature gradient in the boundary layer close to the surface must change drastically since the temperature distribution must remain continuous. The heat-transfer coefficient and the heating rate must also change, since they are both a measure of the thermal gradient in the gas at the wall.

This problem can become quite pronounced when the convective or total heat transfer to an insulating structure is measured with a membrane calorimeter operating at a relatively low temperature. Due to the small size of this type of meter, the sensing surface is near the self-induced surface-temperature discontinuity. Directly at the discontinuity, the heat transfer can be expected, theoretically, to be infinite, as it is at the leading edge of a flat plate. The small membrane will therefore be exposed to heating rates much higher than normal and will not give an accurate description of the heating environment to which the undisturbed structure is exposed. Consequently, the output of the calorimeter must be corrected to some reference heat flux. The desired convective heat-flux measurement is that which would be experienced by an isothermal surface at a known surface temperature.

D. Analysis of Effects of Nonisothermal Surface on Convective-Heating Measurements

1. Analytical Results

Several investigators have studied the effect on convective heat transfer of a step discontinuity in the surface temperature, and the results obtained have been applied to errors that may arise when using a calorimeter that assumes a temperature greatly different from that of the surrounding structure. These results have been substantiated by experimental studies for gas and surface temperatures of moderately low ranges.

The first widely accepted analysis of the local heat-transfer coefficient for turbulent incompressible flow over a flat plate with a step-surface-temperature

discontinuity was presented by Rubesin.[7] Figure 1 defines the system considered. The following equation was given for describing the local heat-transfer coefficient at a point X between L and W:

$$h(X, L) = h(X, 0) \left\{ \frac{T_{w_1} - T_o}{T_{w_2} - T_o} + \frac{T_{w_2} - T_{w_1}}{T_{w_2} - T_o} \left[1 - \left(\frac{L}{X} \right)^a \right]^{-b} \right\} \quad . \tag{5}$$

The exponents a = 39/40 and b = 7/39 were determined from limited experimental data.[8]

Of greater interest is the ratio of the average coefficient between L and W to the local coefficient that would exist at (L + W)/2 in the undisturbed or isothermal case. This average value was obtained by Rubesin through integration of equation 5 between L and W; the resulting ratio is

$$\frac{\bar{h}(W, L)}{h\left(\frac{W + L}{2}, 0\right)} = F\left(\frac{L}{W}\right) + H_1\left(\frac{L}{W}\right) \left[\frac{T_{w_2} - T_{w_1}}{T_{w_2} - T_o} \right] \quad . \tag{6}$$

The functions F(L/W) and H_1(L/W) are geometrical terms that depend upon the exponents 39/40 and 7/39 and are plotted versus (L/W) in Figure 2.

Reynolds, et al.[9,10] made a further study of the problem, concluding that equation 5 holds over a wider range of Reynolds numbers when a = 9/10 and b = 1/9 are used. These values were used by Westkaemper,[11] resulting in a modified term H_2(L/W) in equation 6. The function H_2(L/W) is compared to H_1(L/W) in Figure 2.

Brunner, et al.[12] extended these analyses to include a circular calorimeter, as compared to the square configuration implied in equations 5 and 6. They also gave consideration to nonuniform temperature distribution over the calorimeter itself. The effect of this geometry was to increase the predicted error about 10%. The effective surface temperature of a circular membrane having a parabolic temperature distribution was found to be 0.75 of the center-point value. The combined effects were concluded to be relatively minor in predicting meter errors in that they tend to cancel each other.

2. Application of Theory to Heat-Flux Measurements

In many applications, it is desired to evaluate the heat transfer to an insulating surface directly from the calorimeter measurement rather than to evaluate a heat-transfer coefficient. This can be accomplished in the following manner.

Values of $\bar{h}$ can be determined from the calorimeter measurement by

$$\bar{h} = \bar{q}/(T_o - T_{w_2}) \quad . \tag{7}$$

It is conventional to consider h over both the isothermal noninsulating structure and the isothermal insulating structure (ref. Figure 1) to be equal and defined by

$$h = q_{isn}/(T_o - T_{w_2}) = q_{isi}/(T_o - T_{w_1}) \quad . \tag{8}$$

Consequently, the heat flux to an isothermal (undisturbed) insulating structure is related to q_{isn} and the temperature potentials according to

$$q_{isi} = h\,(T_o - T_{w_1}) = q_{isn} \left[\frac{T_o - T_{w_1}}{T_o - T_{w_2}}\right] \tag{9}$$

From equations 7 and 8, the ratio of $\bar{h}/h$ is obtained as

$$\frac{\bar{h}}{h} = \frac{\bar{q}}{q_{isn}} \quad , \tag{10}$$

and from equations 7, 8, and 10 the ratio $\bar{q}/q_{isi}$ becomes

$$\frac{\bar{q}}{q_{isi}} = \frac{\bar{q}}{q_{isn}} \left[\frac{T_o - T_{w_2}}{T_o - T_{w_1}}\right] \quad . \tag{11}$$

The available theory can therefore be used to predict corrections required for calorimeter measurements, provided that:

1) Gas-stream, surface, and calorimeter temperatures are known.

2) The flow in the boundary layer at the surface approximates the flat-plate flow assumed in the analysis.

3) The distance of the calorimeter from the point of boundary-layer inception is known.

It is unlikely that all of the information above will be accurately known for typical flight conditions. However, based on available flight data, engineering estimates of the required corrections can often be made.

E. Simulation Theory

One of the first steps in an evaluation of a heat-flux meter is to ascertain what, exactly, it should measure. The measurement that is usually of primary concern is the net flux to a heated structure. To obtain this measurement, the heat-flux meter should indicate the heat transfer that would exist at a test station if the meter were not present. In practice, of course, it is rarely possible to achieve this goal because a calorimeter that is placed in a heated structure disturbs the thermal characteristics in the immediate vicinity. Since these thermal disturbances introduced by a calorimeter are often difficult to determine accurately, a practical approach is to 1) minimize the disturbance, 2) recognize its presence as a potential source of error, and 3) attempt to correct for the errors it introduces.

F. Calorimeter Calibration

The foregoing discussion shows how errors in heat-flux measurement are inherent in the installation of a calorimeter when the temperature distribution in the heated structure is disturbed. It would, of course, be desirable to establish a laboratory calibration technique that would always account for and correct these errors. This demand is difficult to fulfill, however, because of the many variables that cannot be sufficiently controlled during either laboratory calibration or actual application of a meter. Furthermore, a valid calibration of this type apparently requires a precise knowledge and laboratory simulation of in-flight conditions. Laboratory simulation of such conditions is often highly impractical.

Although a true single calibration is desirable, its feasibility appears to be questionable. A more practical approach might be to conduct a thorough performance evaluation of the calorimeter and then compare the calibrated-meter output to the actual incident heating. If a general knowledge exists of the environment to which the meter will be exposed, and if the accuracy of the meter can be experimentally determined under conditions designed to simulate the environment, meaningful flight data could be obtained. Information acquired from a study of this type would permit a well grounded evaluation of the expected accuracy of a given meter in a proposed application. Because of the large number of different meters presently being used and the broad spectrum of heating conditions being encountered, this information would be extremely useful in selection of the calorimeter that would best adapt to a given heating environment and indicate the heat flux to the instrumented

structure with the greatest accuracy. With a view to collecting such information, several popular heat-flux meters were experimentally evaluated. Laboratory heating apparatus capable of providing convective, radiant, and combined convective-radiant heating conditions was used, in conjunction with a variety of mounting structures, to approximate a wide range of heating environments.

HEATING APPARATUS

An experimental program was conducted to investigate the magnitude of the errors previously described and to evaluate their effect on current heat-flux calorimeters. The heating apparatus utilized for this study is essentially identical to that used during the previous phases of the program.[4,5] Since this equipment constitutes an integral part of the Phase 3 work, a description of the apparatus is repeated here.

The heating apparatus (see schematic, Figure 3) consists essentially of the 30-tip oxyacetylene heating torch and an electrically heated graphite block. The heating-torch system includes seven manifolded acetylene bottles and a single oxygen bottle, a flowmeter for each gas to insure close reproducible control of heating rates, solenoid valves for automatic operation, and throttling valves for fine control of gas flow. The graphite block is heated by current from a power supply capable of developing 75 kva. This block is bathed in argon during the heat-up period, and a shutter is opened automatically in conjunction with the opening of the gas solenoid valves. The block temperature is monitored and controlled with a Leeds & Northrup Rayotube and power controller.

Figures 4 and 5 (front and rear view, respectively) show the over-all layout of the heating apparatus. The central portion of Figure 4 shows the graphite radiant heater with water-cooled cover and control Rayotube directly above it. The large slotted stand provides variable positioning of the torch, which in this photograph is shown in a horizontal position. Positions of the torch other than horizontal are for convection heating only, without the radiation source. On the right is the water-cooled exhaust duct; on the left is a portion of the instrument panel containing various control switches, throttling valves, and flowmeters.

Figures 6 and 7 are close-up views of the heating zone. In Figure 7, the water-cooled cover has been removed from the graphite block. A 0.125-inch-thick stainless-steel test plate (described below) is shown in place, recessed into the brick base. During warmup, the underside of the radiant heater is covered by a sliding shutter that is actuated by an air cylinder This shutter is visible in Figure 6.

The entire test procedure is automated. The oxygen and acetylene solenoid valves and a solenoid valve controlling air to a pencil-type cylinder driving the shutter are operated by a microswitch sequence timer. The oxygen valve opens first, followed

closely by the acetylene valve. A pilot flame, which is ignited prior to initiation of the timing sequence, ignites the torch at the instant the acetylene valve opens. When both convective and radiant heating are to be used, the graphite heater is brought to equilibrium before the timing sequence is initiated. Equilibrium is determined visually with an optical pyrometer sighted through a hole in the heater cover. The solenoid valve controlling the shutter-actuating air cylinder is opened by the timer in conjunction with the acetylene valve. The result is essentially a step heat input. The test then proceeds for a predetermined period of time, after which a reverse shut-off sequence occurs.

EXPERIMENTAL PROCEDURES

A. Reference Heat-Flux Measurements

In a test program of the type described, it is necessary to obtain an appropriate heat-flux measurement to which all heat-flux-meter data can be referenced and compared. This heat flux should be representative of the heat flux to which the instrumented panel is exposed. The underlying theory and procedure employed in establishing a reference-calorimeter heat-flux measurement is presented below.

Convective-heating rate to a surface is given by

$$q_c = h (T_o - T_w) \quad . \tag{12}$$

The heat-transfer coefficient, h, is dependent upon mass flow rate and gas-stream properties. It can be assumed that h is a constant by maintaining the mass flow rate of both the oxygen and the acetylene constant. Maintaining the gas flows constant will also permit the assumption of constant gas temperature, T_o, since the combustion conditions are invariant. The only remaining variable on the right-hand side of equation 12 is the surface temperature, T_w. The validity of these assumptions is assured by measuring oxygen and acetylene flow with precision flowmeters. The meters used have a 10-inch scale with 100 equal divisions. As noted earlier, each gas line is provided with a throttling valve for fine adjustment so that the flow can be easily reproduced within 1% of a specified value.

Radiant-heating rate to a surface is given by[13]

$$q_r = \sigma \alpha_s \epsilon_r F (T_r^4 - T_w^4) \quad . \tag{13}$$

The geometrical-shape factor, F, is a constant of the system as is the Stefan-Boltzmann constant. The surface absorptivity of the plate surface, α_s, and the emissivity of the graphite block, ϵ_r, will both be about 0.9 and can be assumed to be constant, since the test plate and meters are prepared with a special high-absorptivity high-temperature finish. The radiation-source temperature, T_r, is controlled through a feedback to the power controller from a Rayotube viewing the source. T_r can therefore also be assumed constant. The only remaining variable on the right-hand side of equation 13 is, as in equation 12, the surface temperature, T_w.

The total heating rate to a surface subject to both convective and radiant heating is given by

$$q = q_c + q_r \quad . \tag{14}$$

Since, under any set of constant test conditions to be employed, equations 13 and 14 are shown to be functions of T_w only, q in equation 14 will also be a function of the surface temperature only. This fact provides the basis for the method of evaluating the reference heat flux.

The first step is to determine the true heating rate to a test plate under a given set of mass-flow and/or radiant-heating conditions. This is accomplished by determining the heat stored in a thin standardizing plate as a function of time. The slope of the resulting curve of heat stored versus time is the rate of heat storage. This rate of storage plus the rate of heat loss from the rear surface of the plate is the true heating rate. Separate reference calorimeters were fabricated to measure either purely radiant or convective and total heating.

1. Radiant-Heating Reference Meter

The radiant-heating reference meter consists of a copper slug 0.500 inch in diameter and 0.120 inch thick, suspended in a guard plate of the same thickness and 2 inches square. The slug is separated from this plate by an air gap 0.002 inch wide and is held in place by four strips of Constantan foil (0.1" wide $\times$0.0003" thick) bridging the air gap on the back surface. The back surface is insulated with commercially available Fiberfrax insulation material.

A surface coating of Parsons optical black lacquer (absorptivity > 0.99) is air-brushed on the slug and guard plate. The resulting surface has a deep velvet-black appearance which is maintained after heating to 1000°F several times. The temperature of the copper slug is measured with a Chromel/Alumel thermocouple (0.003 inch in diameter) spot-welded to the back of the slug.

The resultant temperature history is assumed to be the average slug temperature. It can be combined with specific heat data from the literature to give the heat content for the copper slug. The specific heat of copper can be represented by[14,15]

$$c = (0.092 + 1.142 \times 10^{-5} T) \text{ Btu/lb-°F} \quad . \tag{15}$$

The heat content as a function of temperature is then given by

$$Q = \int_0^T c\,dT = (0.092\,T + 0.57\,T^2 \times 10^{-5})\ \text{Btu/lb} \quad . \tag{16}$$

The validity of this device can be best demonstrated by the linearity of its temperature rise under constant heat-flux conditions and especially by the slow decay of the slug temperature when the incident heat flux is reduced to zero. A portion of the cooling period of the radiation reference calorimeter after a typical test is shown in Figure 8. In no case did the slug temperature drop at a rate greater than $\frac{1}{2}$°F/sec, clearly indicating that during the heating periods losses are negligible and all heat absorbed is being stored. Thus the meter consists of an isothermal mass whose heat-flux measurement represents the true heating rate.

2 Convective- and Total-Heating Reference Meter

The measurement of a reference convective and total heat flux is much more difficult than that for radiation. The reference calorimeter must be free from the uncertainties common to typical flight-type calorimeters. Since most problems in heat-flux measurements arise from thermal perturbations of one type or another, the reference total calorimeter should be designed such that the presence of the sensor does not alter the heat transfer being measured. This can best be done by placing a sensor in a thermally infinite thin plate such that the sensor does not influence the plate temperature in any way. The sensor best suited for this application is an in-wall or surface thermocouple plug made of the parent plate material. The plate itself can then be treated as an isothermal mass as in a slug-type calorimeter.

The reference convective-total calorimeter chosen was a 1/8-inch-thick plate of Type 316 stainless steel. (A low-conductivity material was selected to prevent lateral conduction.) Surface and in-wall temperature sensors were made using techniques well established in the manufacture of standard ATL temperature sensors (Delta-Couples). The sensors are made by locating the junction of the thermocouple at the desired depth from the heated surface in a plug of the reference plate material. The instrumented plugs are then pressed into the reference plate, providing a homogeneous system with essentially no thermal disturbance due to the presence of the sensors. The plate surface is painted with Pyromark high-temperature black paint having an absorptivity of approximately 0.9.

Using these sensors, temperature measurements were made at the surface, midplane, and rear of the stainless-steel plate. Test results indicated that under convective heating, the slope of the stainless-steel surface temperature is a valid and consistent measurement of the slope of the average plate temperature and that rear-surface losses are negligible. Therefore, only the surface temperature was used in subsequent tests.

Heat-content (enthalpy) measurements were made as a function of temperature on samples of Type 316 stainless steel taken from the stock from which the test plates and temperature sensors were fabricated. These measurements were conducted by the University of California at Berkeley. The resultant heat-content data represented a maximum uncertainty of $\pm 0.5\%$ and were in good agreement with previous results for Type 316 stainless steel.[5]

Based on the above data, the stainless-steel reference-meter temperature history can be converted to a plot of heat content versus time. The slope of the heat-content curves (measured graphically) then represents the heating rate to the reference meter.

The accuracy of the reference total calorimeter is substantiated by its linear temperature rise during heating under a constant heat flux and by the minimal change in its slug temperature when the incident flux has been reduced to zero (see Figure 8).

Measurements in radiant heating made with the reference radiation calorimeter and the reference total calorimeter were compared to measurements made with a membrane radiometer supplied by an independent manufacturer; all three instruments were found to exhibit excellent agreement. This is discussed further in part E. of the "Experimental Results and Discussion" section of this report.

B. Test Program

The experimental portion of Phase 3 of this program consisted primarily of studying the effects of mounting structure and mounting-structure temperature variations on heat-flux measurements using currently available calorimeters. The effects, in convective heating, of a discontinuity in the surface temperature created by the presence of the calorimeter were also studied. These effects were evaluated to determine the magnitude of the errors in calorimeter measurements which were produced and to define the conditions under which these errors occurred. The data were collected employing heat-flux meters

supplied by NASA, including various radiometers, a copper- and a nickel-slug total calorimeter, and a membrane total calorimeter. Radiant, convective, and combined radiant-convective heating were used in the tests.

A brief study of the effects of a large radiant heat input on a gas-temperature probe was also conducted. The test procedure consisted basically of subjecting a calorimeter to the test conditions that would best promote the desired effects. For example, the copper-slug total calorimeter was mounted in a high-conductivity structure to study certain aspects of cross conduction. Identical heating conditions were then imposed on the appropriate reference meter.

The data collected permitted a critical evaluation of the performance of a specific instrument under particular test conditions. Based on the results of meter performance under the laboratory heating environment, the applicability of the calorimeter calibration to the actual application and any required calibration-correction techniques could be established, provided the proposed application sufficiently resembled the test environment.

C. Data Acquisition

The signal from each thermocouple in a test specimen was amplified and recorded on a Minneapolis-Honeywell Visicorder. The Visicorder was calibrated just prior to each test. A Leeds & Northrup Model 8662 potentiometer was used as a voltage reference.

D. Data Reduction

The technique used to determine the heating rate to the reference meters is described in A. above. The manner in which all other data were reduced depended on the specific meter tested and on the environmental conditions encountered. A complete description of these data-reduction methods is presented with the experimental results.

EXPERIMENTAL RESULTS AND DISCUSSION

A. N-123 Copper-Slug Radiometer

A schematic of the N-123 copper-slug radiometer used for calibration evaluation is shown in Figure 9. The slug itself is 0.188 inch in diameter, 0.259 inch thick, and is instrumented with Chromel/Alumel wire forming an effective junction at the bottom of the slug. The radiometer is provided with a purge gas flow around the window to keep its surface free of foreign material. The purge gas is nitrogen run at 750 psi to a 0.018-inch-diameter surface in the purge line. This provides the recommended flow rate of approximately 3 scfm.

An evaluation of the copper-slug radiometer was conducted to determine the effects of variable mounting conditions and of the purged and unpurged flow conditions on the calibration of the instrument. These tests were performed under radiant heating. A brief test series was also made to investigate whether the calibration of the radiometer is altered by the addition of a large convective heat load to the radiometer flange.

During the tests, the temperature histories at various points of the structure and meter were recorded. The locations of these temperature measurements are shown in Figure 9.

Variable mounting-structure conditions were obtained with a 9-7/8" × 9-7/8" × 1/8" copper plate, which was used in both an uncooled and a water cooled-condition. Thus, a wide range of structural operating temperatures was achieved.

1. Unpurged N-123 Radiometer

The copper slug radiometer was tested without purge gas for both the uncooled and the water-cooled mounting structure. The test procedure consisted of subjecting the radiometer-instrumented structure to a step radiant-heat input. The radiation reference meter was then exposed to an identical radiant-heat flux. Extreme care was taken in placing the slug of the reference meter at the same coordinates relative to the radiation source as the test radiometer.

The experimental data were collected in the form of temperature histories as shown in Figures 10 through 13. These data were for radiant-heating rates varying from 7 to 36 Btu/ft^2-sec. Slopes of the radiometer copper-slug temperature were taken at slug temperatures of 100, 200, 300, 400, 500, and 600°F. These slopes were then

plotted as a function of the reference heat flux, with the radiometer-slug temperature as the parameter. Slopes taken during the cooling cycle, when the incident heat flux was zero, are also included on these calibration curves. The resulting curves are shown in Figures 14 through 19, each graph being for a different slug temperature.

It can be readily concluded from these curves that the calibration of an unpurged N-123 copper-slug radiometer is dependent on the structure in which it is mounted. The two structural conditions tested produced two distinctly different calibrations. The slopes of the two radiometer signals differ 10 to 15% at 30 Btu/ft^2-sec and as much as 75% at 10 Btu/ft^2-sec. The absolute value of this difference varied from 2 to 6°F/sec over the 0 to 40°F/sec slope range.

The zero heat-flux points shown on the calibration curves (Figures 14-19) fall on an extrapolation of the positive-slope curve for the water-cooled structure but not for the uncooled structure. In addition, there is considerably more scatter in the zero-heat-flux points for the uncooled structure. These results might well be expected, however, since the "cooling potential" is relatively constant for the water-cooled structure while it is a more time- and heating- dependent variable for the uncooled structure.

A rather surprising conclusion can be drawn from the data shown in Figures 14 through 19. The data indicate that for a given reference heat flux, the slope of the radiometer signal for a water-cooled structure is much greater than the slope for the same uncooled structure. That is, for the same radiant-heat flux and for the two structural conditions tested, the structure that operated at the higher recorded temperature levels (see Figures 10-13) promoted the greatest heat losses from the radiometer copper slug. Attempts to explain this result in light of the existing data met with little success. Further study would be necessary to explain this discrepancy. However, since the calibration of the radiometer in the unpurged condition was found clearly to depend on the mounting structure employed, i.e., radiometer output is seriously influenced by the type of installation, the value of additional study of the unpurged radiometer appeared questionable in terms of practical applications. Therefore, the tests employing the unpurged radiometer were discontinued.

2. Purged N-123 Radiometer

In order to study the calibration of the radiometer with purge-gas flow conditions, it was necessary to modify the instrument slightly to prevent cooling of the radiation source

by the purge gas. Since the radiometer is located only about $1\frac{1}{2}$ inches from the graphite heater during calibration, the purge gas, under normal operation, would impinge directly on the heater element. This problem was resolved by adding a deflecting ring (shown in the sketch below), which caused the purge gas to flow outward along the flange, not onto the heater.

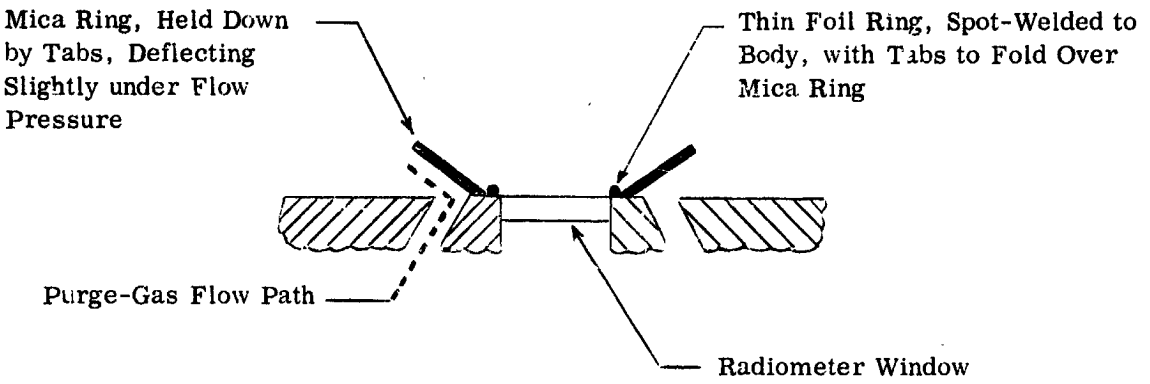

The thin mica ring shown above acted as a flexible flow deflector and, at the same time, permitted most of the incident radiation to pass through it: thus the ring did not alter the heating of the body adjacent to the window.

As previously noted, the purge gas was nitrogen flowing at approximately 3 scfm.

Tests were conducted for radiant-heating rates from 9 to 36 Btu/ft^2-sec as measured by the reference calorimeter. The radiometer was mounted in both the water-cooled and the uncooled copper plates previously described. Typical temperature histories measured during these tests are shown in Figures 20 through 23.

Again, a calibration curve was prepared by plotting the slope of the radiometer-slug temperature as a function of the laboratory reference heat flux, with the slug temperature as the parameter. The results are shown in Figures 24 through 29, each graph being for a different temperature. These curves can also be compared in Figure 30.

Within the range of heat flux and mounting conditions tested, these curves indicate that, for a given slug temperature, the N-123 radiometer, when purged, is not influenced by mounting-structure conditions. It appears, from analysis of the data, that the purge gas provides a relatively constant heat-sink condition which dominates the heat-loss modes.

It can be seen that the temperatures of the copper plate are consistently lower with purge gas than without, indicating that the purge gas is cooling the entire assembly.

The points on the calibration curve taken during cooling (a condition of zero incident heat flux) can be seen to fall on or near the extrapolation of a curve through the positive-slope points for the uncooled as well as the cooled structure. These cooling points also exhibit excellent reproducibility with the zero-heat-flux points determined for the unpurged radiometer when mounted in the water-cooled structure. The noticeable scatter of the cooling points in the unpurged tests was reduced from an average of 2.25°F/sec to 0.94°F/sec, apparently because of the relatively constant cooling effect of the purge gas.

It should be noted that, for a given slug temperature, the calibration curve for the purged radiometer generally falls well within the limits of the two calibration curves obtained with the radiometer in the unpurged environment. Furthermore, the calibration curves for the purged radiometer are, in every case, steeper than for the unpurged radiometer (indicating larger heat losses), giving additional evidence of the cooling effects attributable to the purge gas. These results further substantiate the dominance of the purge gas as the parameter most effective in controlling cross-conduction heat losses from the slug. That is, the heat-loss trends remain relatively constant and independent of the structure temperatures encountered. This result, of course, is extremely useful in aerospace applications because of the large structural temperature variations involved.

It can be concluded from the above tests that the calibration of the radiometer must include operation with purge flow. It can be further concluded that unless adverse structure temperatures are expected in flight, the mounting condition need not be seriously considered in calibration.

3. Combined Radiant-Convective Heating of Purged N-123 Radiometer

A brief test series was conducted to determine if the output of the purged N-123 radiometer is altered by the addition of a large convective heat load to the flange. During the first portion of the test series, combined radiant-convective heating was imposed on the radiometer mounted in a water-cooled structure. For the second portion of the test series, combined radiant-convective heating was to be imposed on the radiometer mounted in an uncooled structure. However, the second portion was not performed because of radiometer malfunction (discussed below). Note that during the first portion of the test series, the

potential cooling effect did not lower the flange temperature even though the radiometer flange was attached to the water-cooled structure. That is, the convective heating clearly caused much higher flange temperatures than previously encountered. This fact can be readily observed in Figures 23, 33, and 34.

Measurement of the reference heat flux, under the heating conditions described, presented somewhat of a problem because the convective-heating source (an oxyacetylene flame) adds an additional radiation component to the radiation from the graphite heater. It was decided, therefore, to measure the two radiation components separately and add these quantities to obtain the combined reference radiant-heat flux.

The heat flux from the radiation source was measured in the usual manner, using the laboratory radiation calorimeter. Next, the radiation from the flame was measured. Such a measurement, however, requires a radiometer with a window so that convective-heating effects can be isolated from radiant-heating effects. It was believed that since the N-125 radiometer itself had been calibrated in the previously described tests, and since very small heat losses were observed at low radiometer-slug temperatures, the N-123 radiometer could be used to measure this radiation component from the flame by employing the calibration curves at hand and using only low-slug-temperature data.

Using the above technique for establishing the radiant-heat loads, the radiant-convective testing was initiated. Test results indicate that the radiation component from the flame was indeed significant: it measured 3 Btu/ft^2-sec on a low-flux total heat test and 7 Btu/ft^2-sec on a higher flux test. Combined radiant-heat loads from both the flame and the radiant source in the two tests were 6 and 11 Btu/ft^2-sec. The magnitude of the total heat load from the convective source to the flange was determined with the reference total calorimeter. Measurements indicated that the total heat load from the flame during these tests was 18 and 19.5 Btu/ft^2-sec. respectively.

The results of the first two combined-heating tests are compared to the original radiation calibration curves for the purged radiometers in Figures 31 and 32. Temperature-history data are indicated in Figures 33 and 34.

At the conclusion of the second combined-heating test, the radiometer copper-slug thermocouple became inoperative and was not readily repairable.

Although the combined radiant-convective heating data gathered are somewhat meager, they are encouraging in that the calibration points fall on the original radiation

calibration curves for the purged radiometer. These results indicate that, within the limitations of the test conditions, a convective load on the flange will not change the purged-radiometer calibration obtained for purely radiant-heating conditions.

Another method that provides an excellent substitution for the separately measured radiation components previously discussed involves measuring the combined radiation by the same method that was employed to measure the flame radiation component, i.e., with the slug radiometer at low sensor temperature. Then if the radiation component that issues from the graphite heater and passes through the flame is desired, the individually measured flame component could be subtracted from the combined-radiation effects measured by the radiometer. However, in view of the excellent agreement exhibited by the data in Figures 31 and 32, it was concluded that this approach would indicate the same radiant-heat loads as those suggested by the separate measurements.

B. Slug-Type Total Calorimeters

The Fenwal copper- and nickel-slug total calorimeters tested were identical in dimensions. The exposed surface was 3.5 inches square, consisting of a 2.5-inch-square sensing surface surrounded by a 0.5-inch bolt flange, as shown in Figure 35.

Due to the popularity of this type of meter, a rather intensive performance evaluation of the two instruments was conducted. The basic purpose of this study was to determine the extent to which the meter calibrations were influenced by mounting structure, mounting-structure temperatures, and mode of heating. Based on the belief that valid calibration curves could be generated, an additional objective was to determine the feasibility of extrapolating the curves into the zero incident-heat-flux region (represented by a negative slope on the temperature-history curves).

Tests were conducted for radiant, convective, and combined radiant-convective heating. All tests employing convective heating were performed at a single downstream position from the point of gas-flow boundary-layer inception.

Two types of mounting structures were investigated. The first type included both water-cooled and uncooled copper structures. The second type consisted of a heat-shield panel fabricated from a stainless-steel frame covered with $\frac{1}{2}$ inch of "M-31" castable high-temperature insulation material* supplied by NASA.

---

* Designated by NASA/George C. Marshall Space Flight Center.

Combining these different heating and structural conditions permitted the calorimeters to be evaluated under a wide variety of heating environments. Figures 36 and 37 illustrate the calorimeter mounting details and the locations of the thermocouples used to obtain the various temperature histories.

1. Copper-Slug Total Calorimeter

Experimental temperature histories at different points in the calorimeter-mounting structure assembly measured for radiant heating, are presented in Figures 38 through 54. The mounting condition and the laboratory reference heat flux for each test are noted on the graphs. Instrumentation problems prevented recording of the copper-mounting-structure temperatures during the initial portion of the test series. The structure temperatures shown for these tests are therefore approximate and were obtained by interpolating subsequent radiant-heating data collected at different heating rates.

Calibration data were generated by plotting the slope of the calorimeter-slug temperature as a function of the reference heat flux, with the temperature of the test-calorimeter slug as the parameter. Slopes of the slug-calorimeter signal were also determined during the meter cooling cycle (zero incident heat flux) and are presented, with the positive-heating slopes in Figures 55 through 58.

Before the actual results are discussed, a brief description of the various trends one could expect from calibration data is presented. If the meter calibration is unaffected by both the heating and the mounting conditions, all calibration data would fall on a single straight line which would pass through a specific point at zero heat flux. This implies a perfectly insulated slug capable of storing all incident energy and producing a signal that is independent of the mode of heating. However, the use of slug-type calorimeters often produces noticeable conductive heat losses due to an effective temperature difference between the slug and the surrounding material. When a calibration curve of the type described (including heating and cooling points) is constructed for a meter whose operation includes these losses, their effect on the calibration curve becomes quite noticeable. For example, if the heat-loss mode depends solely on the presence of a temperature difference, but is independent of the heating conditions that produced the temperature difference, the calibration data will deviate from a straight line but will pass through a specific zero-heat-flux point. Should the temperature difference show a strong dependence on the heating environment (actual heat-flux level,

duration of heating required to reach desired slug temperature, etc.) and the material thermal properties. the calibration curve will again deviate from a straight line but will also exhibit extreme scatter in the zero-incident-heating slopes.

The evident scatter of the calibration data in radiant heating is attributed to lateral-conduction effects in the meter and across the meter-mounting structure interface. The trend of the scatter indicates that the conductive losses are governed by the mounting conditions and by the heating environment of the test structure. A description of the heating environment includes the type of heating, the heating rate, and the duration of heating (the slug temperature achieved).

Due to the degree of data scatter, it is difficult to accurately represent the results of Figures 55 through 58 with a single curve. Each individual test has therefore been identified by connecting the positive- and zero-heat-flux-slope points (determined during calorimeter cooldown) with a separate line..

These calibration data indicate that all tests produced a significant spread in the zero-heat-flux points, with the degree of scatter increasing progressively with meter temperature. The increase at the higher slug temperatures is reasonable, however. because of the large temperature difference established between the copper slug and the structure. Combining the resultant temperature gradient with the high conductivity of the copper slug will obviously promote significant conductive heat losses. as indicated by the data.

Calibration results further show that the mounting structure exerted a strong influence on the instrument calibration; this influence also increased with calorimeter temperature. The significant effect of the mounting structure is that each structure promoted a different heat loss for the same incident heating rate. In fact, due to the presence of these heat losses, the variation in the calibration data obtained for the three structures is of such magnitude that the accuracy in applying the results to an environment different from laboratory conditions is extremely questionable. For example, at a calorimeter temperature of 300°F and a reference heat flux of 20 Btu/ft^2-sec. the copper-slug-calorimeter signal is 27.2°F/sec for the thick copper structure and 34.7°F/sec for the thin (1/8-inch thick) water-cooled structure. For the same reference heat flux and at a transducer temperature of 500°F, these same outputs are -10°F/sec and 9°F/sec, respectively The difference in the readings results in errors of 27.6% at 300°F and 190% at 500°F.

The greatest scatter in the zero-heat-flux points occurs for the thick structure, while the least scatter occurs for the thin water-cooled structure. This result appears reasonable, since the thick structure could conceivably possess the most variable temperature distribution between tests (depending on the heating rate), while the thin water-cooled structure would promote a relatively stable and constant cooling effect. The data further indicate that, generally, the thick copper structure produced the greatest heat losses, even though it did not operate at the lowest structure temperature.

An effect of the heating environment can be seen by noting that, independent of the slug temperature, the conduction losses are lower for the lower heating rates during both heating and cooling portions of the tests. This can be attributed to the fact that when the test assembly is exposed to a low heat flux, smaller temperature gradients are developed due to the combination of the lower heating rate and the prolonged duration of heating required to attain a given slug temperature. This reasoning indicates why the heat losses are the greatest after the test assembly has been heated rapidly.

The trends of lateral-conduction effects can well be anticipated by reviewing the temperature histories. These curves (Figures 38-54) show that, especially at the higher slug temperatures, the temperature differences occurring between the main thermocouple and thermocouple No. 4 can generally produce extreme temperature gradients, which result in lateral conduction. Additional insight concerning these effects is possible by studying the temperature difference between the center of the transducer slug and the groove around its edge (thermocouple No. 1). During initial heating, this gradient promotes heat addition to the slug. However, after sufficient heating, the net effect is such that lateral-conduction losses occur quite readily.

Several attempts were made to achieve a more satisfying correlation of these test results. Typical attempts included plotting the ratio of sensible to incident heat flux versus various dimensionless parameters while trying to incorporate the structure temperature into a meaningful calorimeter performance curve. Unfortunately, these attempts met with little success. It was concluded that the heat losses are dependent on temperature gradients that are too complex to be described by the point temperature measurements made during the tests.

Based on these observations, it has been concluded that data taken with the copper-slug total calorimeter in a structure of unknown temperature history resulting from an unknown heating environment cannot be effectively utilized without some additional temperature information. It can be seen that a measurement of only the calorimeter temperature indicates very little about the structure temperature and the temperature gradients around the calorimeter that control the heat losses. A wide variety of loss gradients can exist at any given calorimeter temperature, and these loss gradients are strongly dependent upon the structure properties and the heating environment. Because of these results, it appears necessary to achieve an exact reproduction of the flight-structure temperatures and heating conditions during the calibration of this type of meter. Since it is often difficult to obtain this information, the obvious limitations and errors introduced by a high-conductivity-slug calorimeter must be accepted.

2. Nickel-Slug Total Calorimeter

It is evident from the previous discussion that the high conductivity of the copper slug plays a prominent role in promoting lateral-conduction effects. It was therefore considered possible that a meter of identical design but possessing a lower thermal conductivity would reduce the heat losses from the calorimeter and thus produce more stable calibration results. With this in mind, a nickel-slug calorimeter, identical in design (ref. Figure 35) to the copper-slug unit, was evaluated.

a. Mounting-Structure Study

Typical temperature histories are presented in Figures 59 through 73. The type of heating and the mounting structure utilized for each test are noted on the graphs. Calibration curves were again constructed and are presented in Figures 74 through 81. The mounting-structure temperatures that occurred for specific calibration points are also shown on these graphs. The calibration data shown for radiant heating and the copper-mounting-structure conditions were collected with the same three copper-mounting-structure conditions utilized during the previous copper-slug-calorimeter performance evaluation.

The results clearly show that the previous effect of mounting-structure conditions on meter calibration has been eliminated through the use of a nickel-slug meter. In addition, the scatter in the zero-heat-flux points that was evident for the copper-slug calorimeter was reduced significantly. For example, under the radiant-heating environment, the average

zero-heat-flux point scatter for the copper-slug meter is 24.3°F/sec with a maximum of 34.8°F; the equivalent scatter for the nickel-slug meter is 3.8°F/sec with a maximum of 4.5°F/sec.

The data obtained for the copper mounting structures further indicated that the nickel-slug calorimeter signal is not influenced by the type of heating. Both convective and radiant heating produced the same calibration curve over the range of test conditions. Finally, the zero-heat-flux points determined for the convective-heating environment fell well within the range of similar radiant data.

Additional testing to determine the influence of a colder mounting structure on the nickel-slug-calorimeter calibration was considered but could not be justified. The results of such a study can be anticipated if one considers the test data obtained to date. Further cooling of a copper mounting structure will merely result in a greater heat loss potential at all heat-flux levels. However, since the cooled and uncooled structures already tested indicated no effect on calorimeter calibration over the tested conditions (convection to the uncooled plate produced temperatures up to about 550°F, while radiation to the cooled plate produced temperatures as low as 200°F), further cooling of the structure cannot be expected to cause any additional effect.

The trends in calibration data exhibited by the nickel-slug total calorimeter when mounted in the M-31-coated heat-shield panel are quite similar to those produced by the copper mounting structure. For example, the data show that, when mounted in M-31 material, the meter can be calibrated by either radiant, convective, or combined radiant-convective heating. Either mode of heating will produce a single calibration curve for the conditions tested.

The zero-heat-flux calibration data collected for the M-31-coated panel were determined only for convective heating, as shown on the calibration curves (Figures 74-81). These points also show the least degree of scatter of all the zero-heat-flux data presented. Since the mounting-structure temperature gradients produced by convective heating are generally more extreme than the gradients resulting from the equivalent radiant heating, and since the greatest heat losses would be expected to occur for convective heating, it is believed that, for the M-31-coated panel, the zero-heat-flux data presented represent the maximum degree of scatter of any combination of convective and radiant heating.

The calibration data also indicate that favorable agreement exists among all zero-heat-flux data collected for the nickel-slug calorimeter. Since these zero-heat-flux points were determined for extreme variations in mounting-structure temperature (a very high- and a very low-conductivity material), coupled with a broad range of different heating environments, their degree of scatter suggests that the heating environment does not significantly affect meter calibration. That is, for a given mounting condition and slug temperature, the type of heating, the actual heat-flux level, and the duration of heating necessary to achieve a specific slug temperature do not exercise significant control during the calibration process.

b. Comparison of Copper Mounting Structure and M-31-Coated Heat-Shield Panel

The calibration curves for the calorimeter mounted in the M-31-coated heat-shield panel (Figures 74-81) agree quite favorably with the data obtained for the copper structure up to laboratory reference heating rates of approximately 15 Btu/ft^2-sec. The indication is, therefore, that for any mode of heating less than 15 Btu/ft^2-sec, calibration data for the nickel-slug meter will exhibit complete independence of mounting structure. Either a high-conductivity material possessing a relatively even temperature distribution or an insulating-type structure with an extremely high surface temperature and large temperature gradient could be employed as the mounting structure during calibration. Either of the two described conditions and any combination of convective-radiant heating (within the limits of the test conditions) would generate identical calibration data.

However, for incident heating rates above 15 Btu/ft^2-sec, the calibration results begin to exhibit two distinct trends. These trends appear to be independent of the method of heating and predominantly determined by mounting-structure conditions. Since these conditions utilize two extremes in thermal conductivity, the deviation present in the calibration data is attributed to conductive heat losses. The slope of the calibration curves determined for both the copper mounting structure and the M-31-coated panel indicates that heat losses from the calorimeter are much more prominent for the copper mounting condition. That is, the slope for the copper-mounting condition increases with heating rate at a noticeably smaller rate than the slope for the insulating mounting condition. Furthermore, the curve for the heat-shield panel approximates a straight line, which suggests that the calorimeter heat-loss effects for this mounting condition are relatively constant and minimal.

Since the M-31-coated heat-shield panel developed very high surface temperatures during convective heating, one might conclude that the absence of heat losses exhibited by the calibration data is not due to the insulating qualities of the M-31 material but is instead due to the increase in heat transfer to the meter resulting from the induced surface-temperature discontinuities (discussed in parts C. and D. of the "Calorimeter-Induced Disturbances" section). However, the presence of this effect can be disregarded because of the different types of heating used to define the calibration curves of Figures 74 through 81. Both of the combined heating tests (radiant and convective heating) shown on the calibration curves are predominantly radiant heating. The measured combined flux of 22 Btu/ft^2-sec resulted from the individually measured components, that is, 16 Btu/ft^2-sec from the radiation source and 12 Btu/ft^2-sec total heating from the convection source; the combined flux of 20 Btu/ft^2-sec was the result of an 18 Btu/ft^2-sec radiant input and a 9 Btu/ft^2-sec total heat load from the convective source. These two tests, in conjunction with the purely radiant-heating data, verify that any effect of a step temperature discontinuity at the meter-structure interface does not alter meter output. It is noted that the individual heating components presented cannot be directly added to give the combined result. Although this discrepancy could not be fully explained using available data, its presence does not justify additional testing.

An interesting result can be seen from a comparison of Figures 36 and 37. Early radiation tests (Figures 38-54) were conducted with the mounting structure of Figure 36, which prevented the presence of large slug-edge temperatures (indicated by the low thermocouple No. 4 readings) and therefore suggested the presence of a high-conductance path for heat losses. However, all succeeding heating tests used the mounting-structure configuration shown in Figure 37, which resulted in consistently high slug-edge temperatures in the vicinity of the mounting bolts for all three types of heating. Since radiant heating on the copper-mounting structure shown in Figure 37 resulted in high temperatures (large thermocouple No. 4 temperature readings), the role of stagnation heating in maintaining large slug-edge temperatures is not as important as one might assume for the tested mounting configurations. In addition, the calibration data from these tests indicate that for the nickel-slug calorimeter mounted in a copper structure and subjected to radiant heating greater than 15 Btu/ft^2-sec, the same heat losses from the nickel slug occur regardless of the slug-edge temperature; i.e., regardless of either of the two mounting methods shown in Figures 36 and 37.

Temperature histories presented in Figures 59 through 73 show that structure temperatures are lower for the M-31-coated panel than for the copper structure. This result is attributed to the significant difference in the thermal conductivities of the two materials. Further, the temperature difference between the center and edge of the slug varies from test to test. However, for similar heating conditions, this temperature difference is greater for the M-31 panel than for the copper structures, but the magnitude of this difference shows no direct correlation with the heat losses. The structure temperature shows even less correlation. It is possible, therefore, that the temperatures measured are not really indicative of the true structural temperature effects.

Although a deviation in the calibration points exists between the M-31-coated panel and the copper mounting structures at the higher heating rates, the over-all influence of this variation need not be of great concern. The calibration points for the M-31-coated panel clearly approach a single calibration curve over all ranges of the three types of heating used. If the calorimeter is actually calibrated in a low-conductivity structure, the calibration can be expected to be quite consistent under any of the three heating modes and valid in a flight environment. Should the calorimeter be calibrated in other mounting structures (similar to the tested copper structures), the calibration will be valid at the lower heat-flux levels but might not be applicable at the higher heat fluxes. Errors of as much as 25 or 30% can be recognized at the higher fluxes if flight-type mounting conditions are not simulated during calibration.

It is of interest to note that some of the calibration points at a slug temperature of 700°F (ref. Figure 79) show a slight deviation from their expected values. A typical example concerns the calibration point for the M-31 mounting condition at a convective-heating rate of 27.2 Btu/ft^2-sec. This discrepancy is caused by the discontinuous change in the specific heat of nickel, which occurs at the Curie temperature of approximately 670°F. The result is a sudden change in the slope of the slug temperature, making the exact slope difficult to determine.

The above discussion indicates that the nickel-slug calorimeter possesses many features that are desirable for a flight transducer. For example, although calibration is usually performed under radiant heating, the calibration curves for a given mounting condition are valid when applied to a purely convective-heating environment. This result

is very encouraging because it gives considerable support to the validity of past calibration and flight measurements employing this type of meter. In addition, the results show that for heat-flux levels below 15 Btu/ft^2-sec, calibration of the nickel-slug total calorimeter mounted in a copper structure under radiant heating is directly applicable to many aerodynamic heating conditions, e.g., when the meter is mounted in an insulating structure and subjected to convective heating.

The ability of this calorimeter to withstand the large variations in flange conditions while maintaining a single calibration indicates that the design incorporates parameters that are highly advantageous to the measurement of convective heat transfer. One of these parameters appears to be the thermal conductivity of the slug. Since the temperature at the center of the slug was not influenced by the variation in flange temperature, the conductivity of the slug can be assumed to be sufficiently low. However, the measured temperature gradients indicate that a similar design incorporating copper as the slug material would be subject to considerable conduction effects.

Another parameter of importance is the size of the slug. Although the slugs in the meters tested are somewhat cumbersome, several advantages are introduced. In addition to physically locating the main thermocouple far from the edges where large temperature variations have been observed, the unusually large slug area provides a buffer area against both thermal and hydrodynamic boundary-layer effects. In view of the high temperatures measured around the mounting bolts, it is obvious that serious stagnation heating effects could develop. Associated with the stagnation flow would be both fluid and thermal turbulence on the downstream side of the bolts. This turbulence occurs on the sensing surface but is apparent-apparently damped-out before reaching the center of the slug. Also, any thermal-boundary-layer perturbations caused by surface-temperature discontinuities appear to be damped-out. A smaller slug, however, could be expected to exhibit some dependence on the edge effects.

To summarize the evaluation of the nickel-slug calorimeter for the test conditions, it can be concluded to be a much better instrument than a copper-slug calorimeter of the same design. In addition, variation in the structure temperature has not been found to noticeably affect the calibration. However, the difference between mounting conditions in a copper plate and in an M-31-coated heat-shield panel does produce a change in calibration. This change, which cannot be directly attributed to a difference in structure

temperature, was, however, accompanied by a change in slug-edge temperatures. The exact mechanisms of these changes were not established.

Based on these results, it can be concluded that calibration generally should be carried out with the calorimeter mounted in an M-31-coated heat-shield panel when the calorimeter is to be used in such a mounting. The calibration itself, however, can be performed under radiant or convective heating; either should produce a valid set of calibration curves.

C. C-1118 Membrane Total Calorimeter

The exposed surface of the C-1118 membrane total calorimeter tested consists of a copper body 0.5 inch in diameter with a 0.2-inch-diameter membrane, as shown in Figure 82

The purpose of this test series was to evaluate the general performance of the meter and to investigate the effect of a meter-induced surface-temperature discontinuity on the measurement of convective heating rates. If the study showed that the surface-temperature discontinuity promoted erroneous structural heating-rate measurements, an investigation of data-correction techniques would be conducted. Finally, a study was conducted to determine whether the heat flux to M-31 insulation material is affected by water absorption by the material.

1. Effect of Surface-Temperature Discontinuity

The effect of a surface-temperature discontinuity in measuring convective-heating rates was studied by mounting the membrane total calorimeter in two thermally different materials. The reference test structure, promoting a basically isothermal surface condition, was a 3/8" × 4" × 12" copper plate. Since the body of the membrane calorimeter was also made from copper, temperature discontinuities at the instrument-structure interface were essentially eliminated, introducing a reference surface condition with no temperature variation except that across the membrane itself.

The nonisothermal surface condition was induced by the large difference between the thermal conductivities of the meter copper body and appropriate mounting structures. Two such nonisothermal mounting structures were fabricated. The first was assembled using commercially available fire bricks. The fire-brick mounting structures tested included both smooth and rough surfaces to permit investigation of any effect of surface-contour mismatch. The second nonisothermal mounting condition incorporated an M-31-coated heat-shield panel identical to the one described in part B. of the "Experimental Results and Discussion" section. The conductivity of the M-31 material is approximately 0.07 Btu/hr-ft-°F.

The tests performed consisted of sequentially imposing a convective heat flux on the laboratory total reference calorimeter and on the membrane calorimeter mounted in the isothermal-surface structure. These tests were then repeated over a wide range of incident-heating rates. Identical convective-heating tests were then conducted for the nonisothermal-surface mounting-structure conditions. During all tests, the reference-calorimeter sensor and the test-meter sensor were situated in the same coordinate position relative to the convection source and were subjected to the same flow starting lengths. This procedure insured constancy and repeatability of test conditions. Additional validation of repeatability was provided by the fine degree with which the gas flow could be controlled and by the excellent reproducibility of the laboratory-reference-calorimeter measurements between the isothermal- and the nonisothermal-surface heating tests. Test series were conducted for calorimeter locations of 6, 15, and 31.6 inches downstream from the point of convective-gas-flow boundary-layer inception in order to compare the theory and data at different values of L/W (see part D.1.of "Calorimeter-Induced Disturbances" section).

a. Surface and Free-Stream Gas-Temperature Measurements

In order to correlate the test results with theoretical predictions, it was necessary to measure the surface temperature of both mounting structures and of the calorimeter body, as well as the free-stream gas temperature. Chromel/Alumel thermocouples were used for all surface-temperature measurements. A thermocouple was attached to the calorimeter body to provide a measurement of the body surface temperature and, in the isothermal case, of the structure surface temperatures, since the entire system is made of high-conductivity copper. The low-conductivity structures were instrumented with a thermocouple just below their surface and approximately 0.3 inch upstream from the calorimeter-structure interface. Surface-temperature measurements showed excellent correlation with calculated values.

Accurate gas-temperature measurements were, of course, more difficult to achieve than surface-temperature measurements because of the extreme temperatures encountered; stoichiometric temperature for complete combustion of oxygen and acetylene is in excess of 5000°F. Thermocouples capable of withstanding these temperatures must be fabricated from refractory metals. Such thermocouples, however, exhibit very poor oxidation resistance and can be expected to last for only a matter of seconds at

temperatures in excess of 3000°F. The free-stream gas temperature was assumed to remain constant for a given incident heat flux. Therefore, if a measurement could be made before the thermocouple oxidized away, the reading would be reasonably valid for the entire test. Thermocouples made from tungsten/tungsten-26% rhenium and platinum/platinum-10% rhodium were placed in the free stream through a fire brick in the same coordinate position as the membrane total calorimeter. A number of gas-temperature measurements were made over a wide range of convective-heating levels at each location downstream from the boundary-layer inception point.

An additional problem arises during evaluation of the gas temperature because of radiation losses from the thermocouple at high temperatures. It is therefore necessary to correct for these losses. This is accomplished by making a heat balance between convective-heat input and radiant losses. Such a heat balance requires a knowledge of the heat-transfer coefficient on the thermocouple wire. The heat-transfer coefficient can be obtained directly from the response time of the thermocouple, which is given by [16]

$$\tau = \frac{\rho c D}{4h} \quad . \tag{17}$$

A heat balance on the thermocouple therefore becomes:

$$\frac{\rho c D}{4\tau} (T_o - T_t) = \epsilon \sigma T_t^4 \quad . \tag{18}$$

If thermocouples of two different sizes are used, it is possible to eliminate all unknowns in equation 18, including ϵ. However, it was found that the resulting computation is extremely sensitive to very small errors in the measured temperature, causing inconsistent results. An emissivity of 0.8 was therefore chosen for the oxidized tungsten, and equation 18 was applied to each thermocouple output. Tests were also run using a ceramic-coated thermocouple. Because of unknowns in properties and variations in diameter, the data were not as consistent as the base-wire data but did indicate the same average free-stream gas temperatures.

Typical surface-temperature and gas-temperature histories are presented in Figures 83 through 86. These data were taken for meter locations of 31.6, 15, and 6 inches downstream from the point of boundary-layer inception. Gas-temperature measurements performed at the 6-inch location resulted in a relatively stable free-stream temperature of 5000°F Varying the gas flow rates, while providing sufficient oxygen for complete

combustion. did not noticeably affect the readings. However, the magnitude of the gas temperature varied significantly with the imposed convective heat flux at the 15- and 31.6-inch locations. This effect was apparently due to radiant and convective energy losses over the longer heating lengths.

b. Heating History of Membrane Total Calorimeter

Typical heating histories obtained with the membrane total calorimeter for both isothermal and different nonisothermal surface mounting conditions under convective heating at the different downstream locations are compared to each other and to the reference measurements in Figures 87 through 90. These curves indicate that during the first several seconds of heating, when the meter is subjected to a nonisothermal surface-temperature condition, the calorimeter output is changing. However, as the test progresses, the membrane-calorimeter output begins slowly to stabilize. In all cases, these calorimeter heat-flux measurements for the nonisothermal-surface conditions were much larger than the relatively constant heat-flux measurements registered by the same calorimeter when mounted in the structure (copper) that produced the isothermal-surface condition. The repeatability of the laboratory-reference-calorimeter heat-flux measurements for a given convective-heating rate was well within 3%, thus indicating the consistency and accuracy in reproduction of heating over the isothermal and nonisothermal surfaces. These experimental results, coupled with the underlying theory, directly suggest that the noticeably increased output of the small membrane calorimeter when mounted in the nonisothermal structure is a result of the surface-temperature discontinuity established at the calorimeter-structure interface.

Because of the response time of the system and flame fluctuation at ignition, stable calorimeter readings could not be determined for the nonisothermal-surface mounting condition until approximately 1 second after ignition, as shown in the heating histories (Figures 87-90). It should be further recognized that the actual calorimeter signal was not a smooth curve, as shown in the heating histories, but was a sawtooth-type curve similar to electrical "noise" signals. This indicates that the membrane calorimeter, due to its extreme sensitivity and short response time, was able to detect the turbulence present in the flame. These turbulent effects, however, did not alter the over-all heat-flux determination or the long-term variations.

It was originally expected that the measurements made with the calorimeter for the isothermal surface condition would agree with the reference measurements. The

fact that the two measurements disagree is of some concern and is discussed in part D. of the "Experimental Results and Discussion" section.

c. Effect on Convective Heat-Transfer Coefficient and Heat-Flux Measurements

Presentations showing the effect of surface-temperature discontinuity on heat-flux measurements can be made in terms of either heat-transfer coefficients or actual heat fluxes. The applicable ratios are:

1) $\bar{h}/h$, the ratio of the average heat-transfer coefficient at the surface of the calorimeter to the local heat-transfer coefficient at the surface of an undisturbed structure (this ratio can be compared to the analytical prediction of equation 6).

2) $\bar{q}/q_{isi}$, the ratio of the heat flux indicated by the calorimeter to the heat flux at the surface of the undisturbed structure (this ratio defines the error in the calorimeter measurement).

These ratios, discussed earlier, were shown to be represented by:

$$\frac{\bar{h}}{h} = \frac{\bar{q}}{q_{isn}} \quad . \tag{10}$$

$$\frac{\bar{q}}{q_{isi}} = \frac{\bar{q}}{q_{isn}} \left[\frac{T_o - T_{w_2}}{T_o - T_{w_1}} \right] \quad . \tag{11}$$

Values of $\bar{q}$, T_{w1}, and T_{w2} were selected from experimental records for constant values of the temperature discontinuity $(T_{w_1} - T_{w_2})$. The corresponding values of q_{isi}, the heat flux to the isothermal surface of the copper structure, were determined for the same value of T_{w_2}. Thus, $\bar{q}$ and q_{isn} were available as actual calorimeter measurements and $\bar{h}/h$ and $\bar{q}/q_{isi}$ could be determined experimentally.

Analytical and experimental results are presented in Figures 91 through 93 for the different downstream locations as a function of the heat flux measured by the laboratory reference calorimeter. Experimental values of the ratio $\bar{h}/h$ (direct measurements) indicate that, in the presence of an 800°F temperature discontinuity at the structure-calorimeter interface and at a 31.6-inch location, the heat-transfer coefficient at the calorimeter surface was 30 to 50% higher than the coefficient that would exist at the surface of the undisturbed structure. There was a comparable increase of 20 to 30% in the heat-transfer coefficient at the 15-inch and 6-inch locations. The ratio $\bar{h}/h$ tended to decrease at higher heat flux for

the test conditions encountered at the 31.6-inch location because the measured gas temperature increased at higher heat flux, with the result that the 800°F discontinuity exerted less influence on the calorimeter measurement.

The analytical expressions of both Rubesin and Westkaemper (equation 6 and Figure 2), evaluated for the test conditions, are also shown in Figures 91 through 93. Experimental values of the ratio $\bar{h}/h$ tend to fall between the two correlations. At the shortest downstream location tested, however, Rubesin's correlation appears to provide a closer estimate of the measured increase in the convective heat-transfer coefficient over a surface-temperature discontinuity.

In many aerospace heating applications, it is desirable to evaluate actual structure-surface heating rates directly from the calorimeter measurements instead of heat-transfer coefficients. It has been shown that these heating rates can be conveniently represented in the form $\bar{q}/q_{isi}$. In the present experiment, $\bar{q}/q_{isi}$ will differ noticeably from $\bar{h}/h$ because of the large temperature potentials involved.

Using equation 11 and the appropriate temperature and membrane-calorimeter measurements, values of $\bar{q}/q_{isi}$ were determined and are presented in Figures 91 through 93. The magnitudes of this ratio indicate that when a membrane calorimeter of this type is mounted in an insulating (heat-shield) structure such that large surface-temperature discontinuities are established, the calorimeter measurement can be an extremely erroneous representation of the actual heat flux to the instrumented structure. For example, the results show that the membrane calorimeter was exposed to a heat flux 90 to 140% greater than that to the insulating structure in the presence of an 800°F temperature discontinuity at the 31.6-inch location. The calorimeter error was 50 to 100% and 40 to 60% at the 15-inch and 6-inch locations, respectively, in the presence of a 1000°F temperature discontinuity. These experimental results are compared in Figures 91 through 93 to predictions of the ratio $\bar{q}/q_{isi}$ calculated from equations 6 and 11 and the corresponding temperature data. This comparison shows good agreement between the actual error in the calorimeter measurements and the predicted error. Tables I through III* present the data and results in tabular form.

The effect on $\bar{h}/h$ and $\bar{q}/q_{isi}$ of different calorimeter-induced surface-temperature discontinuities occurring at a given downstream location (31.6 inches) is illustrated in Figure 91. For the temperature conditions tested $\bar{h}/h$ appears to be relatively independent

* See appendix

of different values of the surface-temperature discontinuity. In fact, recognizing the presence of data scatter, no definite change in experimental values of $\bar{h}/h$ can be detected, even though the surface-temperature discontinuities vary from 340 to 800°F. The predicted values of $\bar{h}/h$ also approach this trend. Experimental determinations of $\bar{q}/q_{isi}$, however, were found to be strongly dependent on the actual magnitude of the surface-temperature discontinuity. This dependence was also noted for the calculated predictions of $\bar{q}/q_{isi}$.

The above-discussed results exhibit special significance, since heat-shield panels are often instrumented with small-diameter membrane calorimeters to determine the convective heat-transfer coefficient over the panel surface. This study shows that if the convective heat-transfer coefficient is determined directly from calorimeter output, calorimeter surface temperature, and free-stream gas temperature, the resultant coefficient will be that represented by $\bar{h}$ in equation 7 (part D.2., "Calorimeter-Induced Disturbances"). It will thus not be the desired value of the convective heat-transfer coefficient and will be in error by the amount $\bar{h}/h$ as indicated in Figures 91 through 93. Of course, if this erroneous convective heat-transfer coefficient is utilized with the gas temperature and the heated-structure surface temperature, the resultant heating rate will exhibit a similar error. If the heating rate to the instrumented structure is taken as the direct output of the calorimeter, without correction for surface-temperature-discontinuity effects, then the error will be large and directly related to $\bar{q}/q_{isi}$ as shown in Figures 91 through 93.

Satisfactory agreement between the test data ($\bar{h}/h$ and $\bar{q}/q_{isi}$) and the theory presented (Rubesin and Westkaemper) indicates that error corrections can be estimated for membrane calorimeters if the conditions of the measurement are known. However, it is doubtful that the necessary information is readily available for the in-flight environments that promote these errors. Thus, the potential errors in both convective heat-transfer coefficients and structural heating-rate measurements that can result from calorimeter-induced surface-temperature discontinuities must be recognized.

It should be realized that the appartus in the present study does not completely satisfy the conditions assumed in the development of the theory presented. For the tests in which the calorimeter was located 6 inches downstream, the gas temperature decreased

slightly in the direction of flow. In the tests at the 31.6-inch location, it was necessary to provide a ceramic duct for most of the distance to prevent mixing of the gas stream with surrounding air. This length of about 10 hydraulic diameters may have been sufficient to allow duct flow to develop. The exact nature of the flow in all tests is another factor pertinent to an evaluation of the test results, but the estimated Reynolds number and the turbulence induced by the combustion process indicate that the flow was indeed turbulent. The comparatively good agreement between data and theory indicates that these factors did not introduce serious complications.

2. Transpiration Study

A preliminary investigation was conducted to determine the magnitude of the effect of water absorption on both the heating of the M-31 material and the heat flux to a calorimeter mounted in an M-31 heat shield panel. A stainless-steel panel coated with M-31 material was instrumented with the C-1118 membrane total calorimeter and with three Chromel/Alumel thermocouples (0.008 inch in diameter) embedded at selected depths in the M-31 material (0.002, 0.101, and 0.251 inch). The thermocouples and calorimeter were placed adjacent to each other at the same distance downstream from the leading edge of the panel. A series of convective-heating tests was then made after the instrumented structure was exposed, prior to each test, to each of the following environmental conditions: 1) a minimum relative humidity of 95% for 24 hours at 100°F, 2) oven drying at 220°F for 24 hours, 3) direct contact with water at room temperature for about 2 hours. The percentage of water-moisture absorption was estimated prior to each test by appropriate weight measurements. Note that condition 2 was used as a reference condition to which the results of conditions 1 and 3 can be compared.

The experimental data collected for this test series are presented as temperature histories of the three thermocouples and heating history of the membrane calorimeter in Figures 94 through 102.

Data presented in Figures 94 through 97 compare temperature histories for environmental conditions 1 and 2 above and for heating from a constant convective source. These curves indicate that when the M-31 insulation material has been preconditioned by exposure to a relative humidity of 95% for 24 hours at 100°F, the temperature distribution varies significantly from that occurring when the insulation has been subjected to oven drying at 220°F for 24 hours. The temperature data collected for the oven-dried cases is typical

of temperature histories determined for previous tests and thus verifies the temperature-measurement procedure. However, the temperature data collected after the insulation was subjected to the humid environment show that a) the rate of increase of the insulation-temperature slopes is generally reduced, and b) in certain cases, negative slopes existed. These results suggest that cooling mechanisms, both evaporative and transpirative, were occurring in the moistened material during the heating test.

Due to recording-instrumentation malfunctions, heating rates of the M-31 material as measured by the C-1118 calorimeter were not obtained for the first set of tests (conditions 1 and 2 described above). However, the heating-history trends can be estimated from data collected for conditions 2 and 3 above; i.e., instrumented structure subjected to oven drying at 220°F for 24 hours (reference condition) and to direct contact with water at room temperature for about 2 hours. A comparison of the heating histories measured for these two conditions is shown in Figures 98 and 99. The initial decrease in the measured heat flux from a constant convective-heating source further indicates that the presence of water (liquid and/or gaseous) in the M-31 insulation material promotes surface and boundary-layer cooling that alters the heat flux to the surface and to the membrane total calorimeter. Temporary reductions of 29% and 25% in the measured heating rate due to water absorption are evident in Figures 98 and 99. Because of the large difference in the heat-flux measurements for these two environmental conditions, three additional heating tests were made with the water-soaked panel to study further the noticeable cooling effects. The results, shown in Figures 100 through 102, confirm the previous decreasing heat-flux trends. The temperature-history records indicate that the two in-wall thermocouples failed. It was impossible, therefore, to accurately determine the temperature variation within the insulation for the last three tests. Comparative heating-history data on the oven-dried condition for the three tests (Figures 100-102) were also unavailable because of the deteriorated condition of the test structure and the limited time allotted for this portion of the study.

The importance of this brief transpiration study is that an effect of water absorption by M-31 heat-shield material on the heat transfer to its surface and to a membrane-calorimeter surface has been measured. This effect is probably due to gas-transpiration cooling by the released vapor. A significant variation in this heat flux was recognized between the wet and dry conditions. In fact, temporary reductions of 29% and 25% in the measured heating rates due to water absorption are evident in Figures 98 and 99, respectively.

D. Radiant-Heating Studies

A series of radiant-heating tests was conducted utilizing three commercially manufactured and calibrated calorimeters. The calorimeters tested were the C-1118 membrane total calorimeter and two membrane purged radiometers (models R-2006 and N-139). The C-1118 and the R-2006 were fabricated and calibrated by the same manufacturer. The N-139 (shown in Figure 103) and the R-2006 are essentially of identical design, with only the sensors being of different size.

Prior to the radiant tests, the C-1118 had undergone extensive convective testing. The sensor coating was therefore badly damaged and required recoating. The emissivity of the original surface was 0.89, as quoted by the manufacturer, and the calibration was based on absorbed heat flux. The new coating (Parsons optical black lacquer) was identical to that used on the radiant reference meter. This type of coating has an emissivity very near 1.0, making the calibration supplied with the C-1118 directly applicable to both absorbed and incidental heat flux.

It was also necessary to correct the manufacturers' calibrations of the radiometers for view angle. Both radiometers were originally calibrated with a radiant source that was effectively infinite in extent. The radiometers, however, have a view angle of only about 150 degrees. The calibrations, therefore, included a correction for the energy not seen by the sensor. In the apparatus used in the tests under discussion, the source was entirely within the view field of the radiometers. The correction automatically made during manufacturer calibration was therefore not applicable and had to be eliminated. This required reduction in the heat flux indicated by the radiometer by a factor corresponding to the ratio of the energy not seen during calibration to the total incident energy. The percentage correction is given by $(1 - F_{rs})$, where F_{rs} is the geometrical shape factor corresponding to a view angle of 150 degrees. The following equation is applicable for an elemental area, with θ being the half angle of the view field.[13]

$$F_{rs} = 2 \int_0^{\theta} \cos\theta \sin\theta \, d\theta \quad . \tag{19}$$

Integrating equation 19 results in:

$$F_{rs} = \left[\sin^2 \theta \right]_0^{\theta} \quad . \tag{20}$$

For a view field of 150 degrees, θ = 75 degrees. Substituting θ = 75 degrees into equation 20, the shape factor is:

$$F_{rs} = 0.933.$$

The correction necessary is 1 - 0.933 or 6.7%. Therefore, all radiometer readings during this test program were reduced 6.7%.

The test procedure for comparing these three transducers was similar to that described for convective testing. The graphite resistance-heated source was brought to an equilibrium temperature, and the temperature, measured by an NBS-traceable optical pyrometer, was recorded. The laboratory reference radiation calorimeter was placed in the test section, the shutter covering the source was opened, the calorimeter signal was recorded, and the shutter was again closed. The C-1118 calorimeter was then placed in the test section and the process repeated. The R-2006 and the N-139 followed in respective order. During the entire test sequence, the source temperature was monitored and the power to the source adjusted as necessary to provide a stable temperature. Six tests of this type were run. All test data were good except for the last test, during which the N-139 lost continuity and no reading was obtained.

In order to compare the readings of the four transducers, the heat flux indicated by each was plotted against that indicated by the laboratory reference meter during the same test; the reference-meter output thus appears as a straight line and serves as a basis of comparison.

The resulting data, with the radiometer readings corrected, are shown in Figure 104. As indicated, the N-139 agrees with the laboratory standard within 4% in all but one test, while the C-1118 and the R-2006 are both considerably higher in all cases. The latter two calorimeters also exhibit significantly more scatter.

It should be noted that two different mounting structures were employed for the radiant-heating study of these three calorimeters. Both the N-139 and the R-2006 radiometers were mounted in low-conductivity brick structures, whereas the C-1118 total calorimeter was mounted in a smooth $\frac{1}{4}$-inch-thick copper structure. Because of the high reflectivity of the copper structure, it reflected more radiation back onto the radiant source than did the rough surface of the brick structure. One might conclude, therefore, that the noticeably larger output of the C-1118 total calorimeter

is a measure of this additional radiation (which has been reflected from the mounting structure to the radiant source). However, the data for the R-2006 radiometer, which was mounted in the brick structure, indicate that such a conclusion is invalid because these data show similarly high heating rates and also exhibit better correlation with the C-1118 total calorimeter than with either the laboratory radiation reference calorimeter or the N-139 membrane radiometer. These facts directly suggest that the variation in the calorimeter heat-flux measurements that have been detected for a given radiation-source temperature cannot be correlated solely to differences in the optical properties of the mounting-structure surfaces but rather is due to a basic disagreement in the calibration of the actual instruments.

Because of the close agreement between the laboratory reference meter and the N-139 calorimeter, the indication is that the error lies in the calibration of both the C-1118 and the R-2006. This conclusion is further substantiated by previous tests employing both the radiation and the total laboratory-reference meters for calibration studies of the nickel-slug calorimeter under radiant and convective heating. For heating rates below 15 Btu/ft^2-sec, the two calibrations showed excellent agreement with one another and with theoretical heat capacities at the lower slug temperatures. These results provide evidence of the consistency between the total and radiant reference calorimeters and also substantiate the absolute magnitudes of measured heat flux. It is believed, therefore, that the reference calorimeters and the N-139 purged membrane radiometer indicate the correct heating rates.

During these tests, another interesting phenomenon was observed. The millivolt signals from both the N-139 and the R-2006 radiometers during a typical test (with both rise and decay periods included) are shown in Figure 105. These curves indicate that the response of the radiometers to either a step input or a step cutoff of heat flux is very slow. The N-139 appears to have a faster response but still exhibits a long-term drift before attaining steady state. The decay time for the R-2006 is particularly slow. The cutoff of heat flux was very nearly a true step change; the shutter closed in less than 0.1 second

The only apparent explanation for the slow response is that the air between the sensor and the window heats up with time, taking heat from the sensing membrane.

The reverse would be true on cooling. The effect does not appear to be a result of sensor response time, since the membrane is inherently a fast-responding device; this fast response is seen in the initial rise and decay of the curves. The long-term upward drift of the signals is not believed to be caused by changes in source temperature, since the temperature was monitored at all times and since no such drift was observed with the C-1118 total calorimeter. In addition, the slow decay of the R-2006 indicates that the problem lies in the instrument.

A brief test series was also conducted to evaluate the performance of a purged radiometer possessing a 7-degree view angle. The purpose of the study was to investigate the calibration of the instrument as a function of both its distance from the radiation source and the magnitude of the purge pressure. Nitrogen gas was used for the purge, with pressures varied from 0 to 60 psig. The instrument, a photosensitive device, was mounted in a 0.125-inch-thick stainless-steel structure and was subjected to radiant heating.

The radiometer originally evaluated lost continuity during the initial portion of the test series. A second radiometer was therefore obtained for the study. However, because of the subsequent delay in testing, the original scope of the test plan had to be reduced. The purge assembly of the second radiometer was found to be defective and had to be replaced with components from the original radiometer.

The data for the second radiometer are presented in the form of transducer-output histories (a calibration curve was not included with the second meter), as shown in Figure 106. The distance between the meter and the radiation source and the gas-purge pressures for each test are shown on the graph. All tests were conducted for the same radiant-heating rate corresponding to a block temperature of 2110°F. Except for the radiometer heating history at the 38.9-inch location, the range of data scatter is about 7.5%. The results at the 38.9-inch location suggest that the radiation source did not completely fill the view field of the radiometer, due to incorrect positioning of the radiometer sensor directly below the center of the source. Varying the purge gas (20 to 60 psig) did not alter the meter output at the 16.8-inch location. The curves also indicate that the response of the radiometer to a step input of heat flux is quite slow; the instrument exhibited a long-term drift before approaching a relatively

constant heat-flux measurement. There is also noticeable data scatter for the two tests at the 16.8-inch location, even though the test conditions were identical. The test results at the 7.5-inch location show that when the purge pressure is constant at 20 psig, the radiometer output approaches a relatively constant value. However, increasing the purge pressure at this meter location causes a noticeable increase in radiometer output. Should the purge pressure be reduced to 20 psig, the transducer output would return to its original measurement. The data collected for this meter location are somewhat surprising in that increasing the purge pressure resulted in a cooling effect on the block and an increased output by the radiometer. Generally, the output of a photosensitive device increases with increasing incident energy. However, these instruments can often exhibit unstable trends, depending on the temperature, the incident energy, and the actual properties of the device.[18]

E. Gas-Temperature Probe

A brief performance study of a NASA-supplied gas-temperature probe (No. 50M10100) was conducted. The probe, shown in Figure 107, possesses a sensing element composed of platinum/platinum-10% rhodium thermocouple material. The purpose of this experimental study was to investigate the effect of large radiant-heating loads on the gas temperature indicated by the instrument.

The probe was mounted with its longitudinal axis normal to both the radiation source and the direction of gas flow; the sensing element was 3.2 inches from the radiation source. Actual testing consisted of exposing the probe to a free-stream gas temperature not exceeding 2500°F; after a steady output was recorded, various radiant-heating levels were imposed on the probe. These steps were then repeated for different free-stream gas temperatures.

The experimental results, recorded in the form of temperature histories, are presented in Figure 108. The data clearly indicate that the output of the gas-temperature probe is readily influenced by radiant-heating effects. That is, when the probe registers a given gas temperature and is then subjected to a step radiant-heating input, the probe output begins to increase. If the radiant-heating condition is eliminated, the higher output progressively decreases to the original free-stream gas-temperature measurement. Apparently during total heating, the guard sleeve (see Figure 107) surrounding the sensing device is heated by the radiation source and thus reradiates to the thermocouple

element. However, this heating condition diminishes when the radiation source is removed. As would be expected, the largest increase in the gas-temperature measurement of the probe due to a given radiant-heating input occurred at the lower gas temperatures. For free-stream gas temperatures of 921 and 1185°F and radiation-source temperatures of 1800 and 2360°F, increases of 4.3 and 9%, respectively, were measured. However, for the same radiation-source temperatures and for free-stream gas temperatures equal to 2196 and 2268°F, increases of only 2.3 and 2%, respectively, were detected.

CONCLUSIONS

The calorimeter designs evaluated were subject to varying degrees of error in the measurement of surface heat flux. These errors are attributed to temperature differences between the meter and the surrounding structure caused by the presence of the meter itself and arise from 1) cross conduction between the meter and the surroundings; and 2) in the case of convective heating, perturbation of the boundary layer by the temperature discontinuity at the meter-structure interface.

The over-all study shows that a single calibration for a given heat-flux meter may not be applicable for all heating environments and mounting conditions.

A thorough experimental evaluation of heat-flux meters on a laboratory scale has proved extremely beneficial in establishing their expected accuracies for various installations and heating conditions. Conclusions regarding each type of meter studied are presented below.

A. Copper-Slug Radiometer (N-123)

For a given radiation-source temperature, the output of the N-123 radiometer, when unpurged, varied significantly and showed a strong dependence on the mounting structure employed. This data scatter and the dependence on mounting structure were eliminated when the radiometer evaluation incorporated the purge-gas flow. A radiometer calibration to be utilized in flight applications should therefore be made while operating with purge gas. The presence of a large convective load on the radiometer did not change the radiometer calibration obtained for purely radiant heating.

B. Total Slug Calorimeters

The copper-slug total calorimeter is strongly influenced by cross-conduction effects and by the heating environment to which the structure is exposed. A nickel-slug total calorimeter is superior to a copper unit because of the significant difference in the conductivities of the two calorimeters. Heat-flux measurements with a large nickel calorimeter were independent of both the mounting structure and the heating conditions for heating rates below 15 Btu/ft^2-sec. For heating rates above 15 Btu/ft^2-sec, the output of the calorimeter was dependent on mounting-structure conditions but independent of the type of heating. Surface-temperature-discontinuity effects at the meter-structure interface were minimized by the large surface area of this calorimeter.

C. Total Membrane Calorimeter (C-1118)

Results obtained with the C-1118 membrane total calorimeter when mounted in M-31-coated heat-shield panels show that the output of this instrument can be an extremely erroneous indication of the convective-heating rate to the structure surface. For the conditions tested, the heat-transfer coefficient at the calorimeter surface is 20 to 50% higher than the coefficient that would exist at the surface of the undisturbed structure, and the calorimeter indicates heat fluxes 40 to 140% higher than would exist at the surface of the undisturbed structure. These errors result from the temperature discontinuity introduced on the surface by the presence of the calorimeter, causing the convective-heating rates to be higher than those experienced by the parent structure. Satisfactory agreement between the data and the theory indicates that corrections can be estimated for membrane-calorimeter measurements if the conditions of the measurement are known.

Effects of water absorption by M-31-coated heat-shield material instrumented with a membrane calorimeter were studied. These effects were found to alter the heating rate to the surface of both the material and the instrument in that temporary reductions of 25% and 29% were evident in the heating rate measured by the membrane calorimeter.

D. Radiant-Heating Studies

Significant scatter in radiant-heating data is evident between the C-1118 membrane total calorimeter and the R-2006 and N-139 membrane radiometers for a given radiation-source temperature. The degree of scatter appears to be independent of the mounting-structure optical properties and is due to a basic disagreement in the techniques used in calibrating the instruments. The output of the photosensitive 7-degree-view-angle radiometer, when operated with purge-gas flow, was dependent on the purge pressure at a distance of 7.5 inches between the radiation source and the radiometer window. No such dependence was evident at the larger distances tested (16.8 and 38.9 inches). However, the radiometer did exhibit noticeable data scatter between successive tests, even though the test conditions were identical.

E. Gas-Temperature Probe

The output of the gas-temperature probe (No. 50M10100) can be influenced by radiant-heating effects.

RECOMMENDATIONS

Since it is difficult to calibrate a heat-flux transducer for universal application, it is recommended that laboratory evaluations of current meters be continued in order to determine their behavior in specific heating environments. Resulting information can then be utilized to predict the accuracy of a calorimeter in actual flight applications if the expected environmental conditions can be reasonably estimated.

The practice of measuring convective heat flux (or convective heat-transfer coefficients) to a structure at elevated temperature using a relatively "cold" calorimeter has been shown to produce results of often dubious value. It is recommended that alternative measurement techniques be investigated for potential elimination of these measurement errors.

NOMENCLATURE

A	Area (ft^2)
a	Exponent in equation 5
b	Exponent in equation 5
c	Specific heat (Btu/lb-°F)
D	Diameter (ft)
dT/dy	Gas-temperature gradient
F_{rs}	Geometric shape factor for radiation
F(L/W)	Geometric function (defined by Figure 2)
H(L/W)	Geometric function (defined by Figure 2)
h(X, L)	Local heat-transfer coefficient at X in equation 5, L < X < W
h(X, 0)	Local heat-transfer coefficient at X with no temperature discontinuity in equation 5
$\bar{h}$(W, L)	Average heat-transfer coefficient over area between L and W in equation 6
h(W + L/2, 0)	Local heat-transfer coefficient at X = (W + L)/2 for the case of an isothermal plate in equation 6
h	Local heat-transfer coefficient (Btu/hr-ft^2-°F)
$\bar{h}$	Average heat-transfer coefficient (Btu/hr-ft^2-°F)
k	Thermal conductivity of a gas (Btu/hr-ft-°F)
L	Approach length to step discontinuity in surface temperature (ft)
Q	Heat content (Btu/lb)
q	Local heat flux (Btu/ft^2-sec)
$\bar{q}$	Average heat flux (Btu/ft^2-sec)
R	Thermal resistance (hr-°F/Btu)
T	Temperature (°F or °R)
t	Time (sec)
W	Approach length to downstream side of temperature discontinuity (ft)
X	Space coordinate in direction of flow (ft)
Y	Space coordinate normal to direction of flow (ft)
α	Thermal diffusivity (ft^2/hr)
α_s	Surface absorptivity
ϵ_r	Emissivity of radiant source

NOMENCLATURE
(concl.)

θ	Half angle of radiometer view field (degrees)
ρ	Density (lb/ft^3)
σ	Stephan-Boltzmann constant
τ	Response time (sec)

Subscripts

aw	Adiabatic wall
c	Convection
isi	Isothermal insulating structure
isn	Isothermal noninsulating structure
m	Calorimeter
o	Free-stream conditions
r	Radiation
s	Structure
t	Indicated by thermocouple
w	Wall surface conditions
1	Upstream of temperature discontinuity
2	Downstream from temperature discontinuity

REFERENCES

1. W. H. Giedt, "The Determination of Transient Temperatures and Heat Transfer at a Gas-Metal Interface Applied to a 40-mm Gun Barrel," Jet Propulsion, April 1955.

2. W. H. Giedt and D. L. Rall, "Temperature Measurement in Solids," Product Engineering, 29, July 21, 1958.

3. R. Gardon, "An Instrument for the Direct Measurement of Intense Radiation," The Review of Scientific Instruments, 24, No. 5, May 1953.

4. "Analytical Investigation of Heat-Flux Meters," Advanced Technology Laboratories, a Division of American-Standard, Final Report, ATL-D-711, 31 October 1961, Contract No. NAS8-1571.

5. "Evaluation of Heat-Flux Meters, Phase 2 - Experimental Investigation," Advanced Technology Laboratories, a Division of American-Standard, Final Report, ATL-D-922, 31 October 1962, Contract No. NAS8-1571.

6. J. C. Westkaemper, "An Analysis of Slug-Type Calorimeters for Measuring Heat Transfer from Exhaust Gases," R. T. F., ARO, Inc., November 1960, Contract No. AF 40(600)-800 S/A 11(60-110).

7. M. W. Rubesin, "The Effect of an Arbitrary Surface-Temperature Variation Along a Flat Plate on the Convective Heat Transfer in an Incompressible Turbulent Boundary Layer," NACA TN 2345, 1951.

8. S. Scesa, "Experimental Investigation of Convective Heat Transfer to Air from a Flat Plate with a Stepwise Discontinuous Surface Temperature," University of California, Berkeley, M. S. Thesis, February 1951.

9. W. C. Reynolds, W. M. Kays, and S. J. Kline, "Heat Transfer in the Turbulent Incompressible Boundary Layer with a Step Wall Temperature Distribution," Stanford University, Department of Mechanical Engineering, 1957.

10. W. C. Reynolds, W. M. Kays, and S. J. Kline, "A Summary of Experiments on Turbulent Heat Transfer from a Nonisothermal Flat Plate," ASME Paper 59-A-157, 1959.

11. J. C. Westkaemper, "On the Error in Plug-Type Calorimeters Caused by Surface-Temperature Mismatch," Journal of the Aerospace Sciences, 28, No. 11, November 1961.

12. D. Brunner, J. Suddarth, and R. Miller, "Minuteman Calorimeter Technical Evaluation," The Boeing Company, Report No. D2-13562, August 1962.

13. W. H. Giedt, Principles of Engineering Heat Transfer, New York, D. Van Nostrand Company, Inc. (1957), p 372.

14. C. F. Lucks and H. W. Deem, "Thermal Properties of Thirteen Metals," ASTM Special Technical Publication No. 227, February 1958.

15. A. Goldsmith, T. E. Waterman, and H. J. Hirschborn, Handbook of Thermophysical Properties of Solid Materials, The MacMillan Company, Revised Edition (1961).

REFERENCES
(concl.)

16. H. S. Carslaw and S. C. Jaeger, Conduction of Heat in Solids, London, Oxford University Press, Second Edition (1959), p 75.

17. Max Jakob, Heat Transfer, Volume II, New York, John Wiley and Sons (1957), p 394.

18. Kurt S. Lion, Instrumentation in Scientific Research, New York, McGraw-Hill Book Co. (1959), p 262.

ILLUSTRATIONS

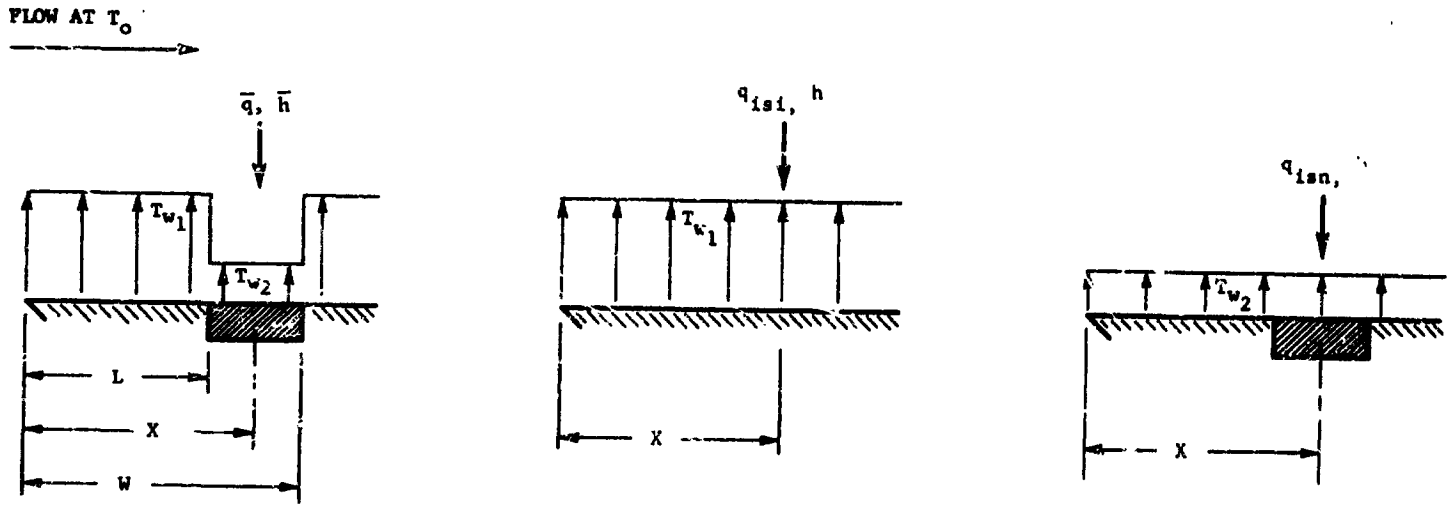

a. Nonisothermal Insulating Structure with Temperature Discontinuity due to Presence of Calorimeter

b. Isothermal Insulating Structure without Surface-Temperature Discontinuity

c. Isothermal Noninsulating (Copper) Structure with Structure at Calorimeter Temperature

ANALYTICAL MODELS

FIGURE 1

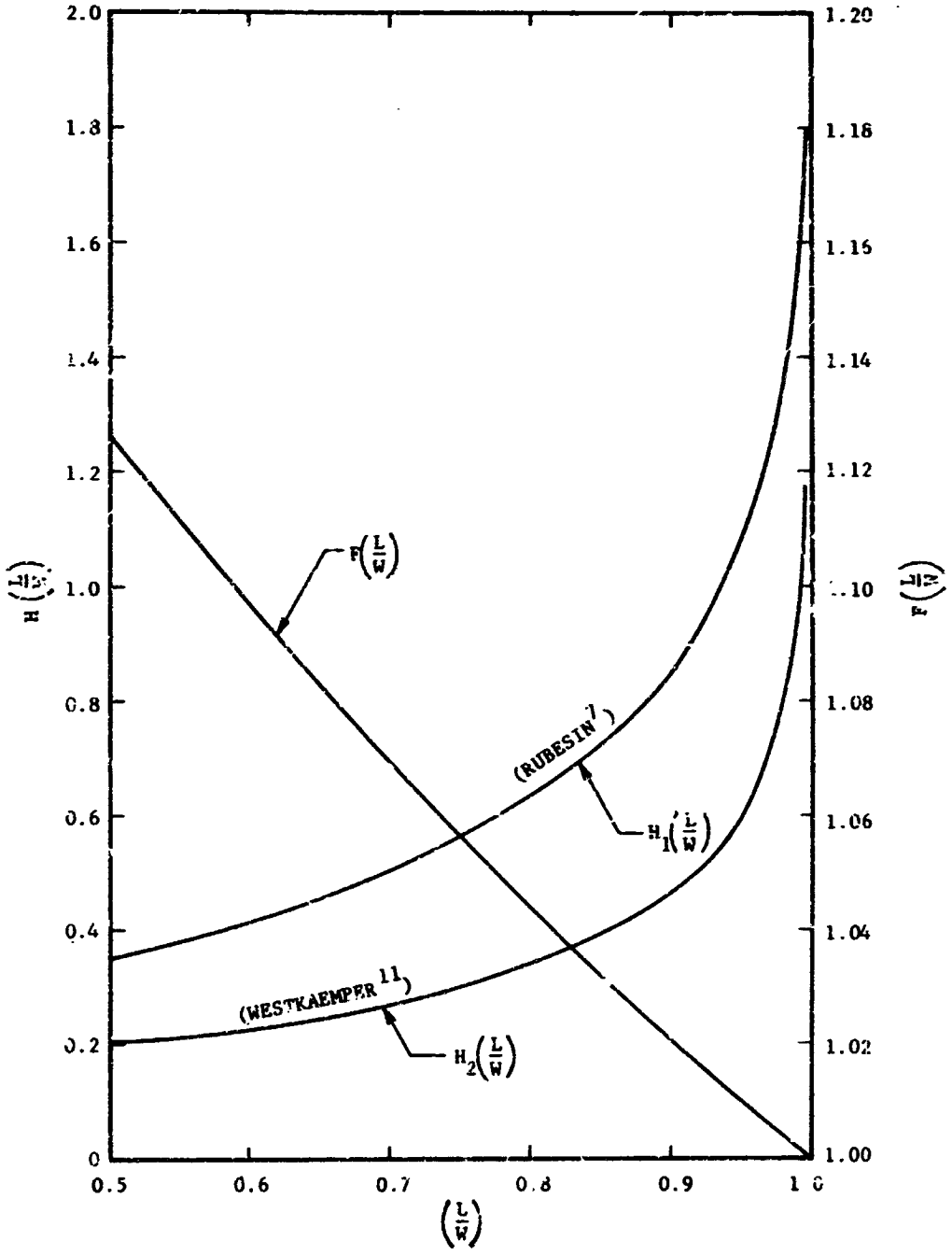

NUMERICAL VALUES OF COEFFICIENTS IN EQUATION 6

FIGURE 2

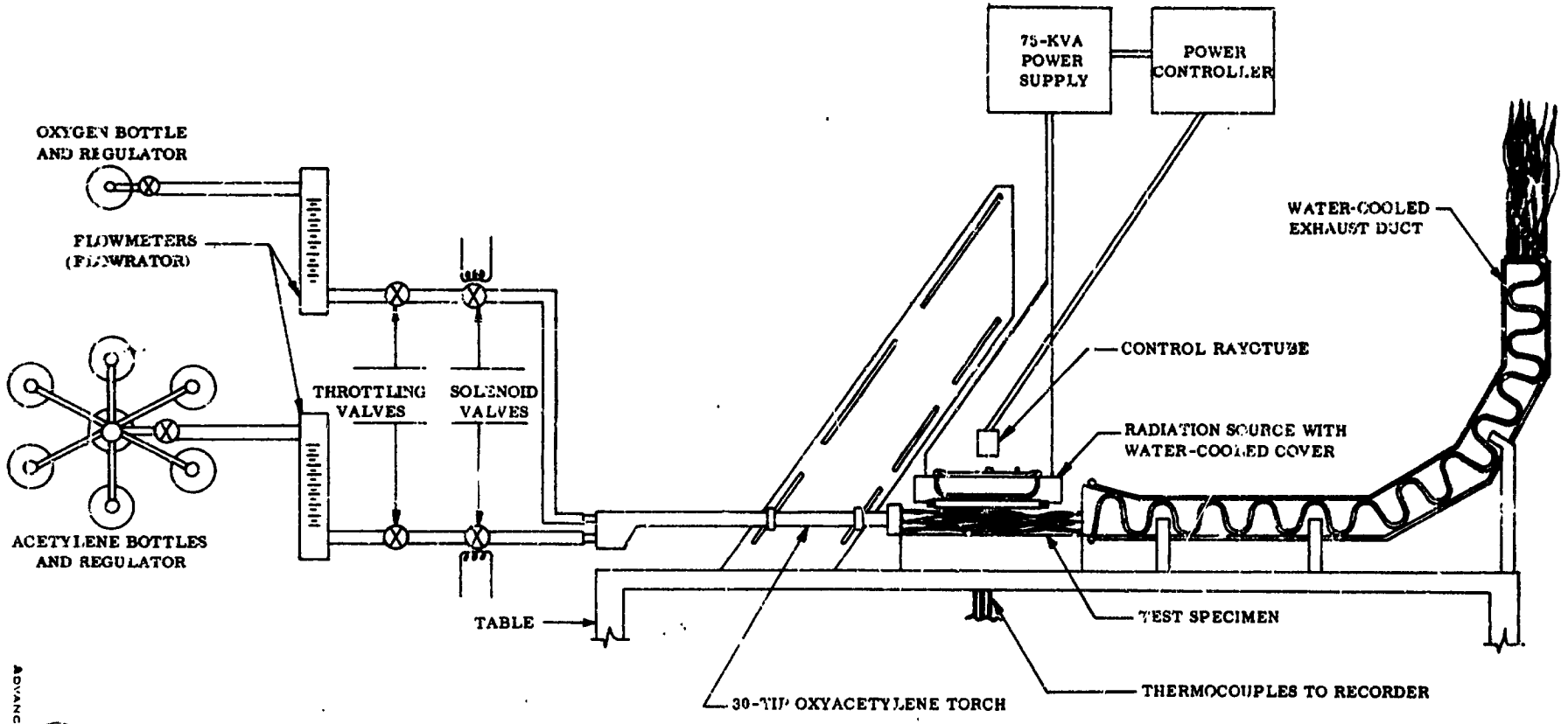

EXPERIMENTAL HEATING APPARATUS

FIGURE 3

LABORATORY HEATING APPARATUS
FRONT VIEW

FIGURE 4

LABORATORY HEATING APPARATUS
REAR VIEW

FIGURE 6

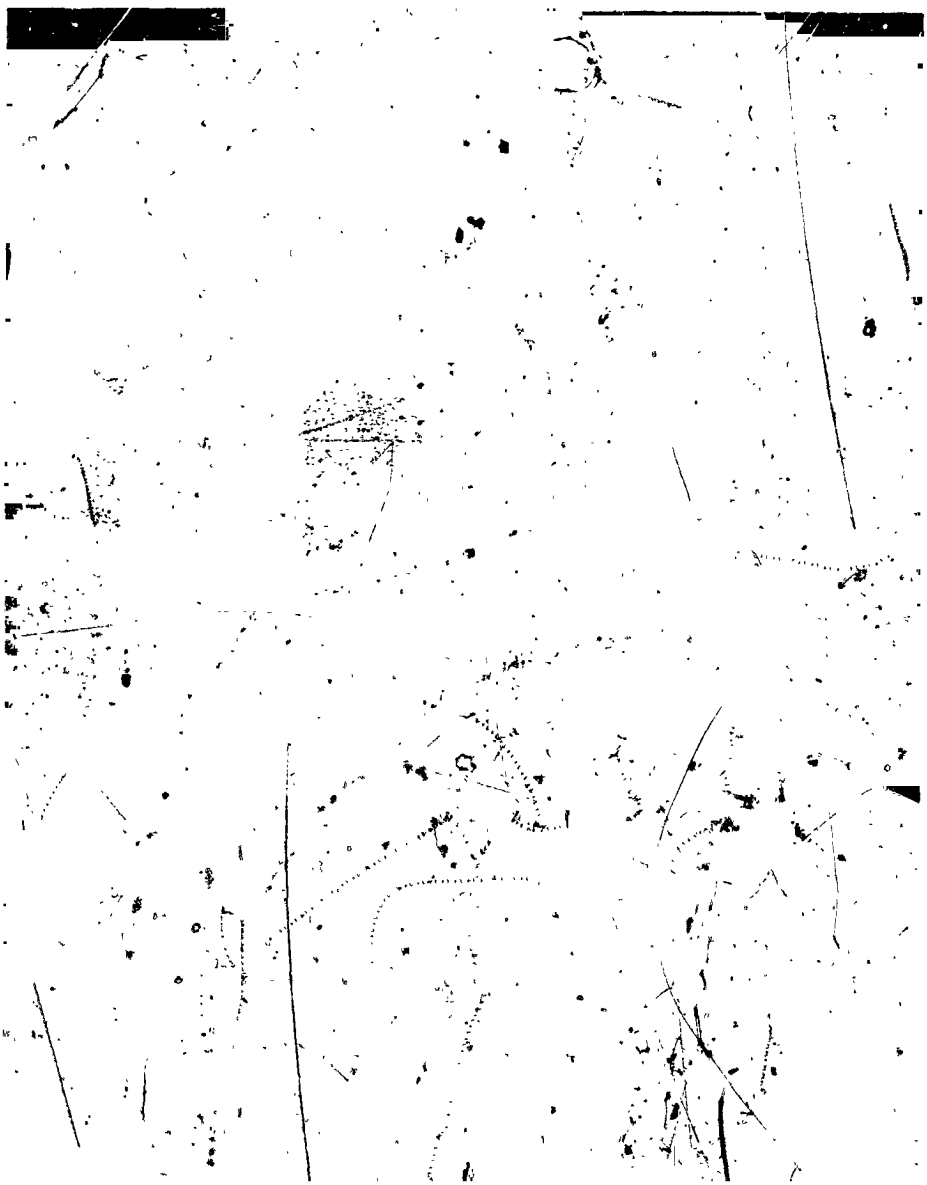

HEATING APPARATUS TEST SECTION

FIGURE 6

INTERNAL VIEW OF RADIANT HEATER AND TEST SECTION

FIGURE 7

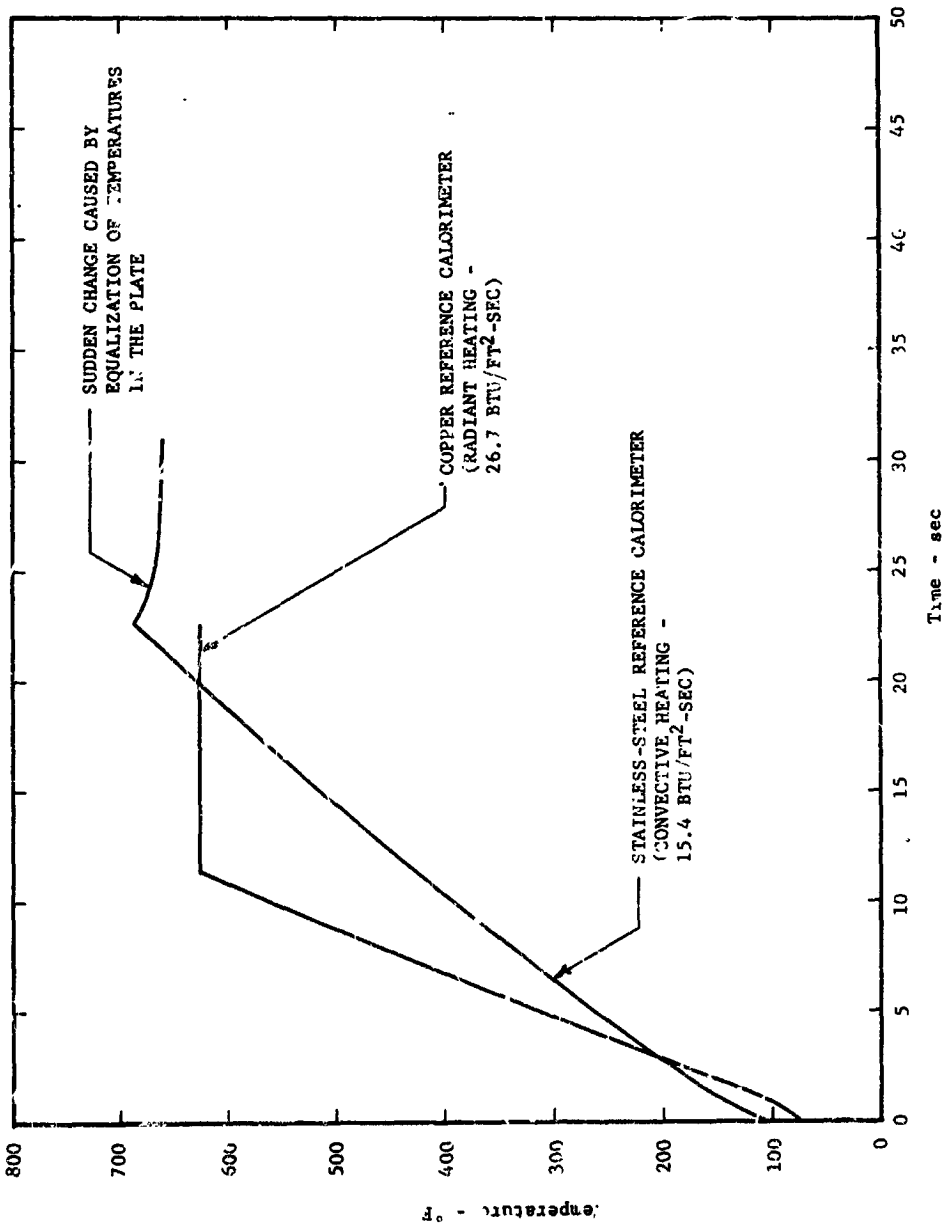

TEMPERATURE HISTORIES OF LABORATORY REFERENCE CALORIMETERS
DURING TYPICAL HEATING TESTS

FIGURE 8

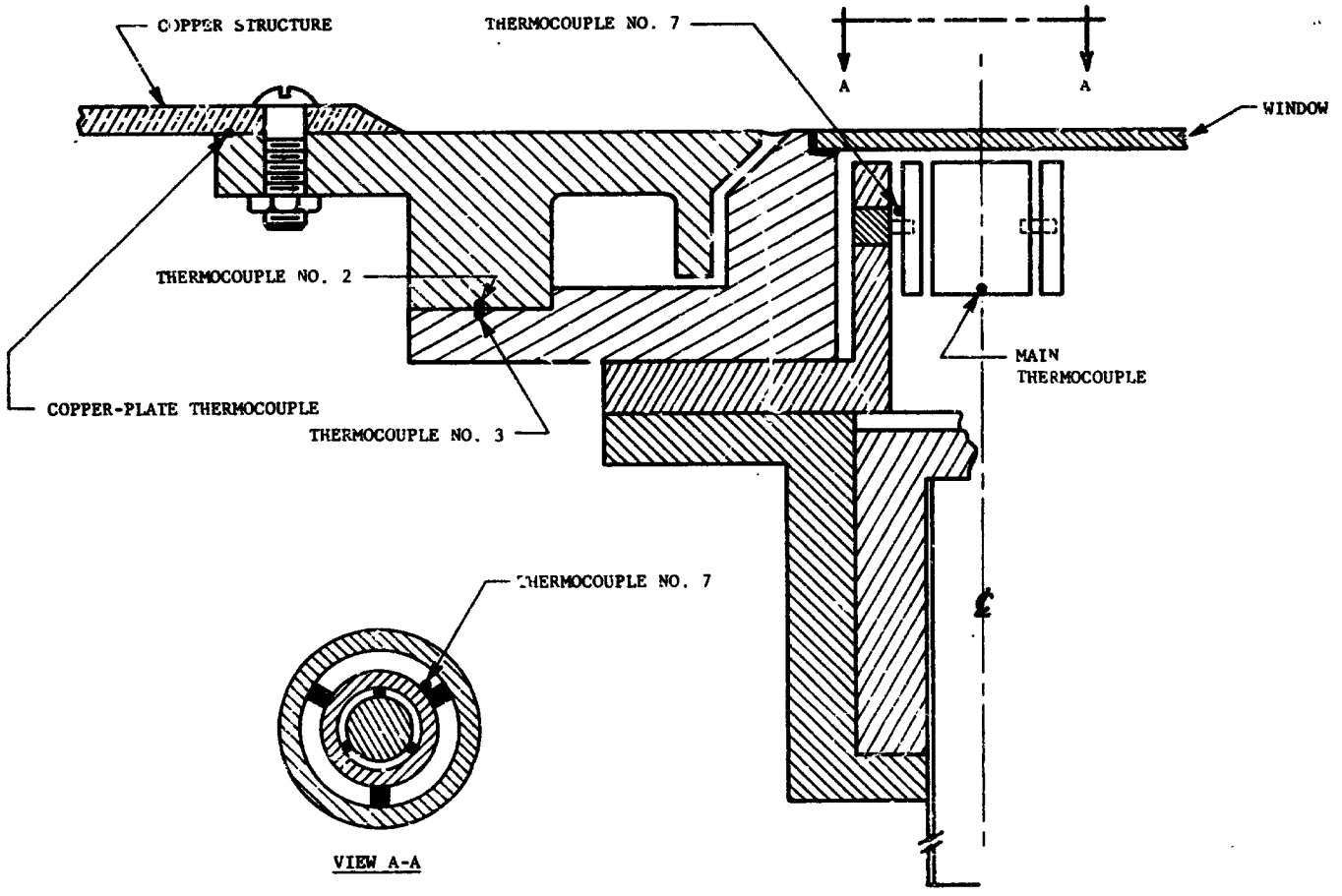

SCHEMATIC OF PURGED N-123 COPPER-SLUG RADIOMETER
(SHOWING THERMOCOUPLE LOCATIONS)

FIGURE 9

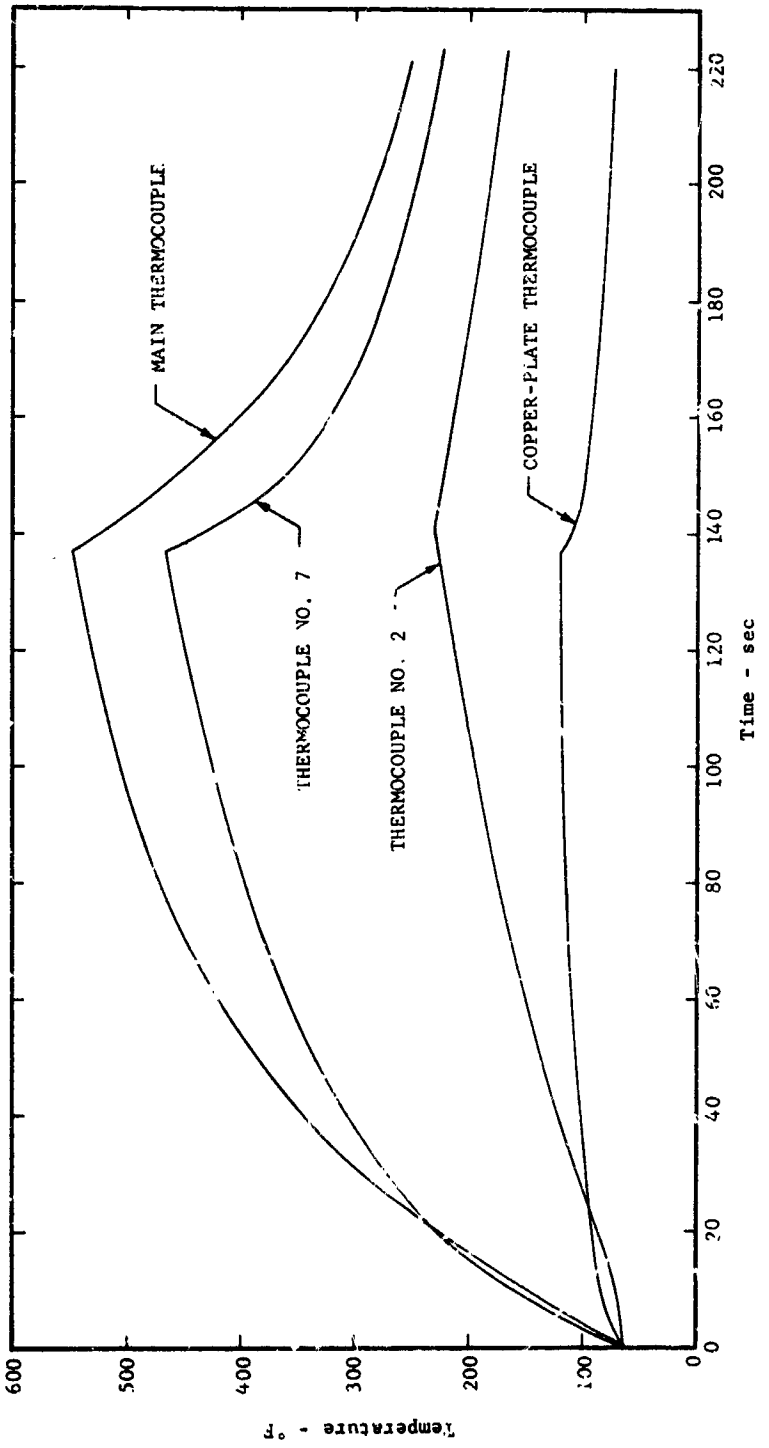

TEMPERATURE HISTORIES OF UNPURGED N-123 RADIOMETER MOUNTED IN WATER-COOLED 1/8"-THICK COPPER PLATE UNDER RADIANT HEATING
(Reference Heat Flux = 7.3 Btu/ft^2-sec)

FIGURE 10

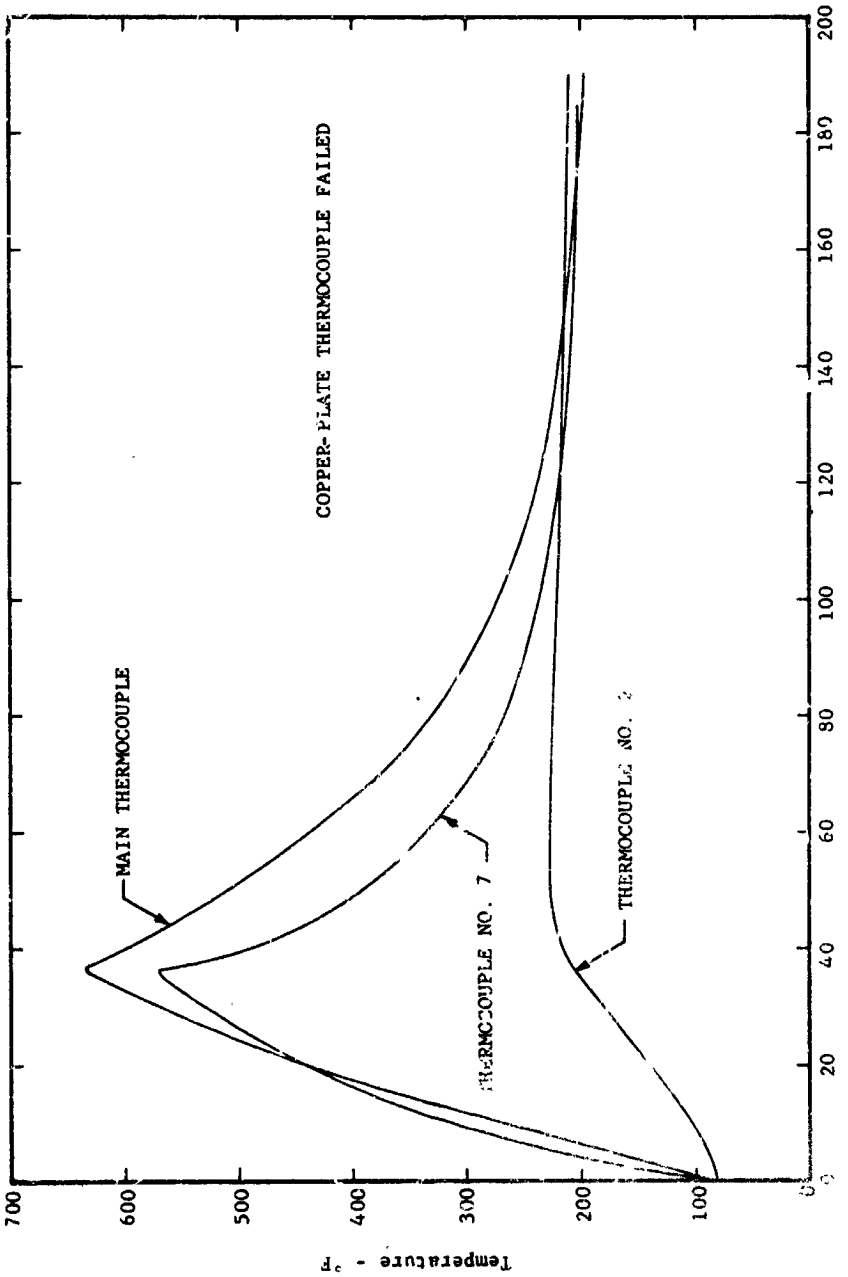

TEMPERATURE HISTORIES OF UNPURGED N-23 RADIOMETER MOUNTED IN UNCOOLED 1/8"-THICK COPPER PLATE UNDER RADIANT HEATING
(Reference Heat Flux = 17.4 Btu/ft²-sec)

FIGURE 11

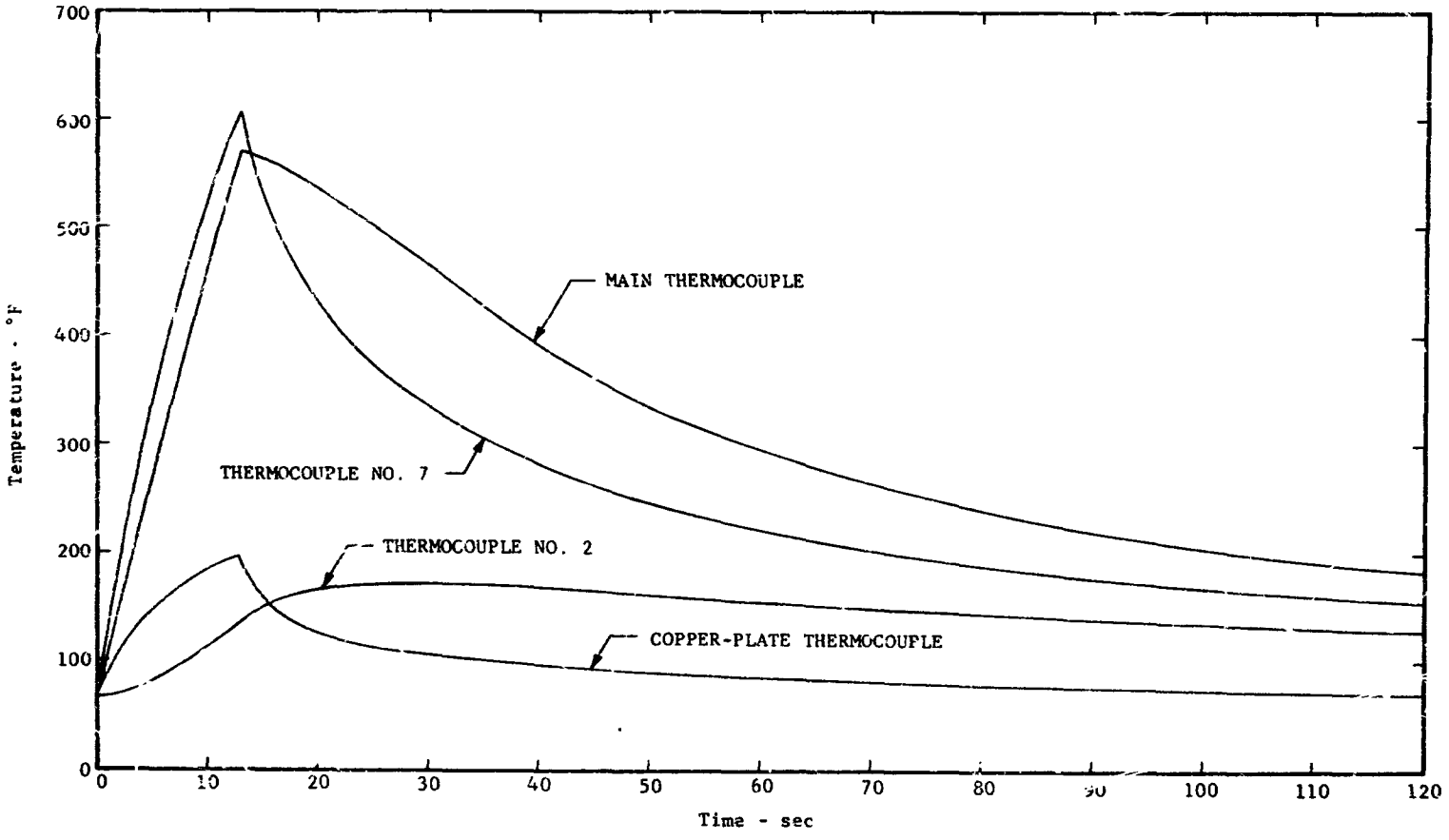

TEMPERATURE HISTORIES OF UNPURGED N-123 RADIOMETER MOUNTED IN WATER-COOLED 1/8"-THICK COPPER PLATE UNDER RADIANT HEATING
(Reference Heat Flux = 30.8 Btu/ft^2-sec)

FIGURE 12

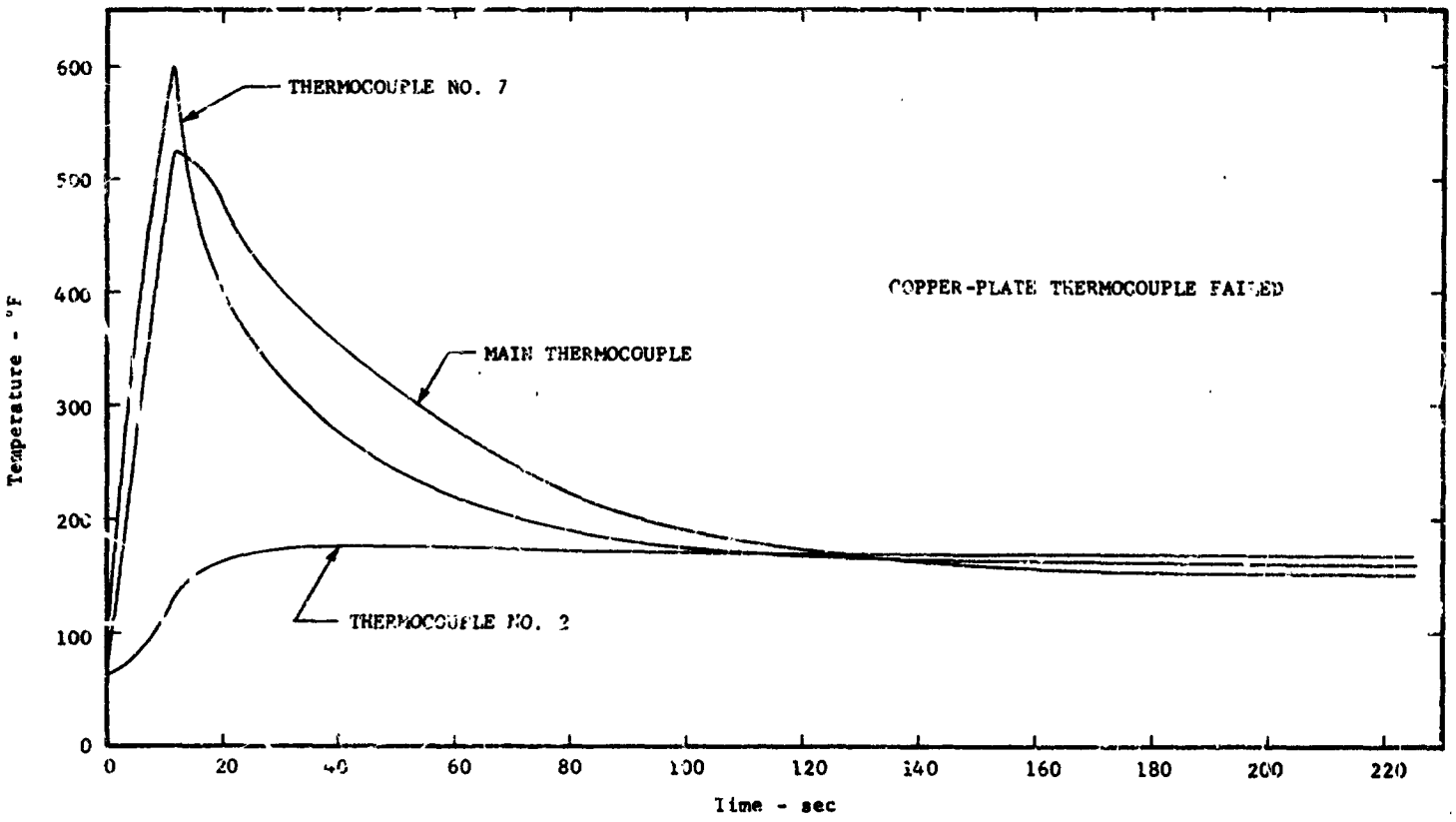

TEMPERATURE HISTORIES OF UNPURGED N-123 RADIOMETER MOUNTED IN UNCOOLED 1/8"-THICK COPPER PLATE UNDER RADIANT HEATING
(Reference Heat Flux = 36.1 Btu/ft^2-sec)

FIGURE 13

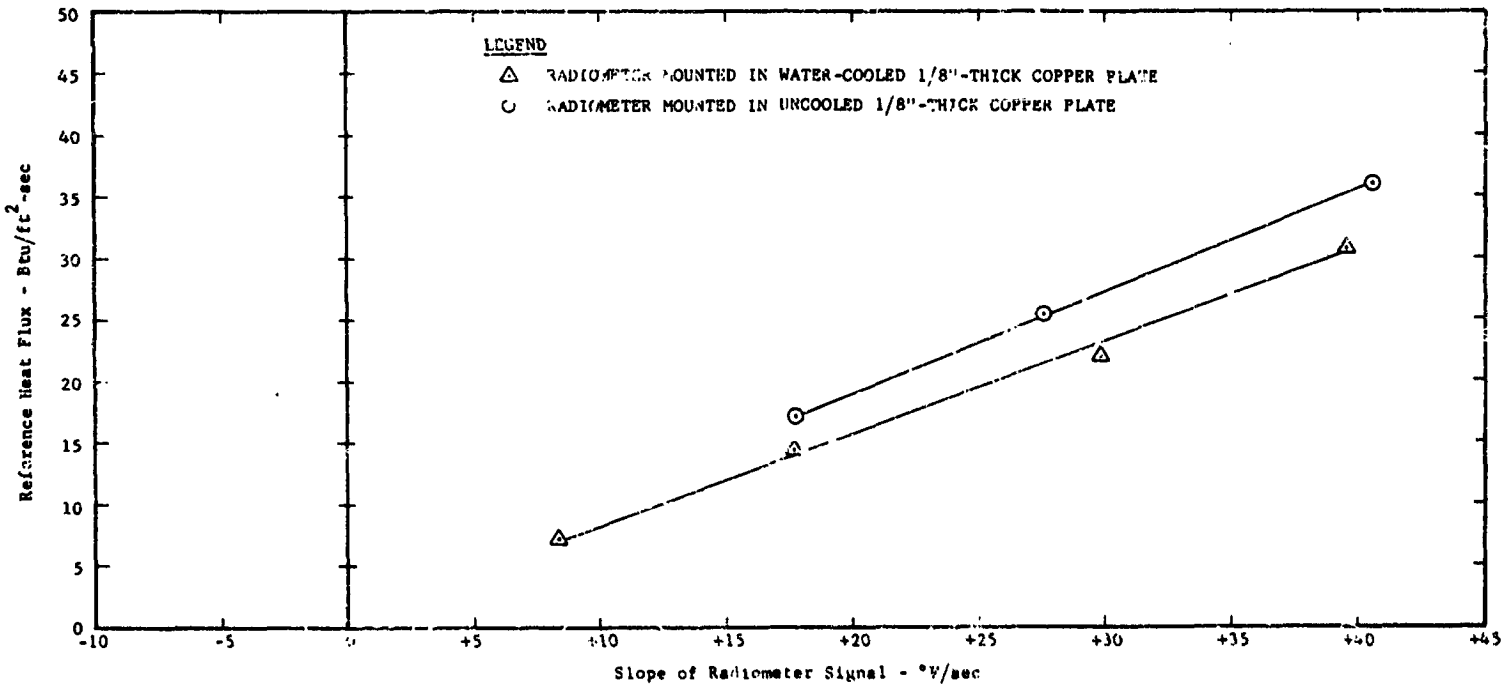

UNPURGED N-123 RADIOMETER CALIBRATION AT 100°F UNDER RADIANT HEATING

FIGURE 14

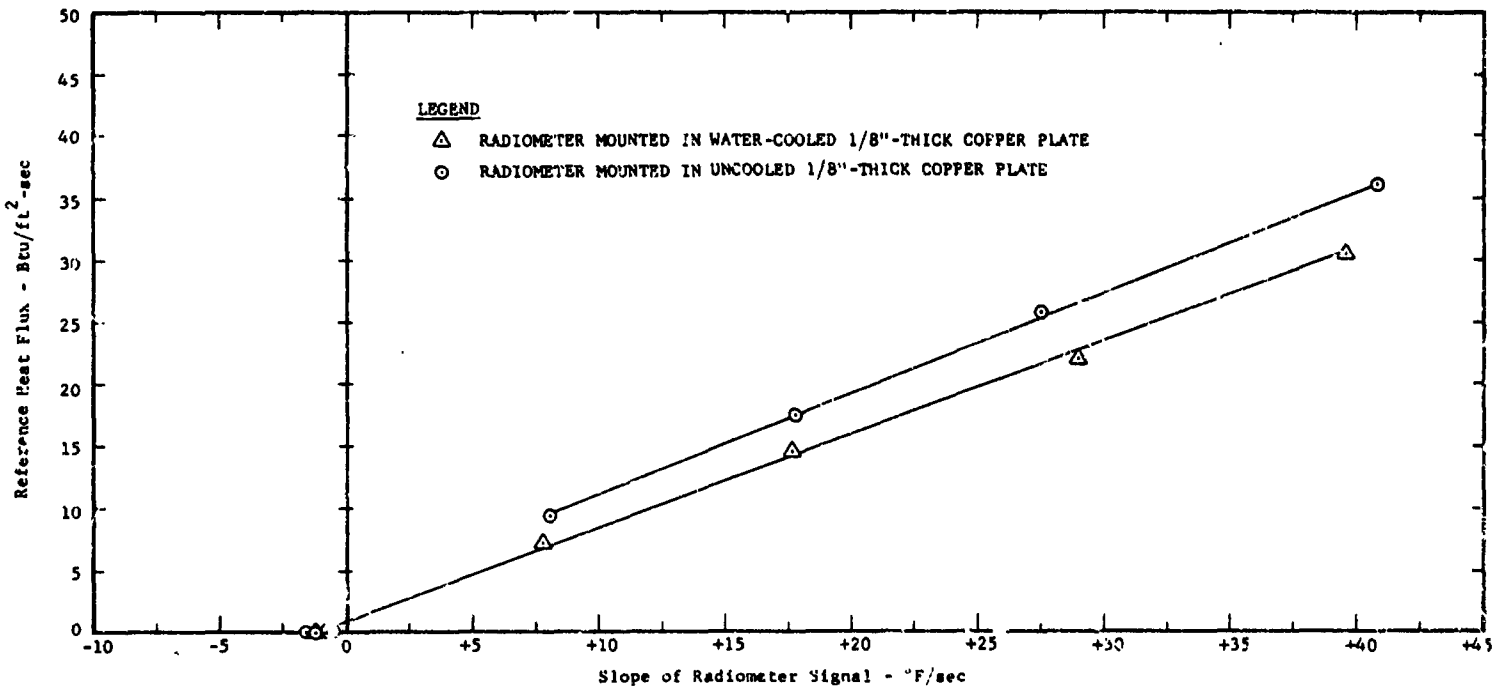

UNPURGED N-123 RADIOMETER CALIBRATION AT 200°F UNDER RADIANT HEATING

FIGURE 15

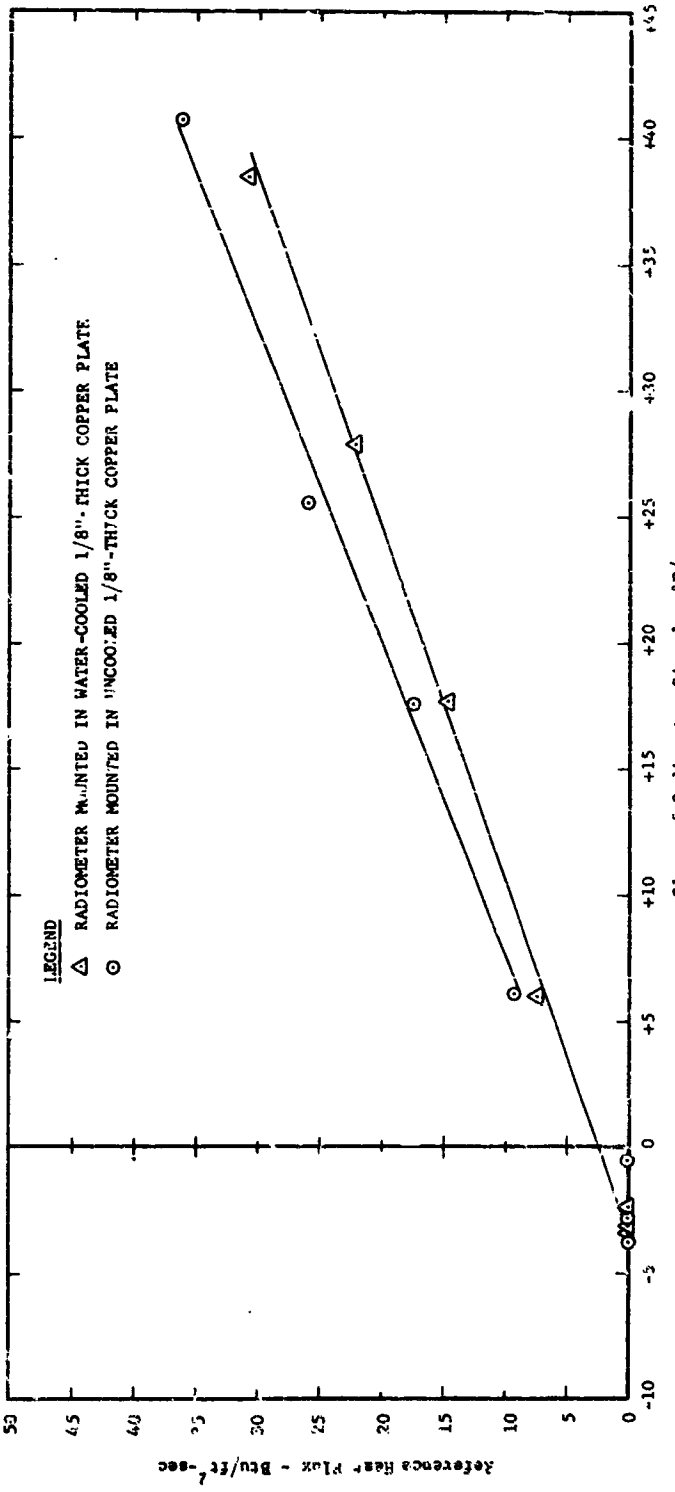

UNPURGED N-123 RADIOMETER CALIBRATION AT 300°F UNDER RADIANT HEATING

FIGURE 16

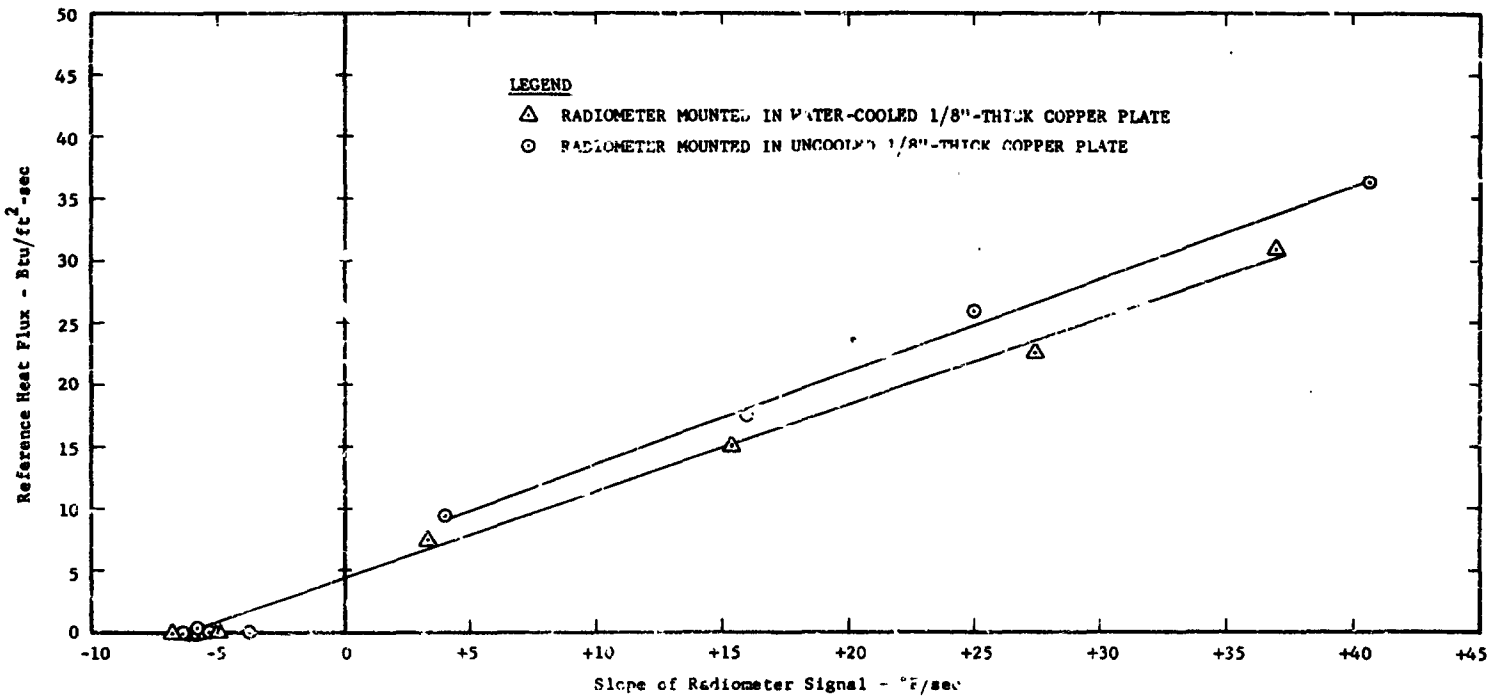

UNPURGED N-123 RADIOMETER CALIBRATION AT 400°F UNDER RADIANT HEATING

FIGURE 17

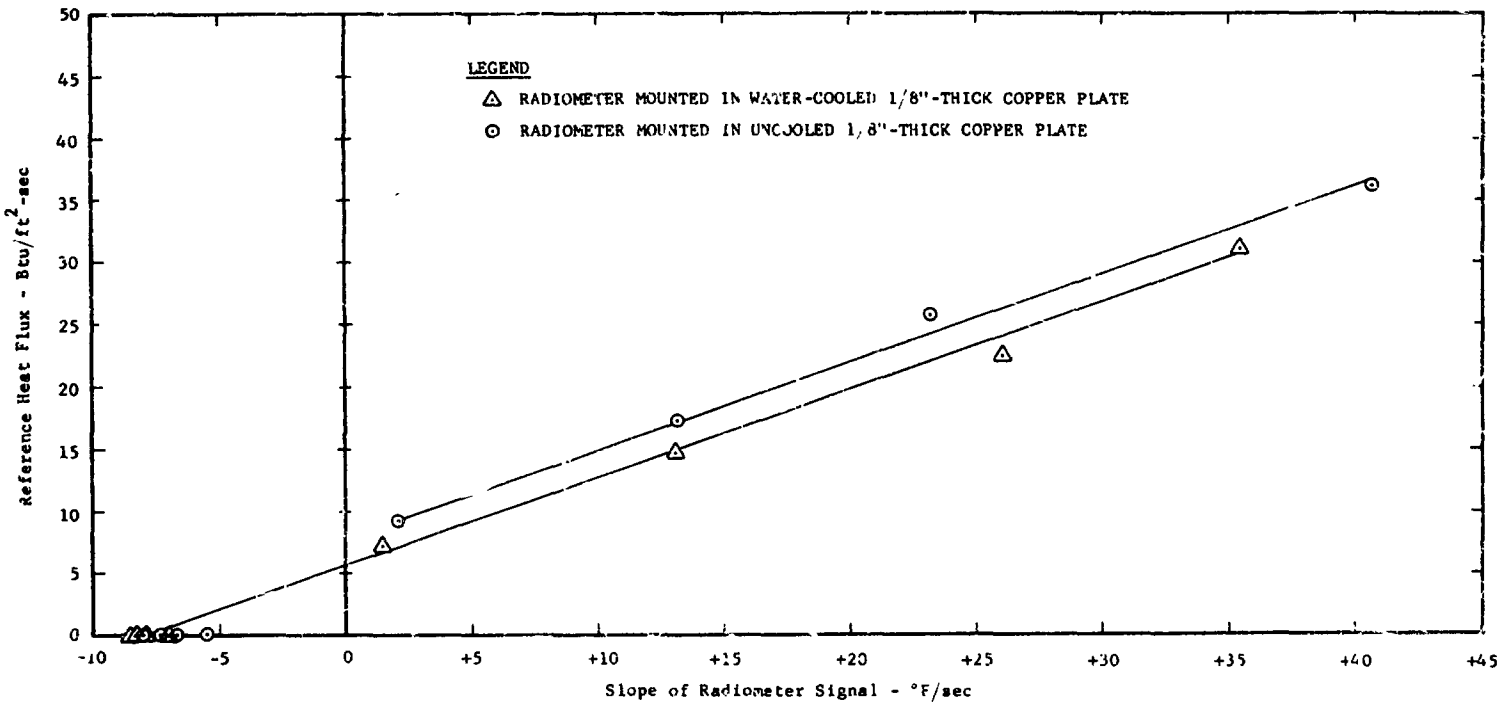

UNPURGED N-123 RADIOMETER CALIBRATION AT 500°F UNDER RADIANT HEATING

FIGURE 18

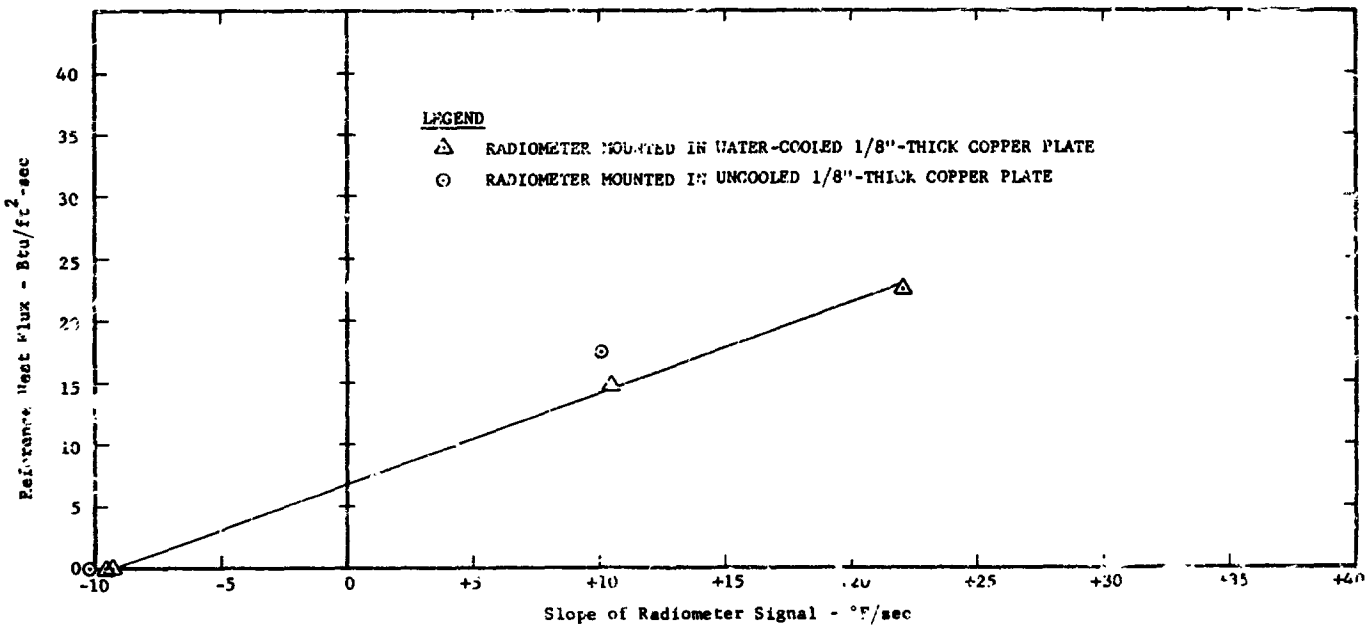

UNPURGED N-123 RADIOMETER CALIBRATION AT 600°F UNDER RADIANT HEATING

FIGURE 19

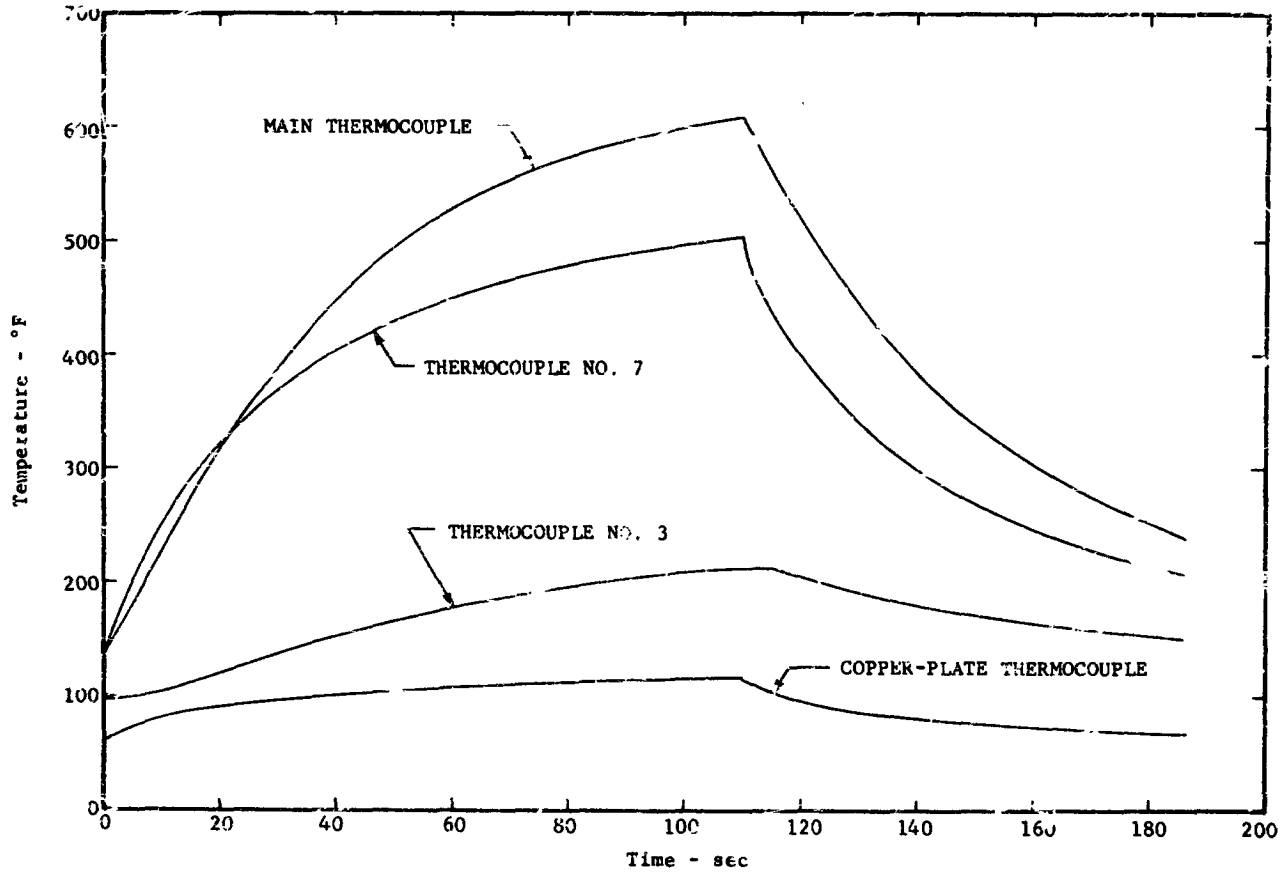

TEMPERATURE HISTORIES OF PURGED N-123 RADIOMETER MOUNTED IN WATER-COOLED 1/8"-THICK COPPER PLATE UNDER RADIANT HEATING
(Reference Heat Flux = 9.3 Btu/ft^2-sec)

FIGURE 20

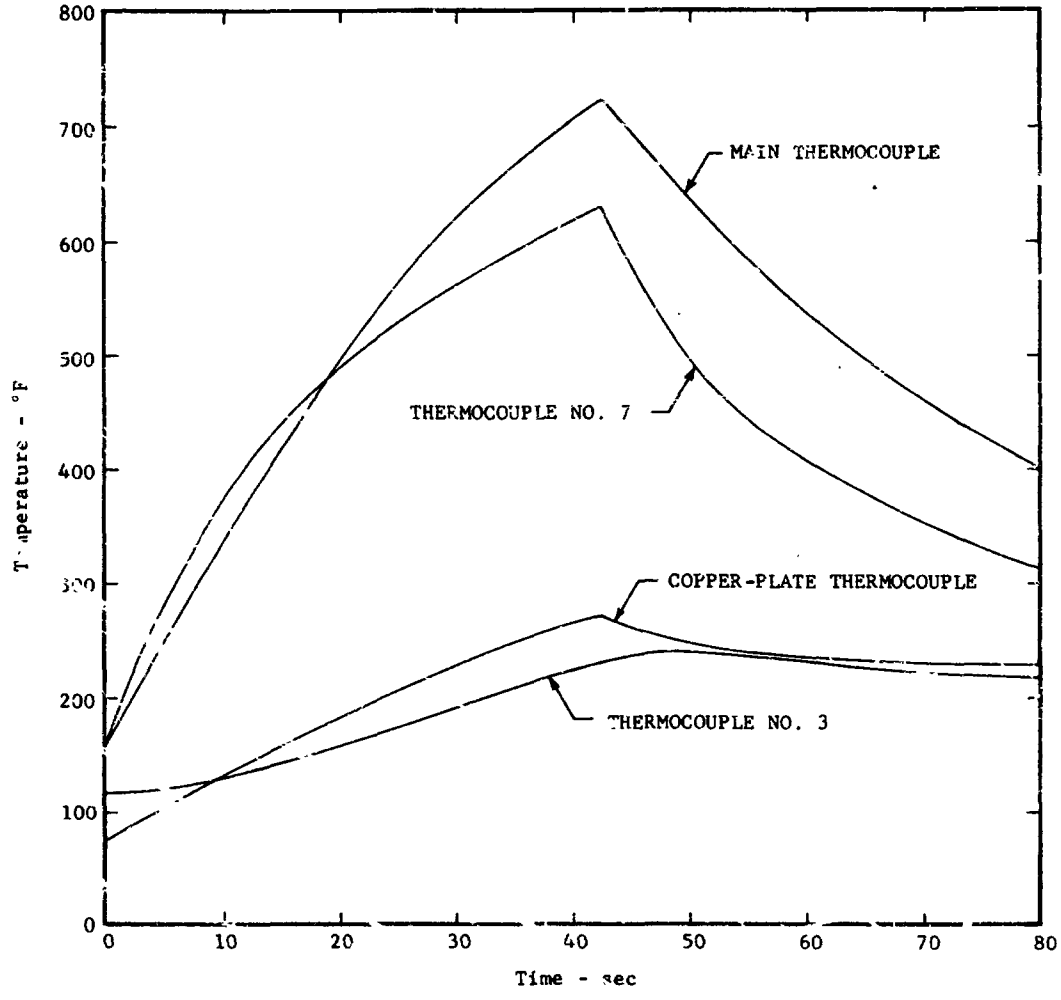

TEMPERATURE HISTORIES OF PURGED N-123 RADIOMETER MOUNTED IN UNCOOLED 1/8"-THICK COPPER PLATE UNDER RADIANT HEATING
(Reference Heat Flux = 17.2 Btu/ft^2-sec)

FIGURE 21

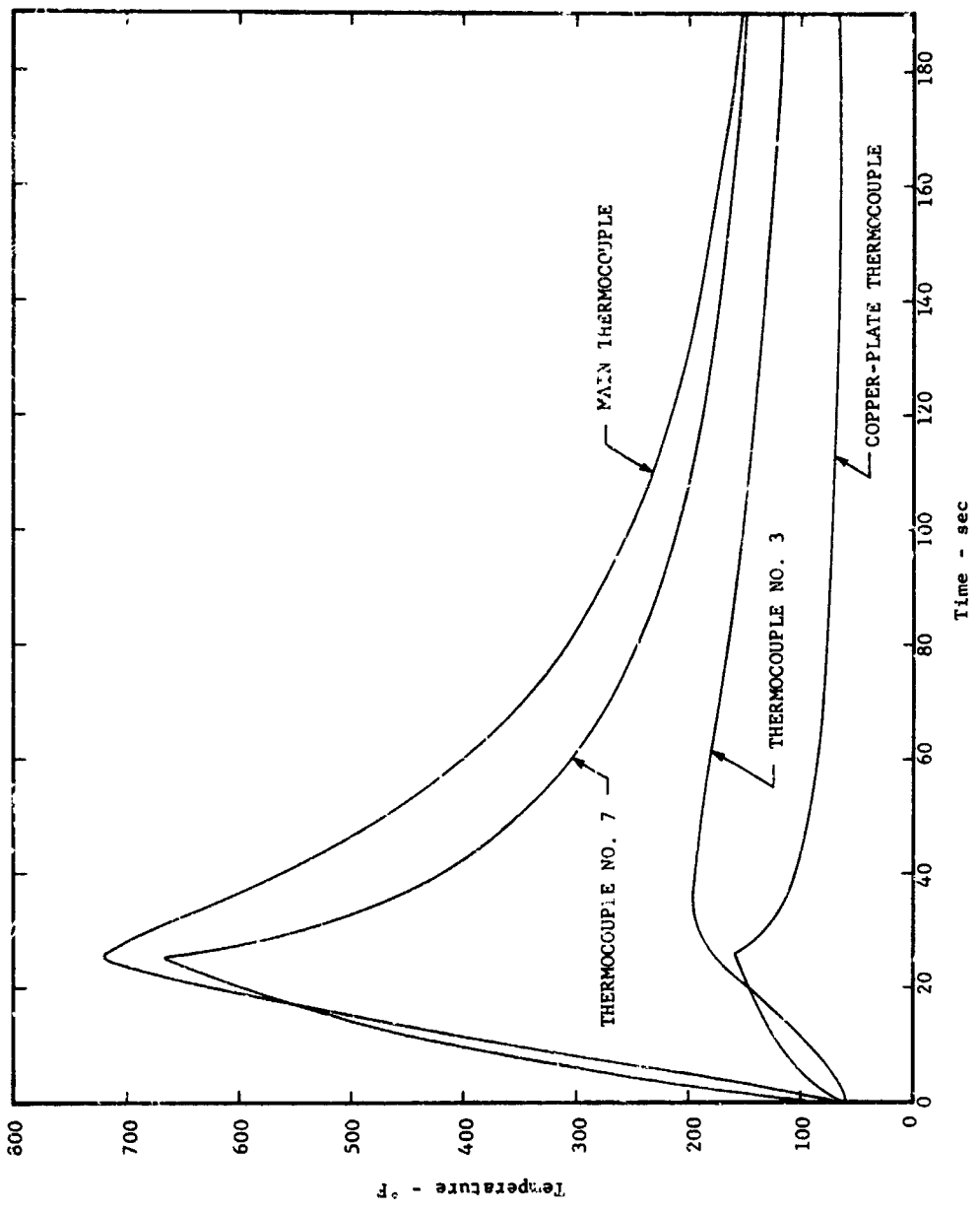

TEMPERATURE HISTORIES OF PURGED N-123 RADIOMETER MOUNTED IN WATER-COOLED 1/8"-THICK COPPER PLATE UNDER RADIANT HEATING
(Reference Heat Flux = 26.7 Btu/ft^2-sec)

FIGURE 22

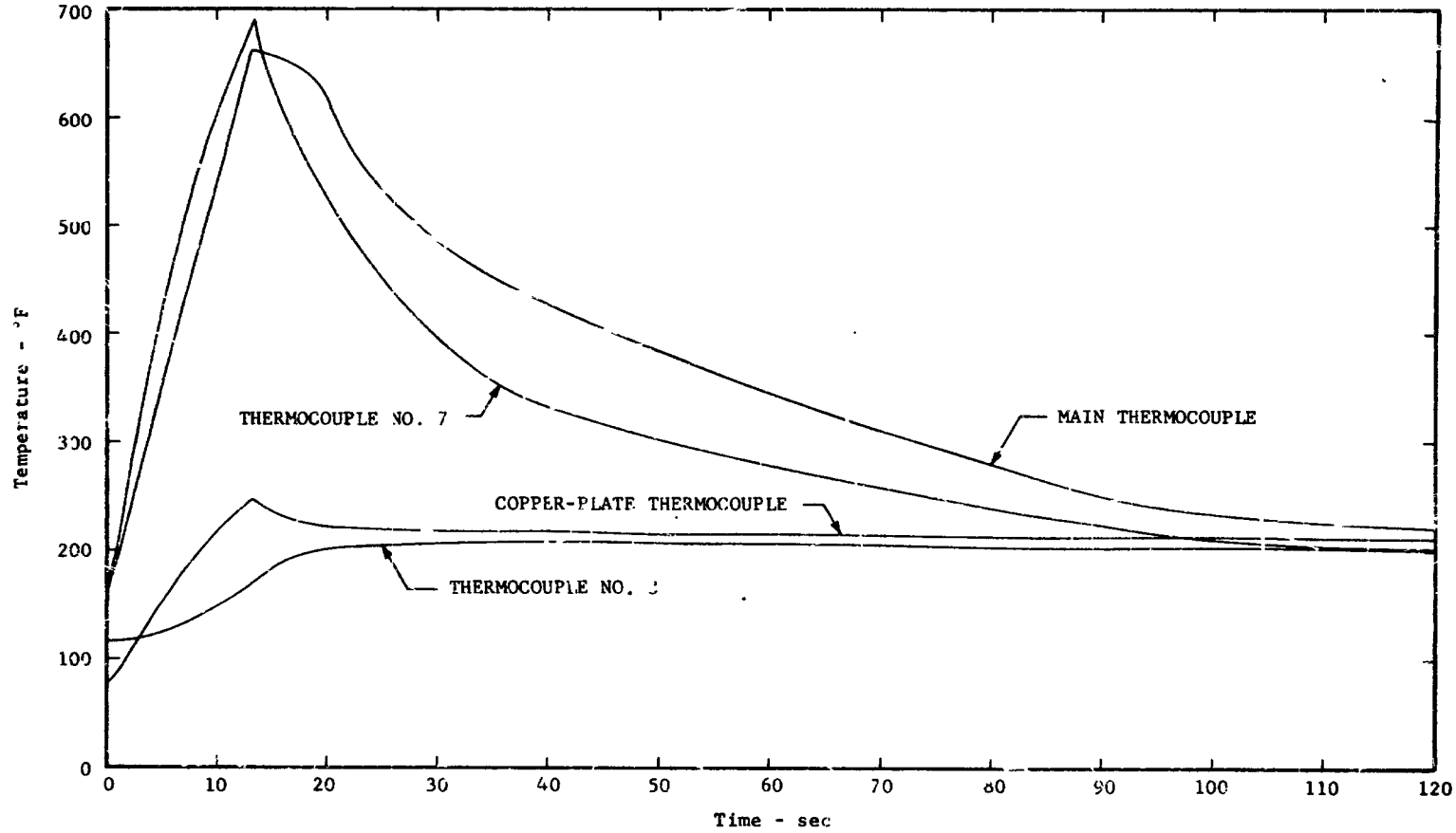

TEMPERATURE HISTORIES OF PURGED N-123 RADIOMETER MOUNTED IN UNCOOLED 1/8"-THICK COPPER PLATE UNDER RADIANT HEATING
(Reference Heat Flux = 37.2 Btu/ft^2-sec)

FIGURE 23

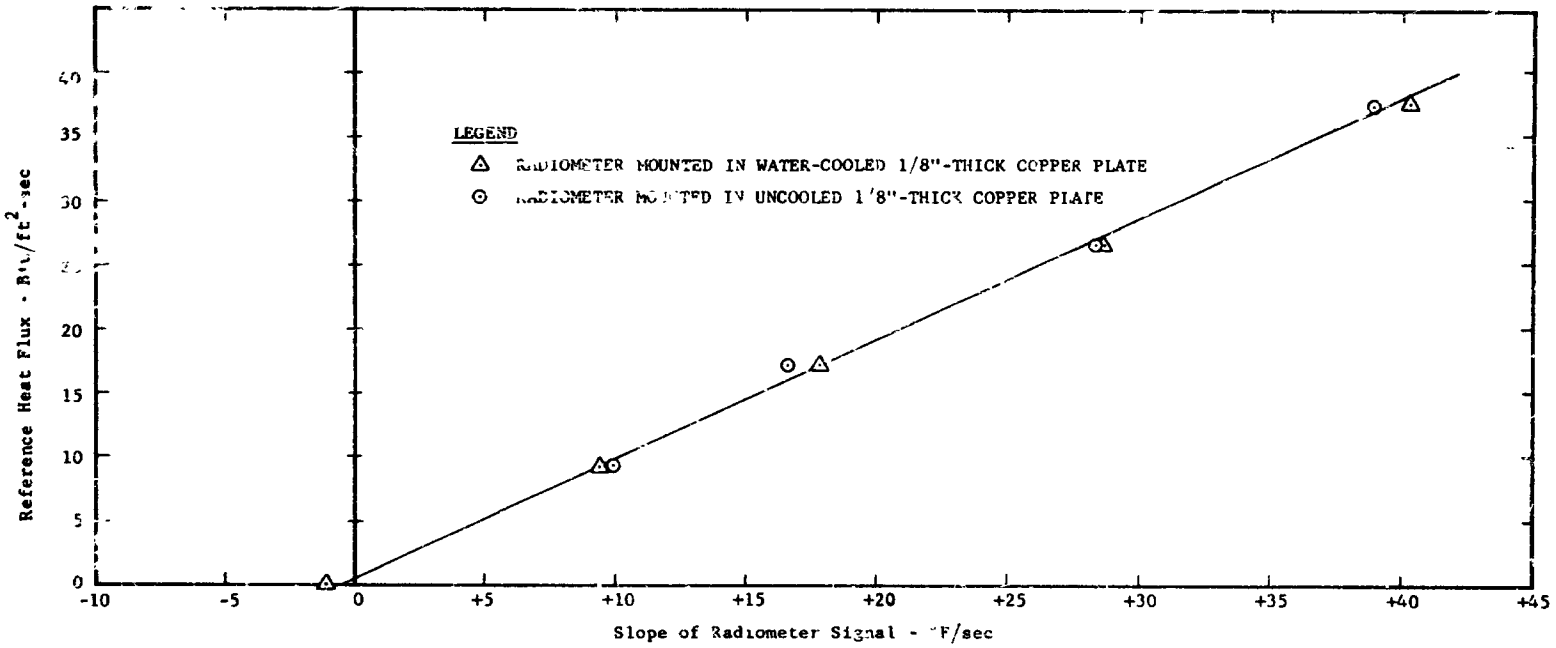

PURGED N-125 RADIOMETER CALIBRATION AT 200°F UNDER RADIANT HEATING

FIGURE 24

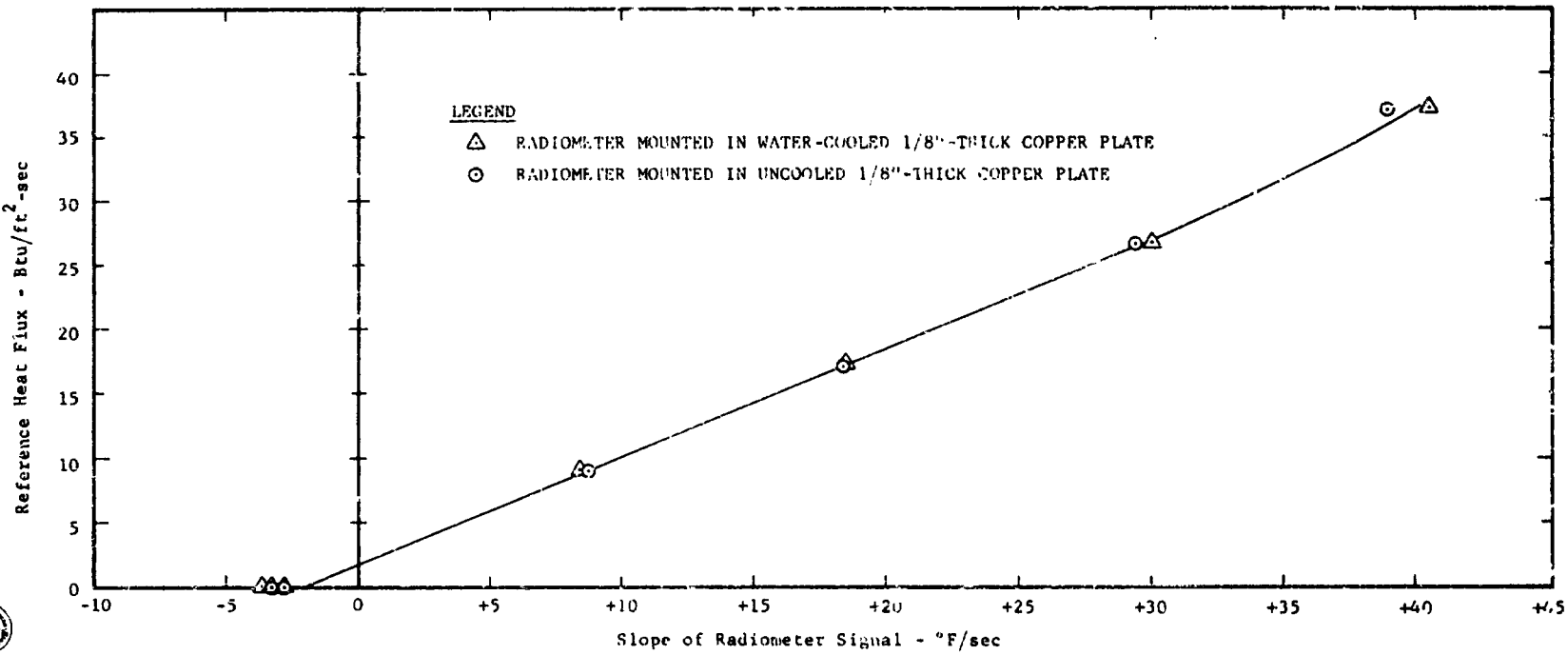

PURGED N-123 RADIOMETER CALIBRATION AT 300°F UNDER RADIANT HEATING

FIGURE 25

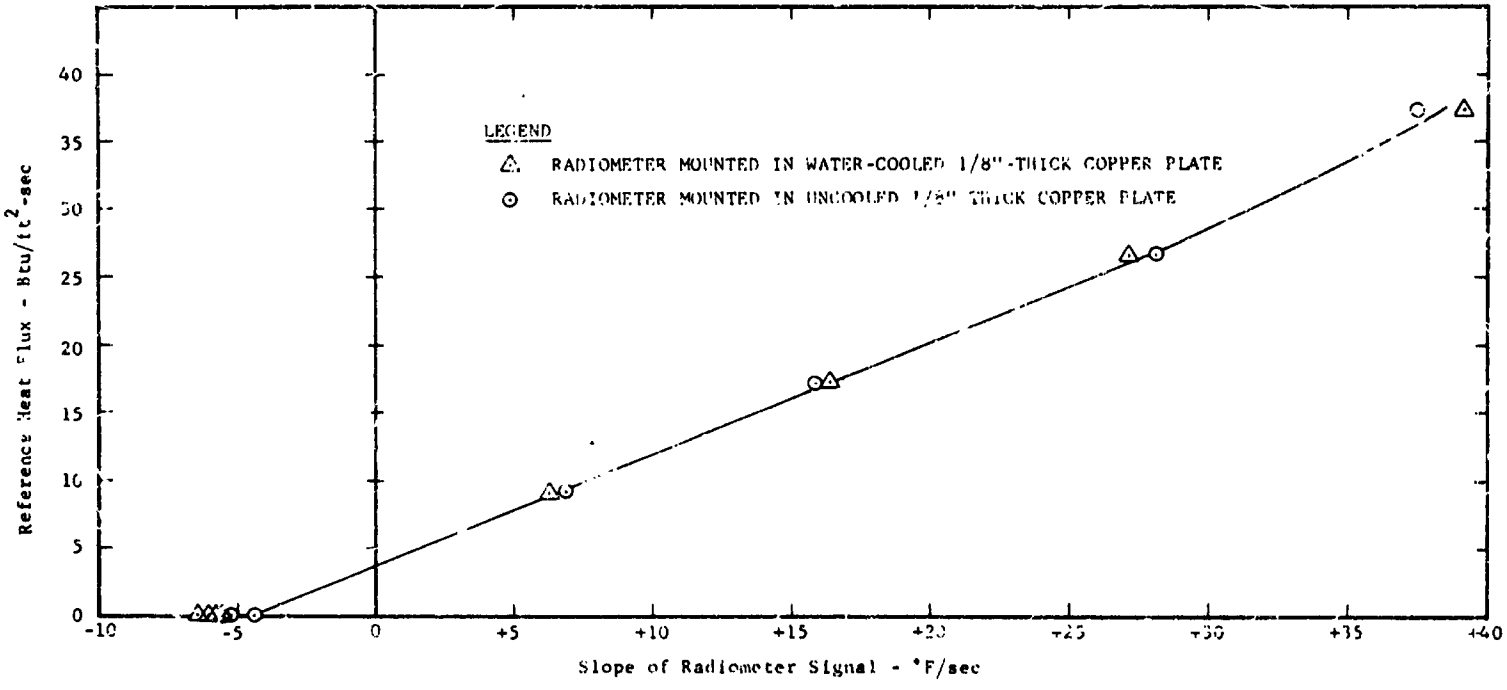

PURGED N-123 RADIOMETER CALIBRATION AT 400 F UNDER RADIANT HEATING

FIGURE 26

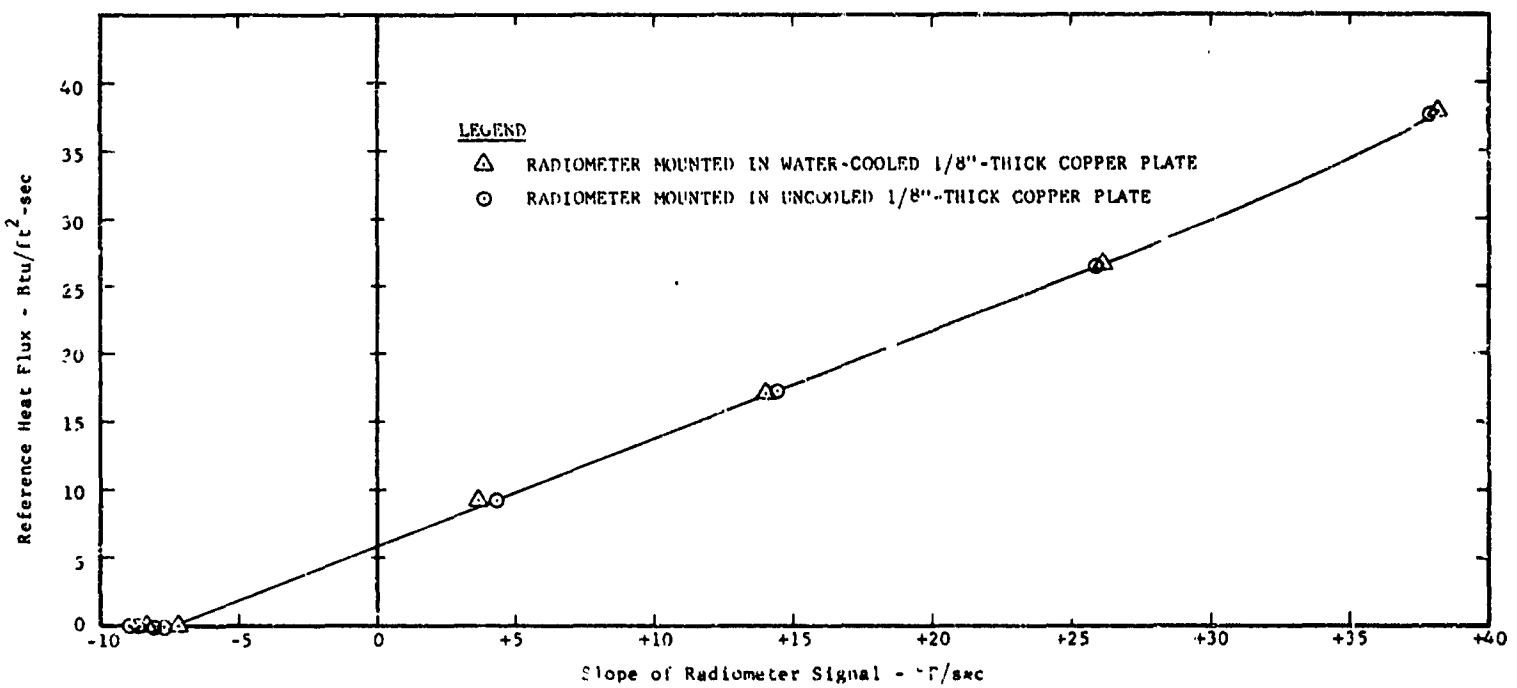

PURGED N-123 RADIOMETER CALIBRATION AT 500°F UNDER RADIANT HEATING

FIGURE 27

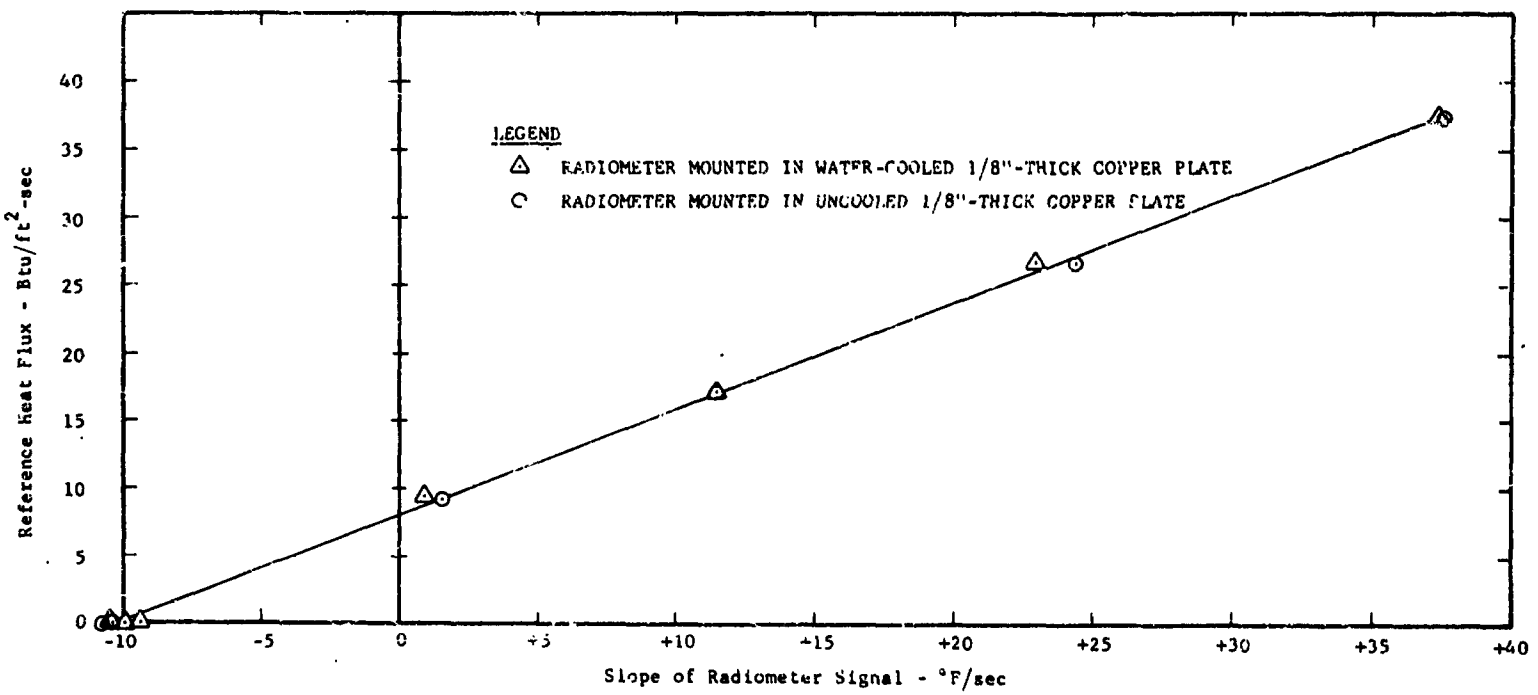

PURGED N-123 RADIOMETER CALIBRATION AT 600°F UNDER RADIANT HEATING

FIGURE 28

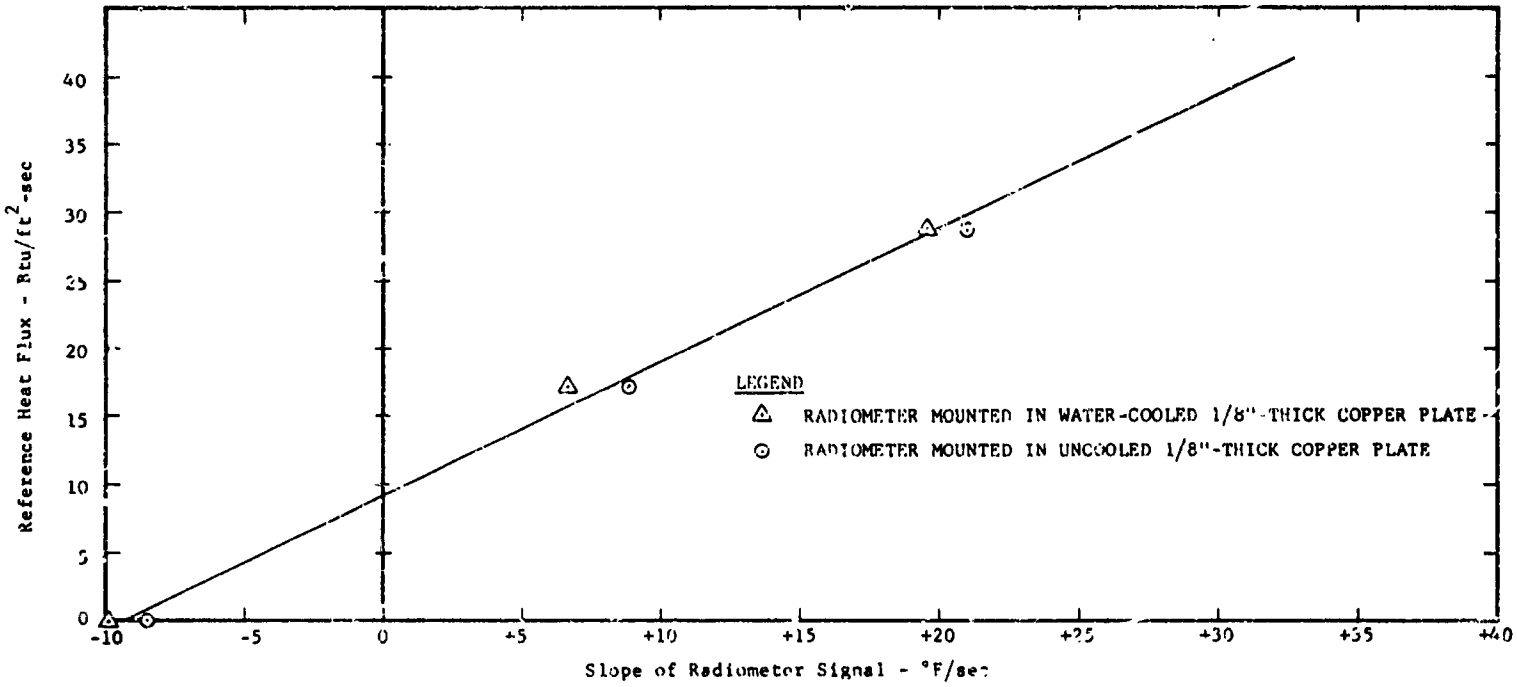

PURGED N-123 RADIOMETER CALIBRATION AT 700°F UNDER RADIANT HEATING

FIGURE 29

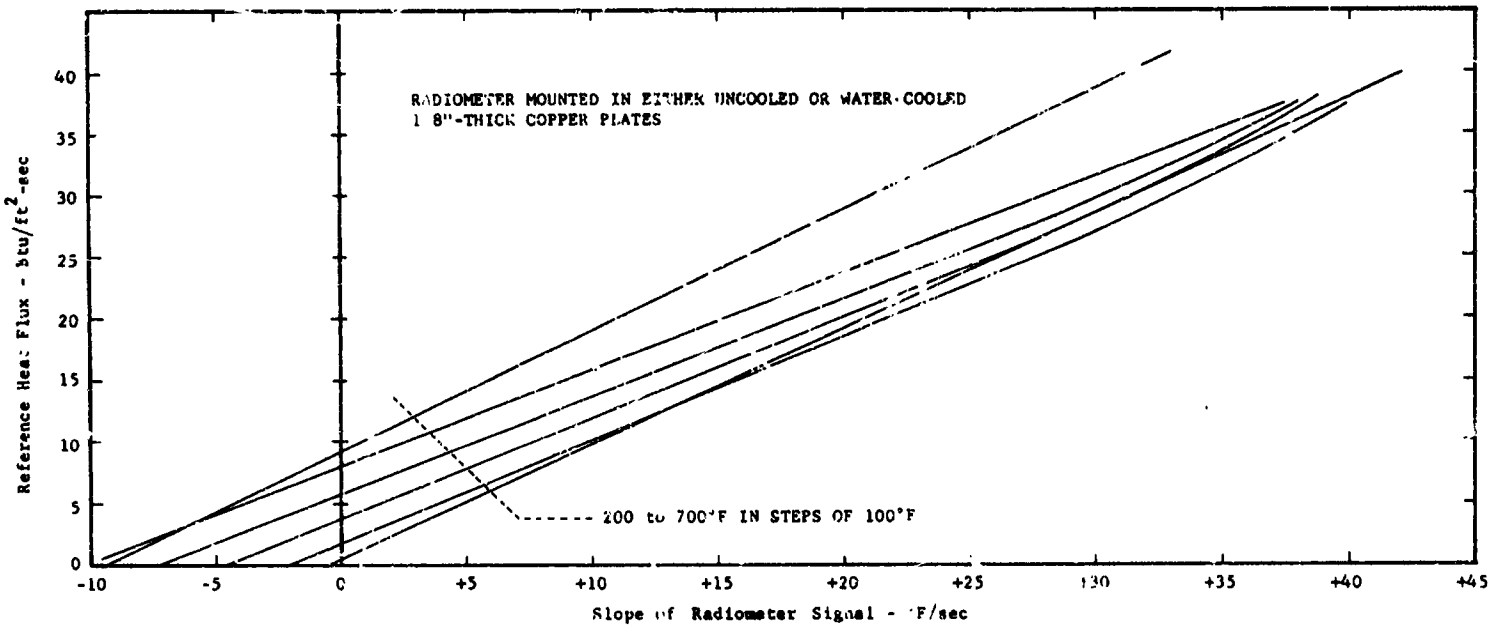

PURGED N-123 RADIOMETER CALIBRATION CURVES
FOR INDICATED COPPER-SLUG TEMPERATURES UNDER RADIANT HEATING

FIGURE 30

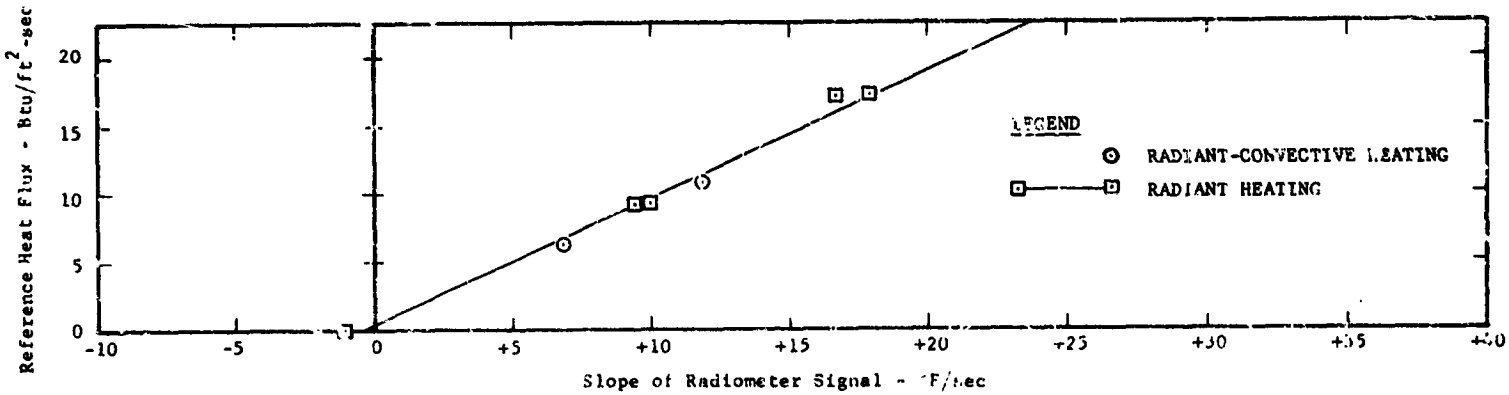

COMPARISON OF CALIBRATIONS UNDER COMBINED RADIANT-CONVECTIVE AND RADIANT HEATING AT 200°F FOR PURGED N-123 RADIOMETER

FIGURE 31

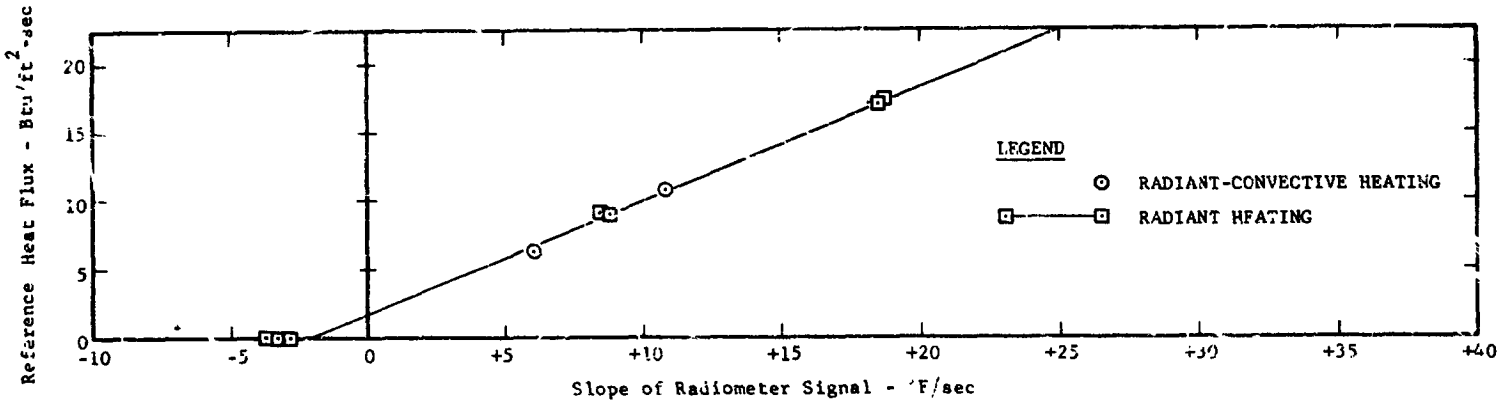

COMPARISON OF CALIBRATIONS UNDER COMBINED RADIANT-CONVECTIVE AND RADIANT HEATING AT 300°F FOR PURGED N-123 RADIOMETER

FIGURE 32

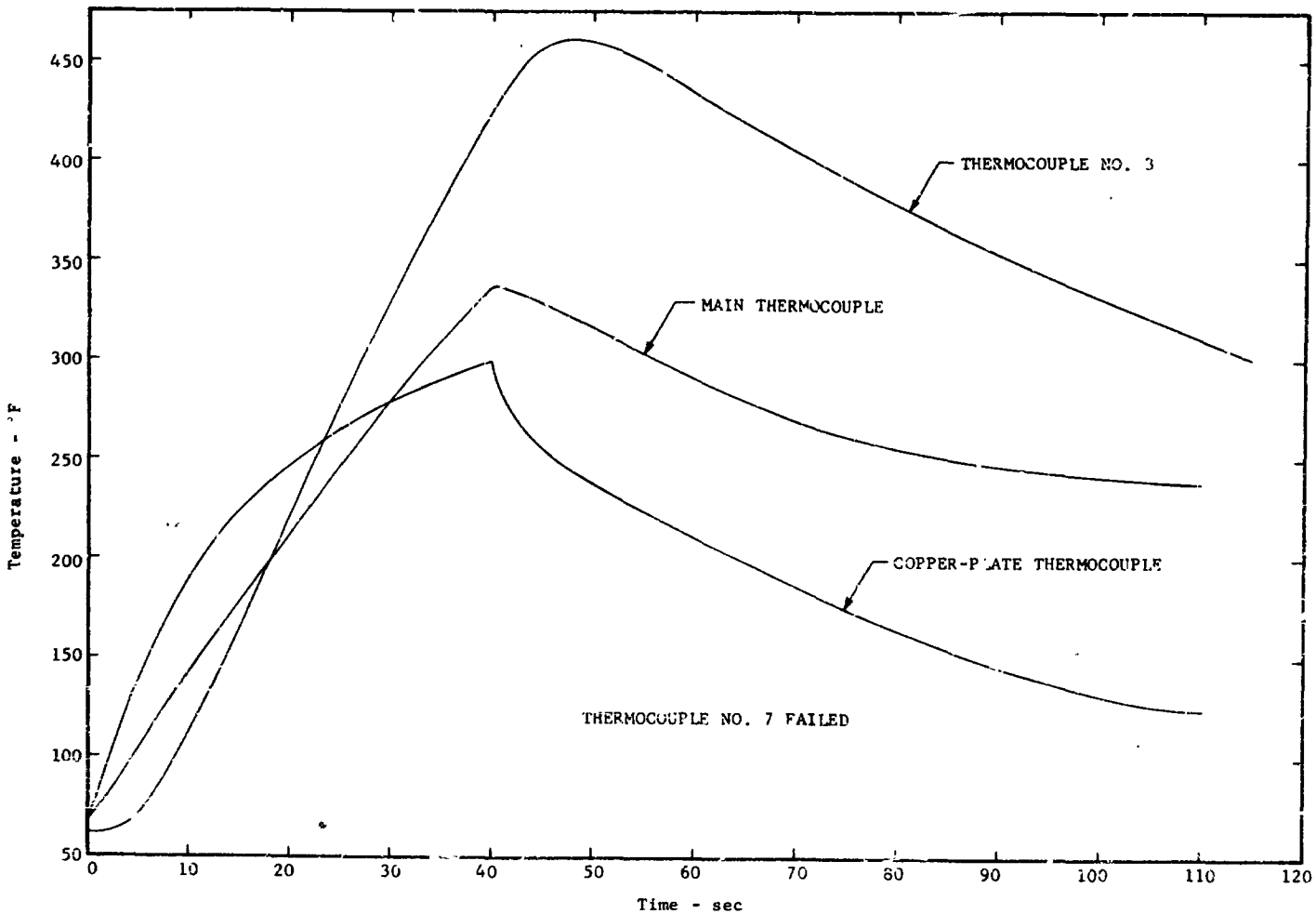

TEMPERATURE HISTORIES OF PURGED N-123 RADIOMETER MOUNTED IN WATER-COOLED 1/8"-THICK COPPER PLATE UNDER COMBINED RADIANT-CONVECTIVE HEATING
(Reference Heat Flux = 6.3 Btu/ft^2-sec)

FIGURE 33

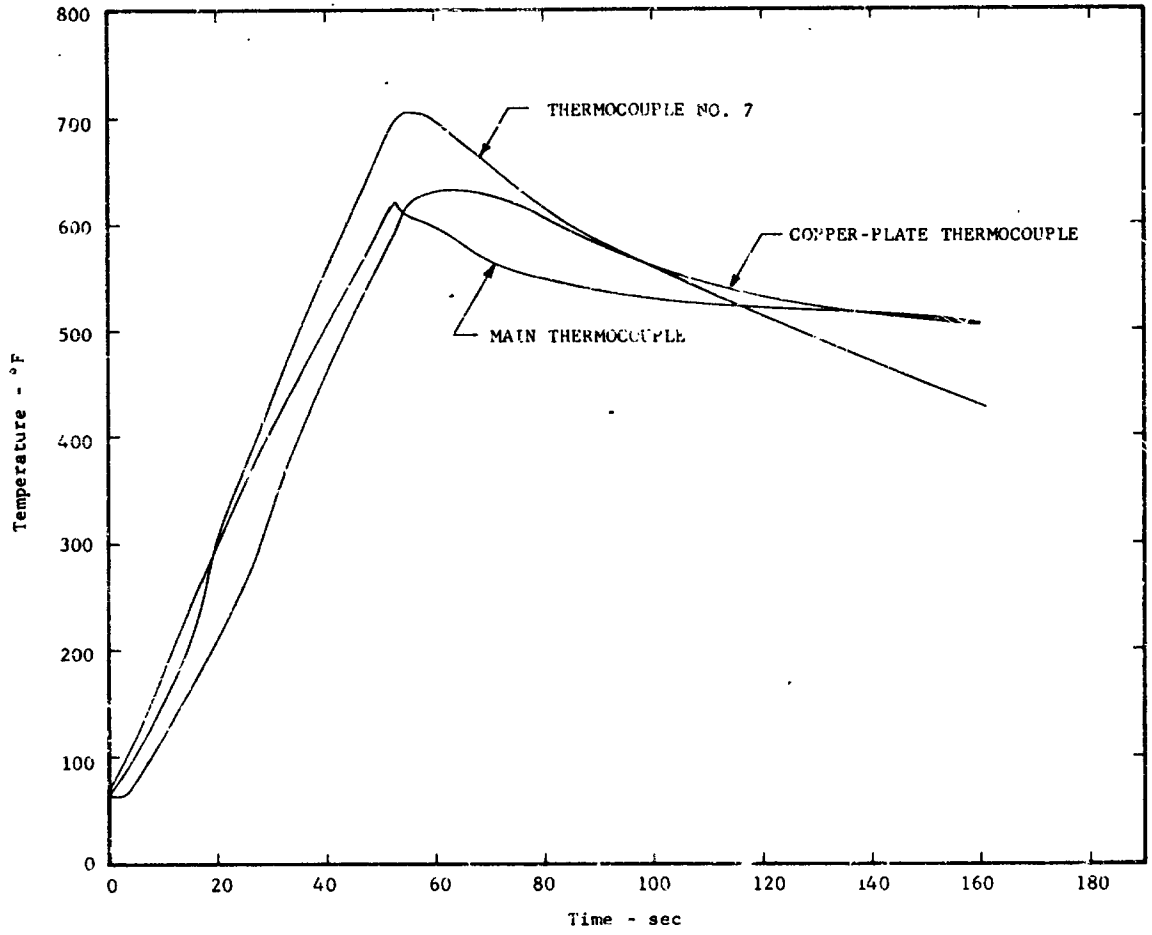

TEMPERATURE HISTORIES OF PURGED N-123 RADIOMETER MOUNTED IN WATER-COOLED 1/8"-THICK COPPER PLATE UNDER COMBINED RADIANT-CONVECTIVE HEATING
(Reference Heat Flux = 11 Btu/ft^2-sec)

FIGURE 34

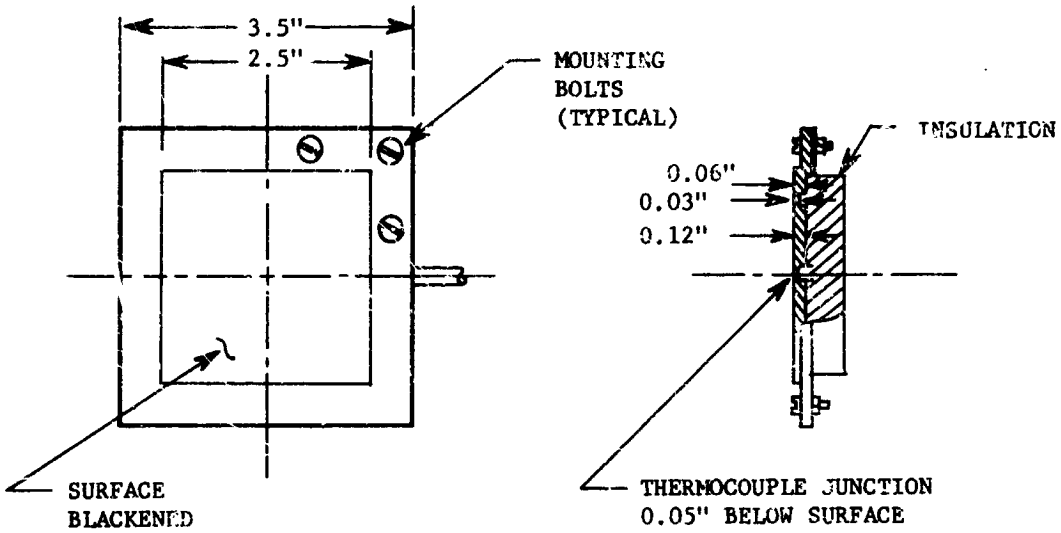

DIMENSIONS OF FENWAL COPPER- AND NICKEL-SLUG TOTAL CALORIMETERS

FIGURE 35

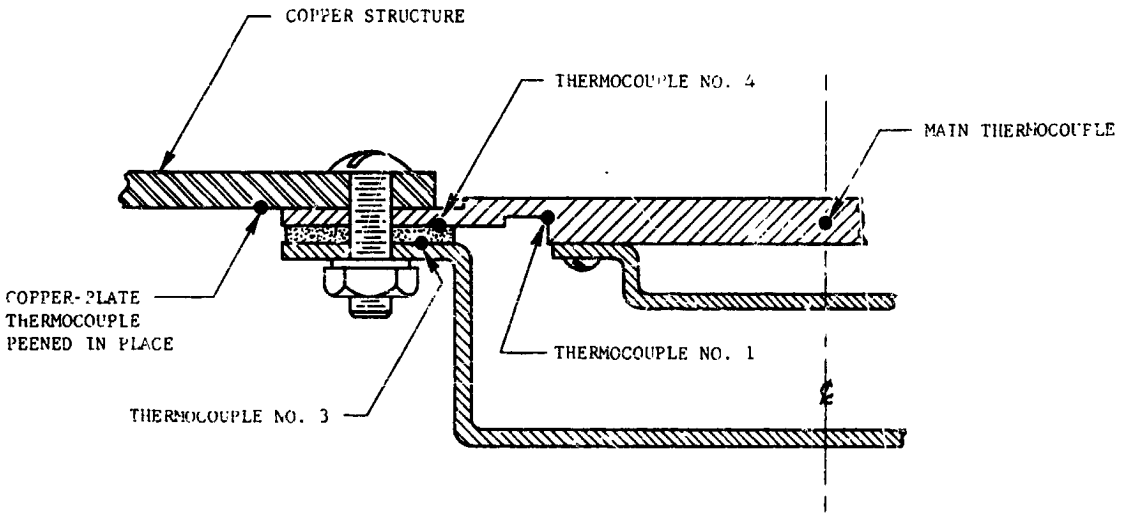

MOUNTING CONDITION AND THERMOCOUPLE LOCATION FOR RADIANT-HEATING TESTS ON FENWALL COPPER-SLUG TOTAL CALORIMETER AND EARLY RADIANT-HEATING TESTS ON FENWAL NICKEL-SLUG TOTAL CALORIMETER

FIGURE 36

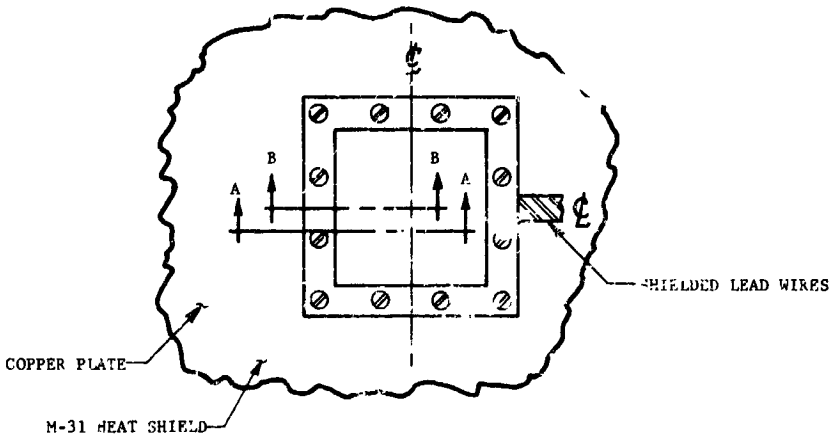

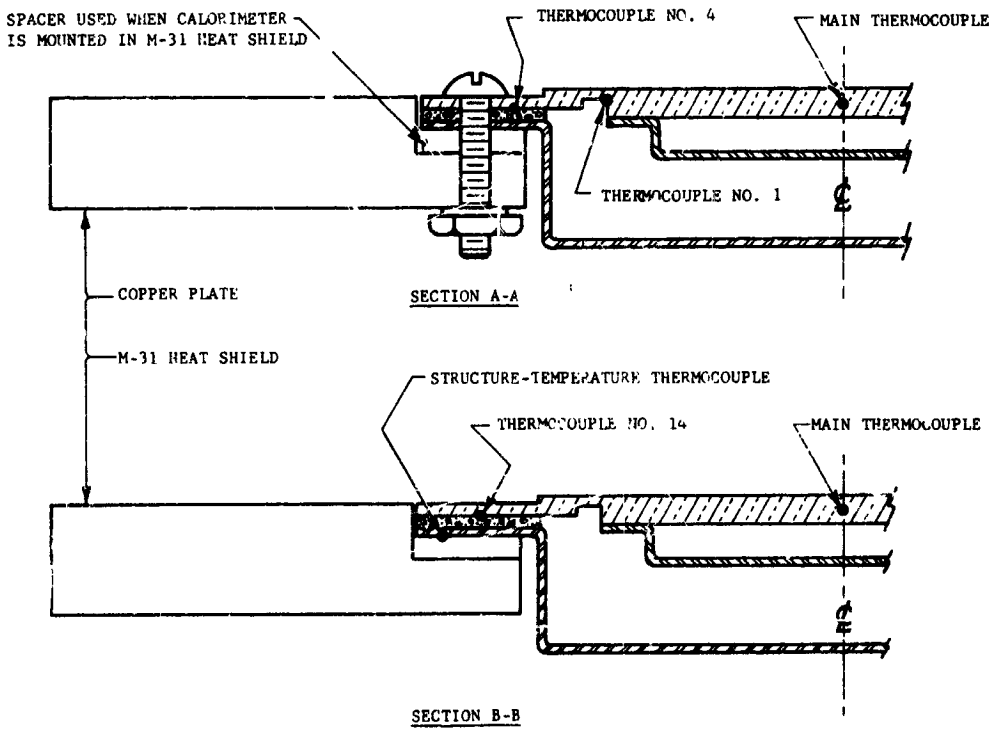

MOUNTING CONDITION AND THERMOCOUPLE LOCATION FOR FENWAL NICKEL-SLUG TOTAL CALORIMETER MOUNTED IN 1/8"-THICK COPPER PLATE AND IN M-31 HEAT-SHIELD MATERIAL

FIGURE 37

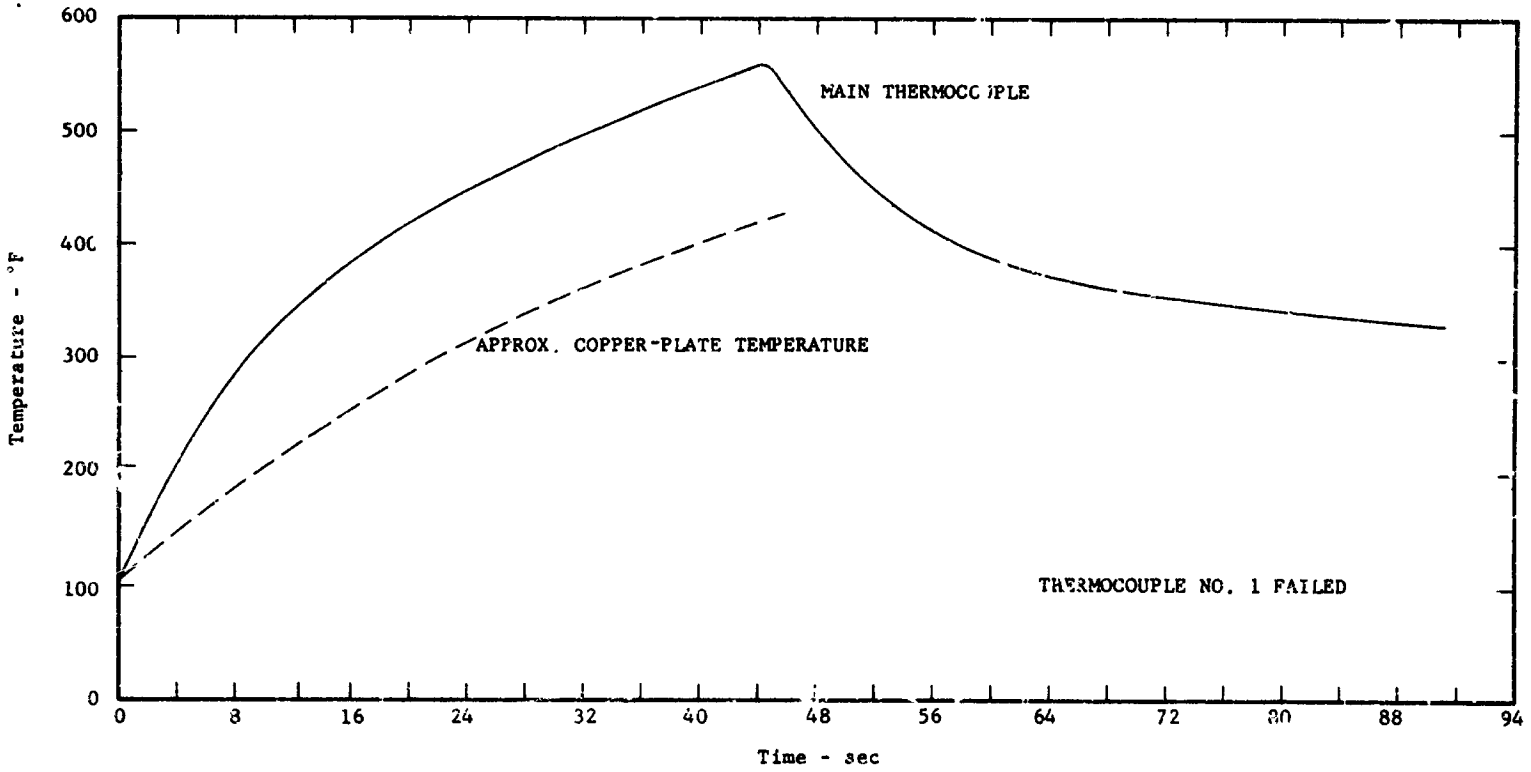

TEMPERATURE HISTORIES OF COPPER-SLUG TOTAL CALORIMETER MOUNTED IN UNCOOLED 1/8"-THICK COPPER PLATE UNDER RADIANT HEATING
(Reference Heat Flux = 15.1 Btu/ft^2-sec)

FIGURE 38

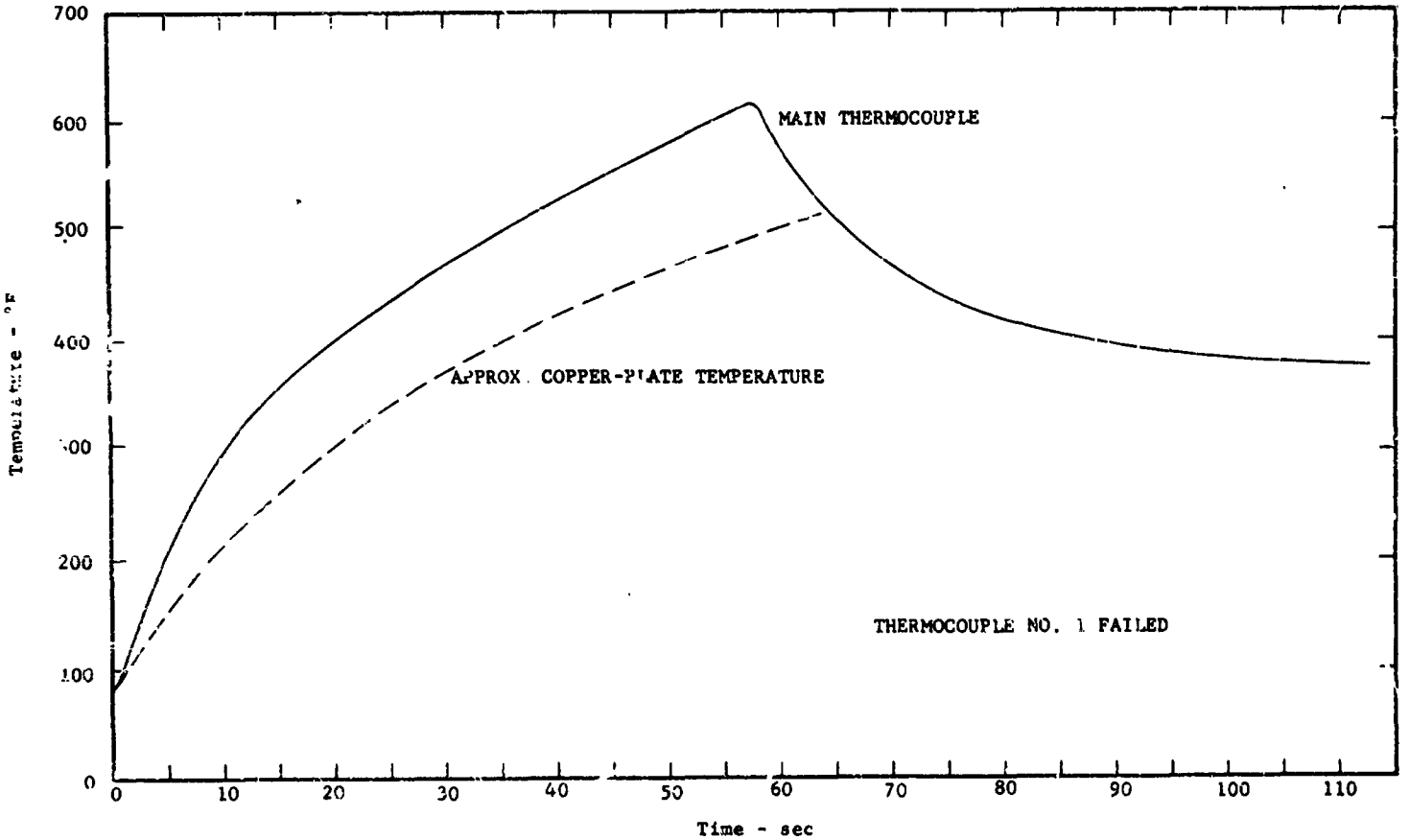

TEMPERATURE HISTORIES OF COPPER-SLUG TOTAL CALORIMETER MOUNTED IN UNCOOLED 1/8"-THICK COPPER PLATE UNDER RADIANT HEATING
(Reference Heat Flux = 18.0 Btu/ft^2-sec)

FIGURE 39

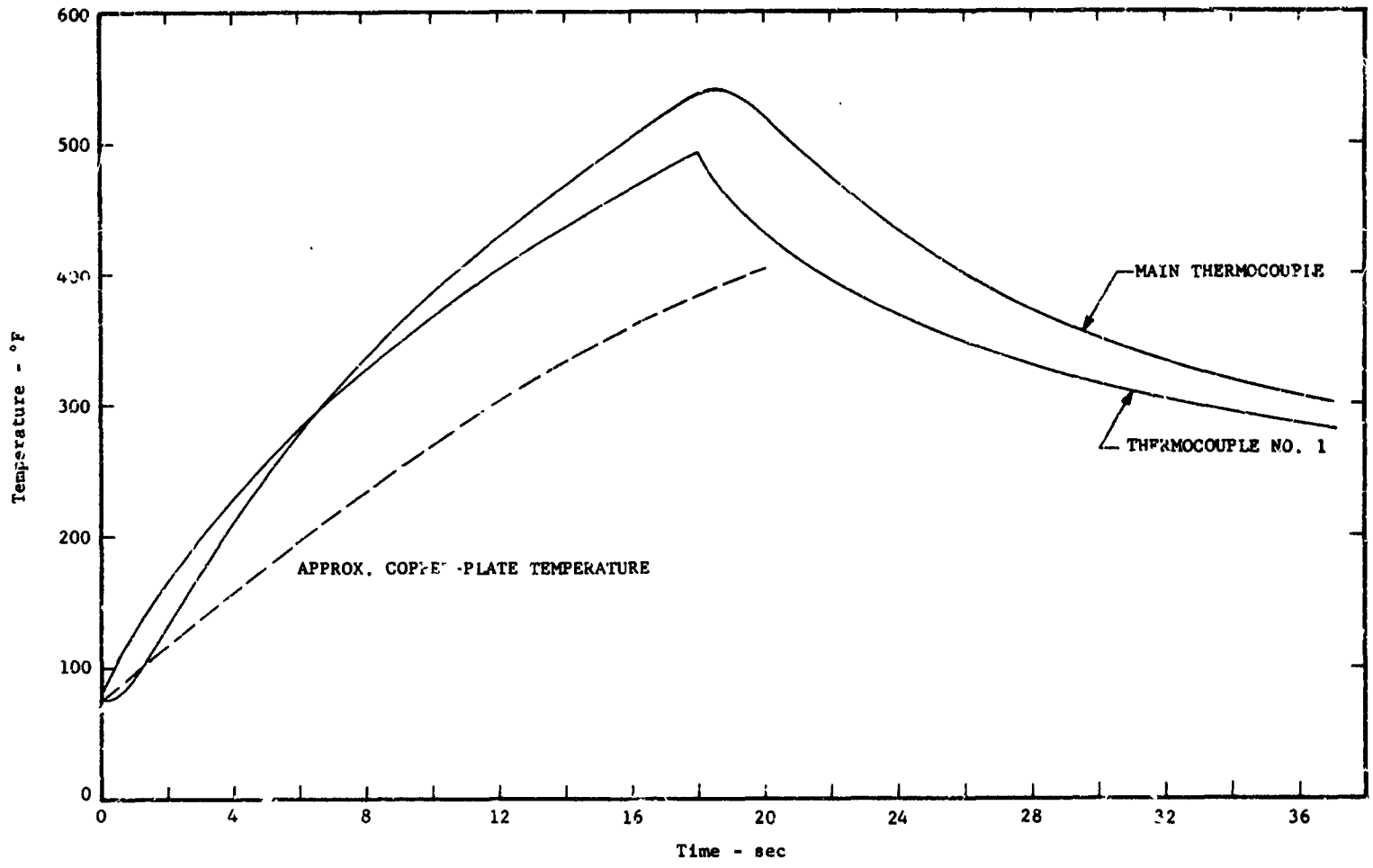

TEMPERATURE HISTORIES OF COPPER-SLUG TOTAL CALORIMETER MOUNTED IN UNCOOLED 1/8"-THICK COPPER PLATE UNDER RADIANT HEATING
(Reference Heat Flux = 27.5 Btu/ft^2-sec)

FIGURE 40

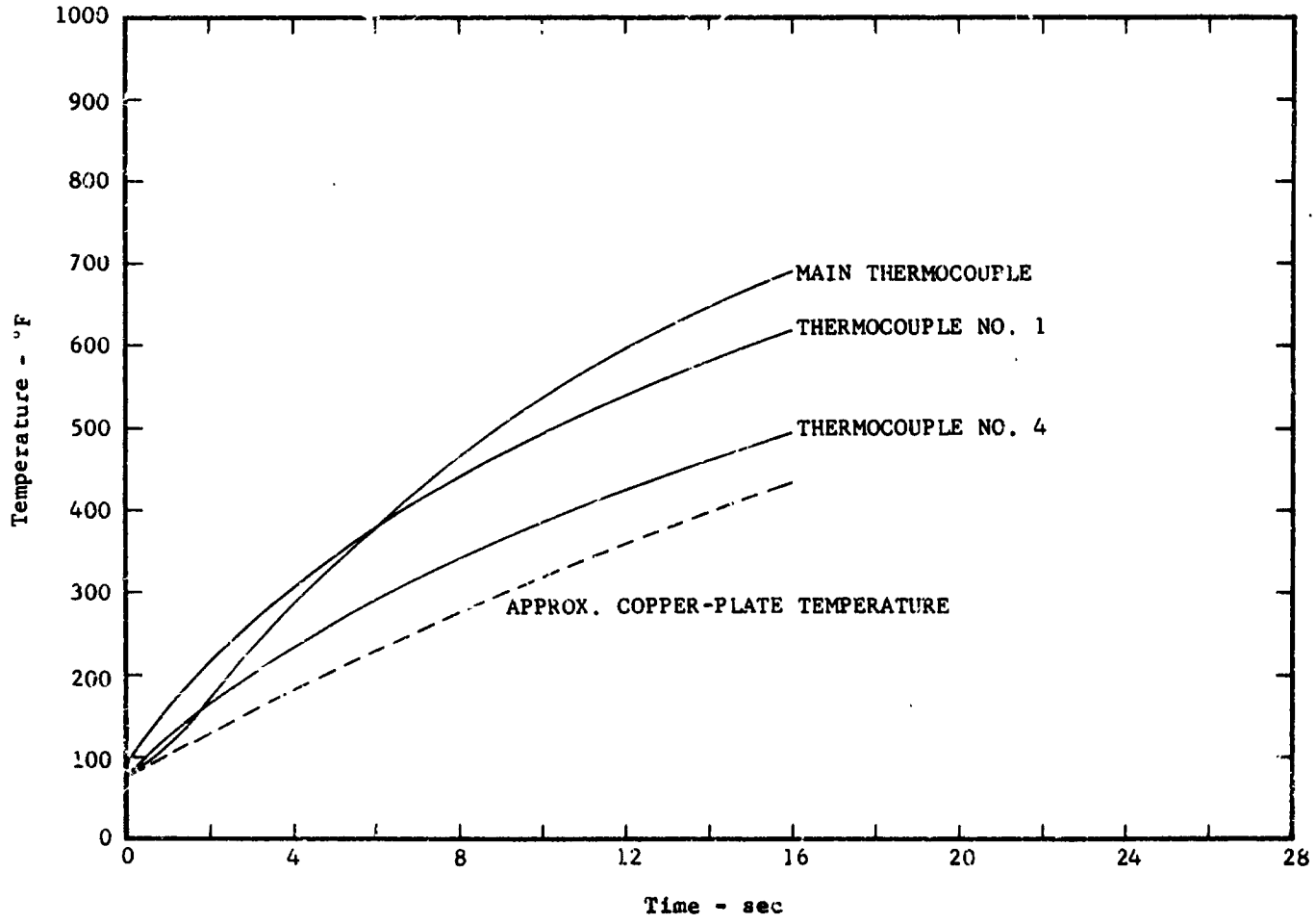

TEMPERATURE HISTORIES OF COPPER-SLUG TOTAL CALORIMETER MOUNTED IN UNCOOLED 1/8"-THICK COPPER PLATE UNDER RADIANT HEATING
(Reference Heat Flux = 37.5 Btu/ft^2-sec)

FIGURE 41

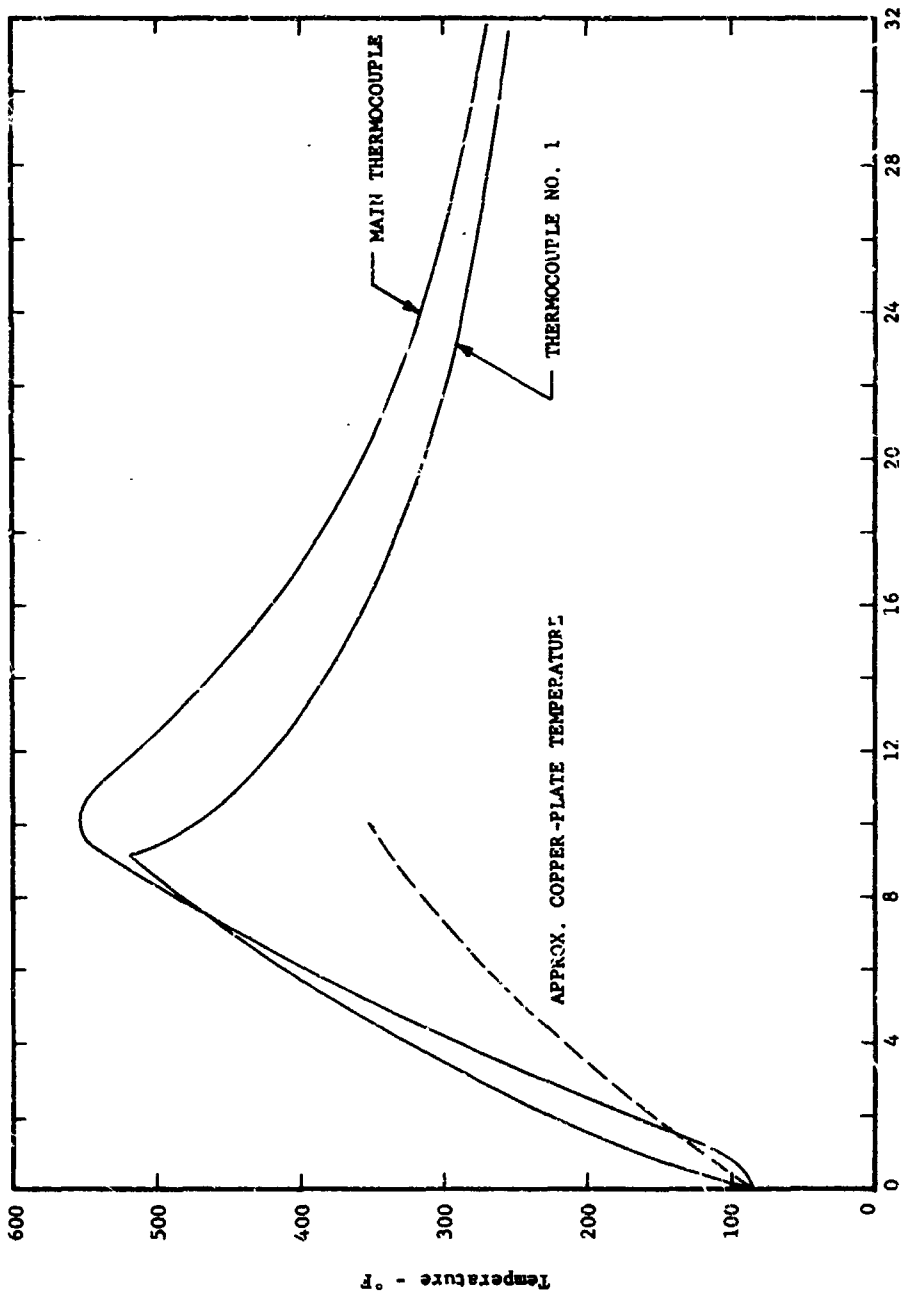

TEMPERATURE HISTORIES OF COPPER-SLUG TOTAL CALORIMETER MOUNTED IN UNCOOLED 1/8"-THICK COPPER PLATE UNDER RADIANT HEATING
(Reference Heat Flux = 40.8 Btu/ft^2-sec)

FIGURE 42

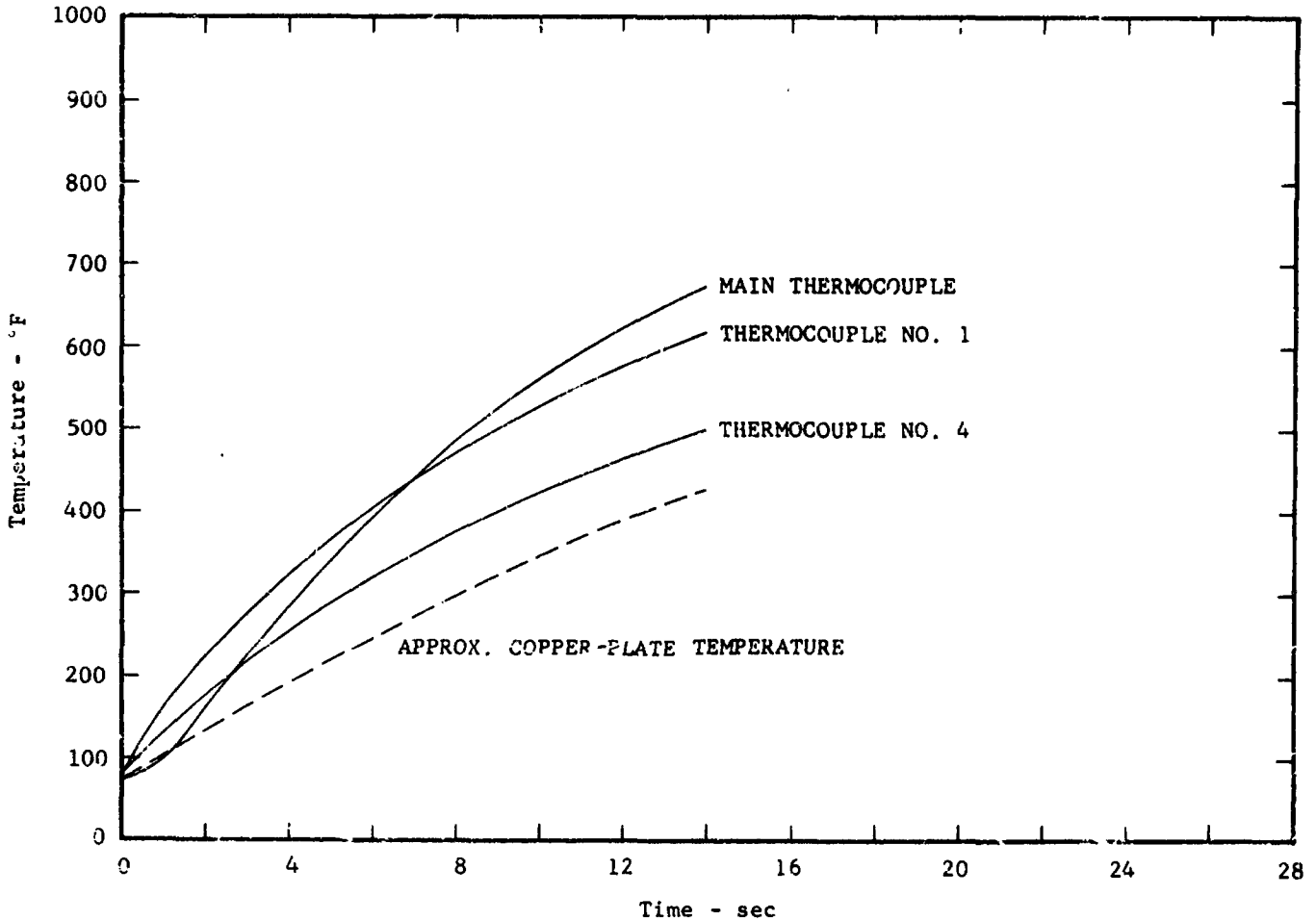

TEMPERATURE HISTORIES OF COPPER-SLUG TOTAL CALORIMETER MOUNTED IN UNCOOLED 1/8"-THICK COPPER PLATE UNDER RADIANT HEATING
(Reference Heat Flux = 41.0 Btu/ft^2-sec)

FIGURE 43

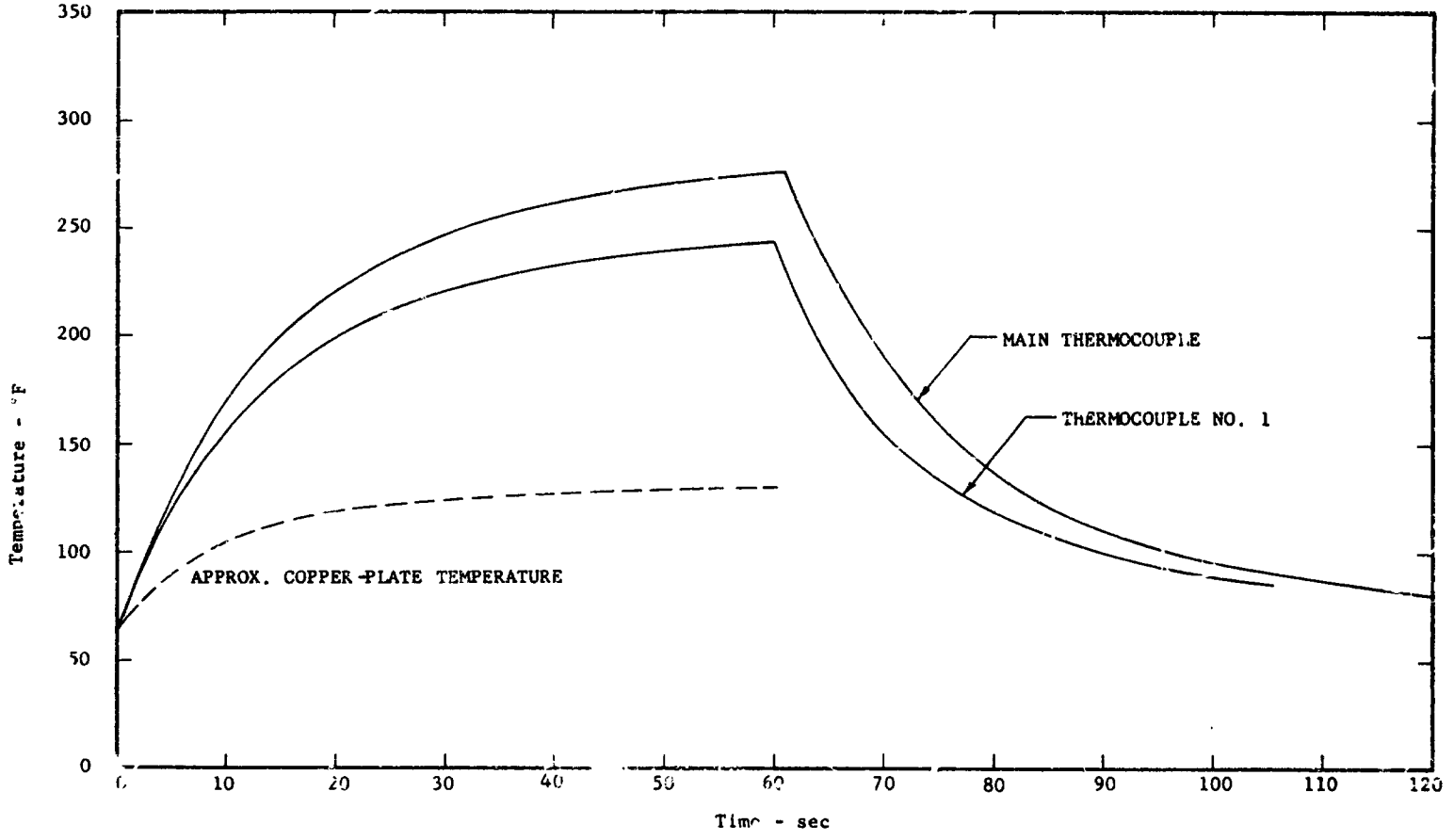

TEMPERATURE HISTORIES OF COPPER-SLUG TOTAL CALORIMETER MOUNTED IN WATER-COOLED 1/8"-THICK COPPER PLATE UNDER RADIANT HEATING
(Reference Heat Flux = 7.6 Btu/ft^2-sec)

FIGURE 44

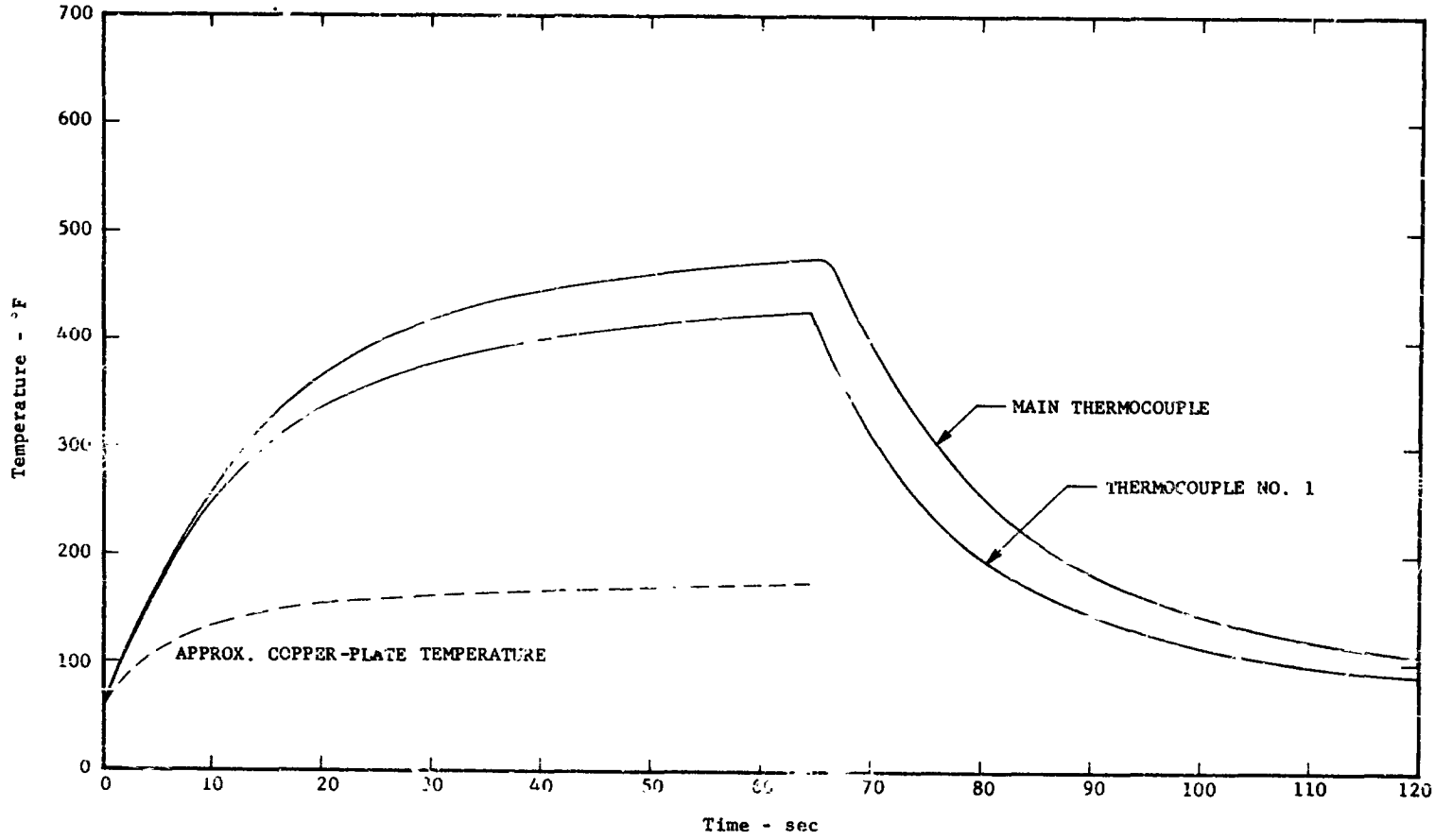

TEMPERATURE HISTORIES OF COPPER-SLUG TOTAL CALORIMETER MOUNTED IN WATER-COOLED 1/8"-THICK COPPER PLATE UNDER RADIANT HEATING
(Reference Heat Flux = 13.1 Btu/ft^2-sec)

FIGURE 45

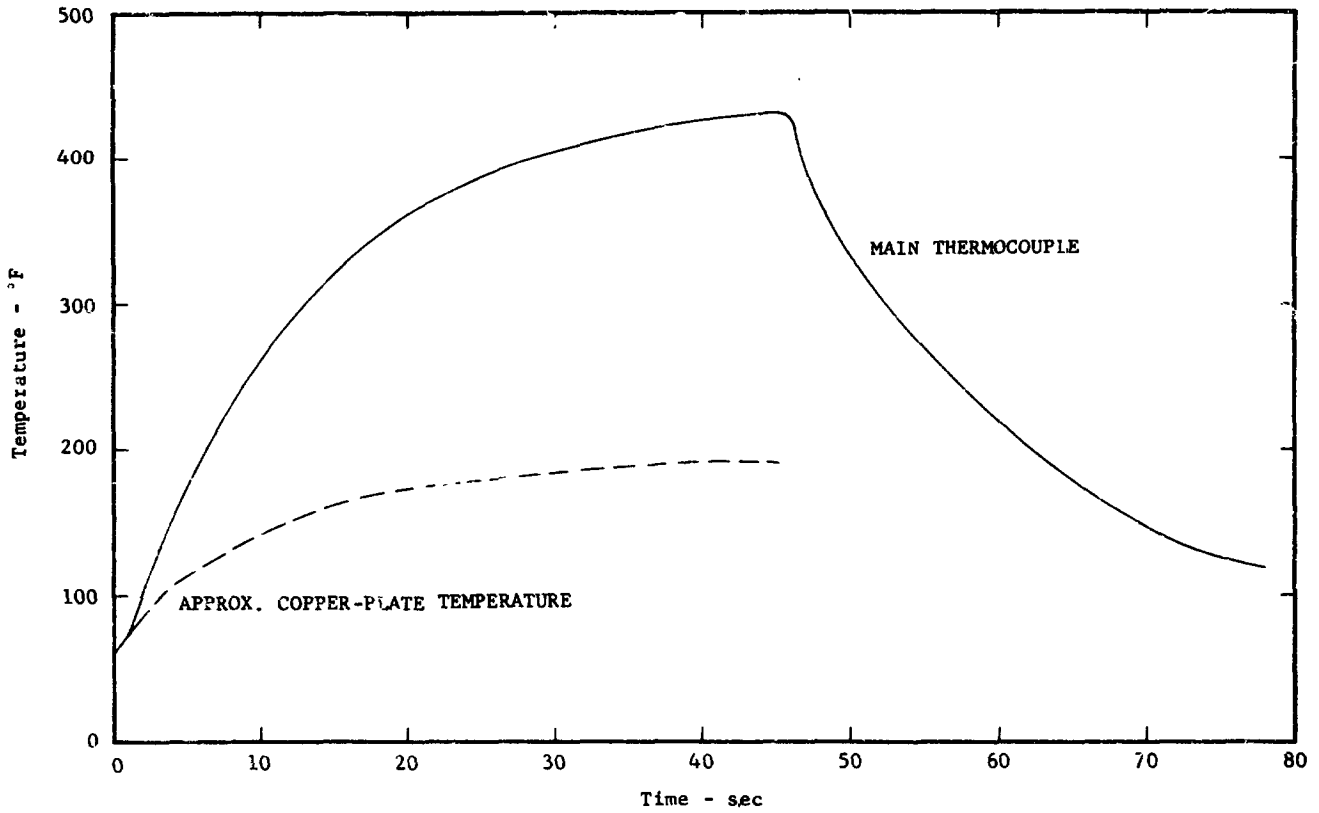

TEMPERATURE HISTORIES OF COPPER-SLUG TOTAL CALORIMETER MOUNTED IN WATER-COOLED 1/8"-THICK COPPER PLATE UNDER RADIANT HEATING
(Reference Heat Flux = 15.9 Btu/ft.^{2}-sec)

FIGURE 46

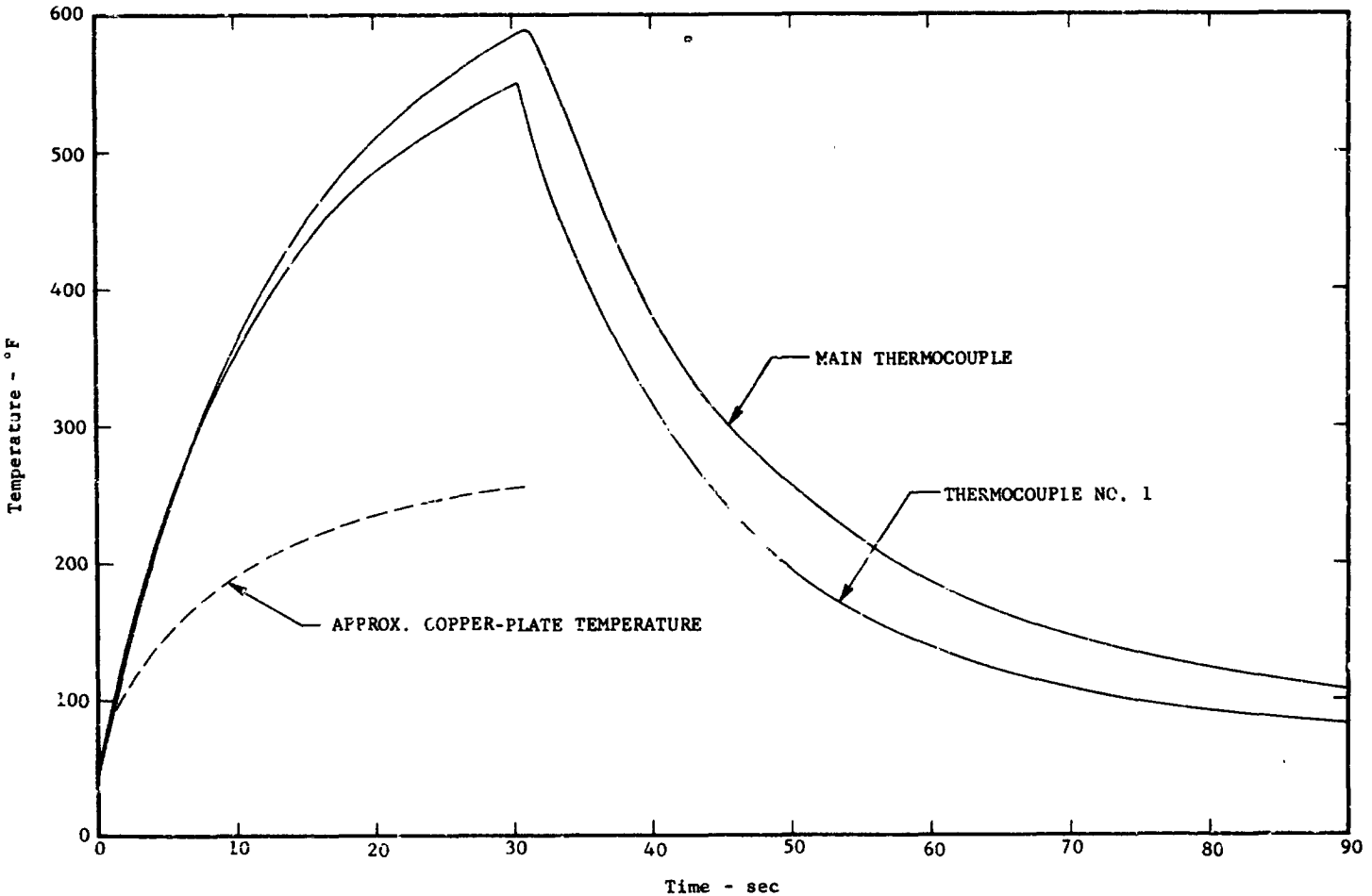

TEMPERATURE HISTORIES OF COPPER-SLUG TOTAL CALORIMETER MOUNTED IN WATER-COOLED 1/8"-THICK COPPER PLATE UNDER RADIANT HEATING
(Reference Heat Flux = 22.9 Btu/ft^2-sec)

FIGURE 47

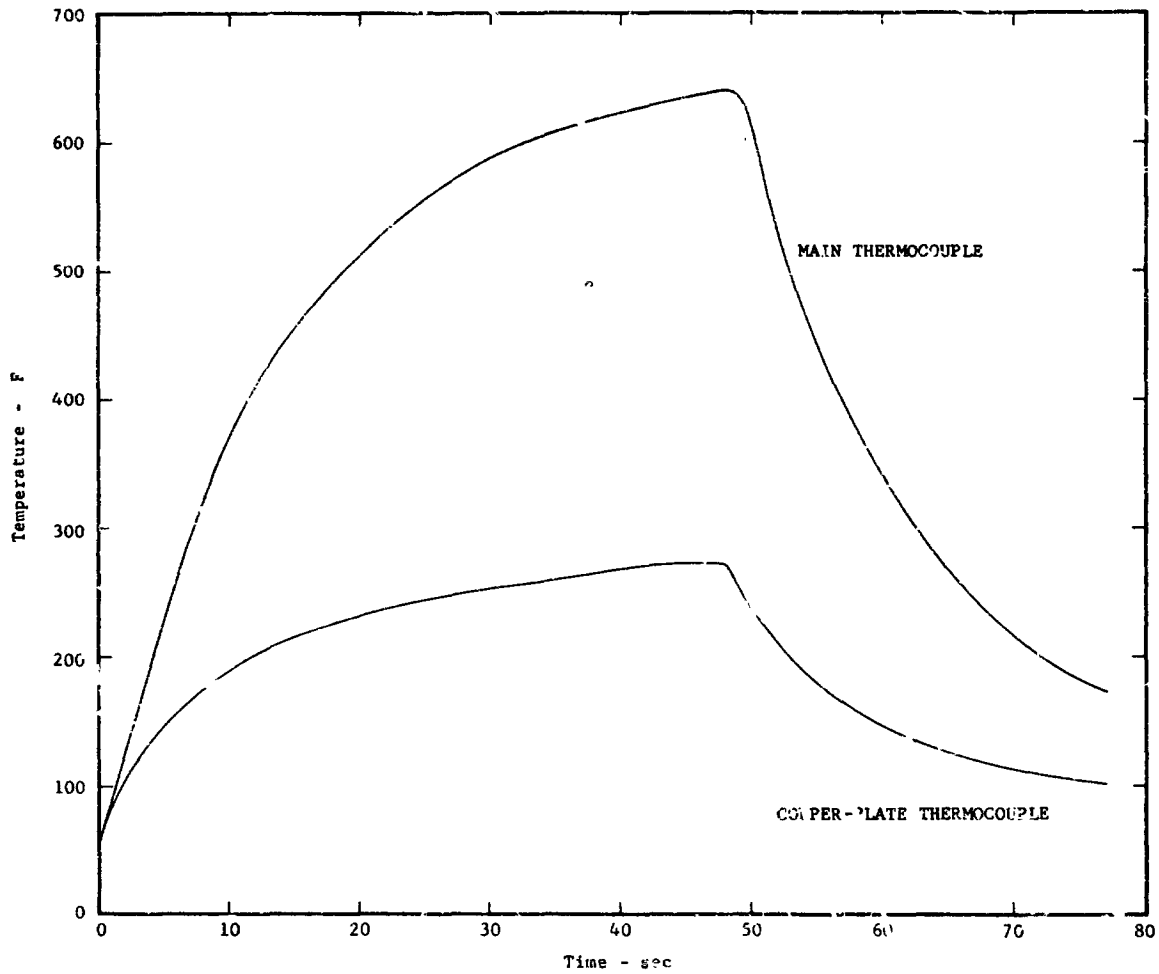

TEMPERATURE HISTORIES OF COPPER-SLUG TOTAL CALORIMETER MOUNTED IN WATER-COOLED 1/8"-THICK COPPER PLATE UNDER RADIANT HEATING
(Reference Heat Flux = 23.1 Btu/ft^2-sec)

FIGURE 48

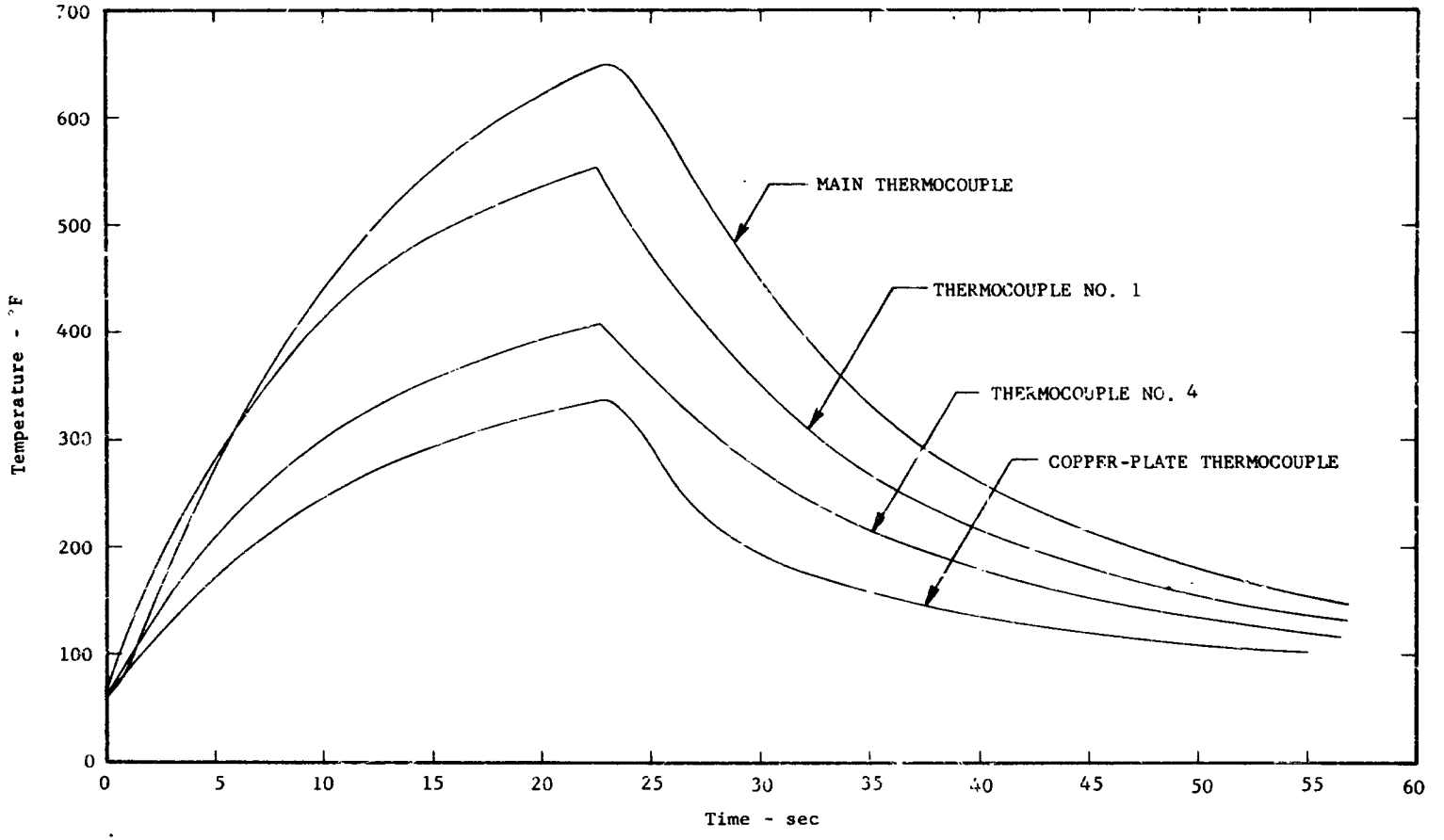

TEMPERATURE HISTORIES OF COPPER-SLUG TOTAL CALORIMETER MOUNTED IN WATER-COOLED 1/8"-THICK COPPER PLATE UNDER RADIANT HEATING
(Reference Heat Flux = 26.7 Btu/ft^2-sec)

FIGURE 49

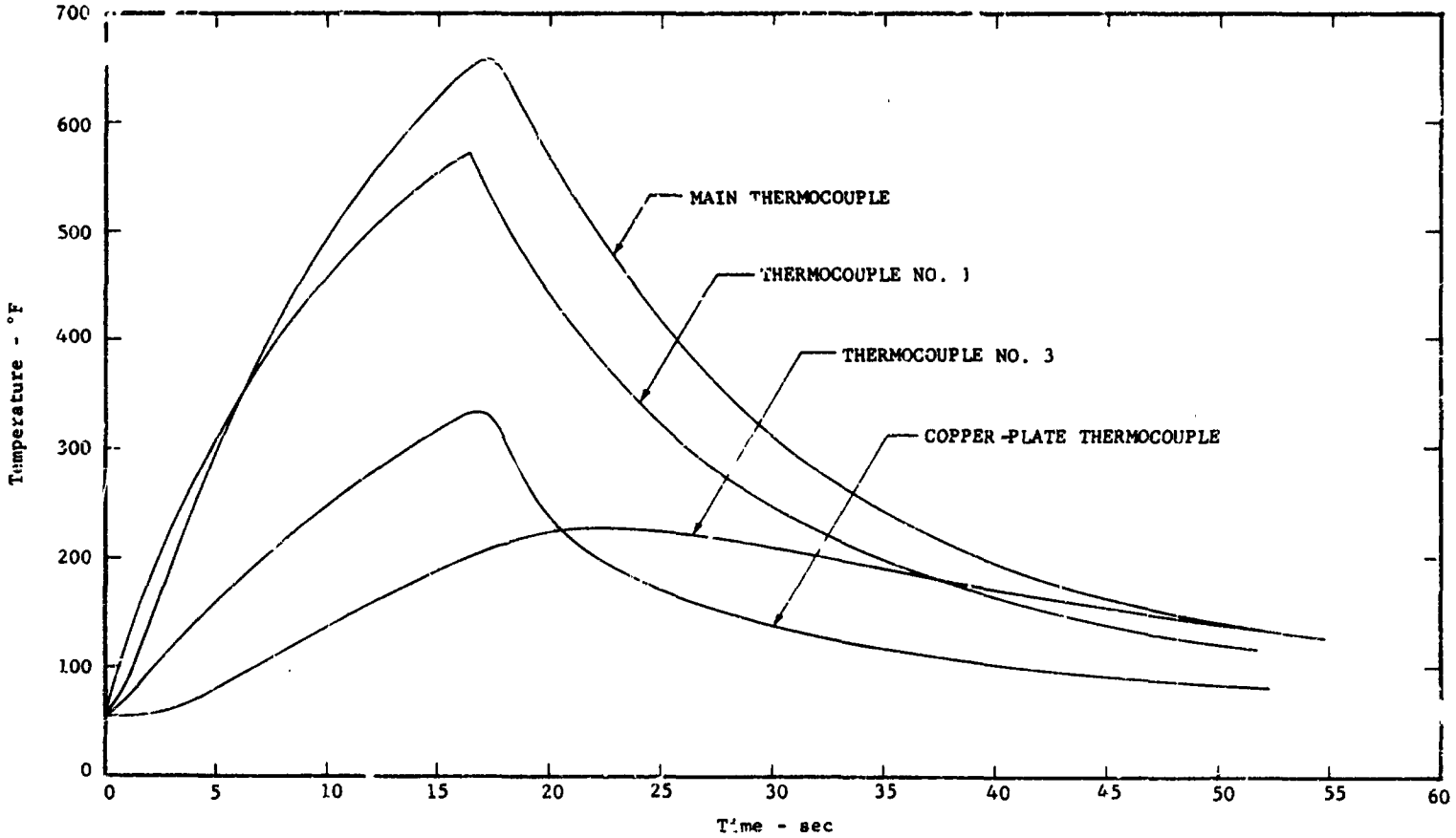

TEMPERATURE HISTORIES OF COPPER-SLUG TOTAL CALORIMETER MOUNTED IN WATER-COOLED 1/8"-THICK COPPER PLATE UNDER RADIANT HEATING
(Reference Heat Flux = 33.5 Btu/ft^2-sec)

FIGURE 50

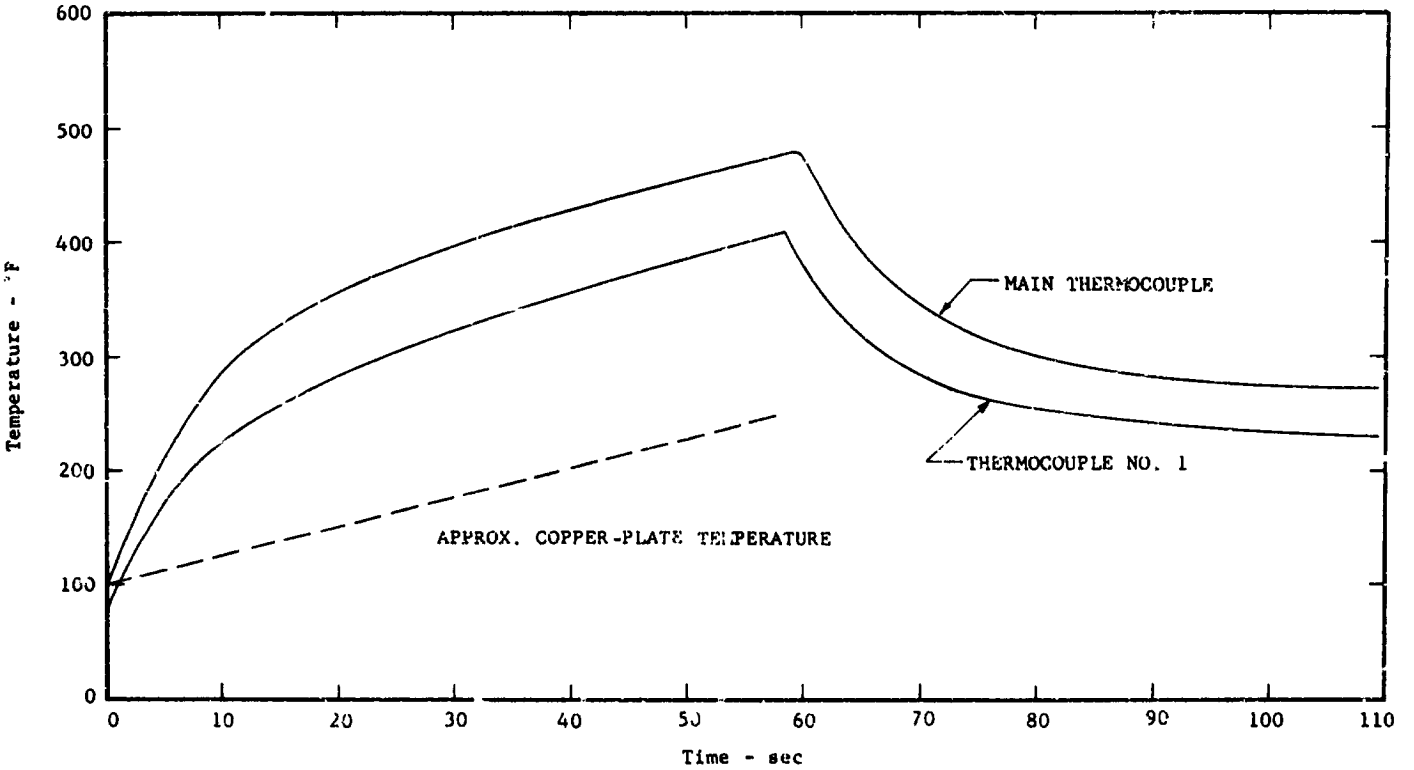

TEMPERATURE HISTORIES OF COPPER-SLUG TOTAL CALORIMETER MOUNTED IN TWO UNCOOLED 1/8"-THICK COPPER PLATES UNDER RADIANT HEATING
(Reference Heat Flux = 14.3 Btu/ft^2-sec)

FIGURE 51

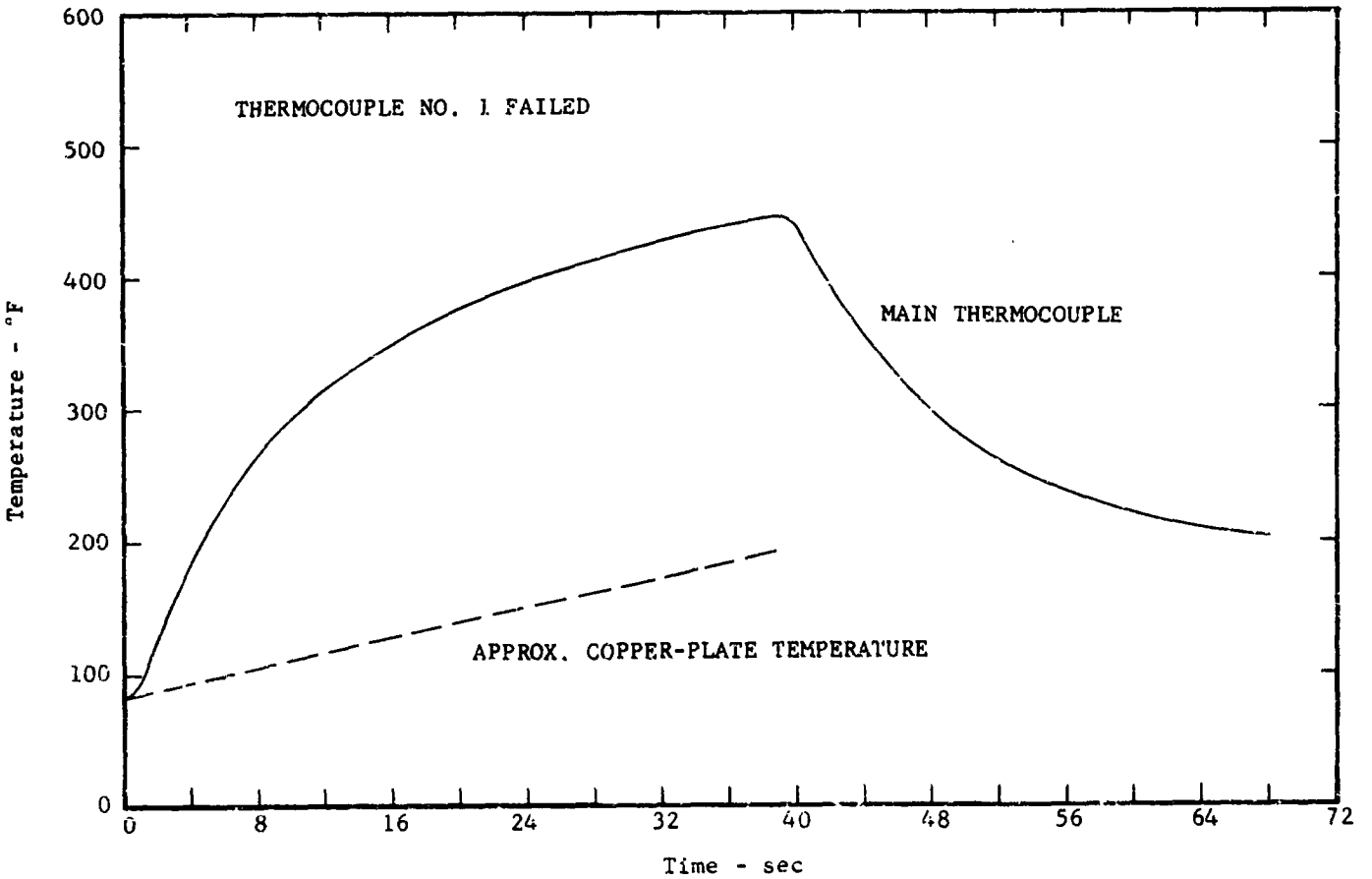

TEMPERATURE HISTORIES OF COPPER-SLUG TOTAL CALORIMETER MOUNTED IN TWO UNCOOLED 1/8"-THICK COPPER PLATES UNDER RADIANT HEATING
(Reference Heat Flux = 14.6 Btu/ft^2-sec)

FIGURE 52

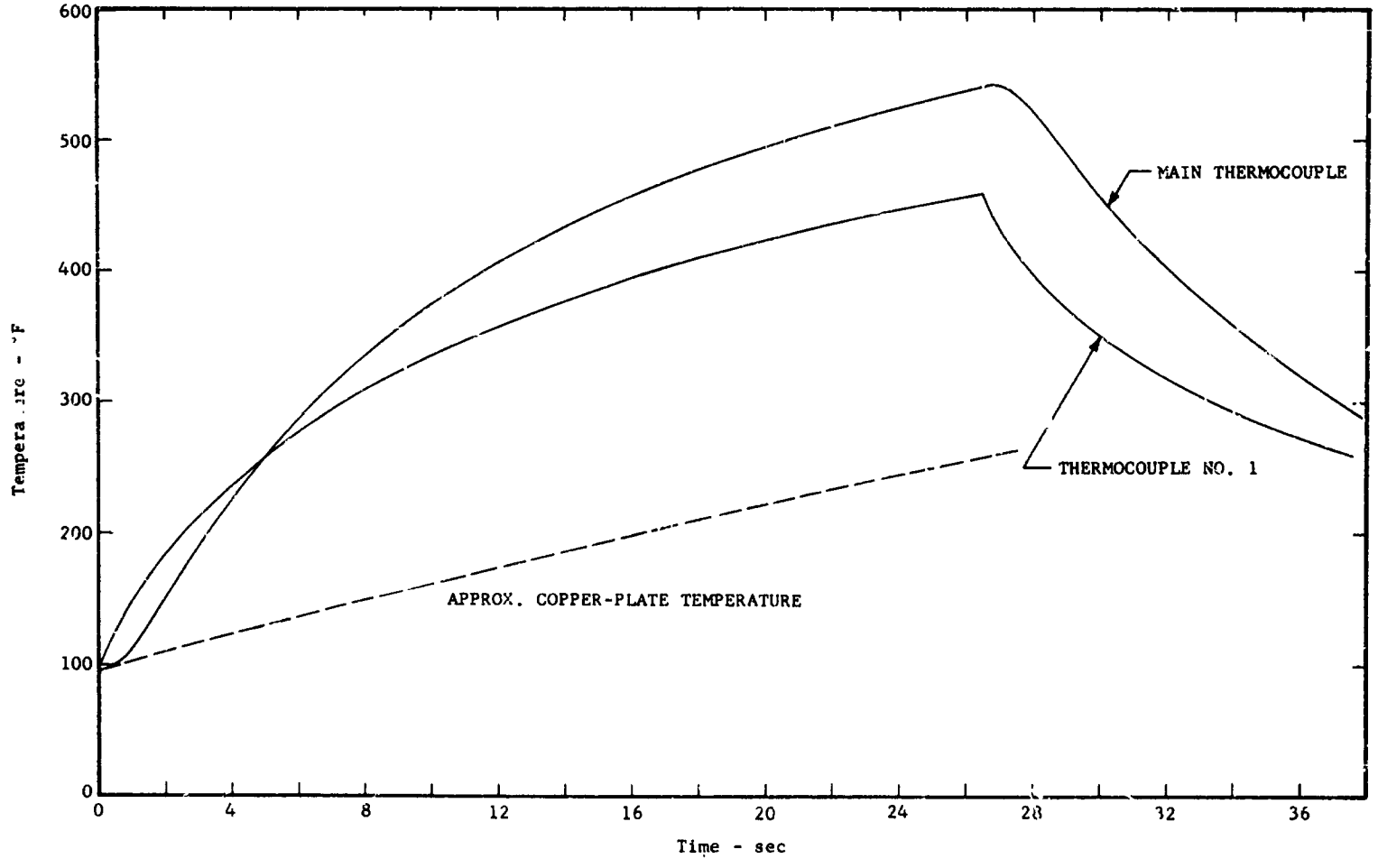

TFMPERATURE HISTORIES OF COPPER-SLUG TOTAL CALORIMETER MOUNTED IN TWO UNCOOLED 1/8"-THICK COPPER PLATES UNDER RADIANT HEATING
(Reference Heat Flux = 27.1 Btu/ft^2-sec)

FIGURE 53

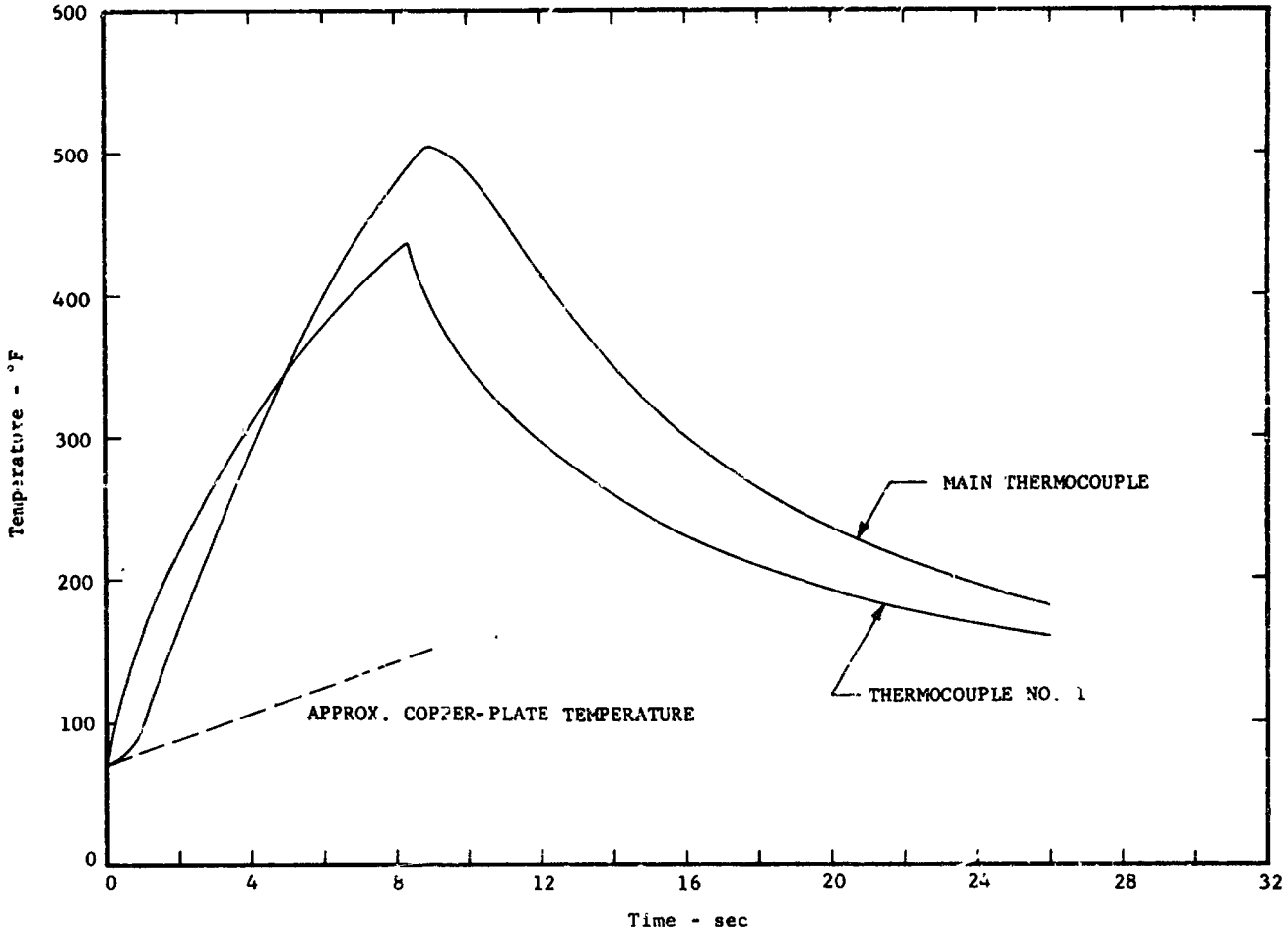

TEMPERATURE HISTORIES OF COPPER-SLUG TOTAL CALORIMETER MOUNTED IN TWO UNCOOLED 1/8"-THICK COPPER PLATES UNDER RADIANT HEATING
(Reference Heat Flux = 43.5 Btu/ft^2-sec)

FIGURE 54

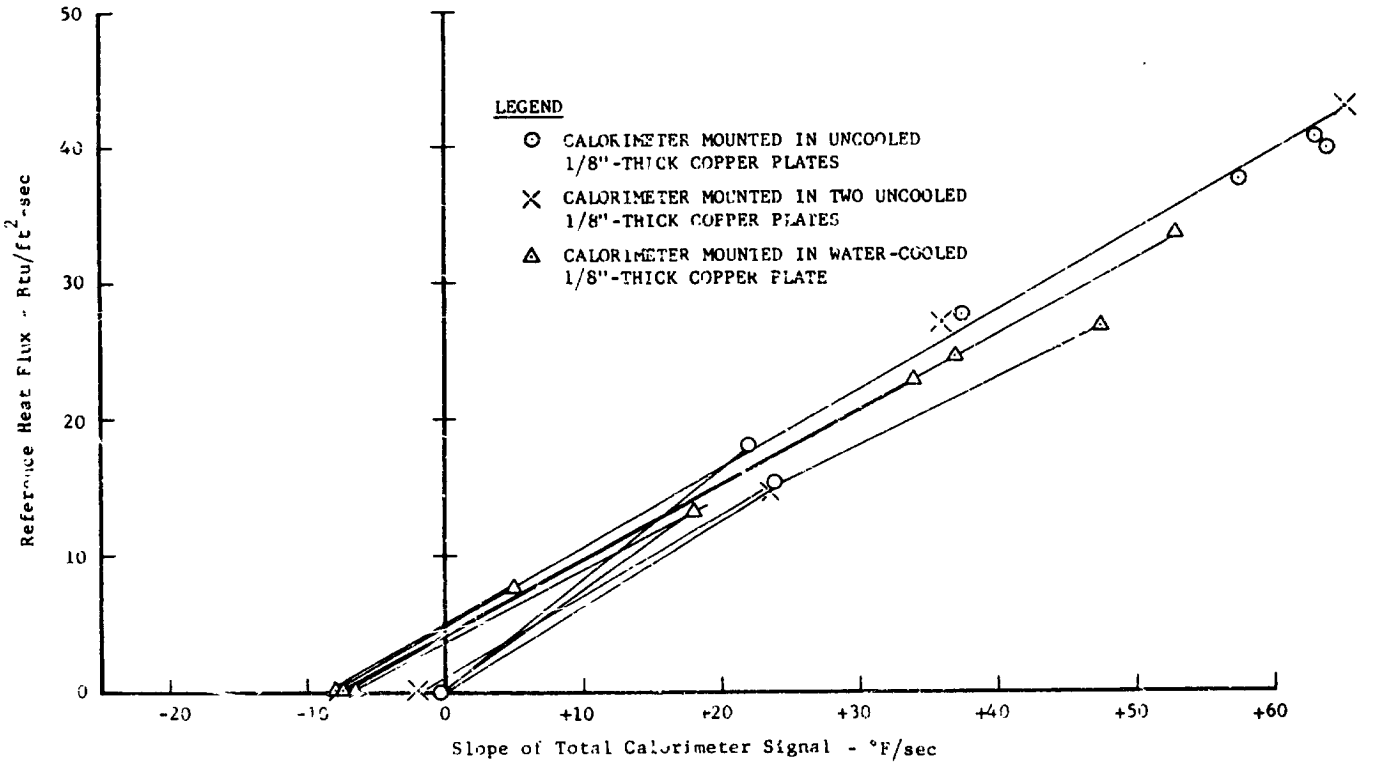

COPPER-SLUG TOTAL CALORIMETER CALIBRATION AT 200°F UNDER RADIANT HEATING

FIGURE 55

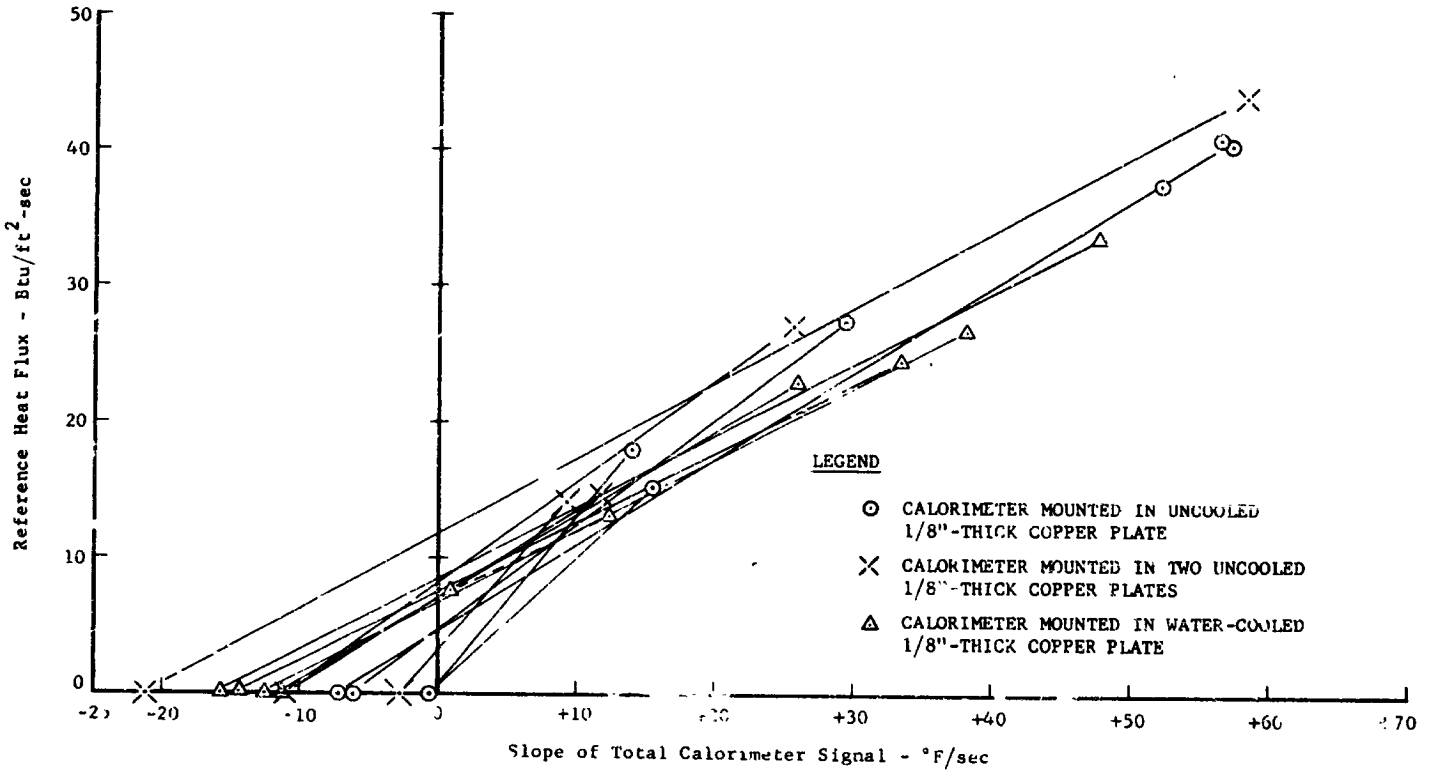

COPPER-SLUG TOTAL CALORIMETER CALIBRATION AT 300°F UNDER RADIANT HEATING

FIGURE 56

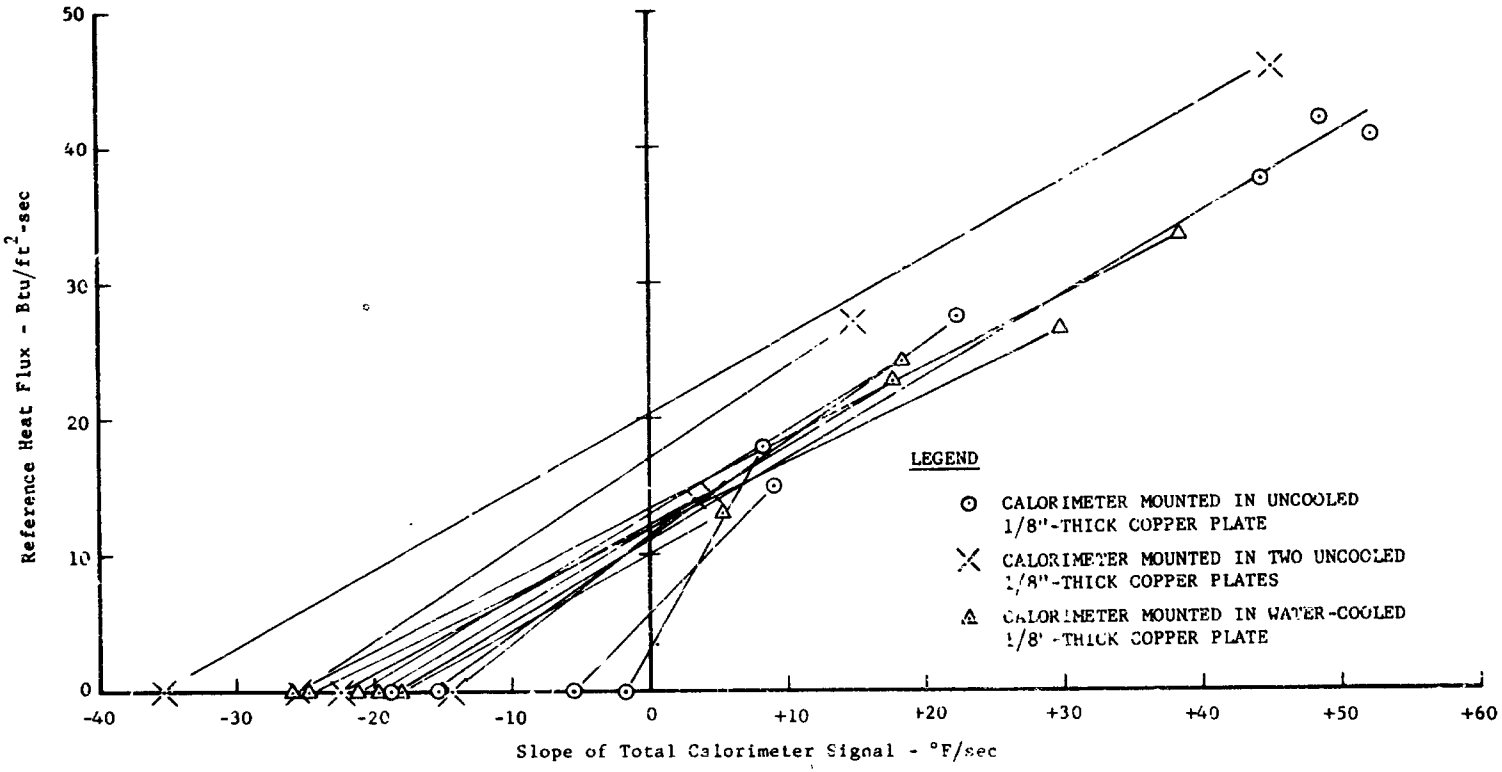

COPPER-SLUG TOTAL CALORIMETER CALIBRATION AT 400°F UNDER RADIANT HEATING

FIGURE 57

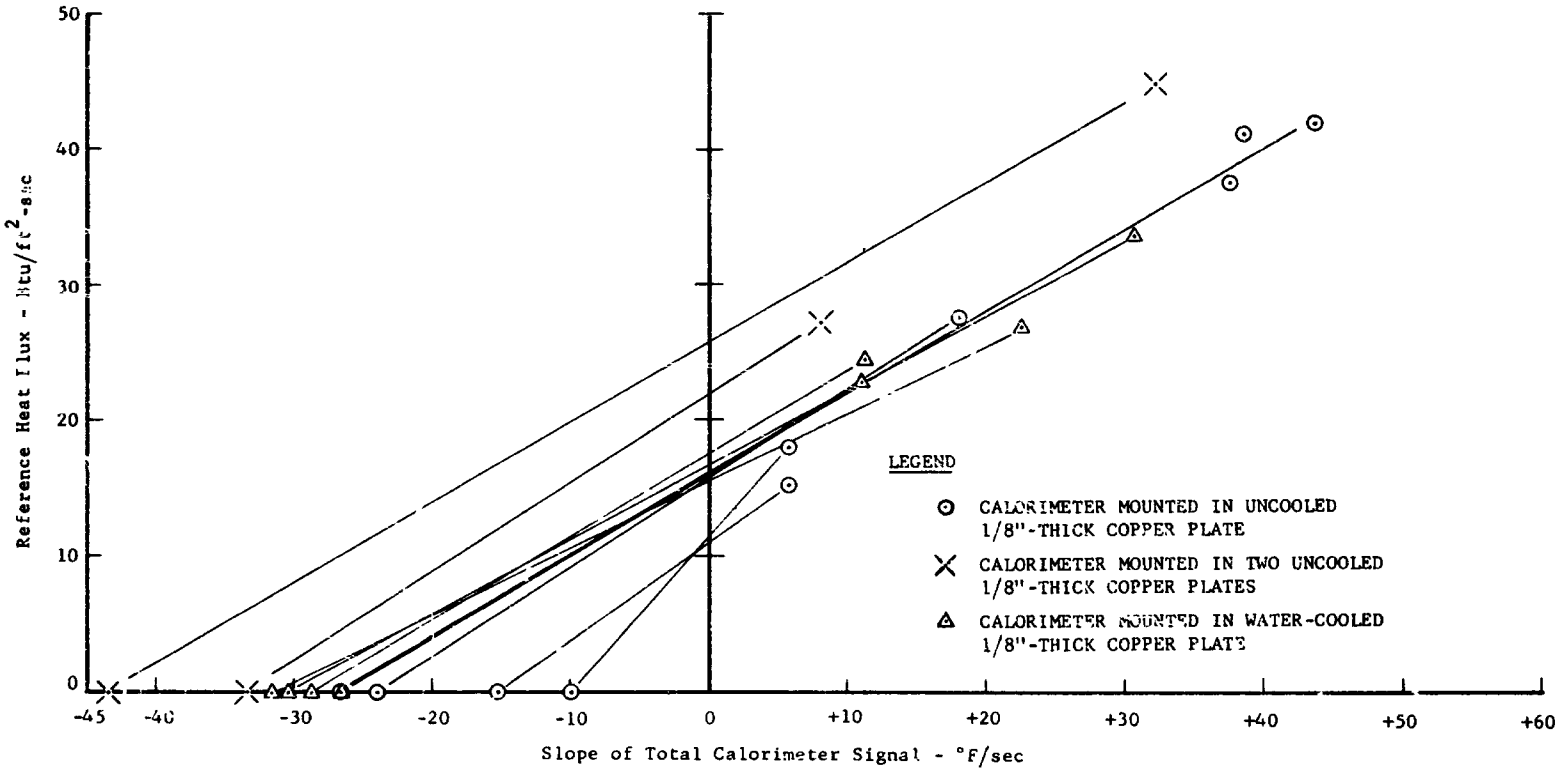

COPPER-SLUG TOTAL CALORIMETER CALIBRATION AT 500°F UNDER RADIANT HEATING

FIGURE 58

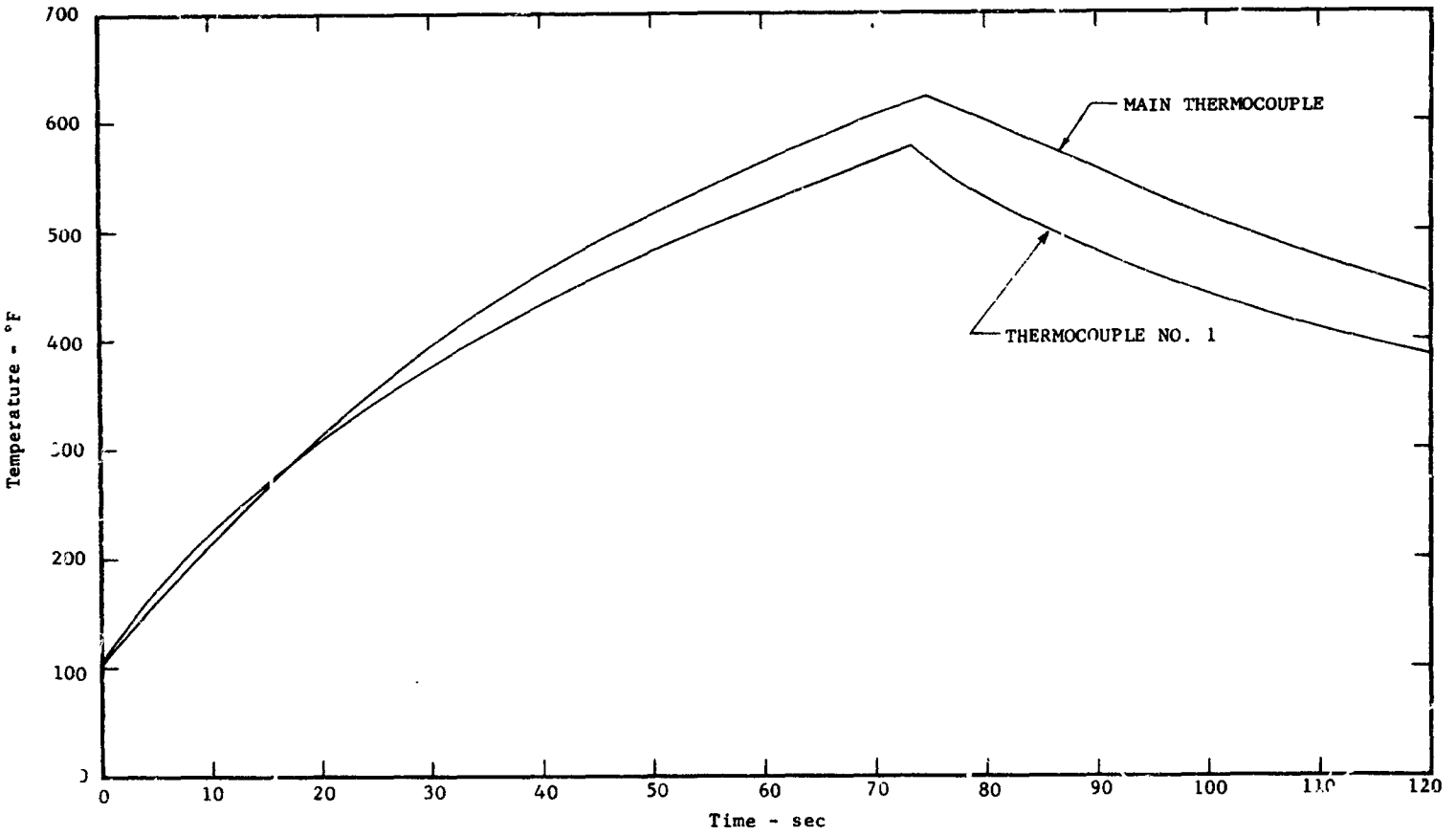

TEMPERATURE HISTORIES OF NICKEL-SLUG TOTAL CALORIMETER MOUNTED IN UNCOOLED 1/8"-THICK COPPER PLATE UNDER RADIANT HEATING
(Reference Heat Flux = 6.3 Btu/ft^2-sec)

FIGURE 59

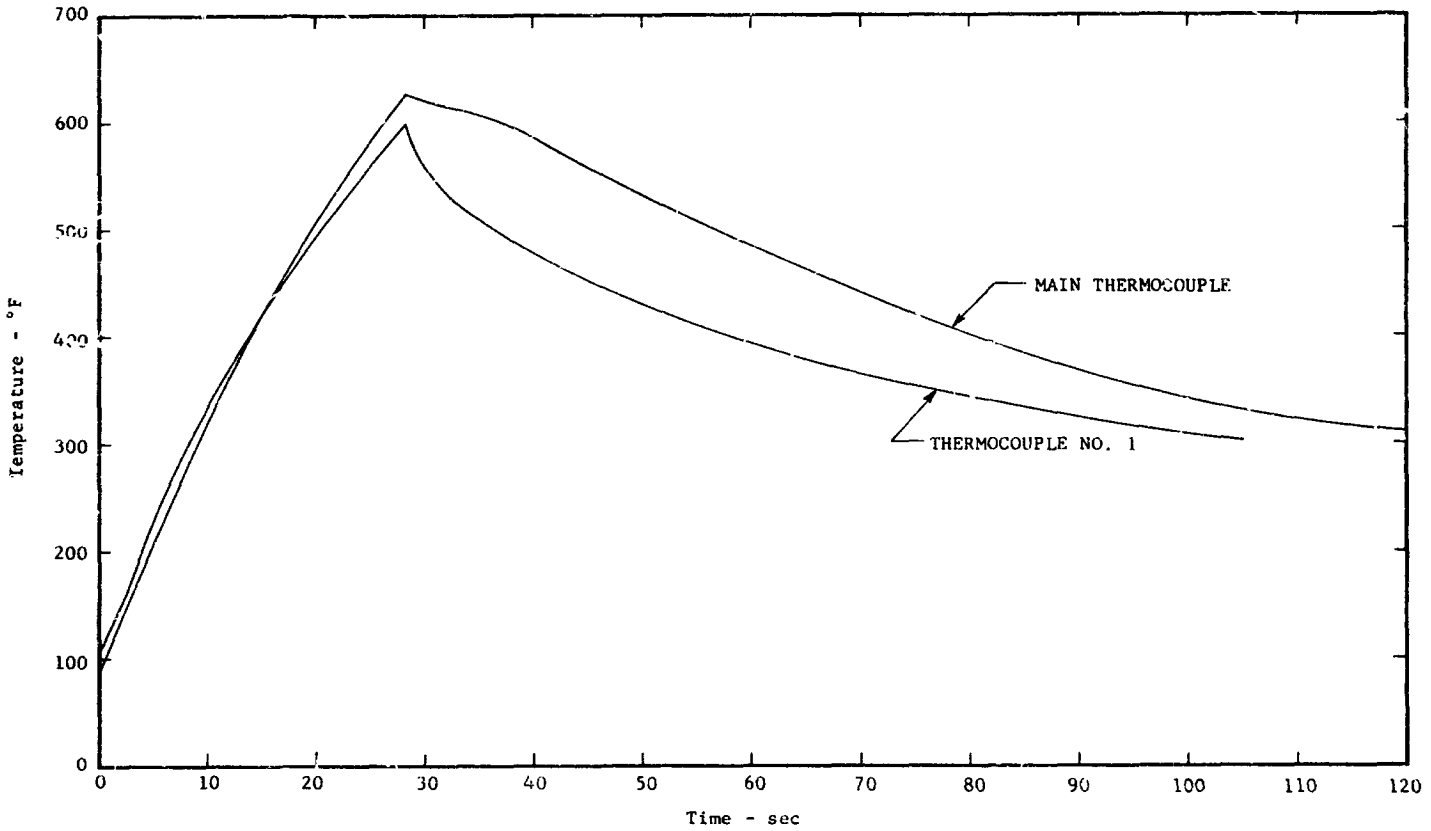

TEMPERATURE HISTORIES OF NICKEL-SLUG TOTAL CALORIMETER MOUNTED IN UNCOOLED 1/8"-THICK COPPER PLATE UNDER RADIANT HEATING
(Reference Heat Flux = 11.9 Btu/ft^2-sec)

FIGURE 60

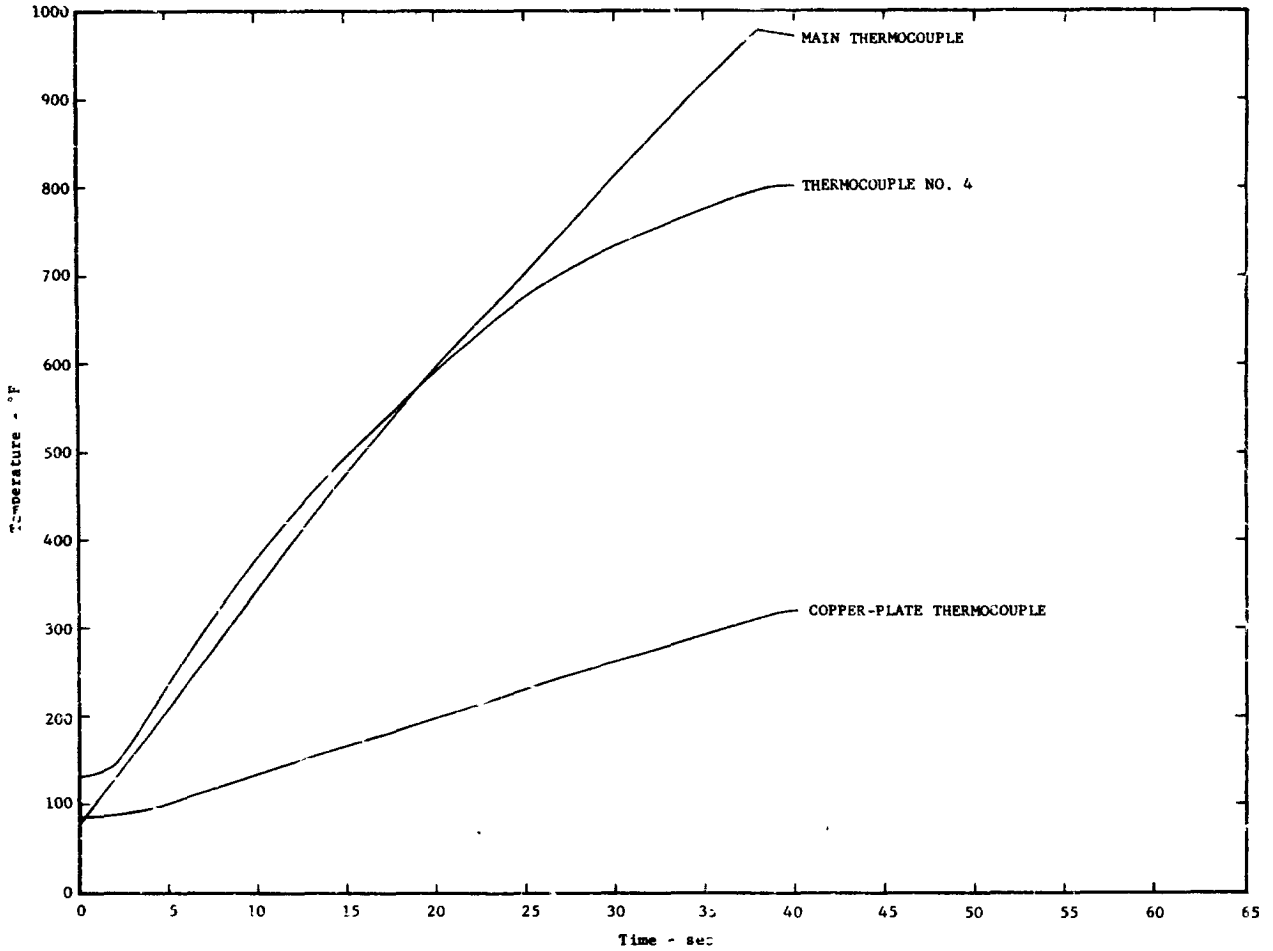

TEMPERATURE HISTORIES OF NICKEL-SLUG TOTAL CALORIMETER MOUNTED IN UNCOOLED 1/8"-THICK COPPER PLATE UNDER RADIANT HEATING
(Reference Heat Flux = 19.7 Btu/ft^2-sec)

FIGURE 61

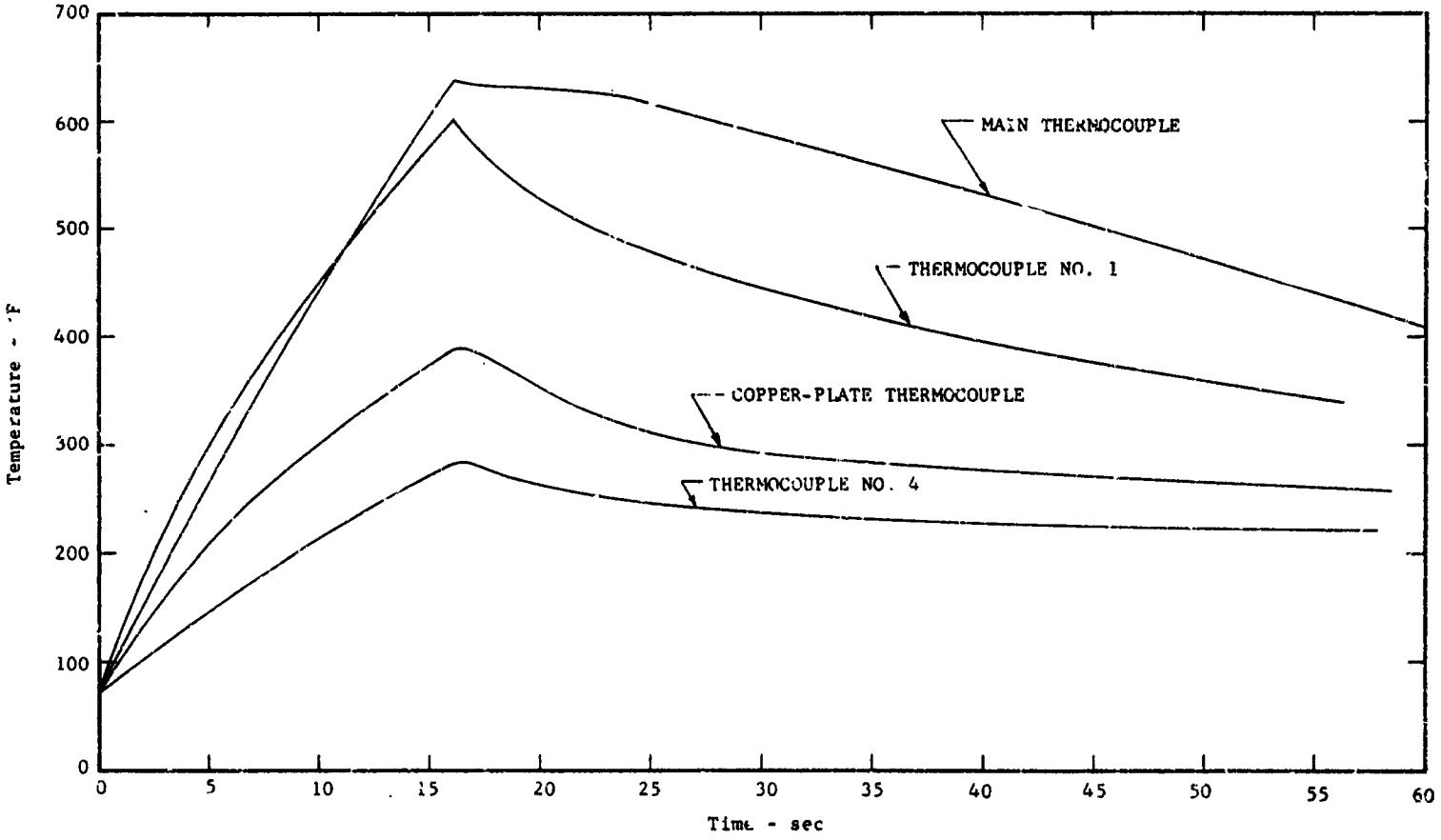

TEMPERATURE HISTORIES OF NICKEL-SLUG TOTAL CALORIMETER MOUNTED IN UNCOOLED 1/8"-THICK COPPER PLATE UNDER RADIANT HEATING
(Reference Heat Flux = 26.8 Btu/ft^2-sec)

FIGURE 62

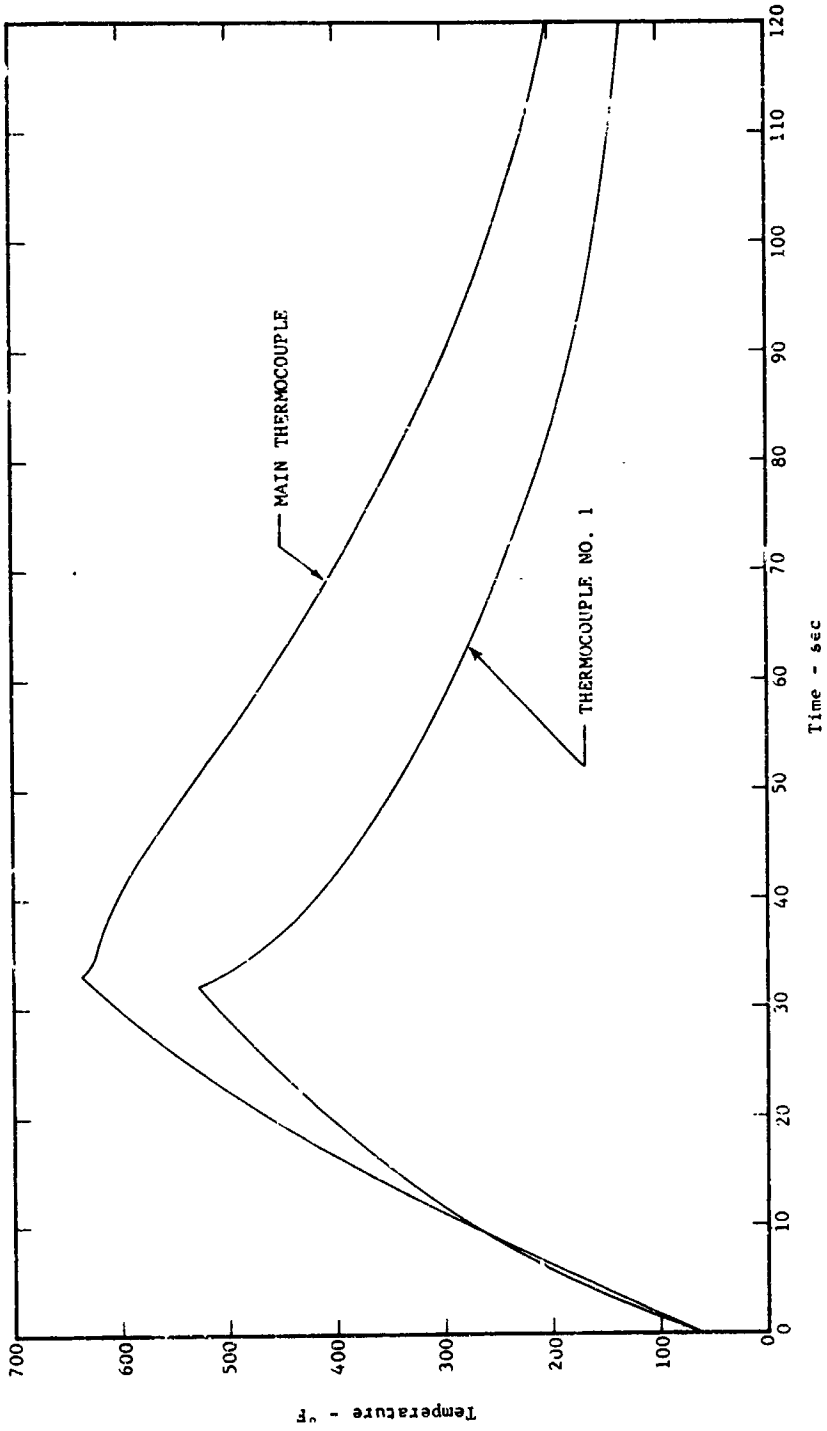

TEMPERATURE HISTORIES OF NICKEL-SLUG TOTAL CALORIMETER MOUNTED IN WATER-COOLED 1/8"-THICK COPPER PLATE UNDER RADIANT HEATING
(Reference Heat Flux = 12.6 Btu/ft^2-sec)

FIGURE 63

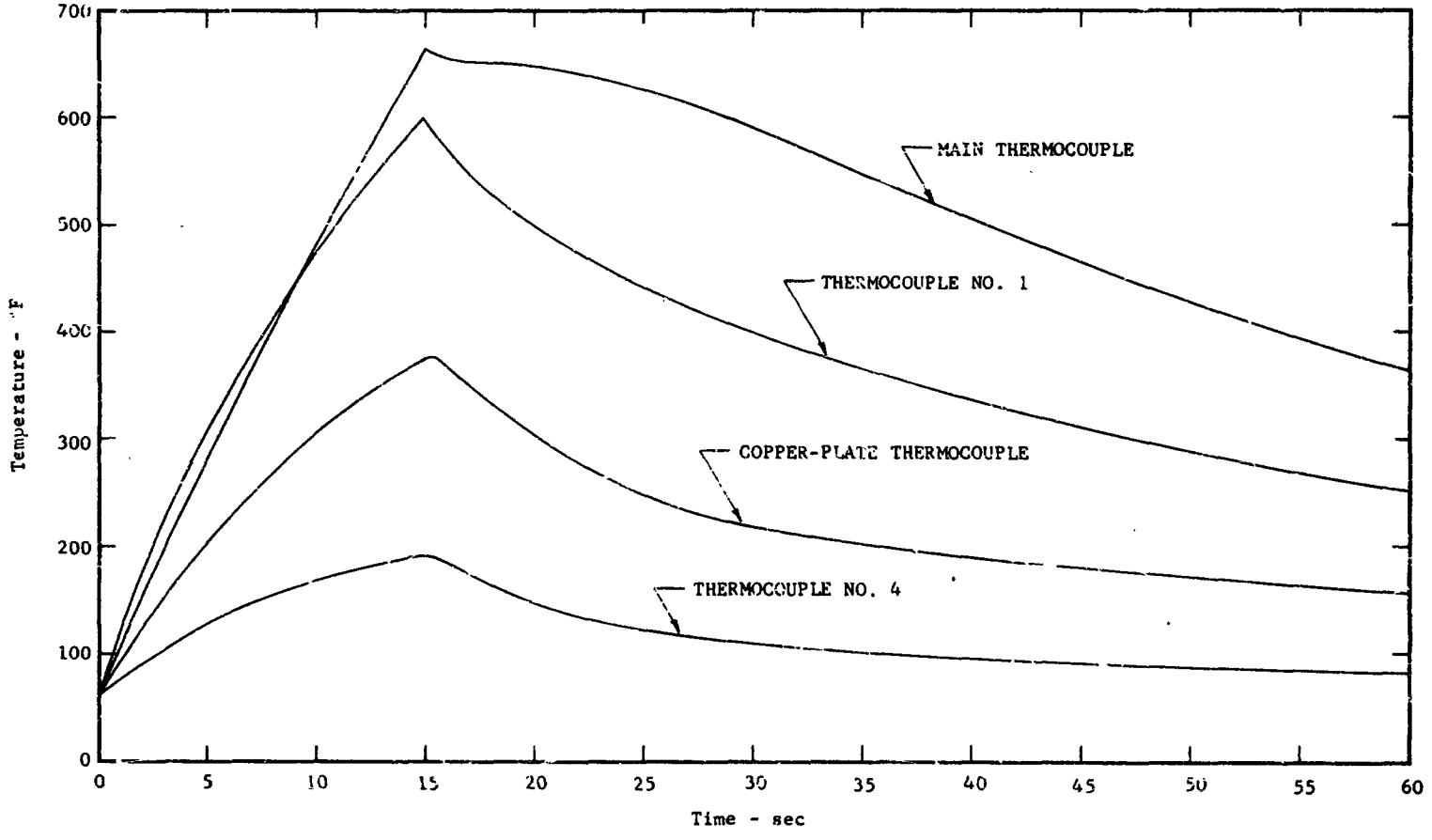

TEMPERATURE HISTORIES OF NICKEL-SLUG TOTAL CALORIMETER MOUNTED IN WATER-COOLED 1/8"-THICK COPPER PLATE UNDER RADIANT HEATING
(Reference Heat Flux = 30.9 Btu/ft^2-sec)

FIGURE 64

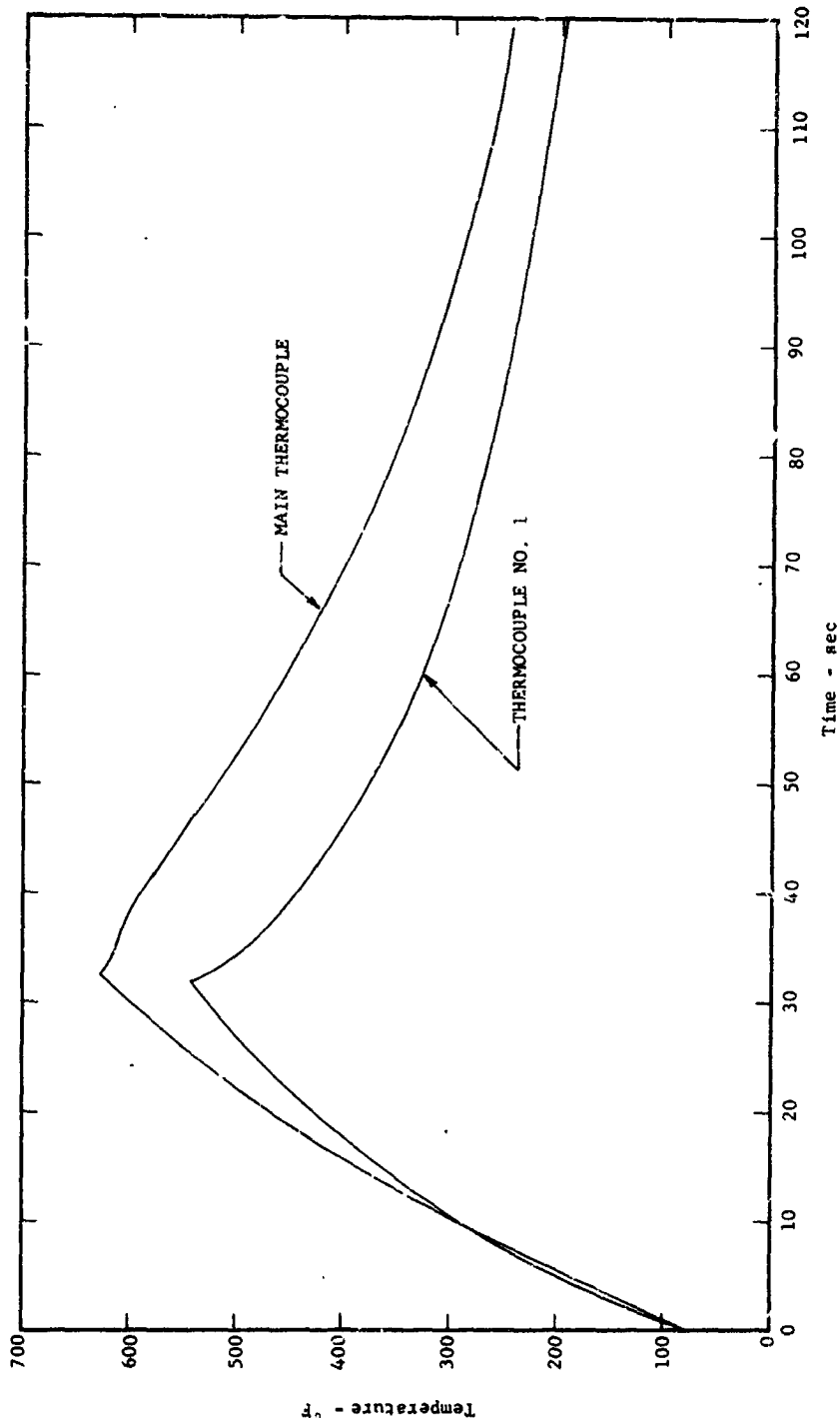

TEMPERATURE HISTORIES OF NICKEL-SLUG TOTAL CALORIMETER MOUNTED IN
TWO UNCOOLED 1/8"-THICK COPPER PLATES UNDER RADIANT HEATING
(Reference Heat Flux = 11.9 Btu/ft^2-sec)

FIGURE 65

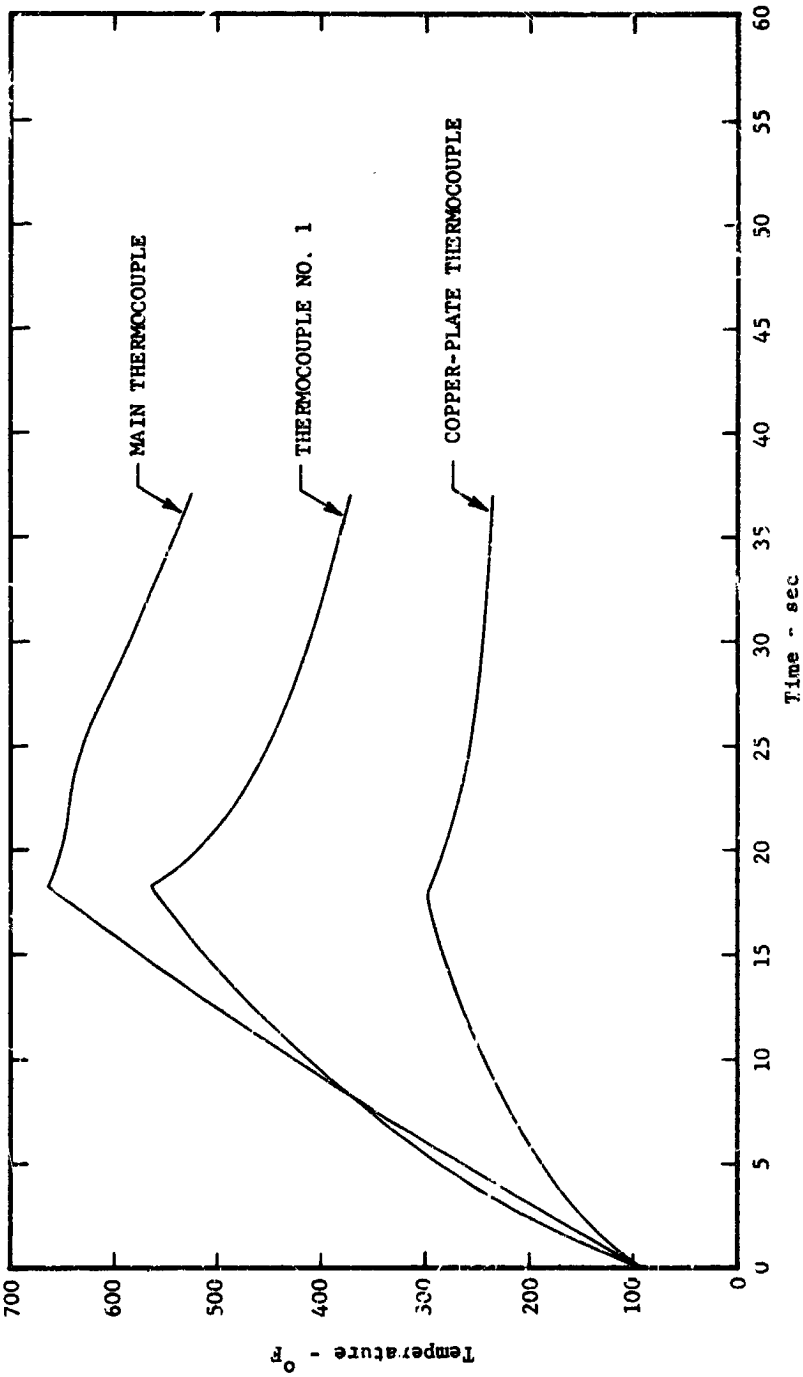

TEMPERATURE HISTORIES OF NICKEL-SLUG TOTAL CALORIMETER MOUNTED IN TWO UNCOOLED 1/8" THICK COPPER PLATES UNDER RADIANT HEATING
(Reference Heat Flux = 24.0 Btu/ft^2-sec)

FIGURE 66

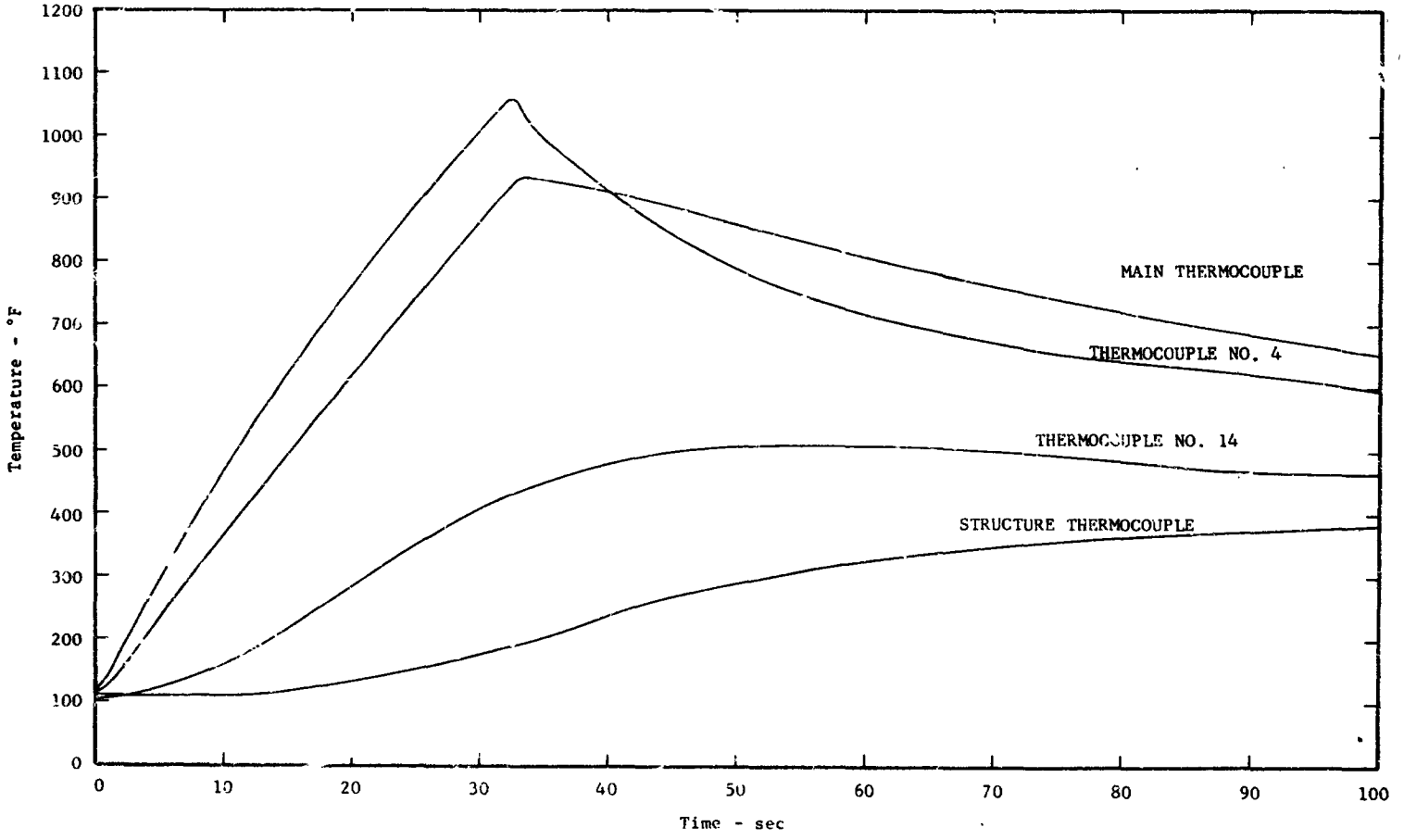

TEMPERATURE HISTORIES OF NICKEL-SLUG TOTAL CALORIMETER MOUNTED IN M-31 HEAT-SHIELD PANEL UNDER RADIANT HEATING
(Reference Heat Flux = 21.6 Btu/ft^2-sec)

FIGURE 67

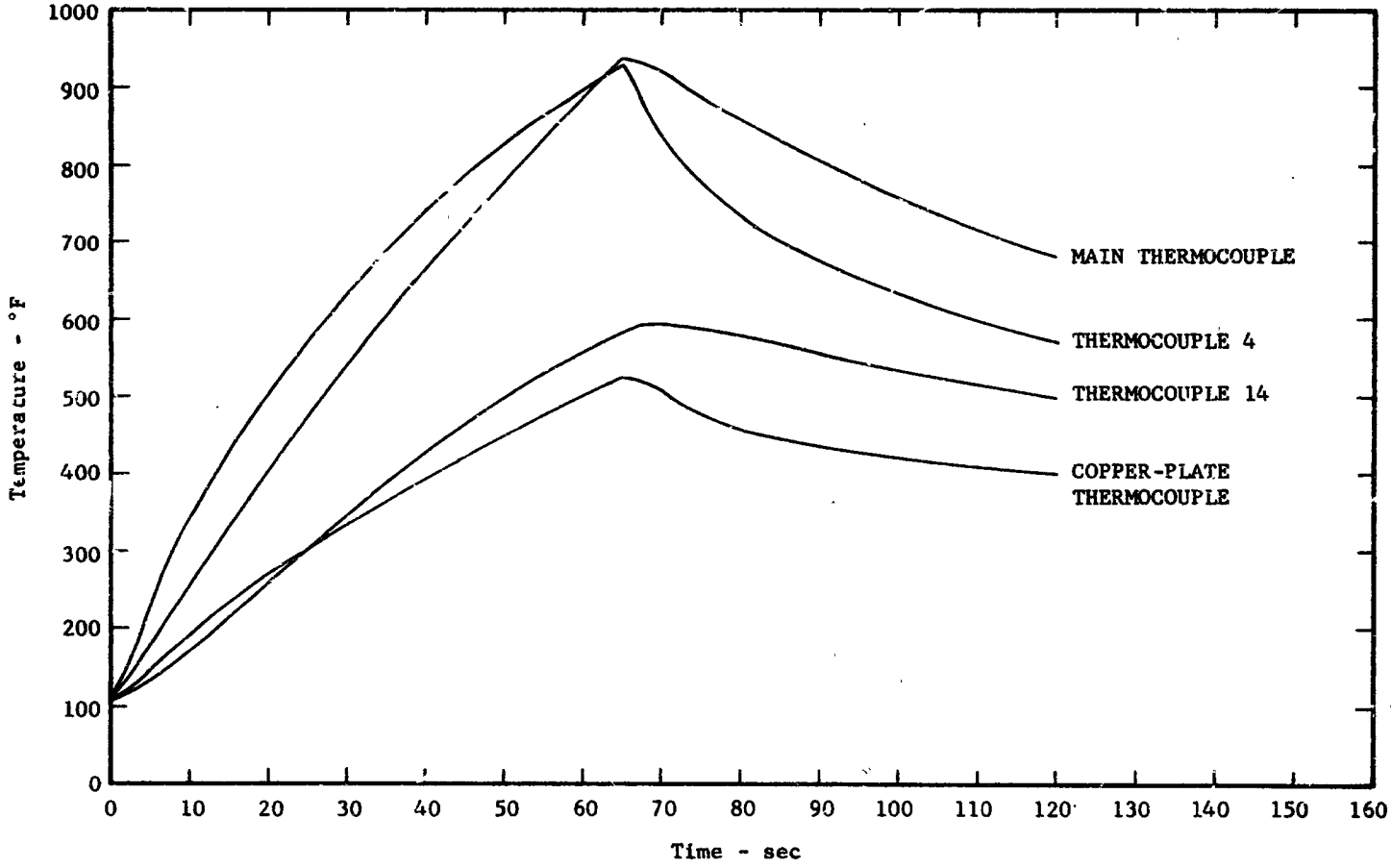

TEMPERATURE HISTORIES OF NICKEL-SLUG TOTAL CALORIMETER MOUNTED IN UNCOOLED 1/8"-THICK COPPER PLATE UNDER CONVECTIVE HEATING
(Reference Heat Flux = 10 Btu/ft^2-sec)

FIGURE 68

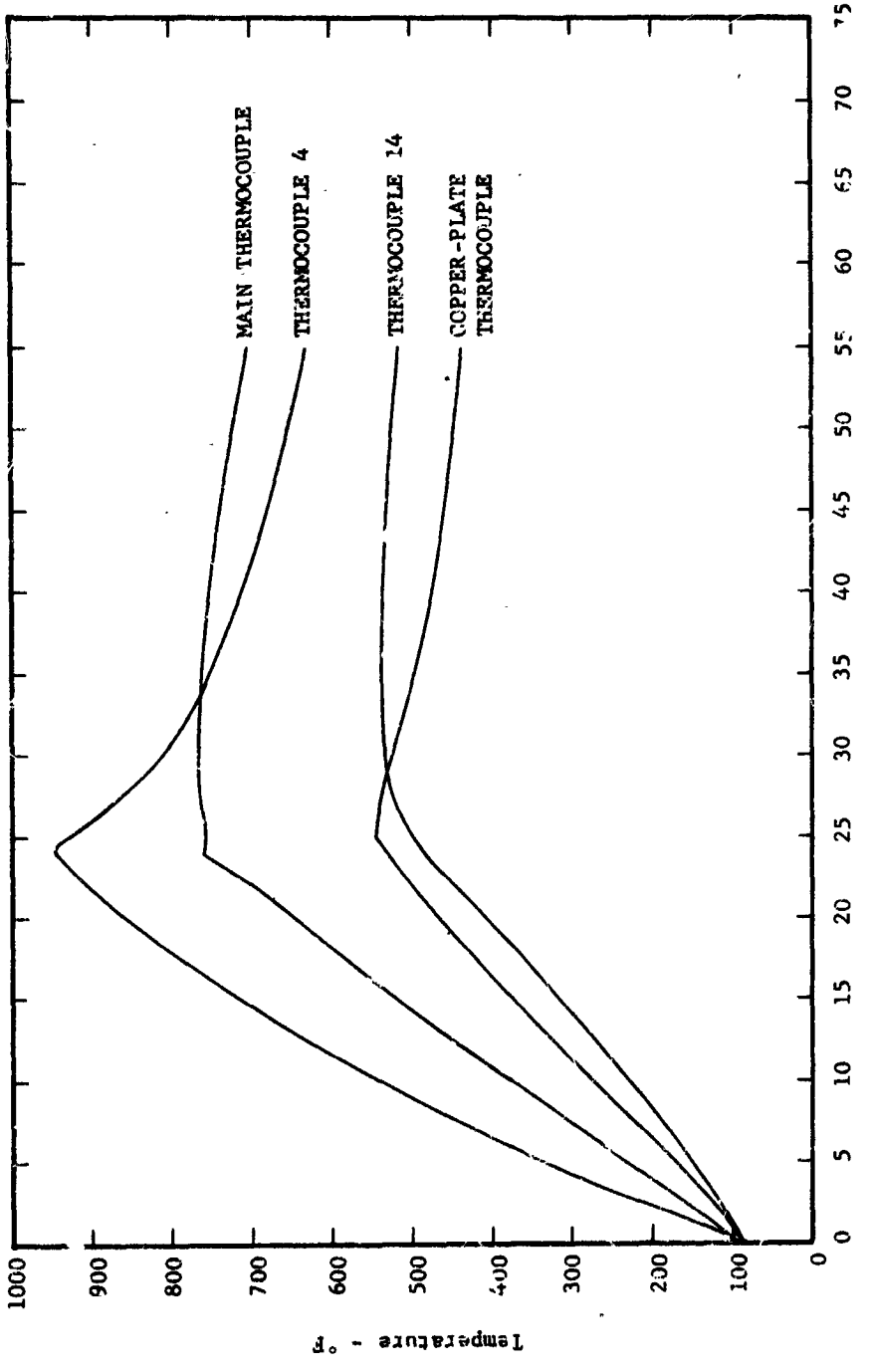

TEMPERATURE HISTORIES OF NICKEL-SLUG TOTAL CALORIMETER MOUNTED IN UNCOOLED 1/8"-THICK COPPER PLATE UNDER CONVECTIVE HEATING
(Reference Heat Flux = 18.3 Btu/ft^2-sec)

FIGURE 69

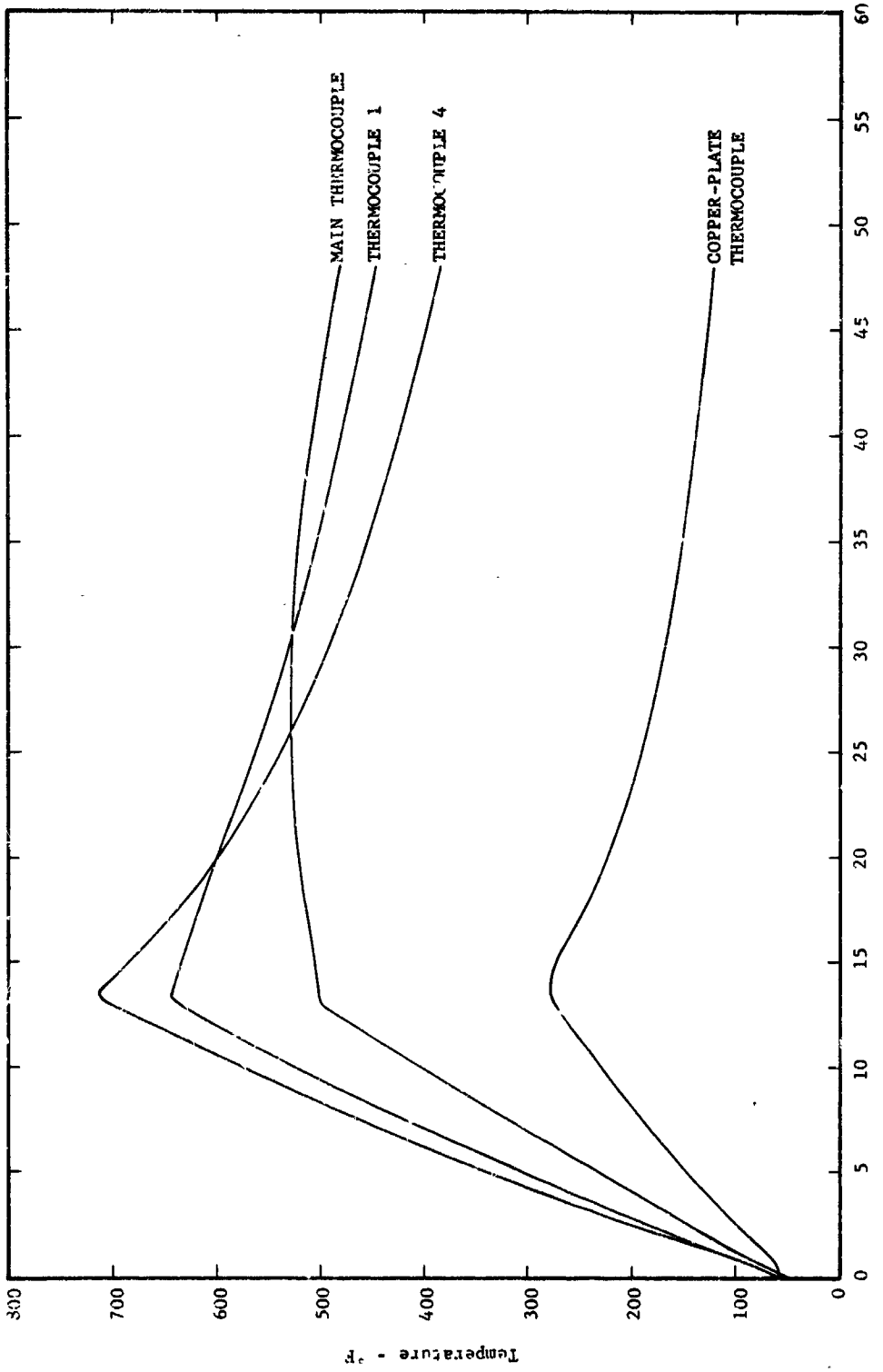

TEMPERATURE HISTORIES OF NICKEL-SLUG TOTAL CALORIMETER MOUNTED IN WATER-COOLED 1/8"-THICK COPPER PLATE UNDER CONVECTIVE HEATING
(Reference Heat Flux = 23.8 Btu/ft^2-sec)

FIGURE 70

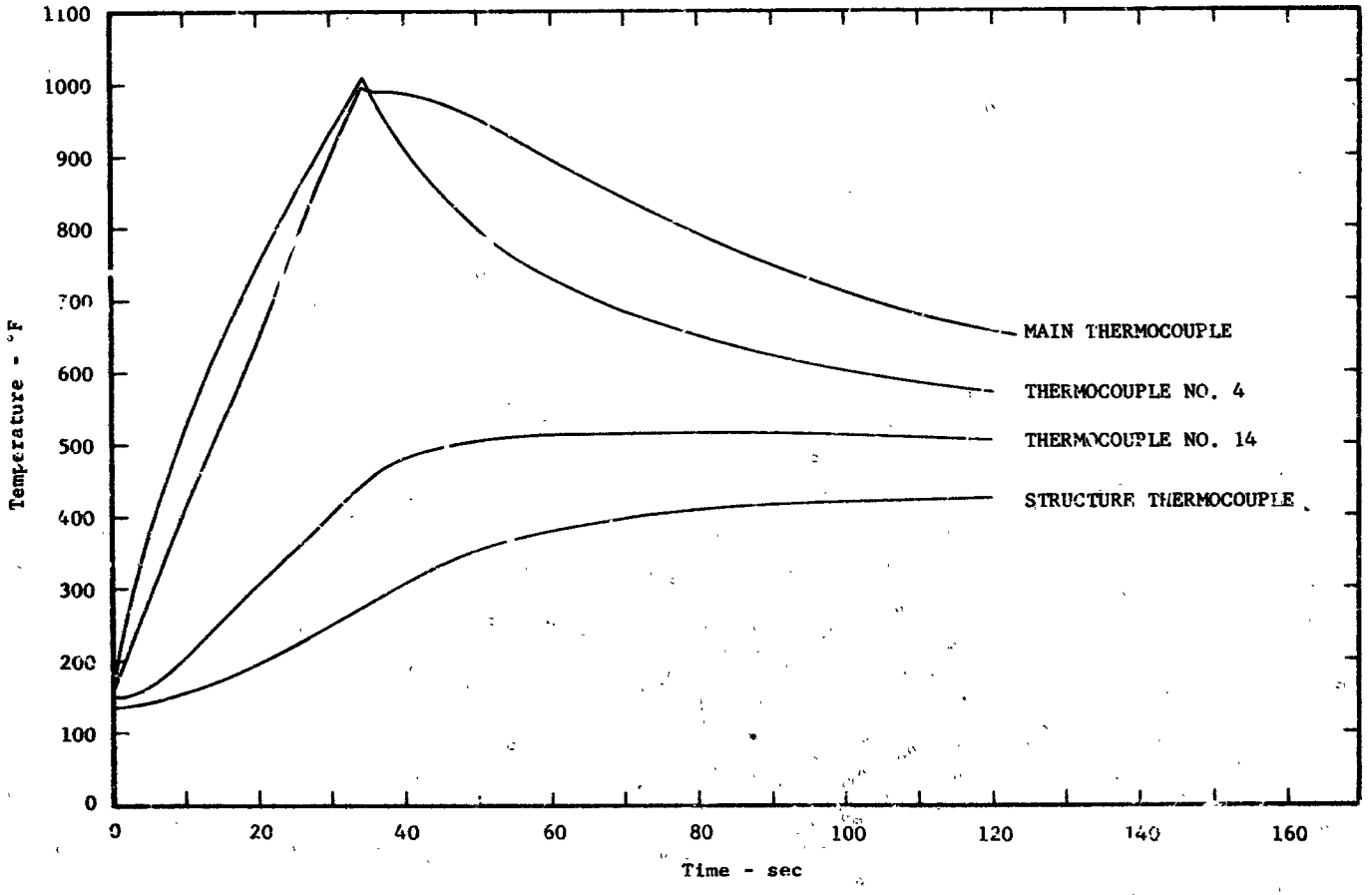

TEMPERATURE HISTORIES OF NICKEL-SLUG TOTAL CALORIMETER MOUNTED IN M-31 HEAT-SHIELD PANEL UNDER CONVECTIVE HEATING
(Reference Heat Flux = 15.4 Btu/ft^2-sec)

FIGURE 71

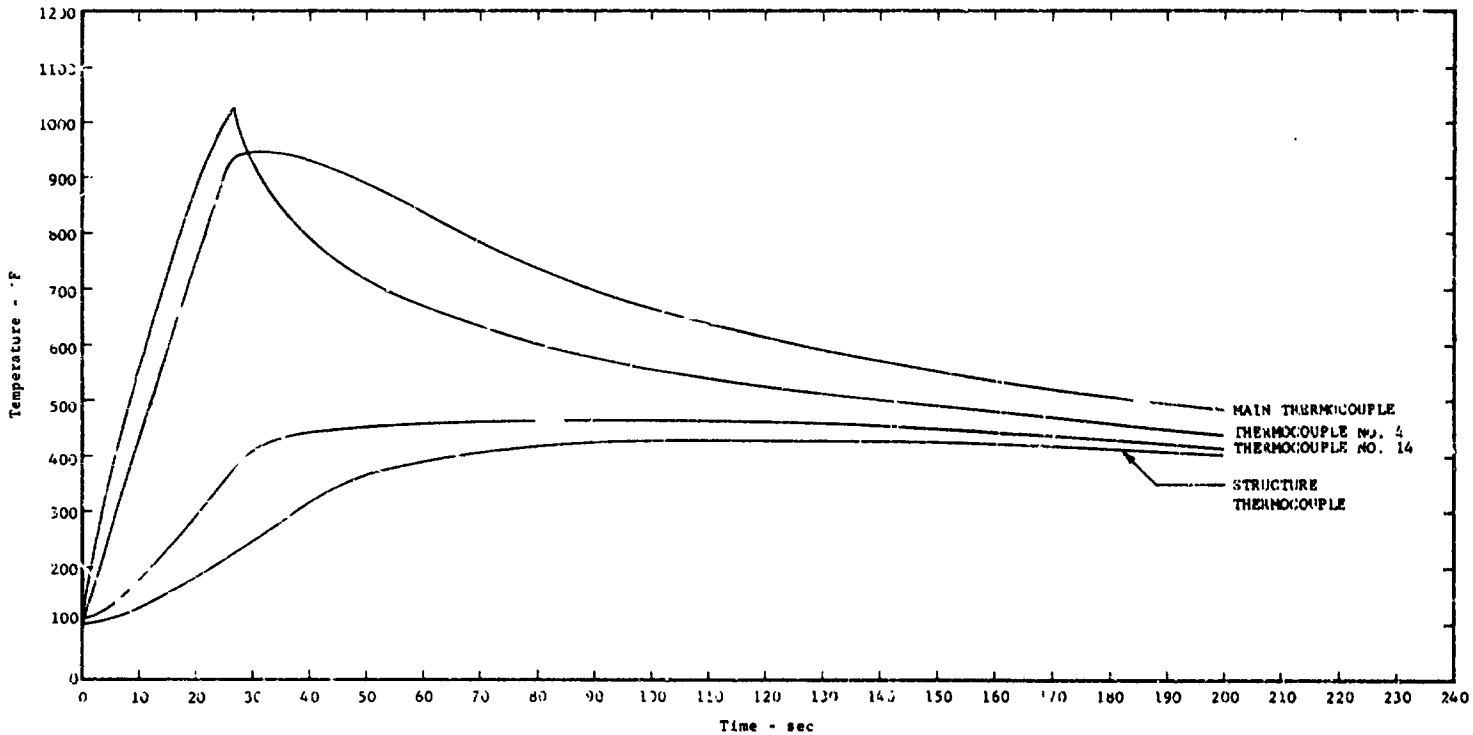

TEMPERATURE HISTORIES OF NICKEL-SLUG TOTAL CALORIMETER MOUNTED IN M-31 HEAT-SHIELD PANEL UNDER CONVECTIVE HEATING

(Reference Heat Flux = 20.12 Btu/ft^2-sec)

FIGURE 72

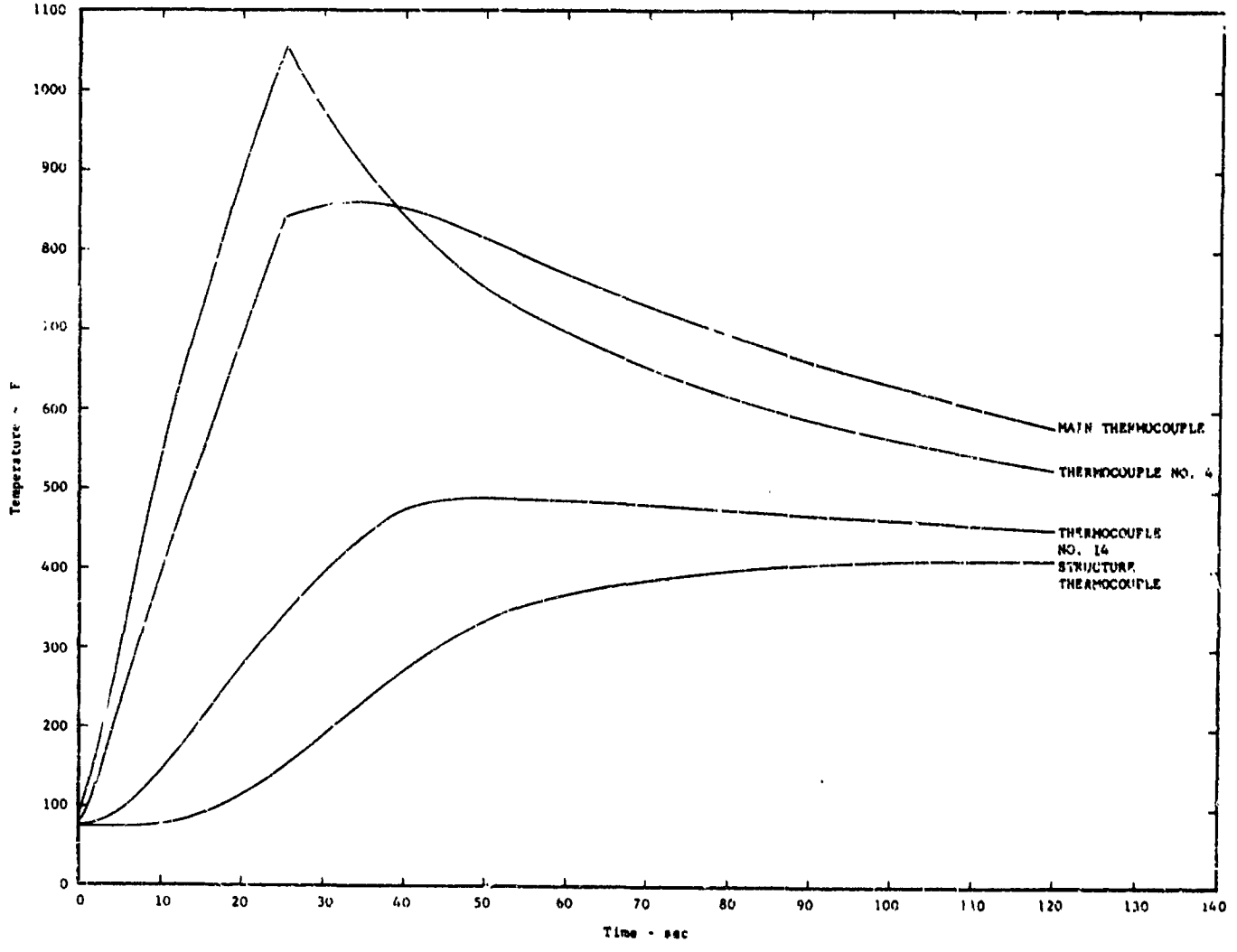

TEMPERATURE HISTORIES OF NICKEL-SLUG TOTAL CALORIMETER MOUNTED IN M-31 HEAT-SHIELD PANEL UNDER COMBINED RADIANT-CONVECTIVE HEATING
(Reference Heat Flux = 19.5 Btu/ft^2-sec)

FIGURE 73

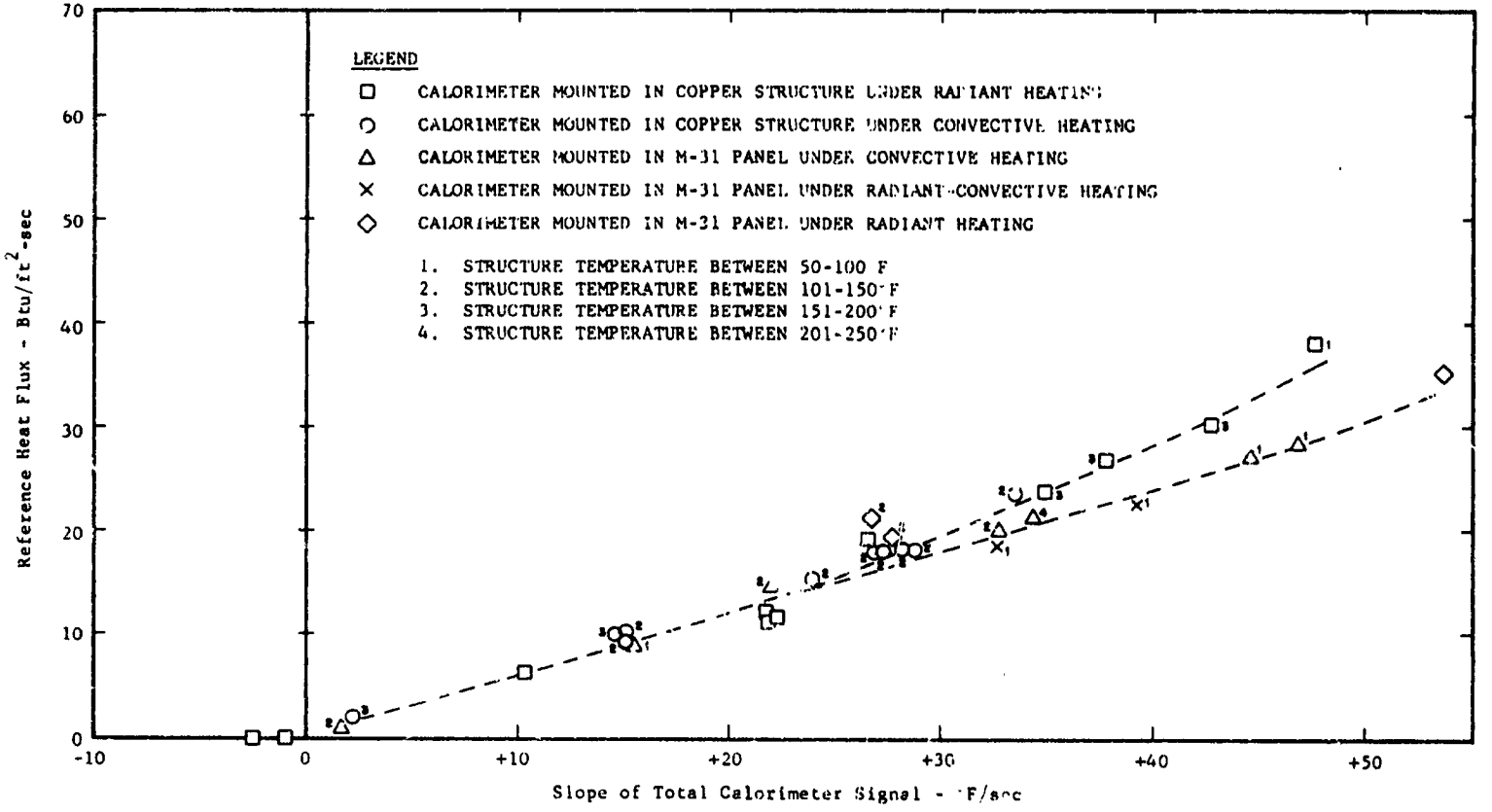

NICKEL-SLUG TOTAL CALORIMETER CALIBRATION AT 200°F FOR INDICATED CONDITIONS

FIGURE 74

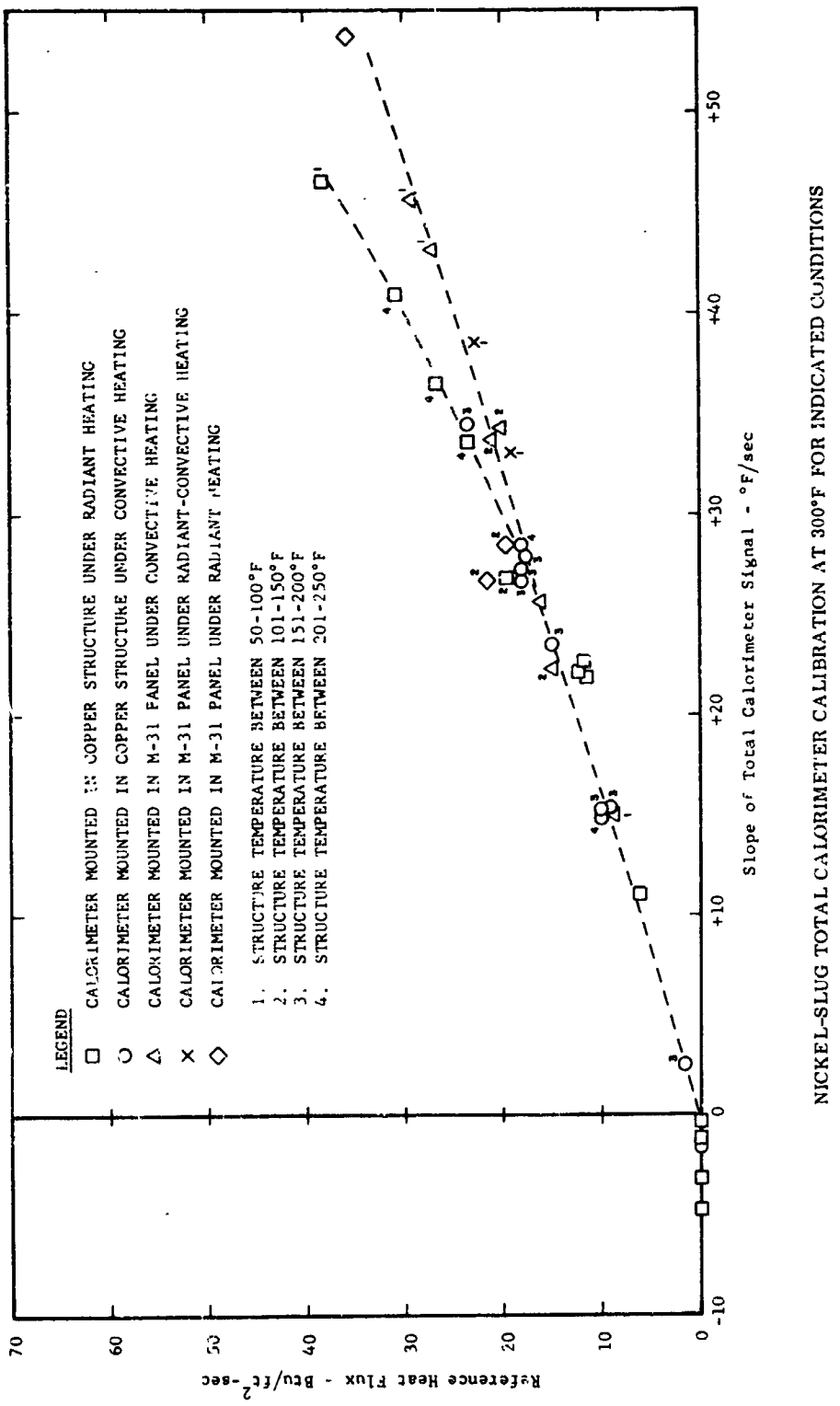

NICKEL-SLUG TOTAL CALORIMETER CALIBRATION AT 300°F FOR INDICATED CONDITIONS

FIGURE 75

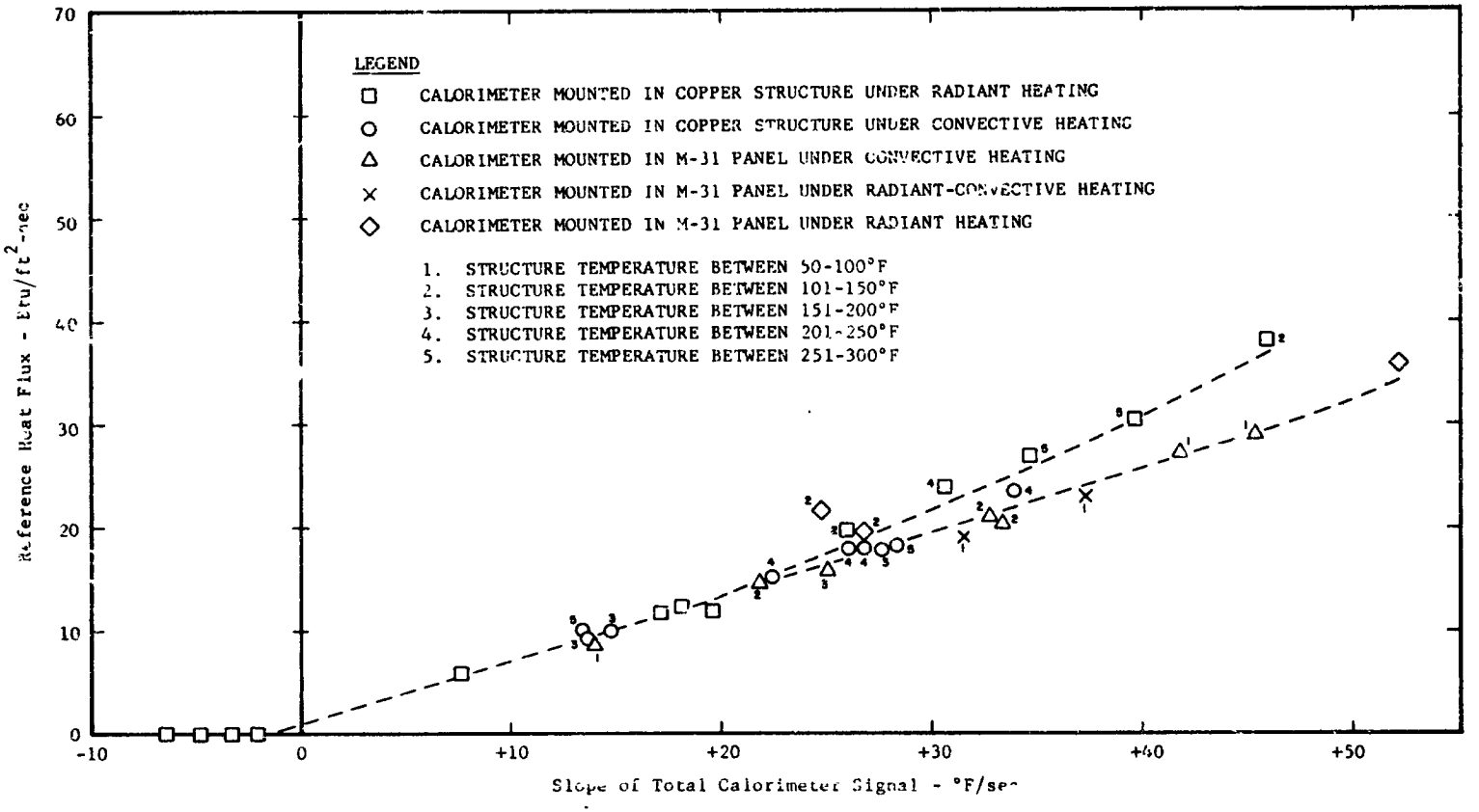

NICKEL-SLUG TOTAL CALORIMETER CALIBRATION AT 400°F FOR INDICATED CONDITIONS

FIGURE 76

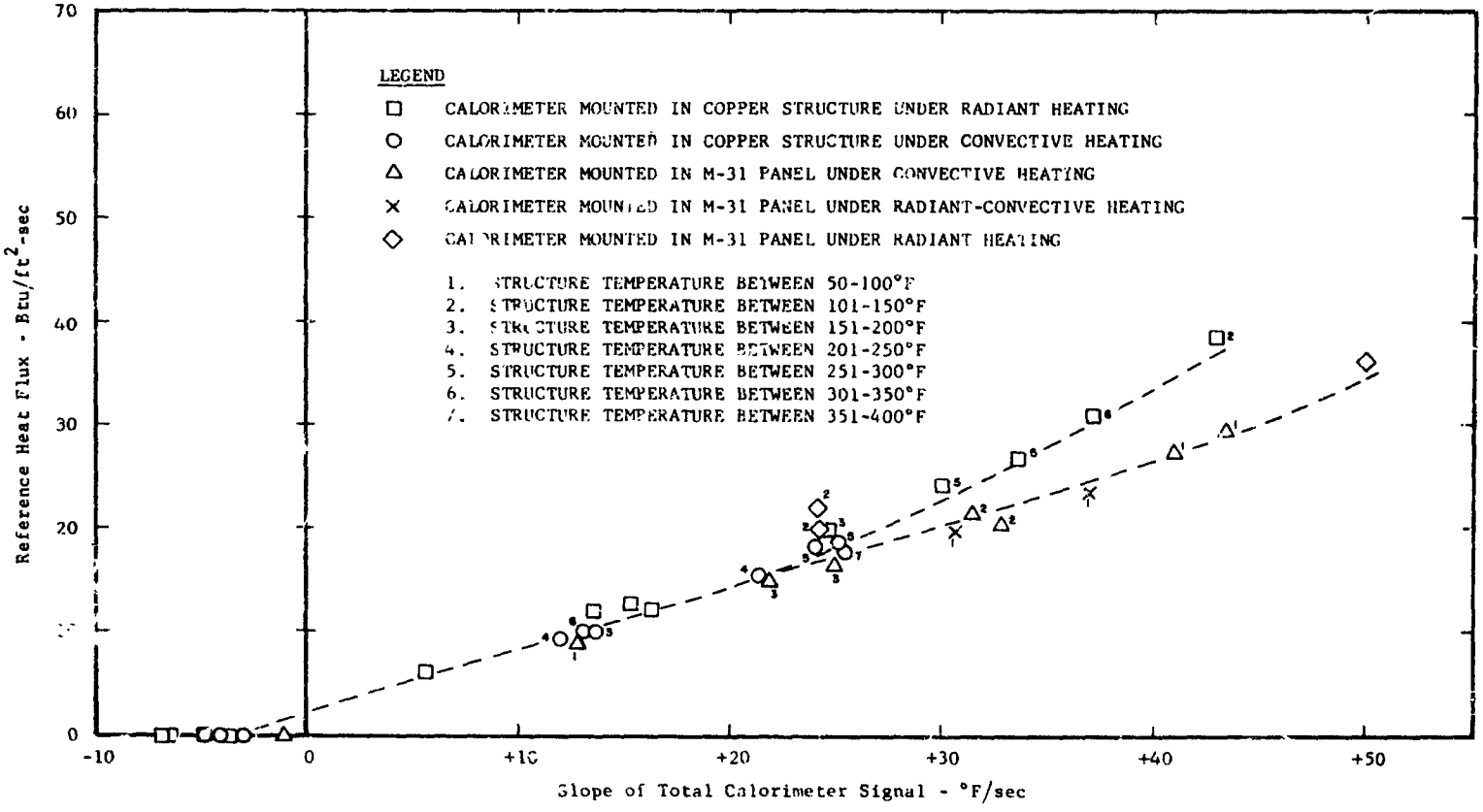

NICKEL-SLUG TOTAL CALORIMETER CALIBRATION AT 500°F FOR INDICATED CONDITIONS

FIGURE 77

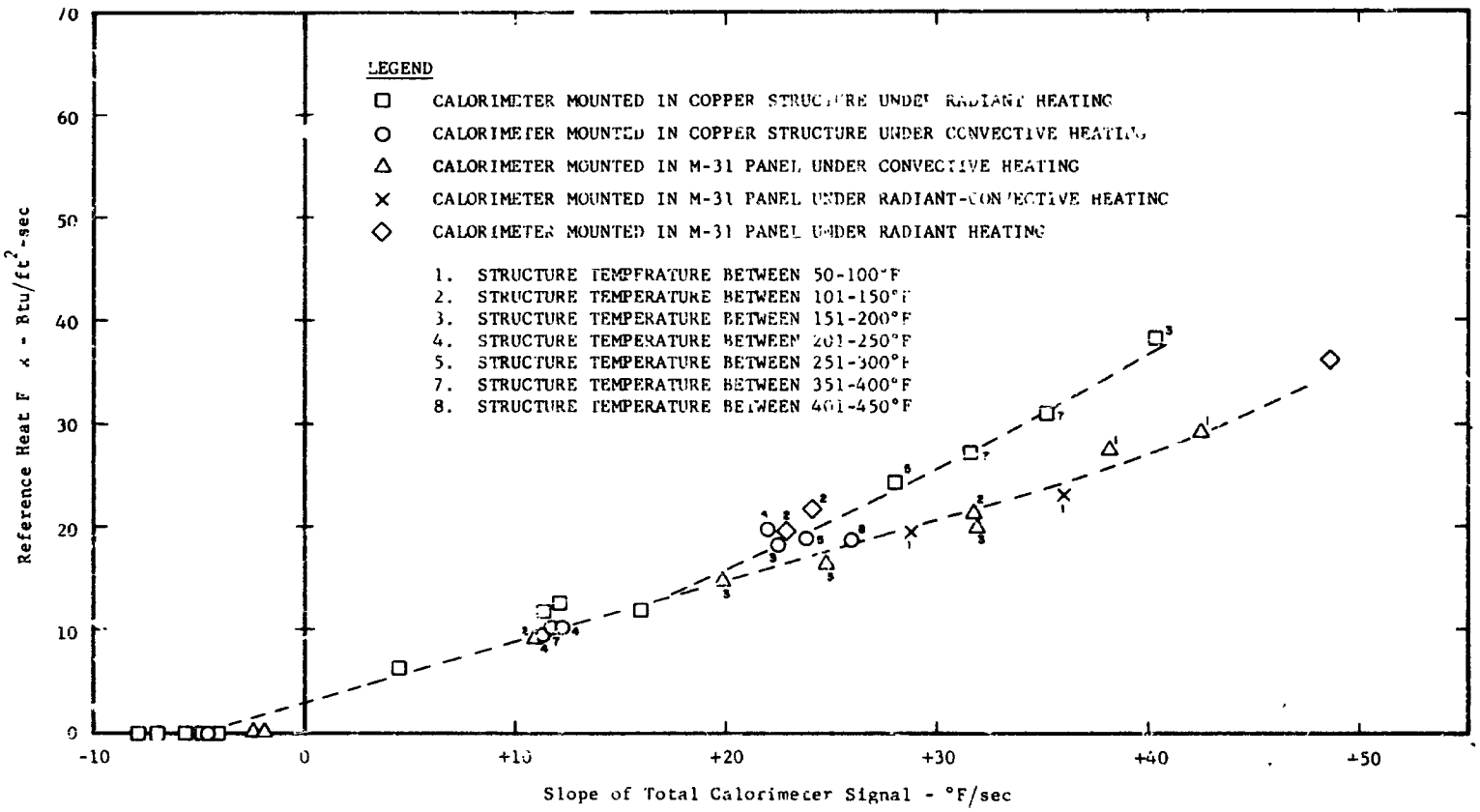

NICKEL-SLUG TOTAL CALORIMETER CALIBRATION AT 600°F FOR INDICATED CONDITIONS

FIGURE 78

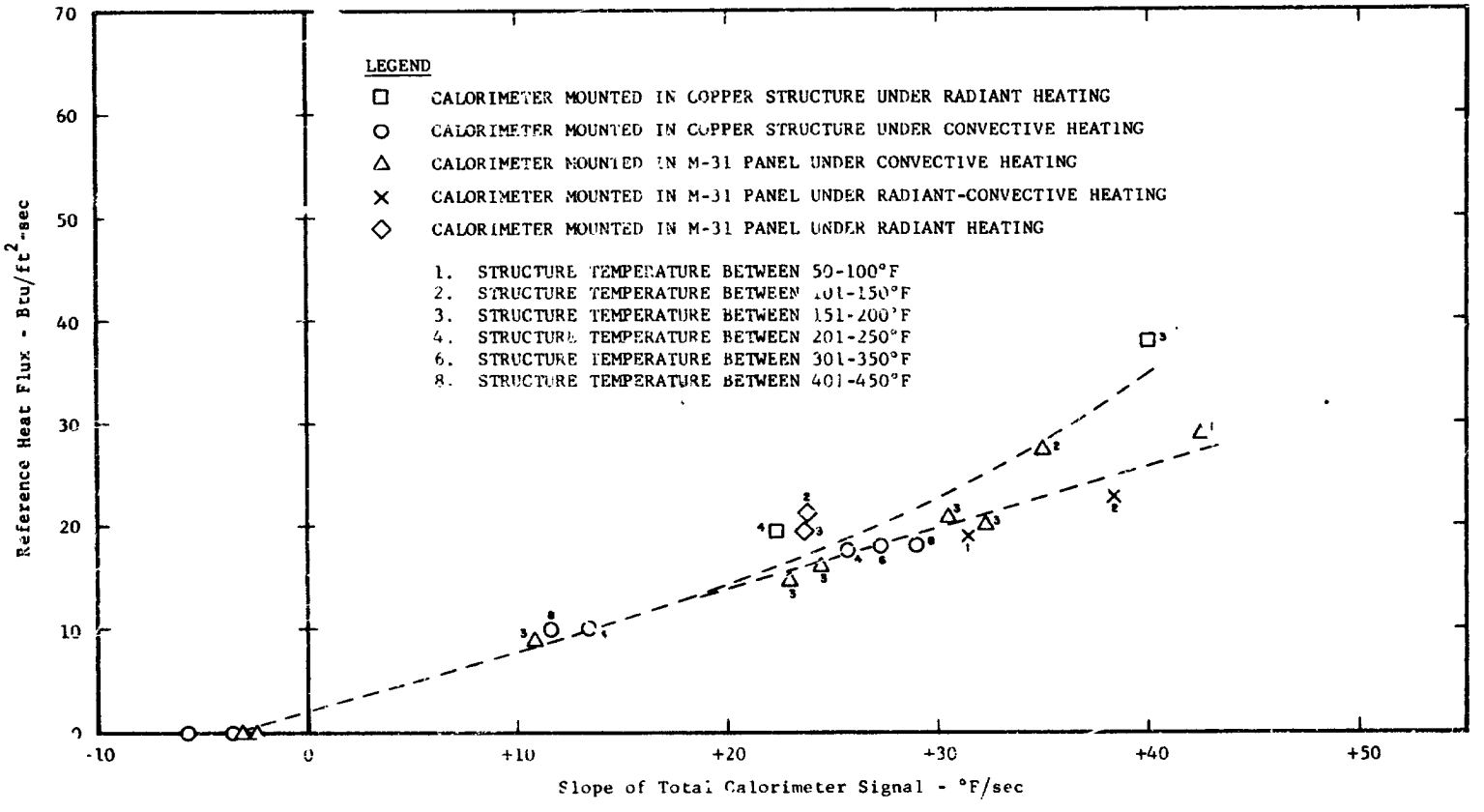

NICKEL-SLUG TOTAL CALORIMETER CALIBRATION AT 700°F FOR INDICATED CONDITIONS

FIGURE 79

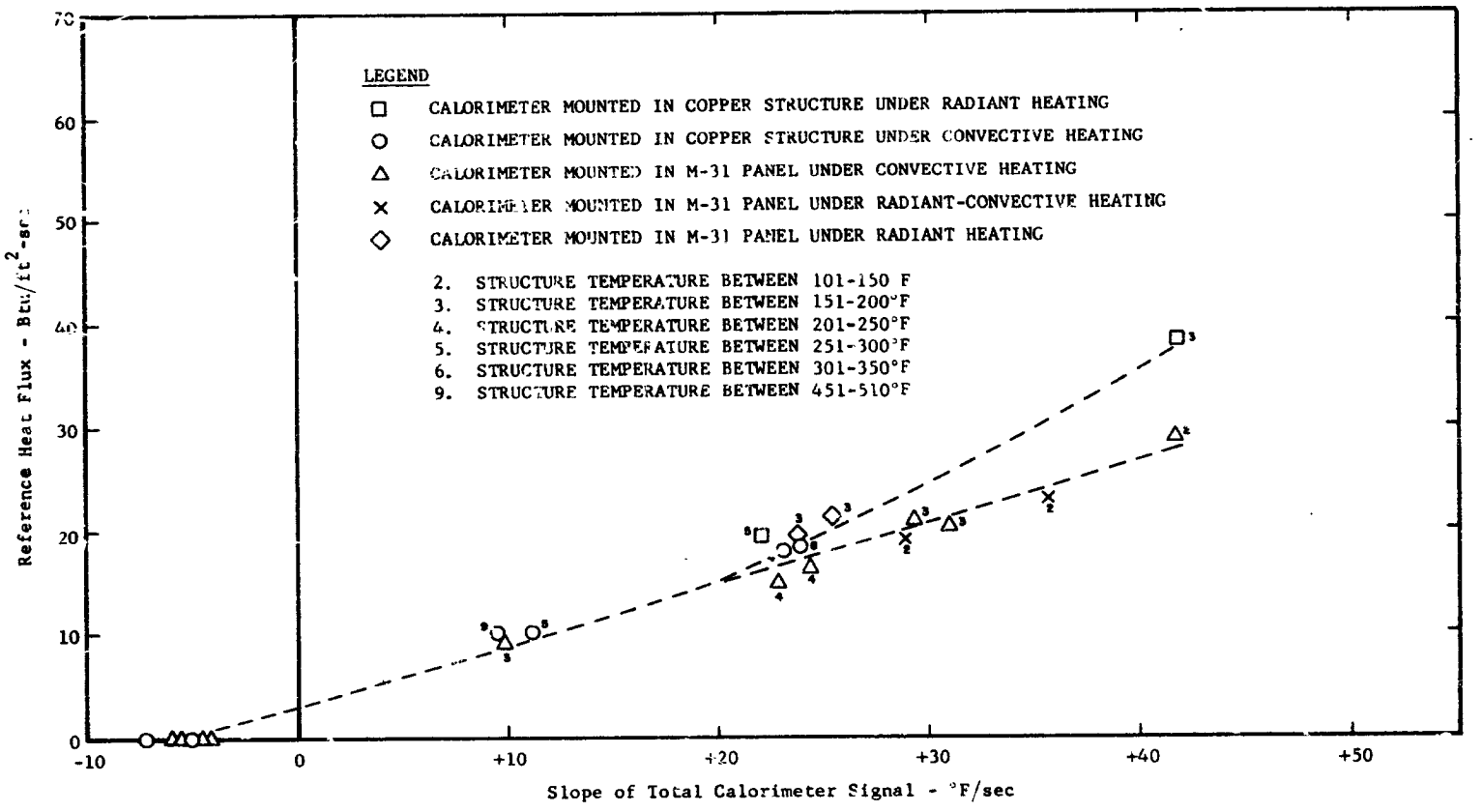

NICKEL-SLUG TOTAL CALORIMETER CALIBRATION AT 800°F FOR INDICATED CONDITIONS

FIGURE 80

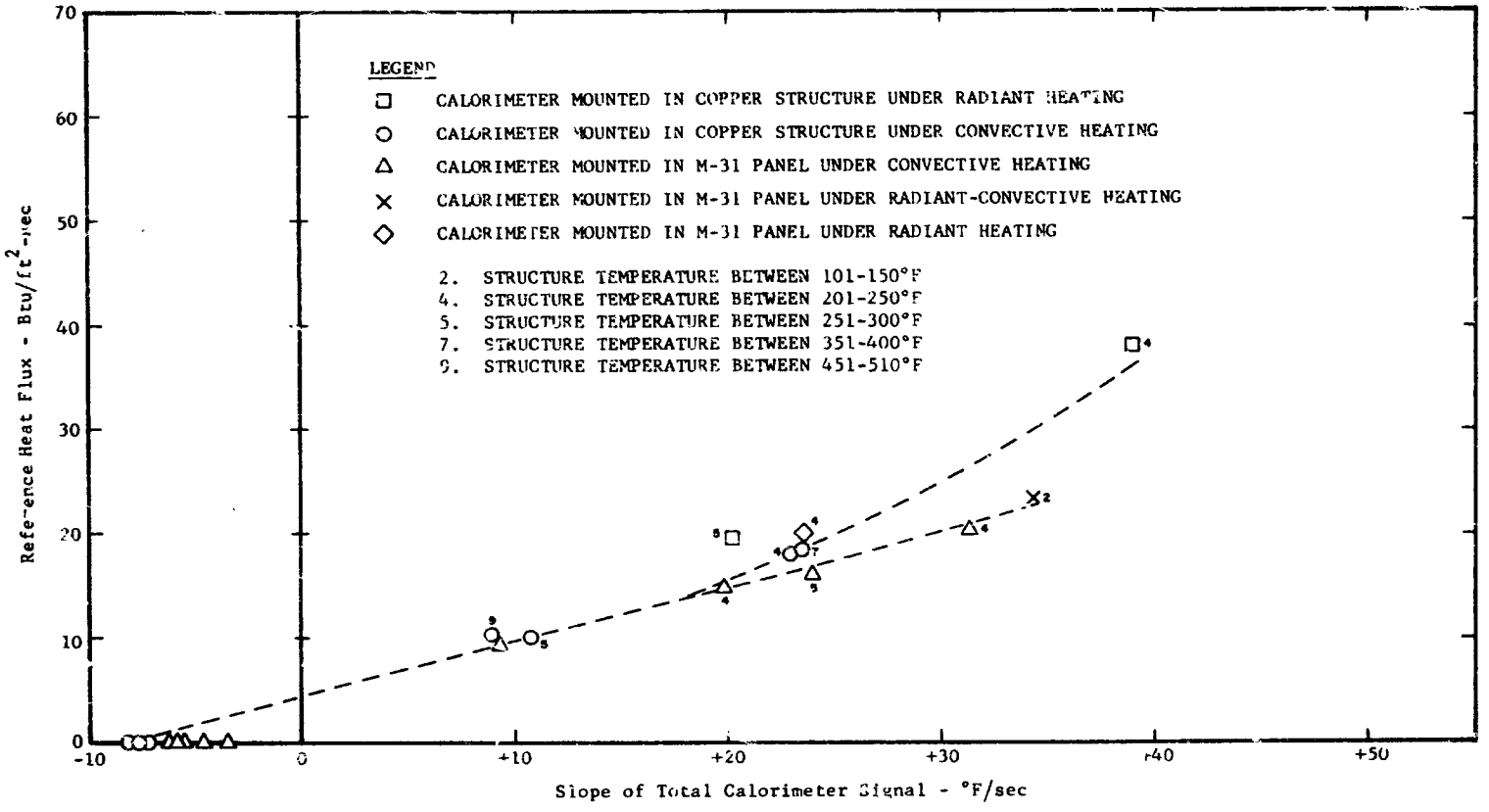

NICKEL-SLUG TOTAL CALORIMETER CALIBRATION AT 900°F FOR INDICATED CONDITIONS

FIGURE 81

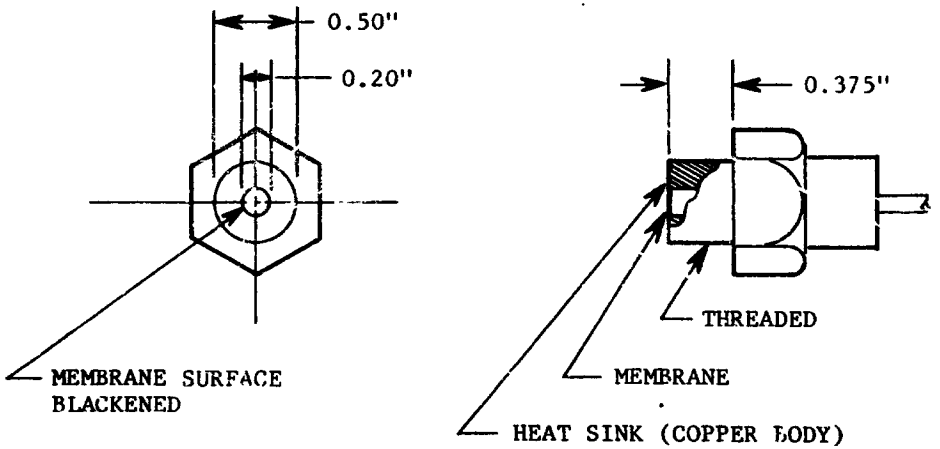

DIMENSIONS OF MEMBRANE TOTAL CALORIMETER

FIGURE 82

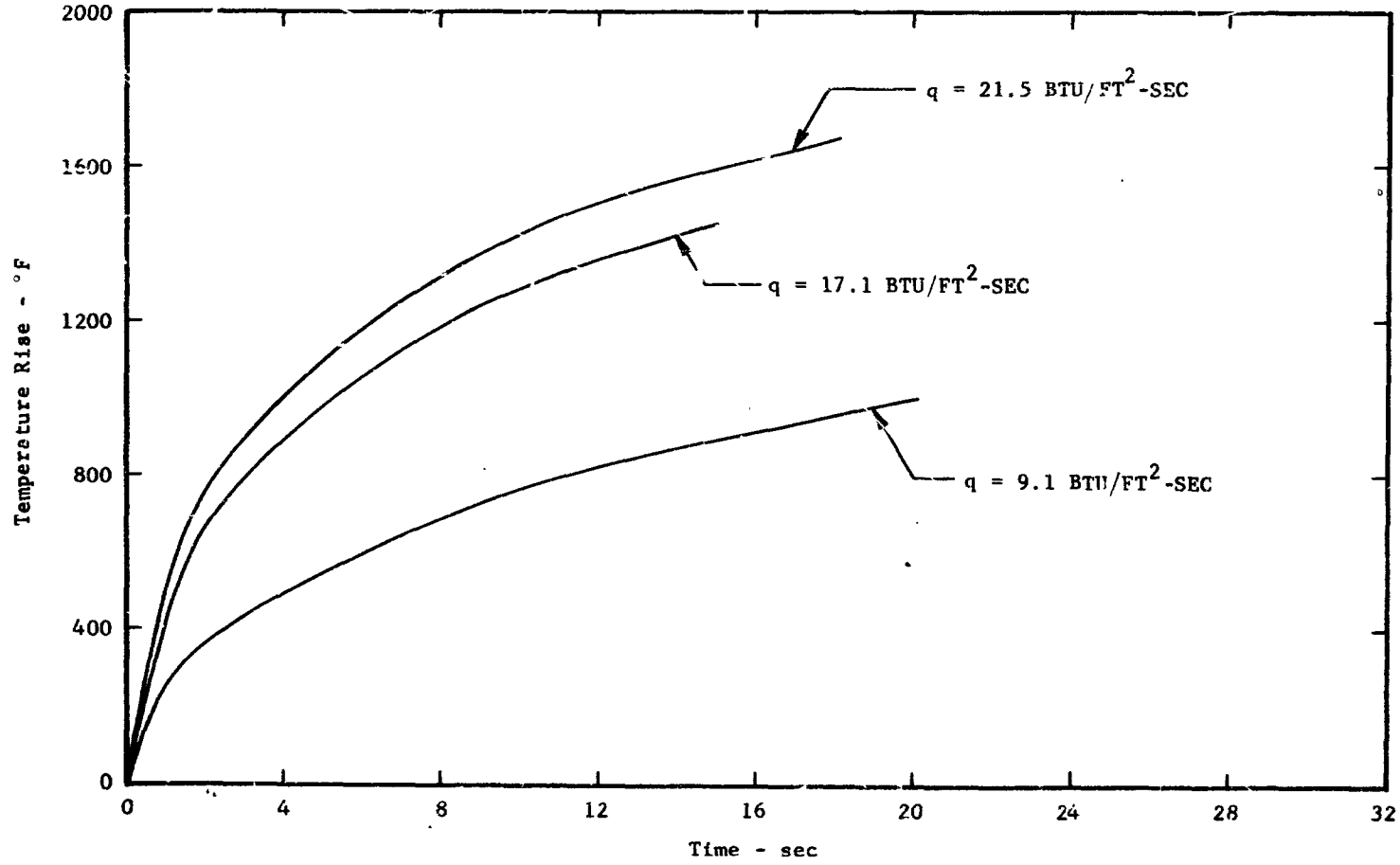

SURFACE-TEMPERATURE RISE OF SMOOTH FIRE BRICK UNDER CONVECTIVE HEATING
6.0 INCHES DOWNSTREAM FROM POINT OF BOUNDARY-LAYER INCEPTION

FIGURE 83

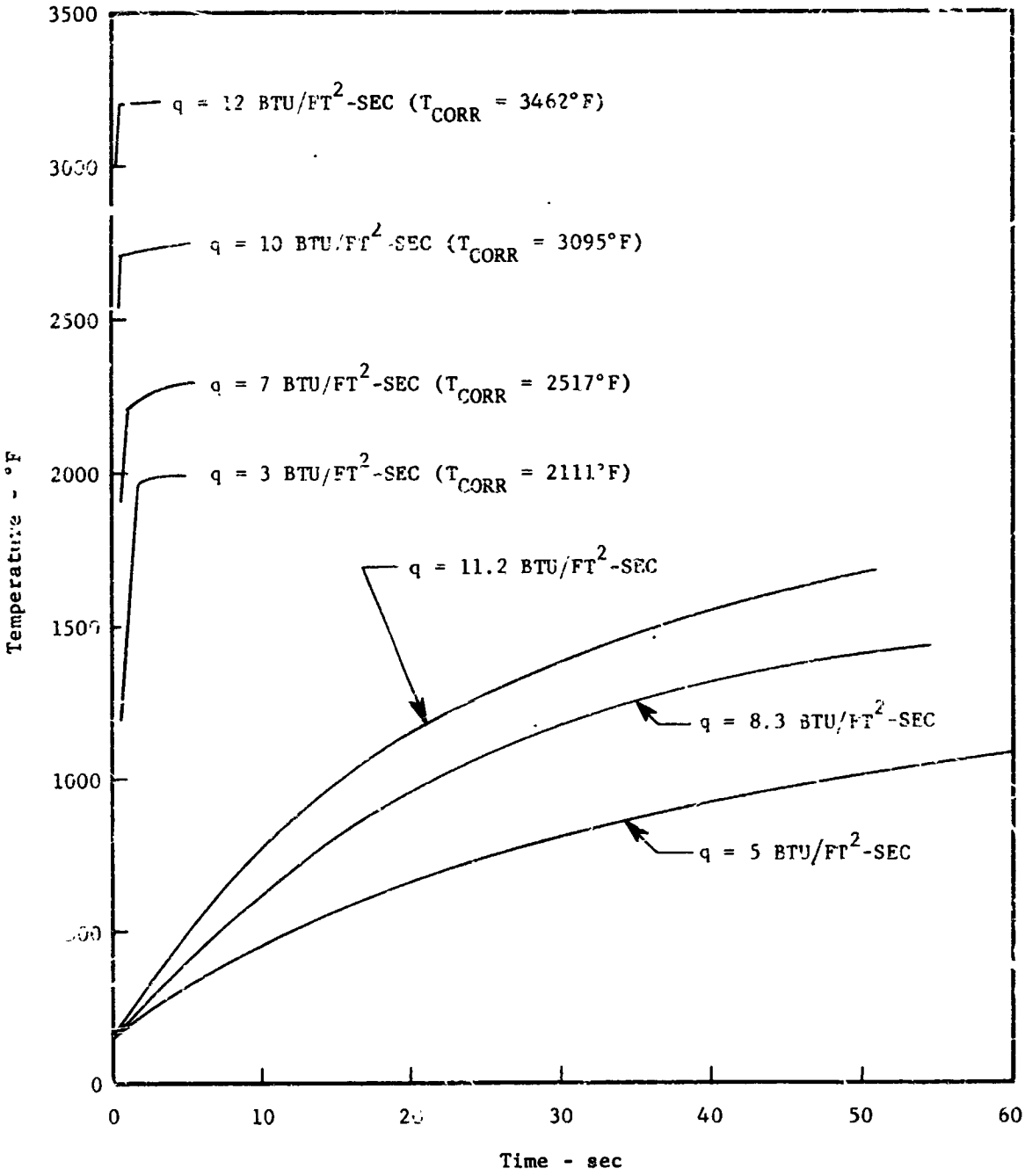

M-31 HEAT-SHIELD-PANEL SURFACE-TEMPERATURE AND FREE-STREAM GAS-TEMPERATURE MEASUREMENTS UNDER CONVECTIVE HEATING 31.6 INCHES DOWNSTREAM FROM POINT OF BOUNDARY-LAYER INCEPTION

FIGURE 84

American-Standard
ADVANCED TECHNOLOGY LABORATORIES DIVISION

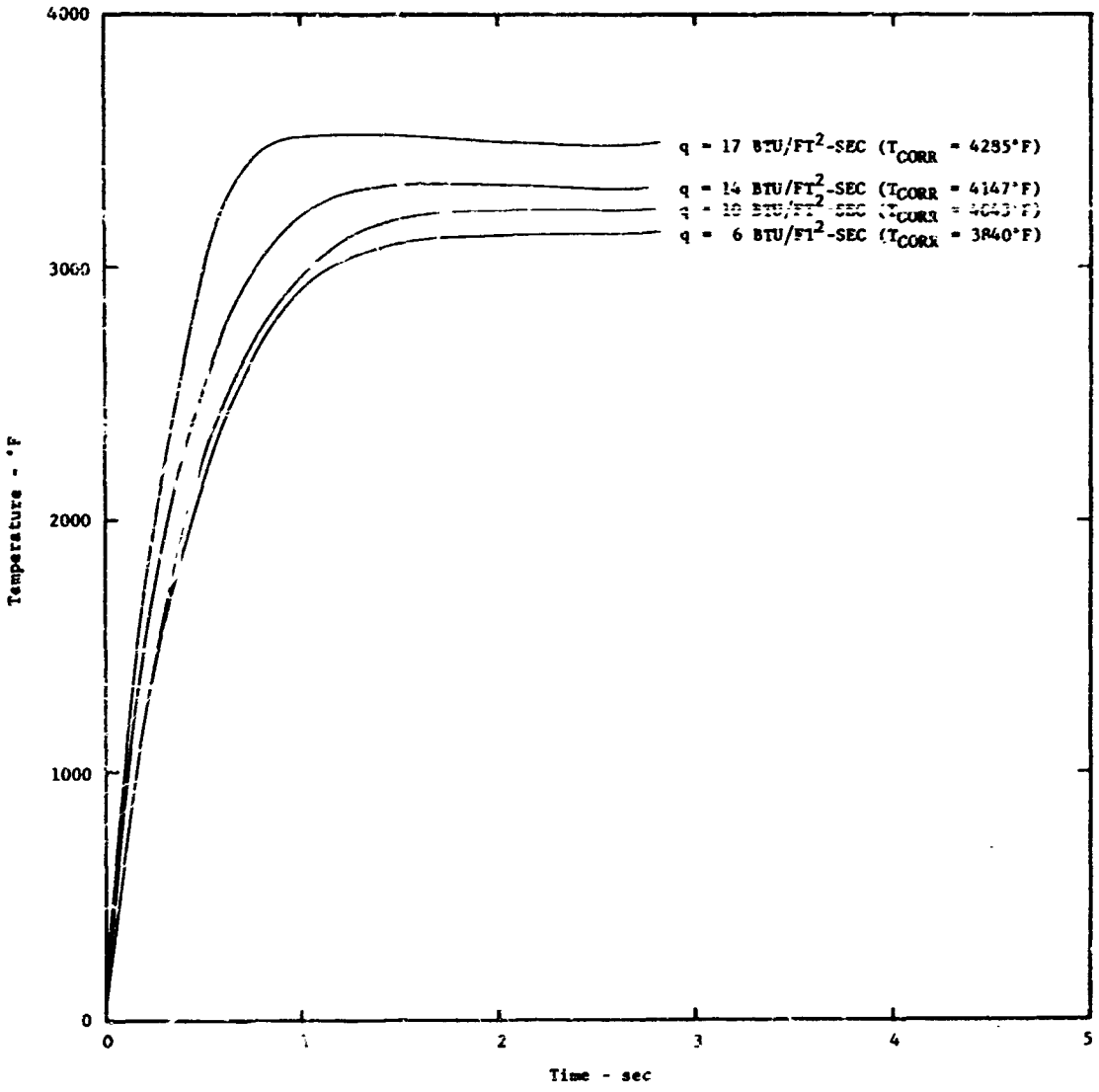

FREE-STREAM GAS-TEMPERATURE MEASUREMENTS UNDER CONVECTIVE HEATING 15.0 INCHES DOWNSTREAM FROM POINT OF BOUNDARY-LAYER INCEPTION

FIGURE 85

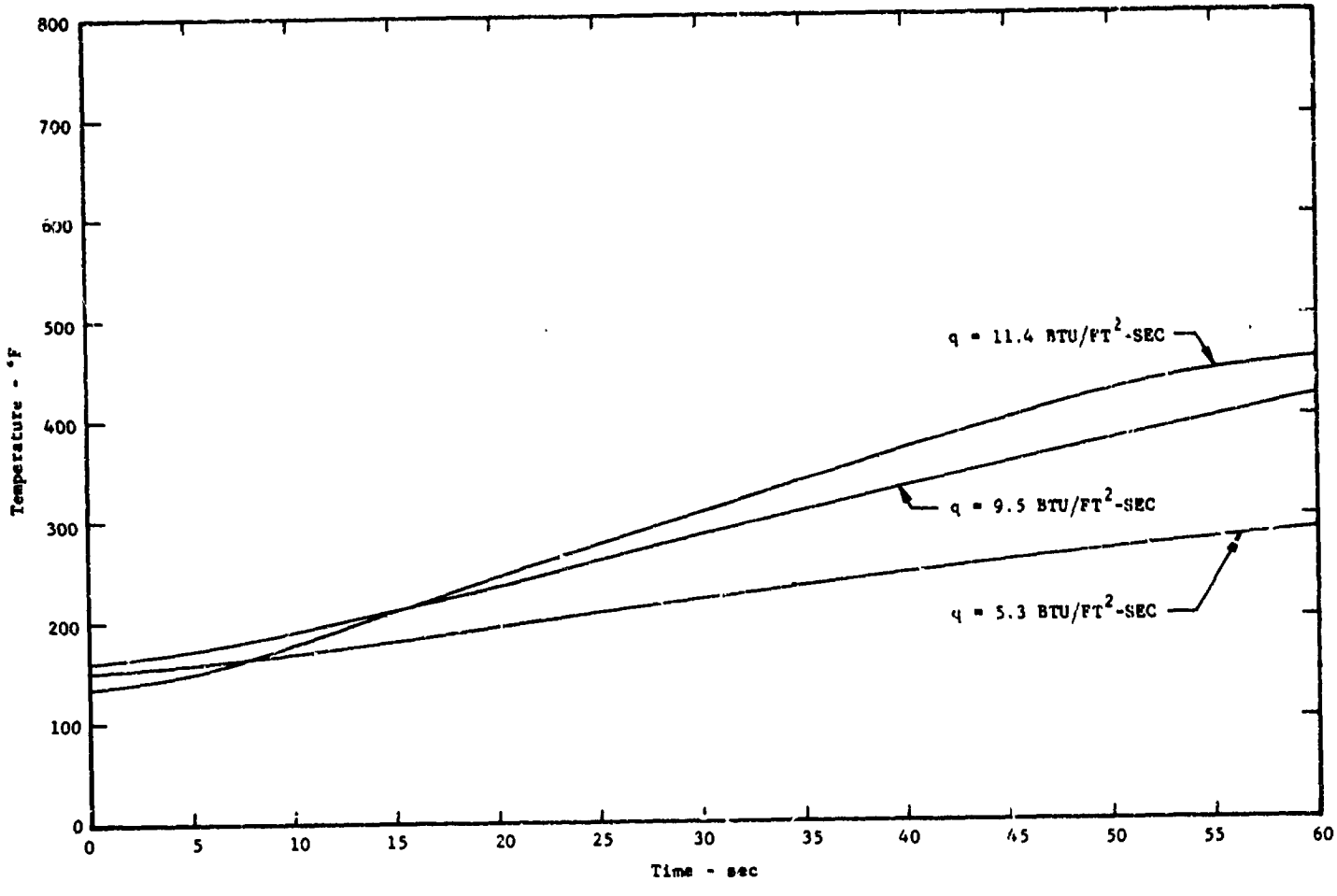

TYPICAL SURFACE-TEMPERATURE HISTORIES OF MEMBRANE TOTAL CALORIMETER AND COPPER (ISOTHERMAL) MOUNTING STRUCTURE UNDER CONVECTIVE HEATING 31.6 INCHES DOWNSTREAM FROM POINT OF BOUNDARY-LAYER INCEPTION

FIGURE 86

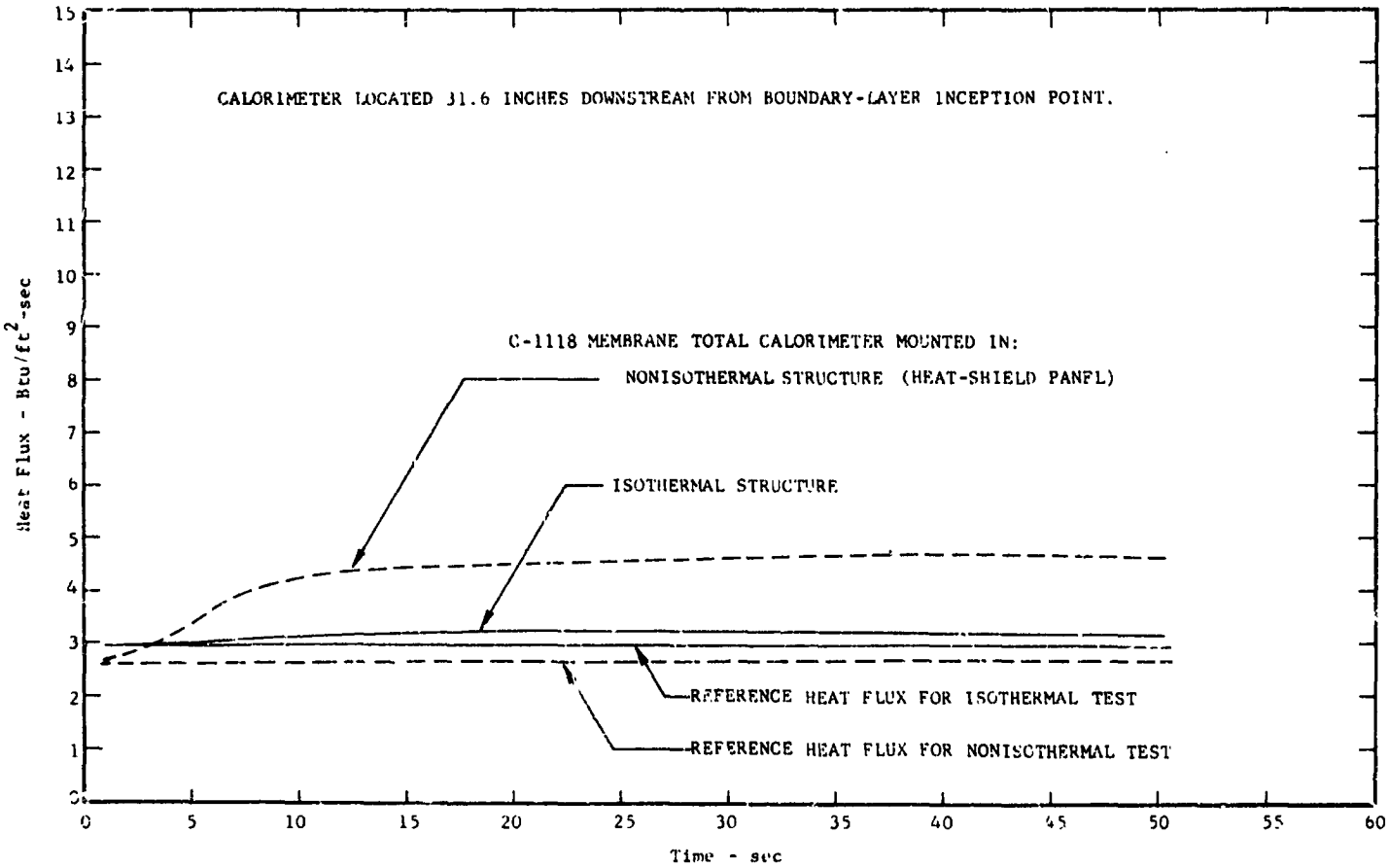

TYPICAL HEATING HISTORIES OF MEMBRANE TOTAL CALORIMETER UNDER INDICATED MOUNTING CONDITIONS AND LOW-RANGE CONVECTIVE HEATING

FIGURE 87

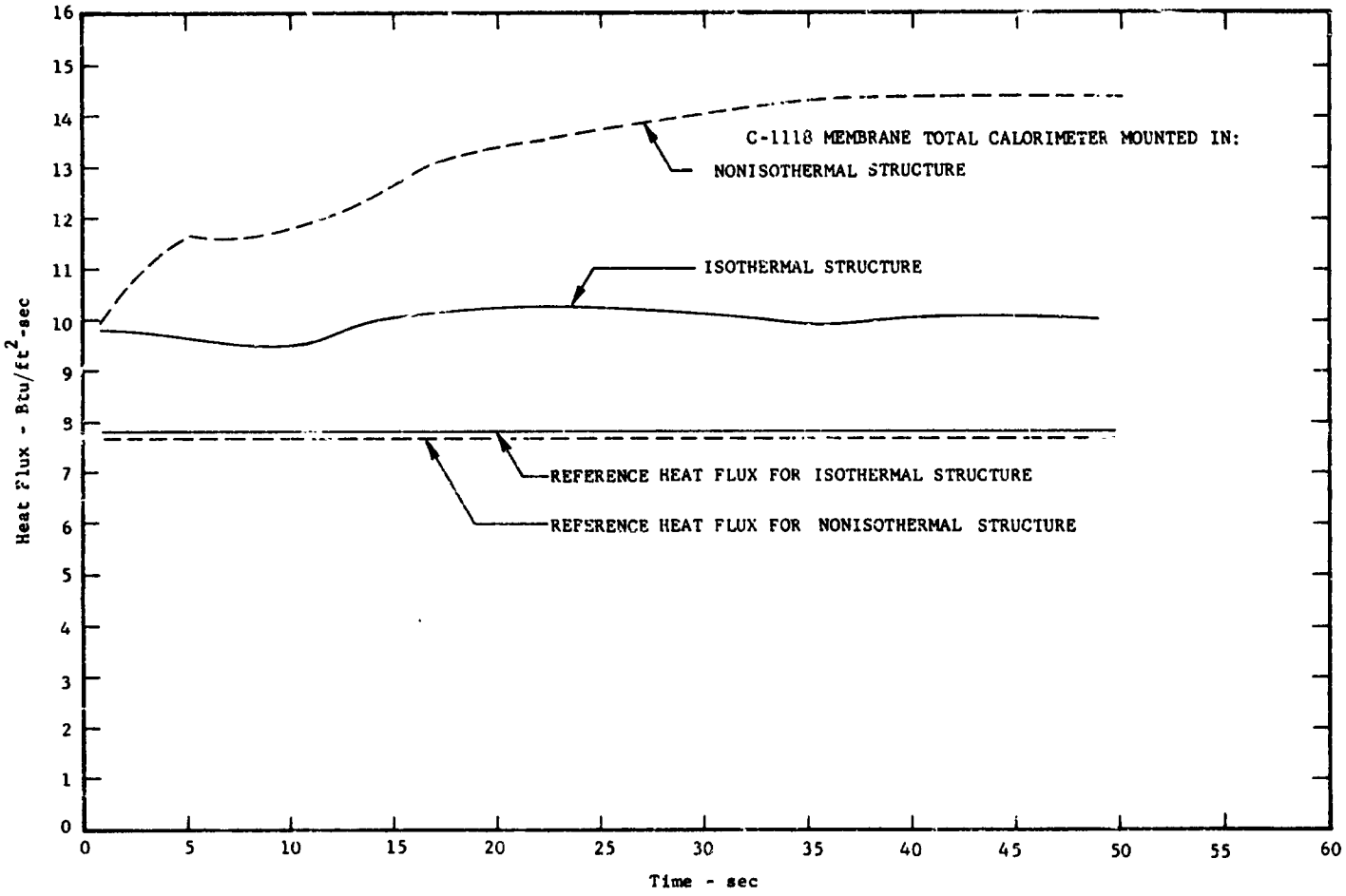

TYPICAL HEATING HISTORIES OF MEMBRANE TOTAL CALORIMETER UNDER INDICATED MOUNTING CONDITIONS AND MEDIUM-RANGE CONVECTIVE HEATING
(Nonisothermal Structure: M-31 Coated Heat-Shield Panel)

FIGURE 88

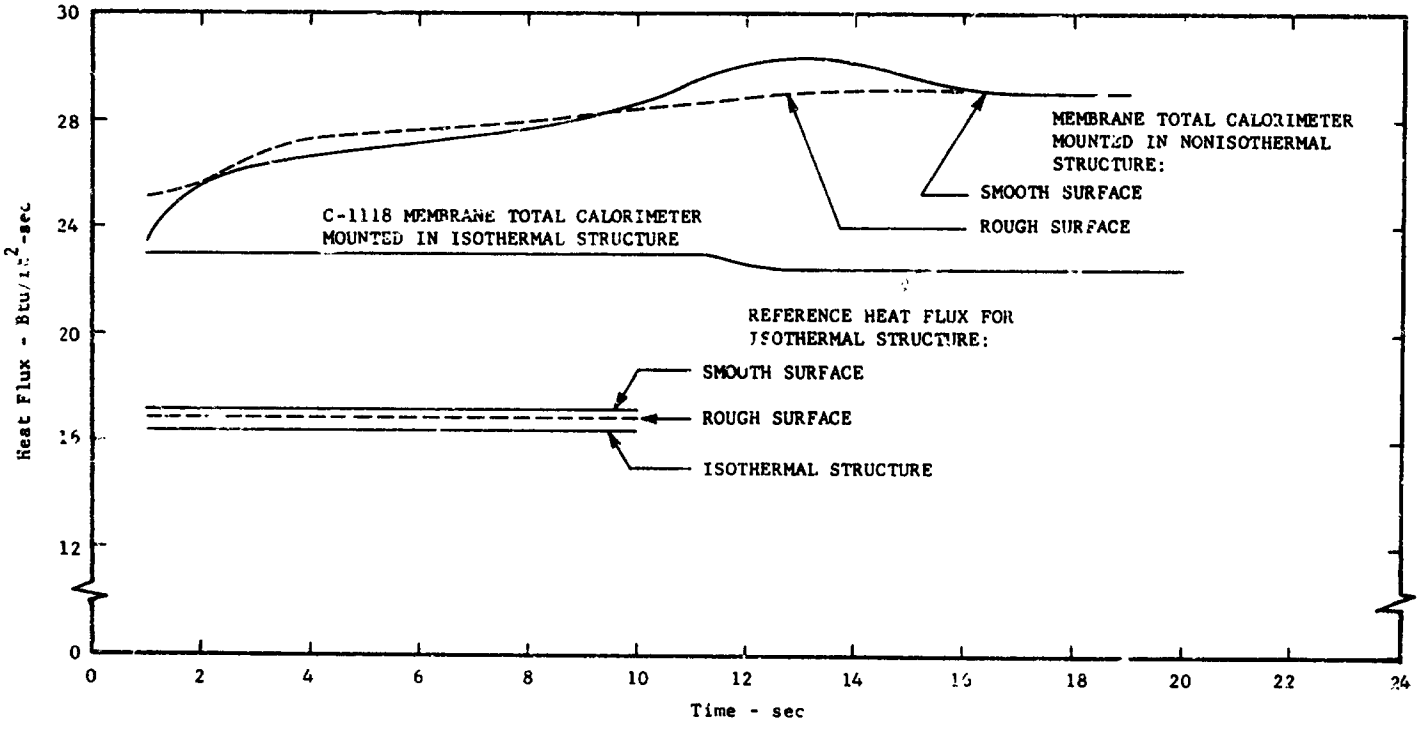

TYPICAL HEATING HISTORIES OF MEMBRANE TOTAL CALORIMETER UNDER INDICATED MOUNTING CONDITIONS AND MEDIUM-RANGE CONVECTIVE HEATING
(Nonisothermal Structure: Commercially Available Fire Brick)

FIGURE 89

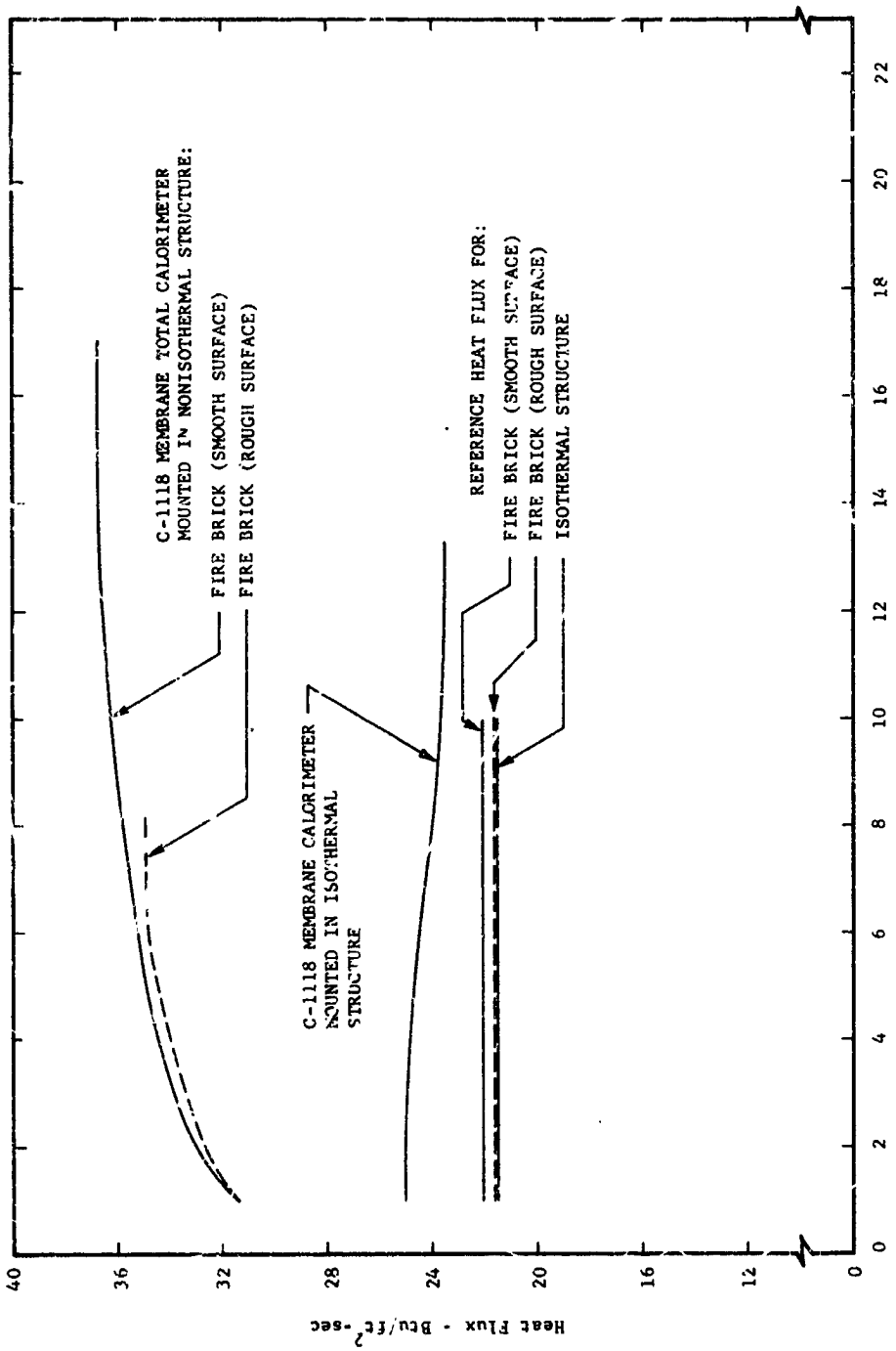

TYPICAL HEATING HISTORIES OF MEMBRANE TOTAL CALORIMETER UNDER INDICATED MOUNTING CONDITIONS AND HIGH-RANGE CONVECTIVE HEATING

FIGURE 90

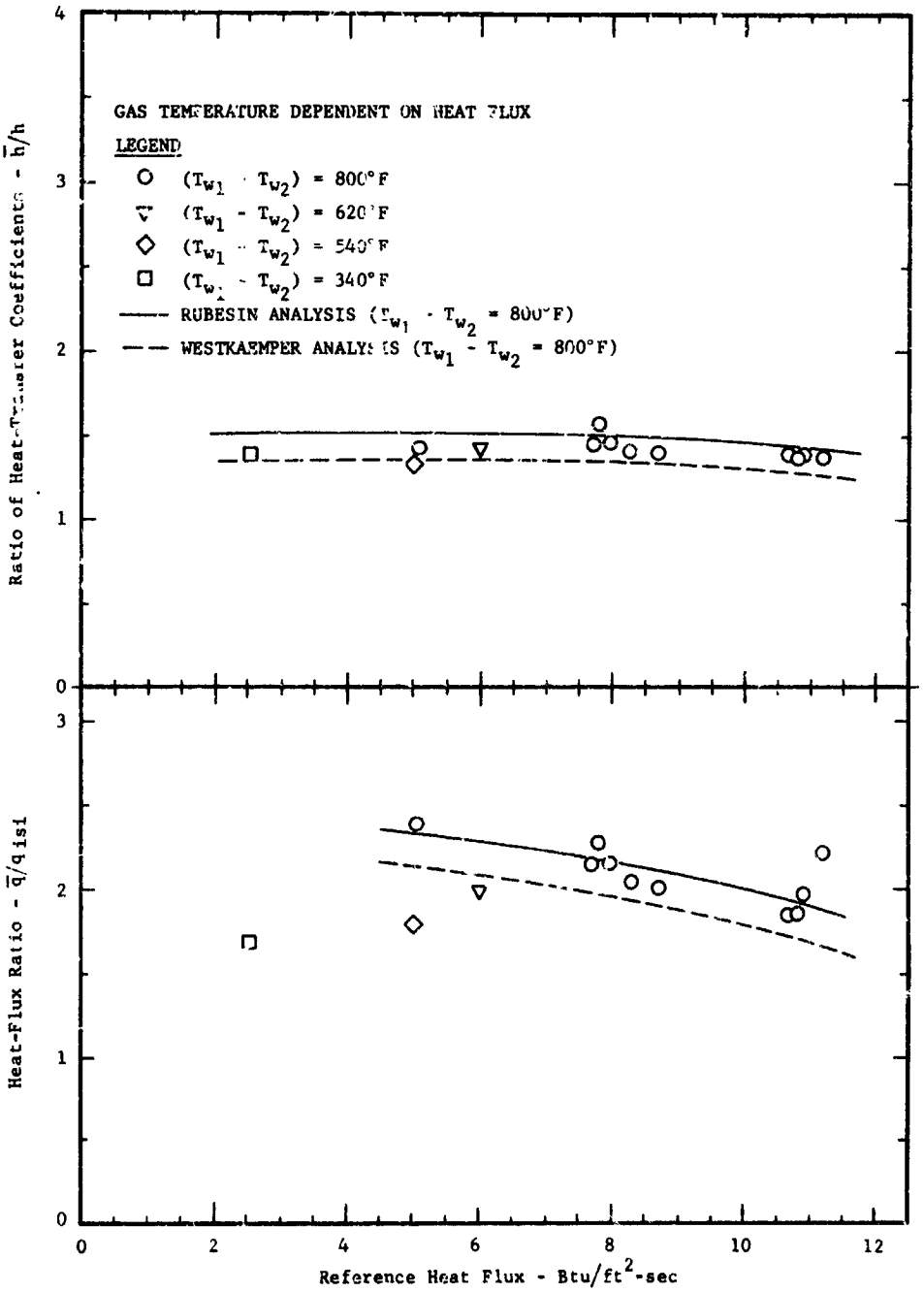

PERFORMANCE OF C-1118 MEMBRANE TOTAL CALORIMETER UNDER CONVECTIVE HEATING 31.8 INCHES DOWNSTREAM FROM POINT OF BOUNDARY-LAYER INCEPTION

FIGURE 91

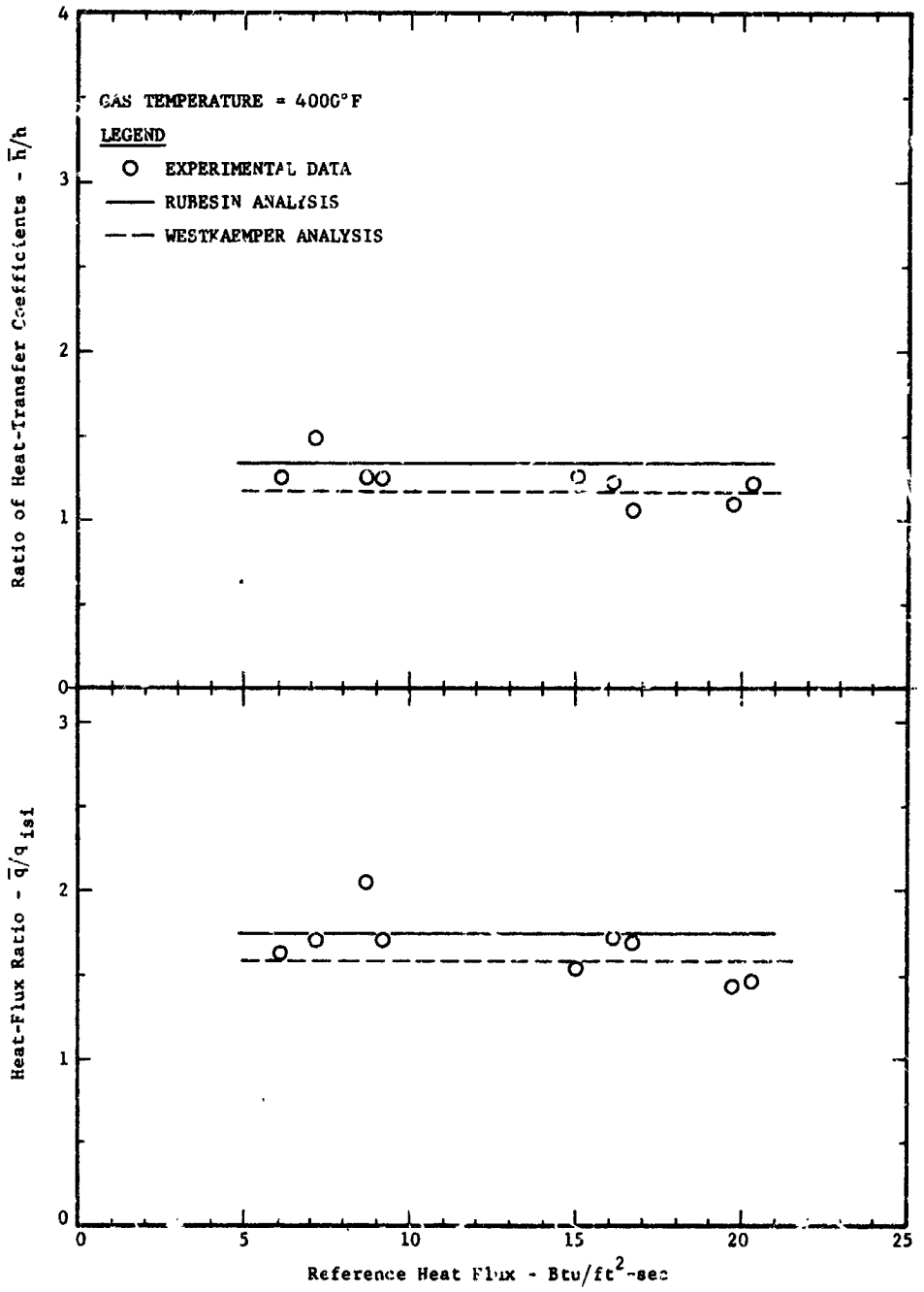

PERFORMANCE OF C-1118 MEMBRANE TOTAL CALORIMETER UNDER CONVECTIVE HEATING 15.0 INCHES DOWNSTREAM FROM POINT OF BOUNDARY-LAYER INCEPTION

FIGURE 92

American-Standard
ADVANCED TECHNOLOGY LABORATORIES DIVISION

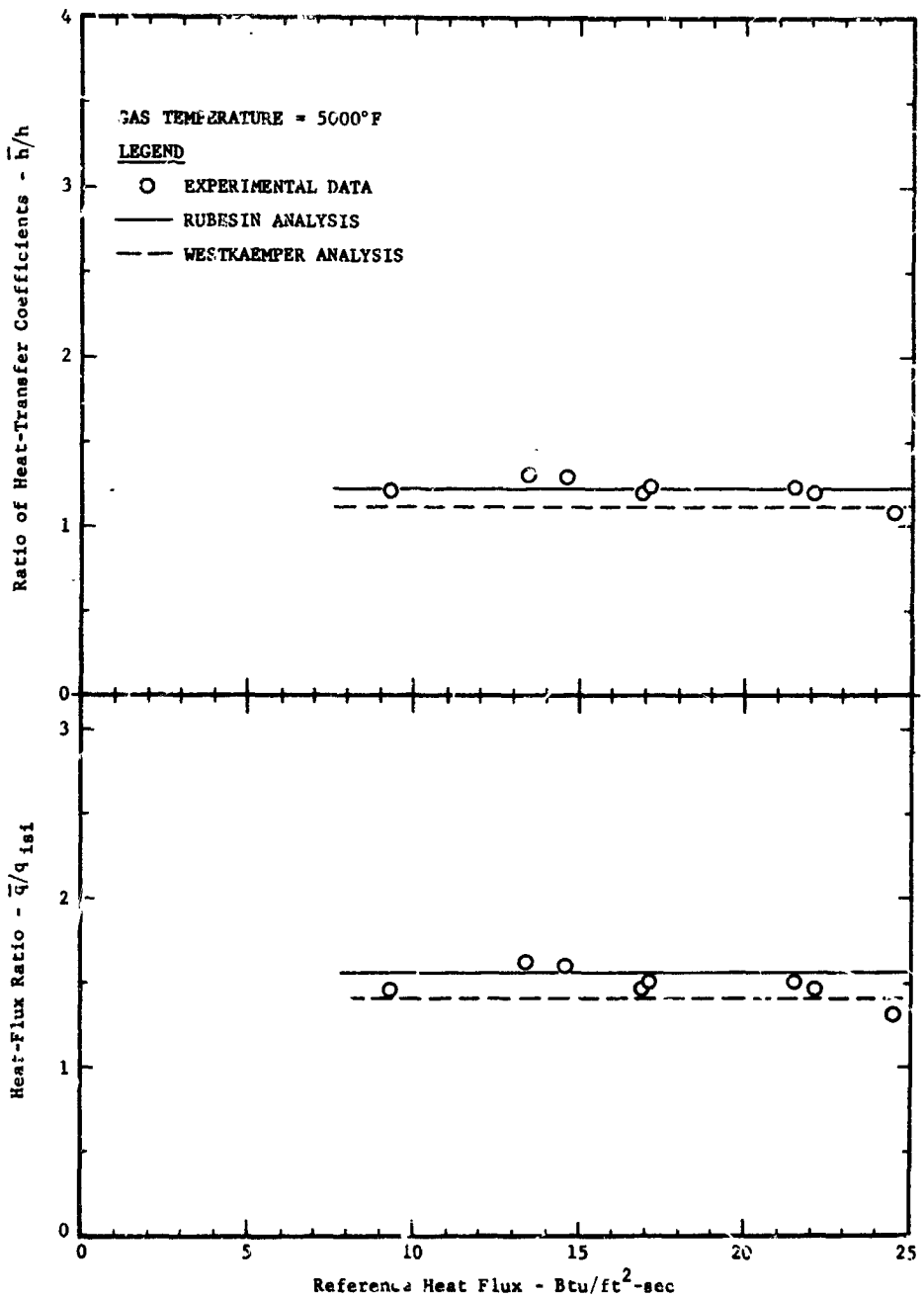

PERFORMANCE OF C-1118 MEMBRANE TOTAL CALORIMETER UNDER CONVECTIVE HEATING 6.0 INCHES DOWNSTREAM FROM POINT OF BOUNDARY-LAYER INCEPTION

FIGURE 93

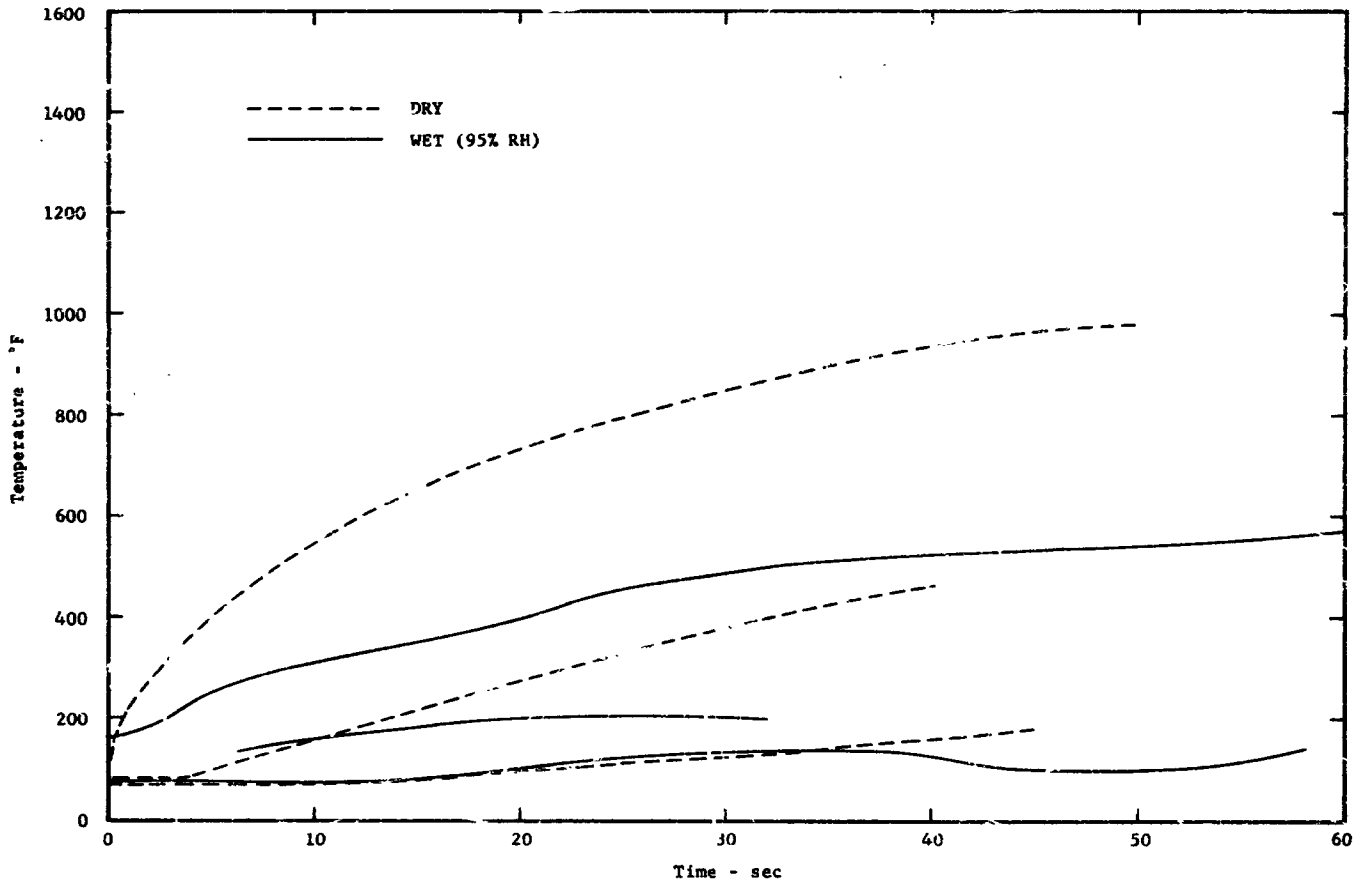

TEMPERATURE HISTORIES AT VARIOUS DEPTHS IN M-31 HEAT-SHIELD MATERIAL
UNDER CONVECTIVE HEATING
(Approximate Heat Flux Indicated by Laboratory Reference Calorimeter = 8 Btu/ft^2-sec)

FIGURE 94

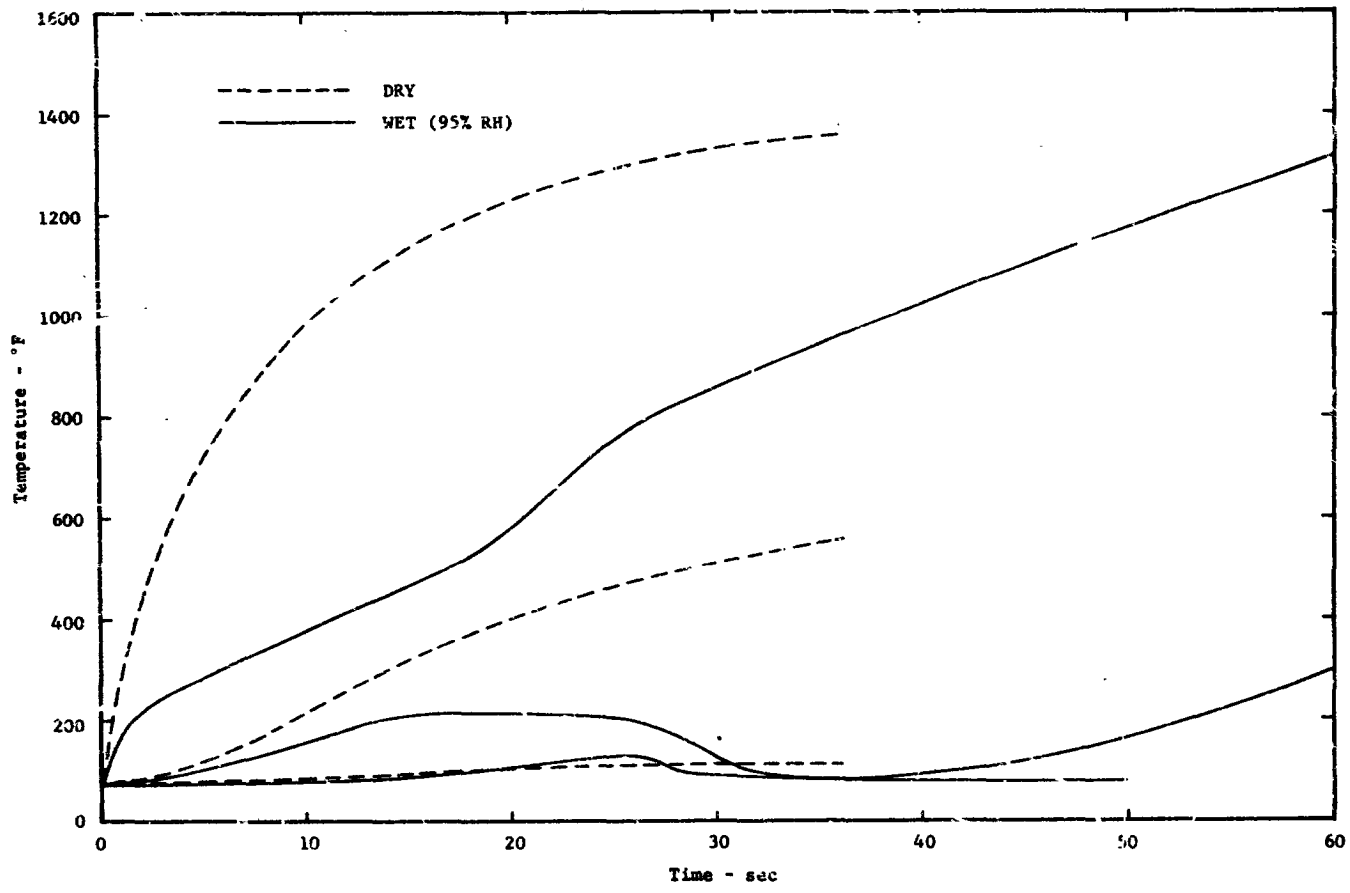

TEMPERATURE HISTORIES AT VARIOUS DEPTHS IN M-31 HEAT-SHIELD MATERIAL
UNDER CONVECTIVE HEATING
(Approximate Heat Flux Indicated by Laboratory Reference Calorimeter = 12 Btu/ft^2-sec)

FIGURE 95

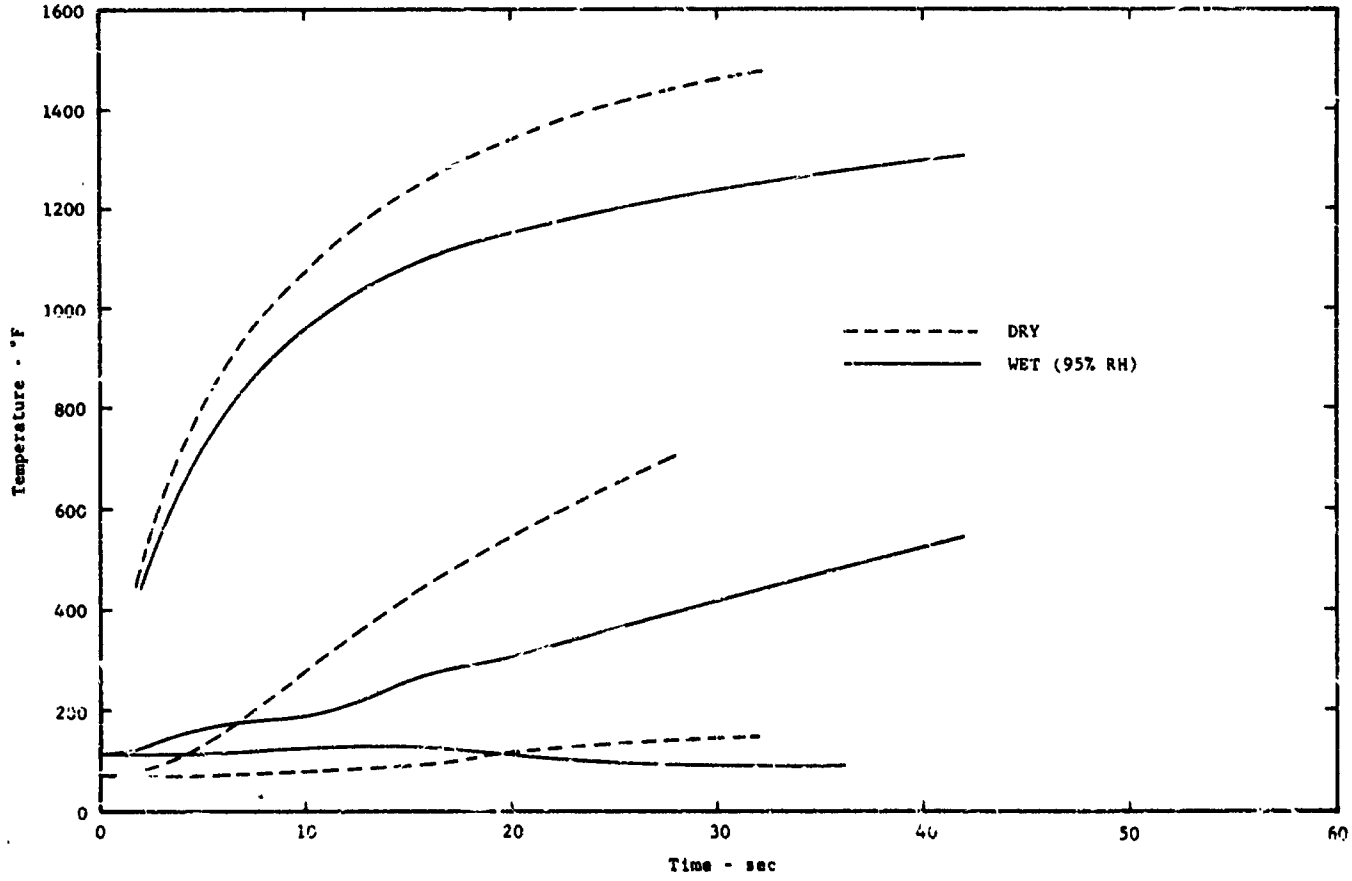

TEMPERATURE HISTORIES AT VARIOUS DEPTHS IN M-31 HEAT-SHIELD MATERIAL
UNDER CONVECTIVE HEATING
(Approximate Heat Flux Indicated by Laboratory Reference Calorimeter = 16 Btu/ft^2-sec)

FIGURE 96

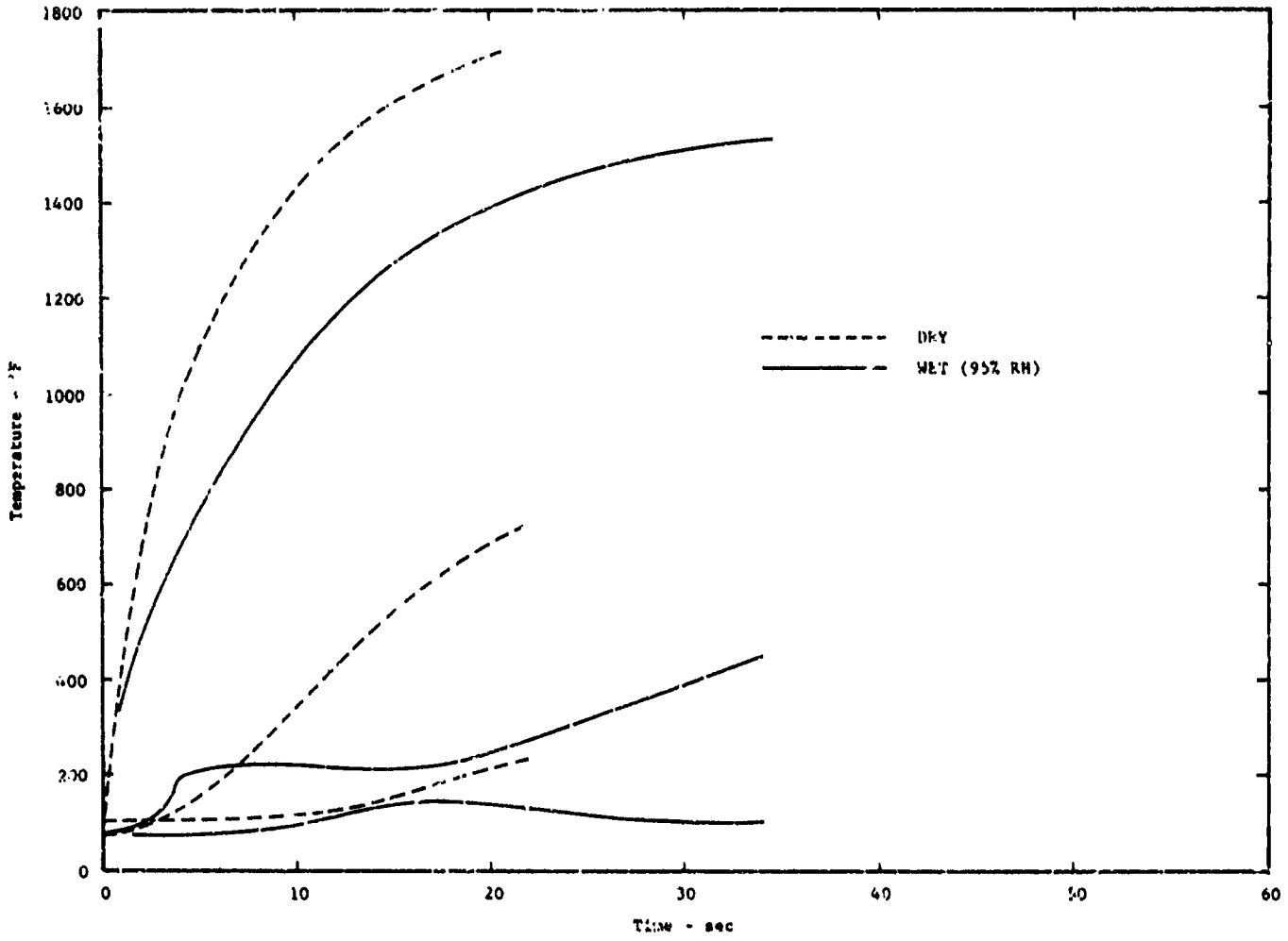

TEMPERATURE HISTORIES AT VARIOUS DEPTHS IN M-31 HEAT-SHIELD MATERIAL
UNDER CONVECTIVE HEATING
(Approximate Heat Flux Indicated by Laboratory Reference Calorimeter = 10 Btu/ft^2-sec)

FIGURE 97

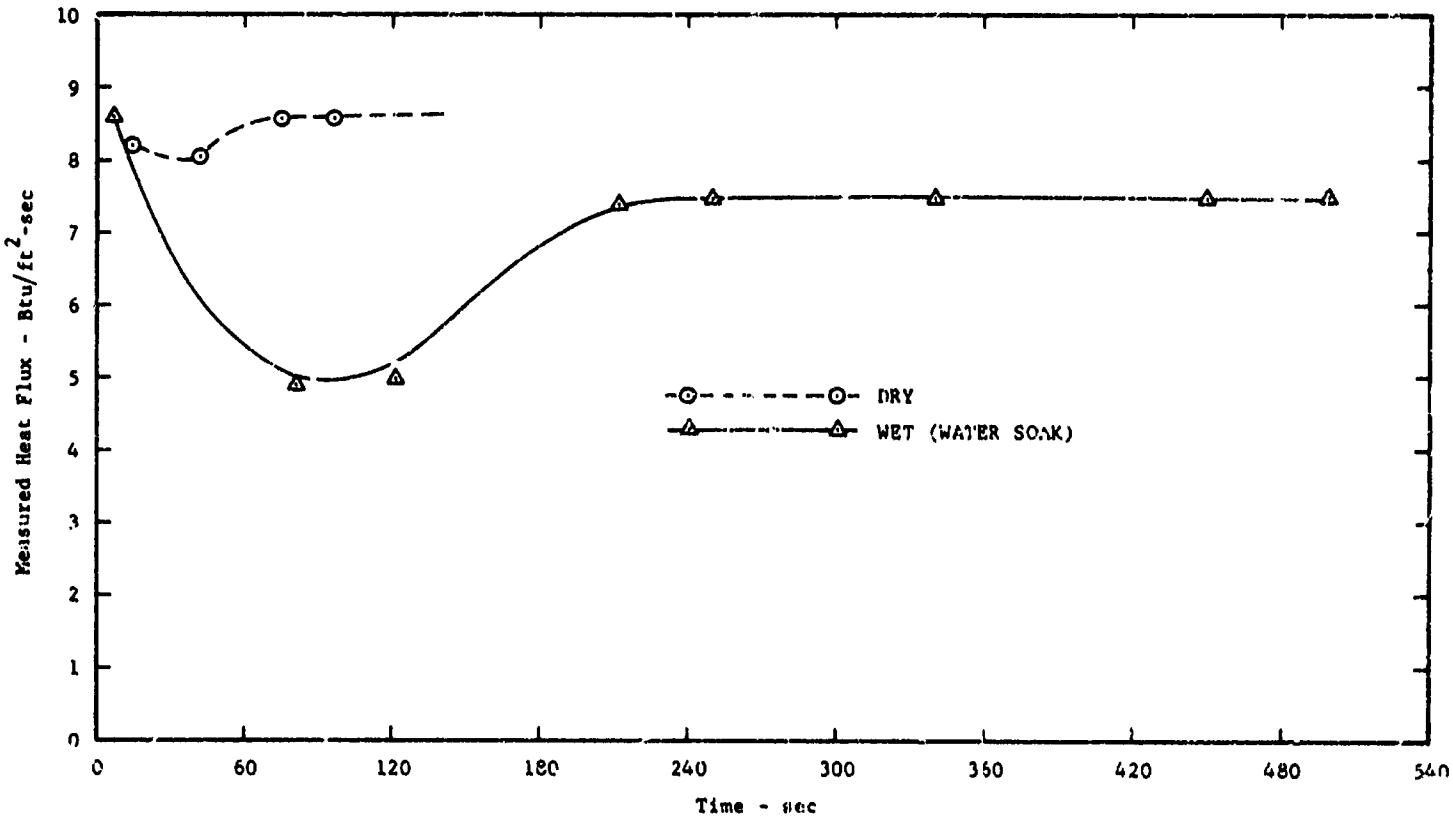

HEATING HISTORY OF C-1118 MEMBRANE TOTAL CALORIMETER MOUNTED IN M-31 HEAT-SHIELD MATERIAL UNDER CONVECTIVE HEATING
(Approximate Heat Flux Indicated by Laboratory Reference Calorimeter = 4 Btu/ft^2-sec)

FIGURE 98

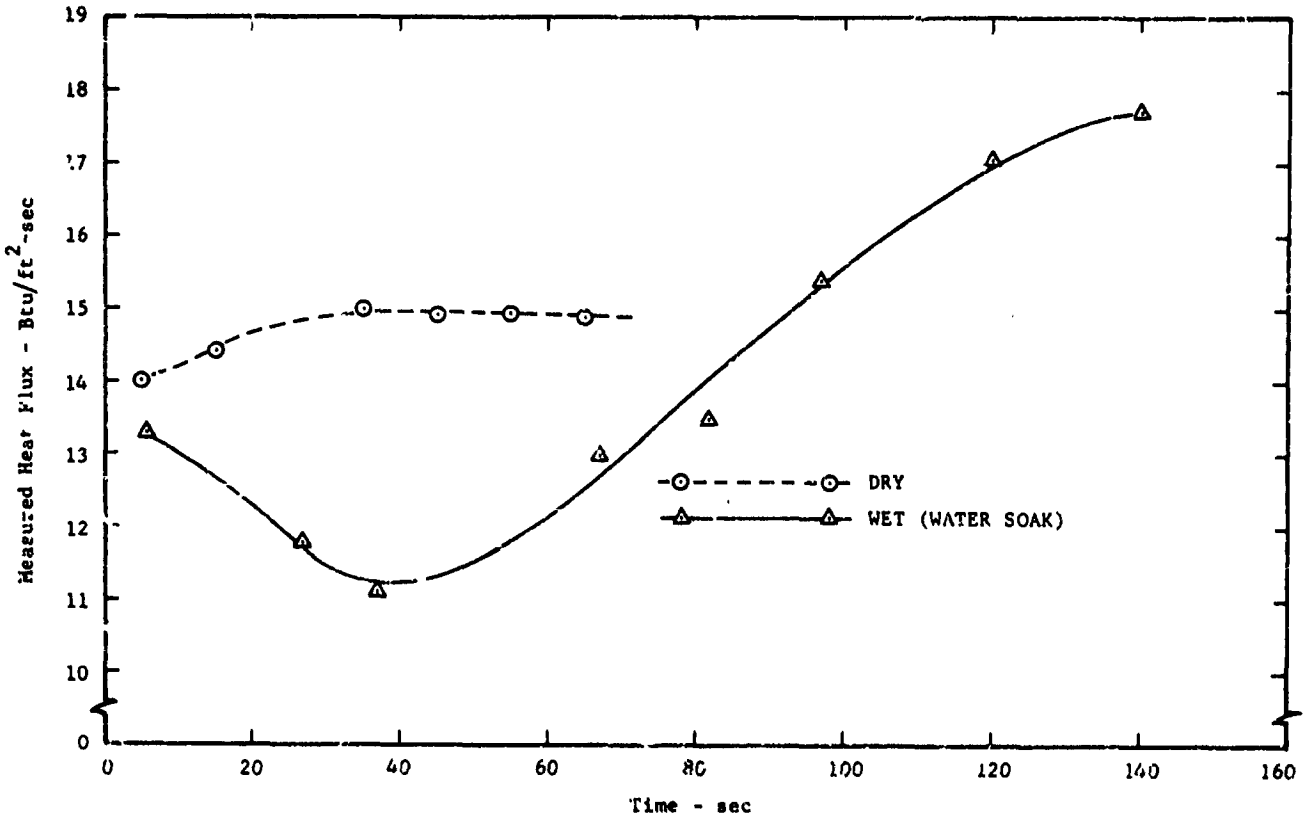

HEATING HISTORY OF C-1118 MEMBRANE TOTAL CALORIMETER MOUNTED IN M-31 HEAT-SHIELD MATERIAL UNDER CONVECTIVE HEATING
(Approximate Heat Flux Indicated by Laboratory Reference Calorimeter = 6 Btu/ft^2-sec)

FIGURE 99

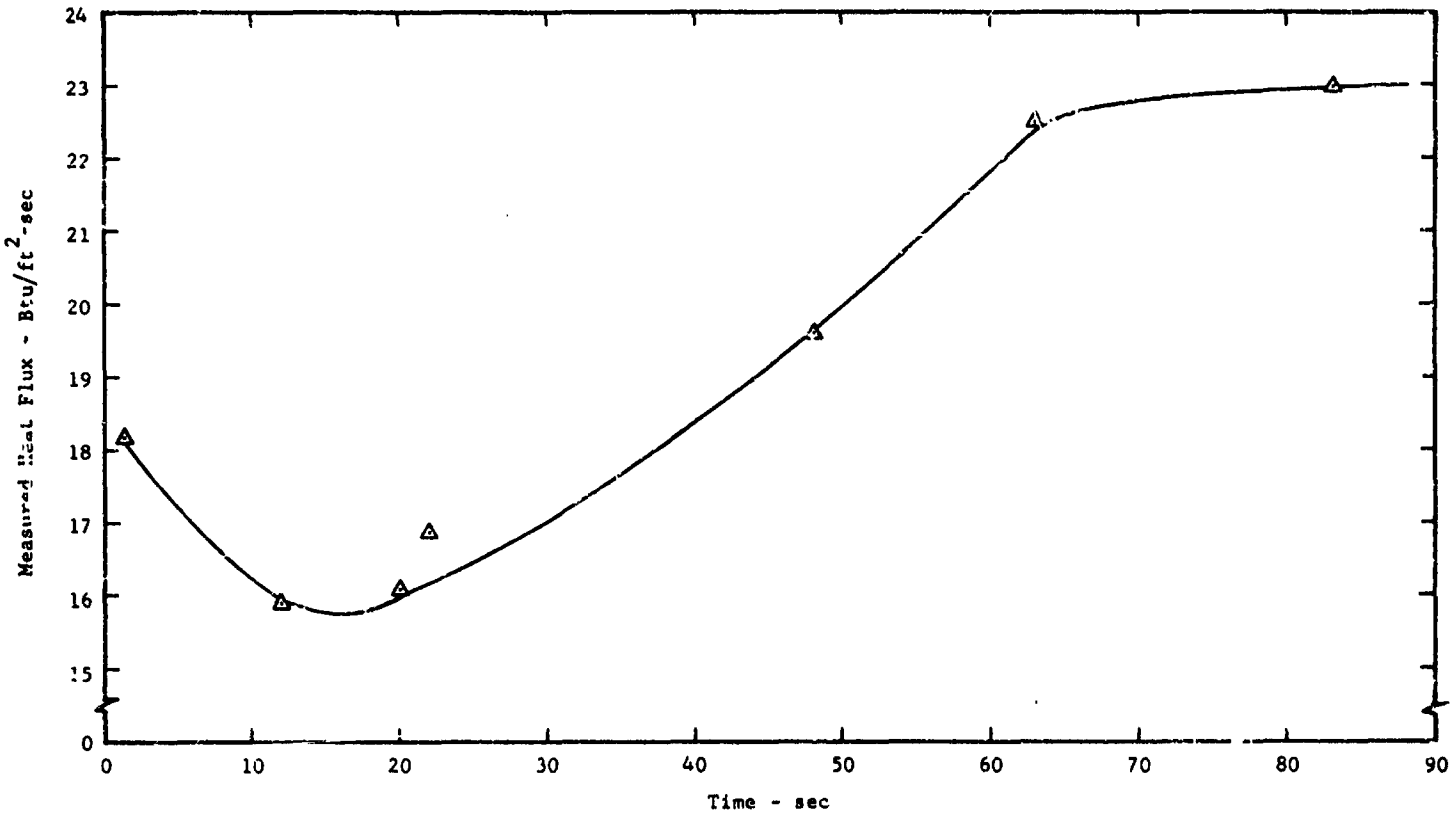

HEATING HISTORY OF C-1118 MEMBRANE TOTAL CALORIMETER MOUNTED IN WATER-SOAKED M-31 HEAT-SHIELD MATERIAL UNDER CONVECTIVE HEATING
(Approximate Heat Flux Indicated by Laboratory Reference Calorimeter = 17 Btu/ft^2-sec)

FIGURE 100

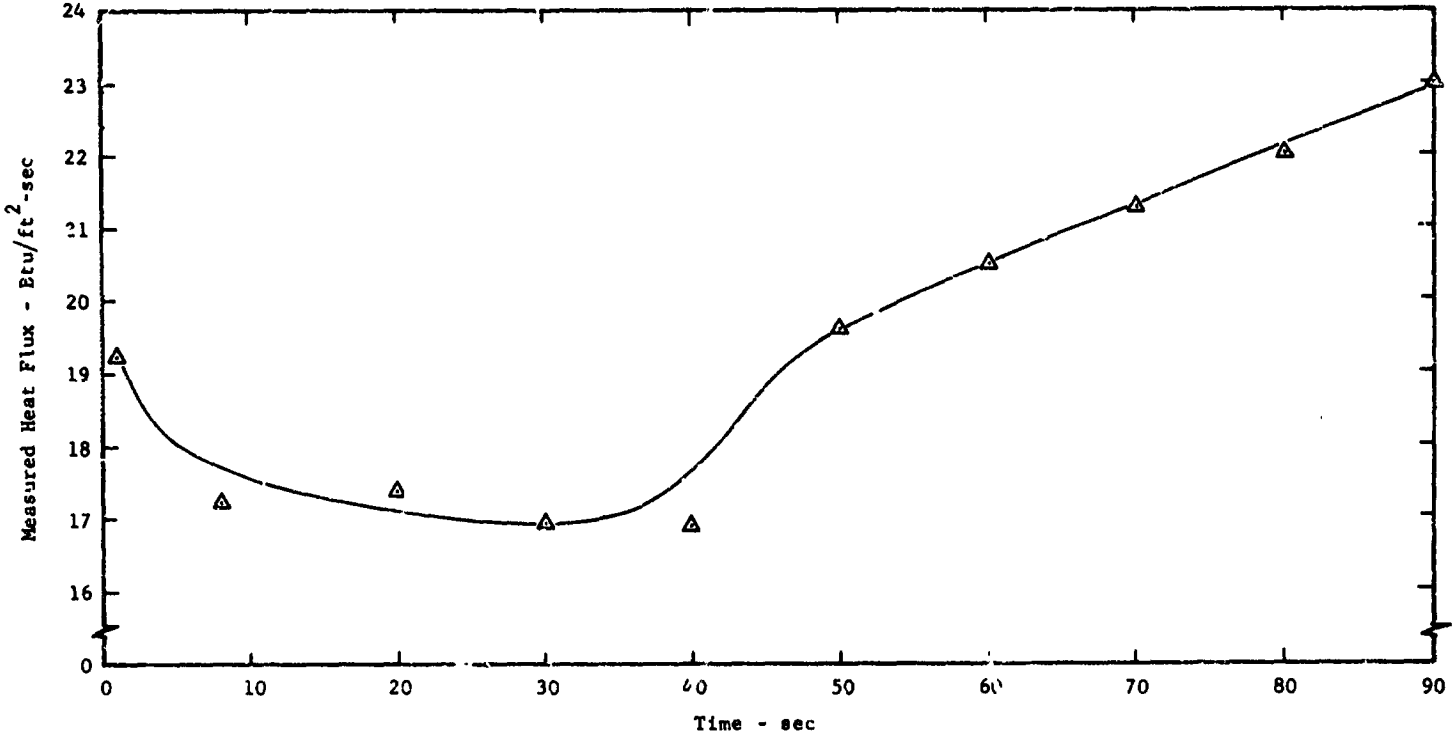

HEATING HISTORY OF C-1115 MEMBRANE TOTAL CALORIMETER MOUNTED IN WATER-SOAKED M-31 HEAT-SHIELD MATERIAL UNDER CONVECTIVE HEATING
(Approximate Heat Flux Indicated by Laboratory Reference Calorimeter = 16 Btu/ft^2-sec)

FIGURE 101

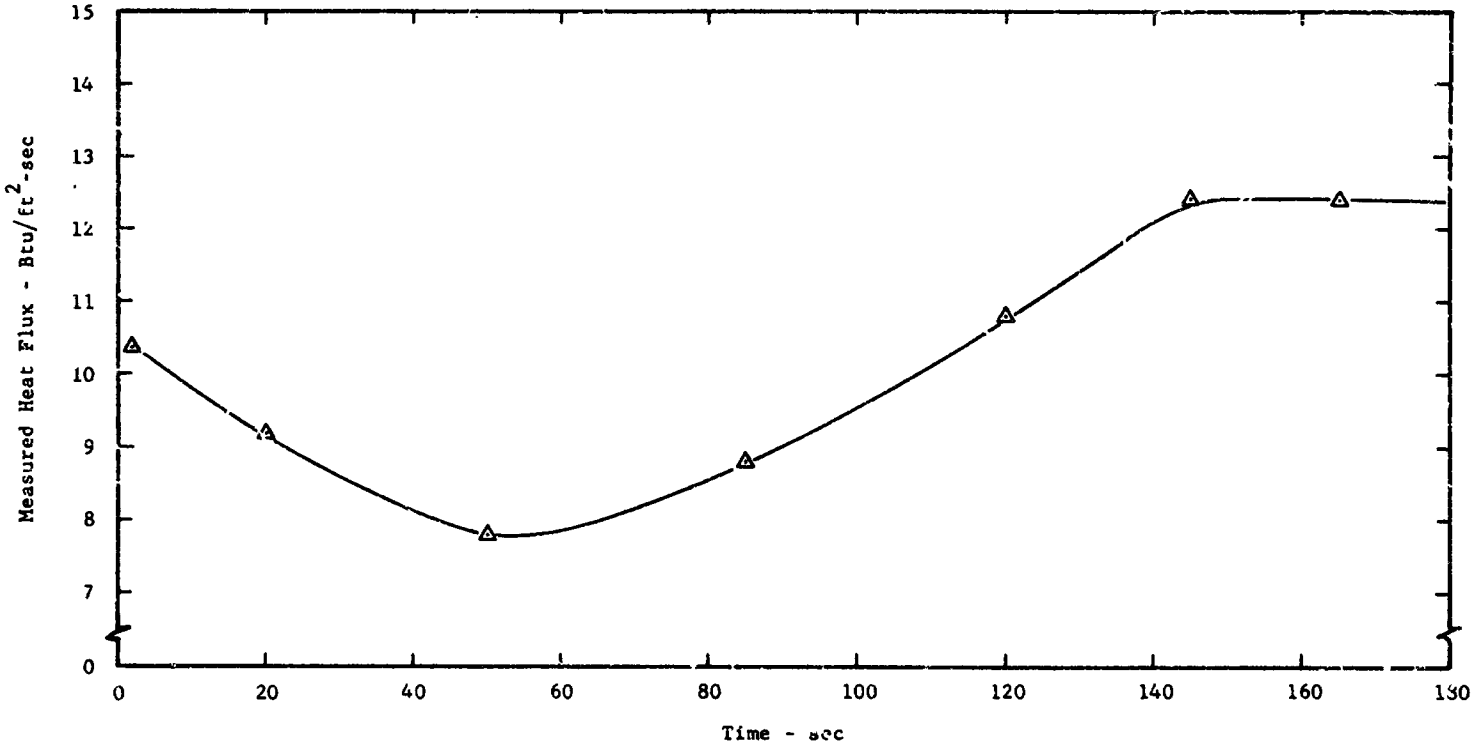

HEATING HISTORY OF C-1118 MEMBRANE TOTAL CALORIMETER MOUNTED IN WATER-SOAKED M-31 HEAT-SHIELD MATERIAL UNDER CONVECTIVE HEATING
(Approximate Heat Flux Indicated by Laboratory Reference Calorimeter = 8 Btu/ft^2-sec)

FIGURE 102

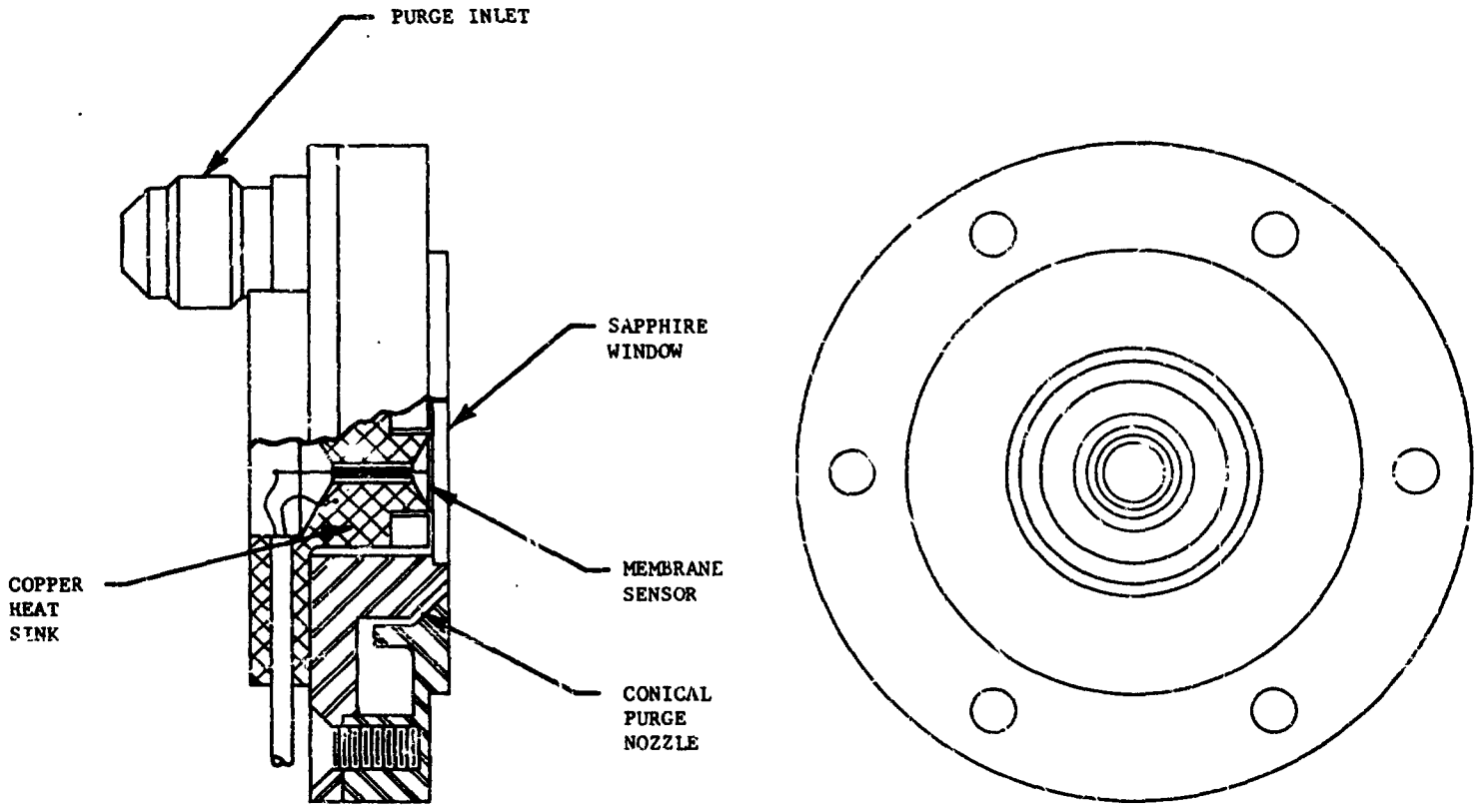

N-139 MEMBRANE PURGED RADIOMETER

FIGURE 103

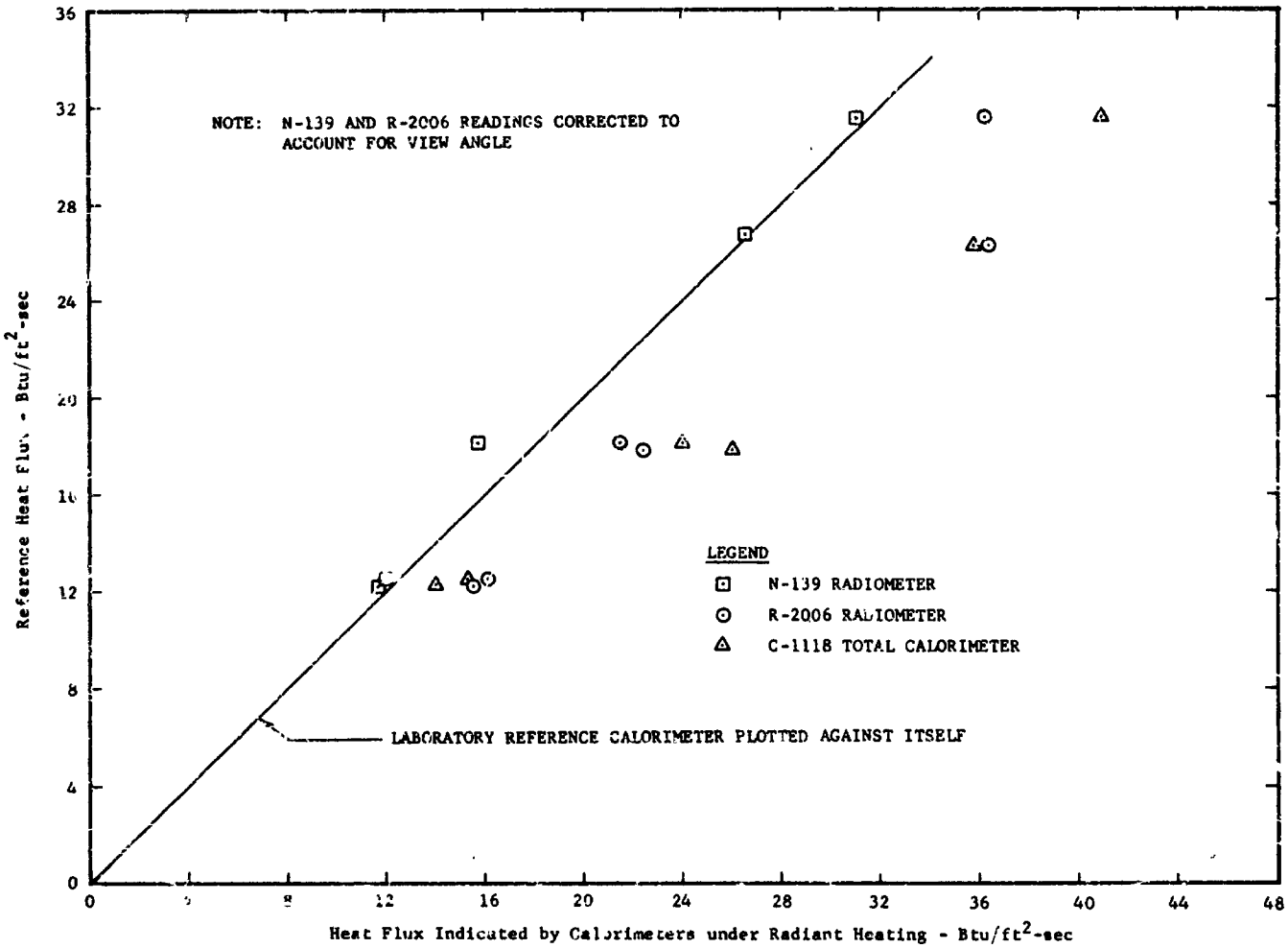

COMPARISON OF LABORATORY REFERENCE CALORIMETER WITH COMMERCIAL MEMBRANE CALORIMETERS UNDER RADIANT HEATING

FIGURE 104

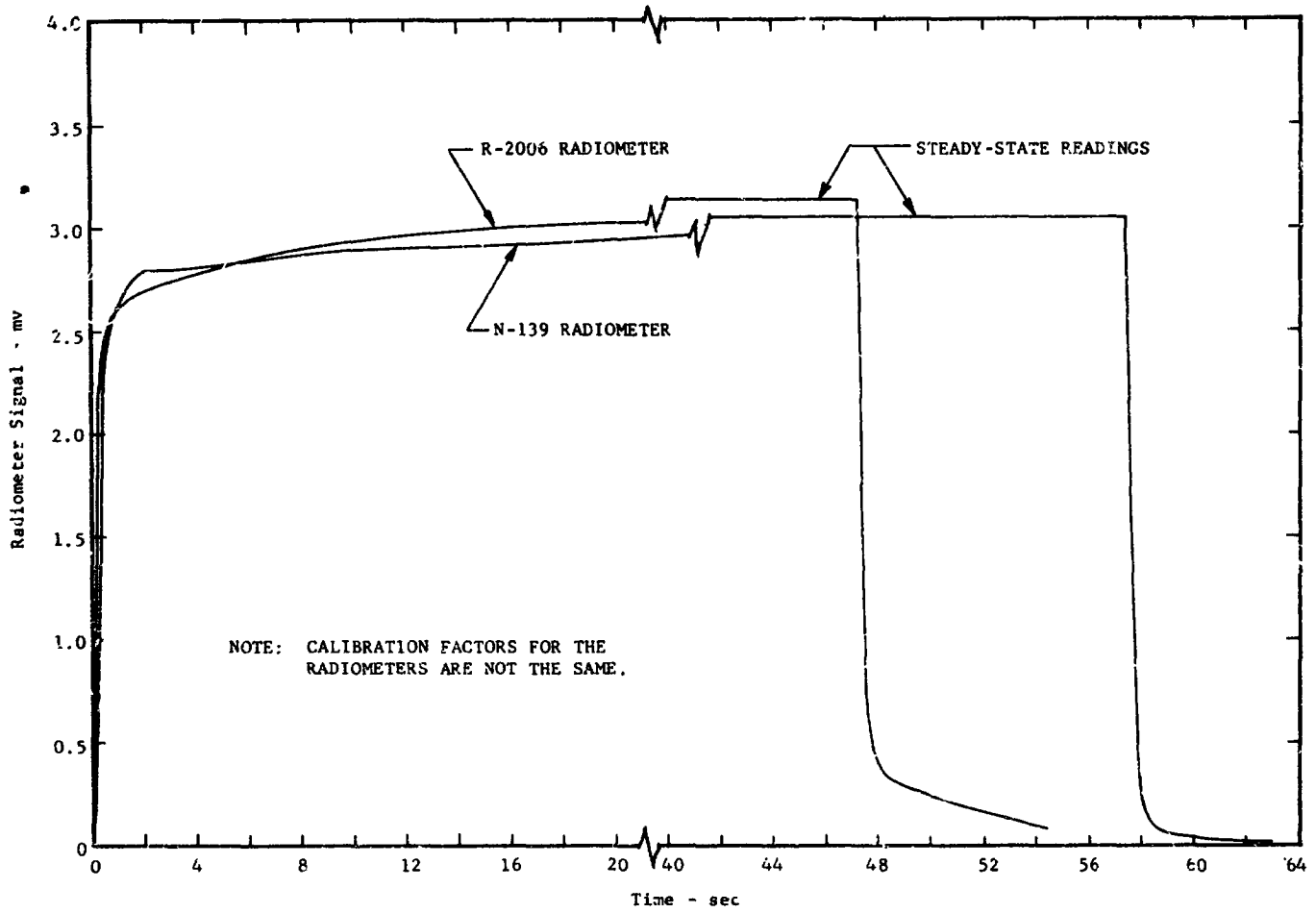

RESPONSE OF N-139 AND R-2006 MEMBRANE RADIOMETERS TO STEP INPUT AND STEP CUTOFF OF HEAT FLUX

FIGURE 105

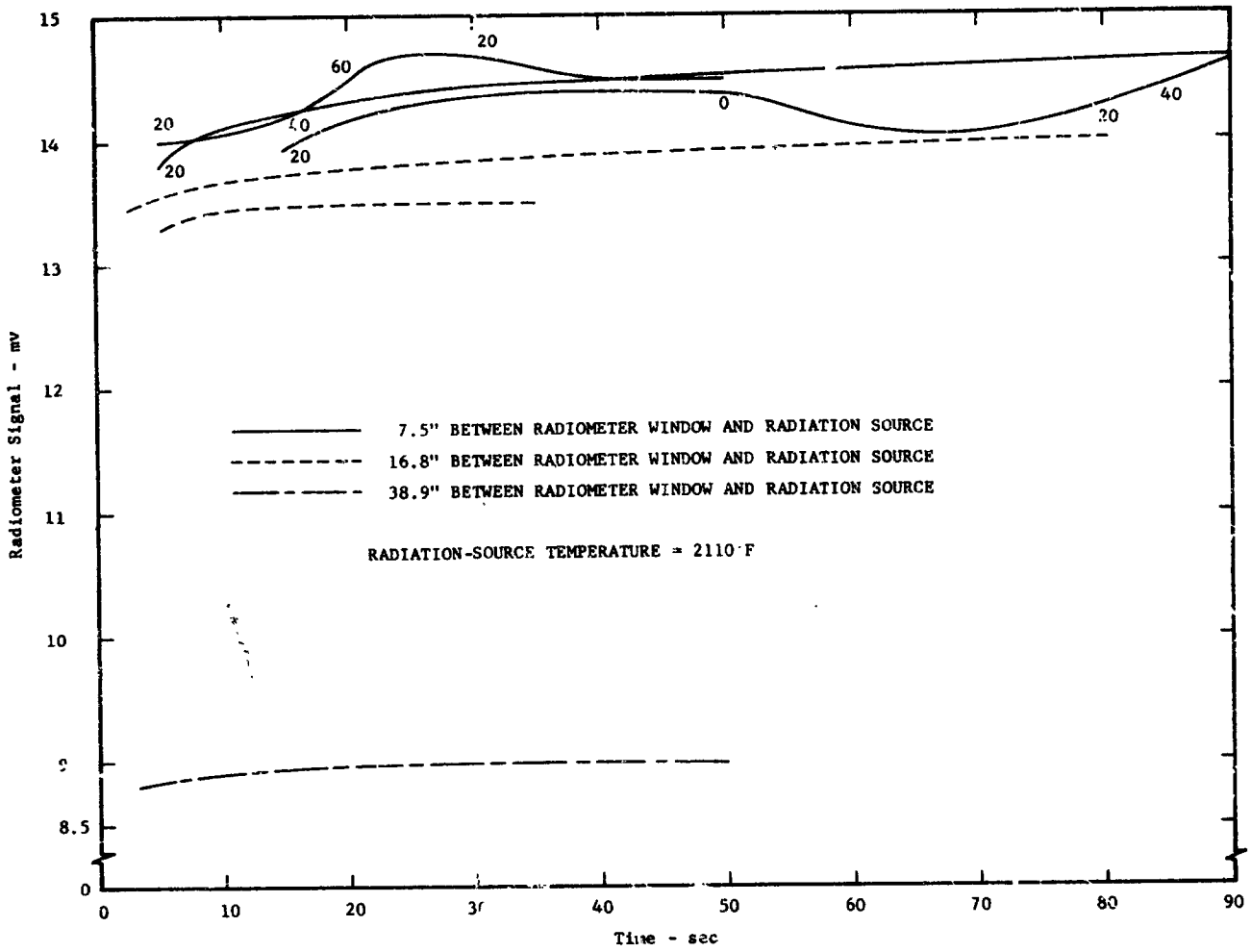

RADIOMETER-SIGNAL HISTORIES FOR DIFFERENT RADIOMETER DISTANCES FROM RADIANT-HEATING SOURCE

FIGURE 36

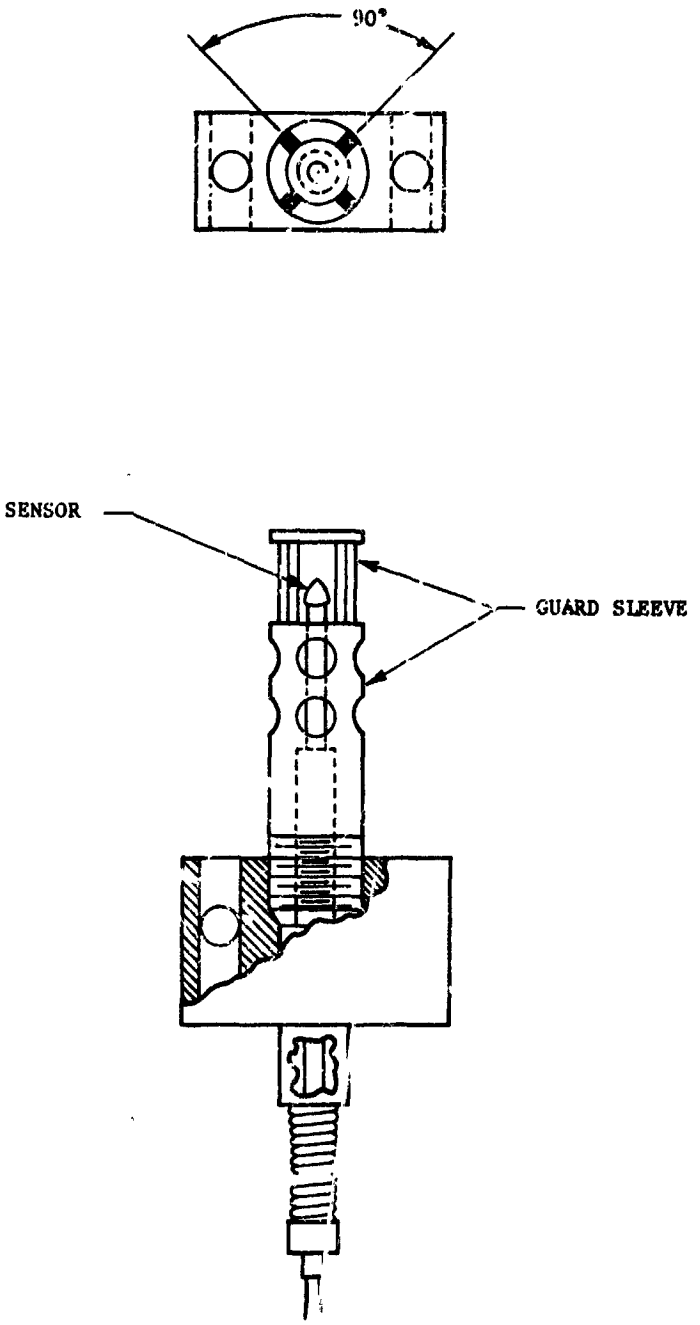

GAS-TEMPERATURE-PROBE (NO. 50M10100) CONFIGURATION

FIGURE 107

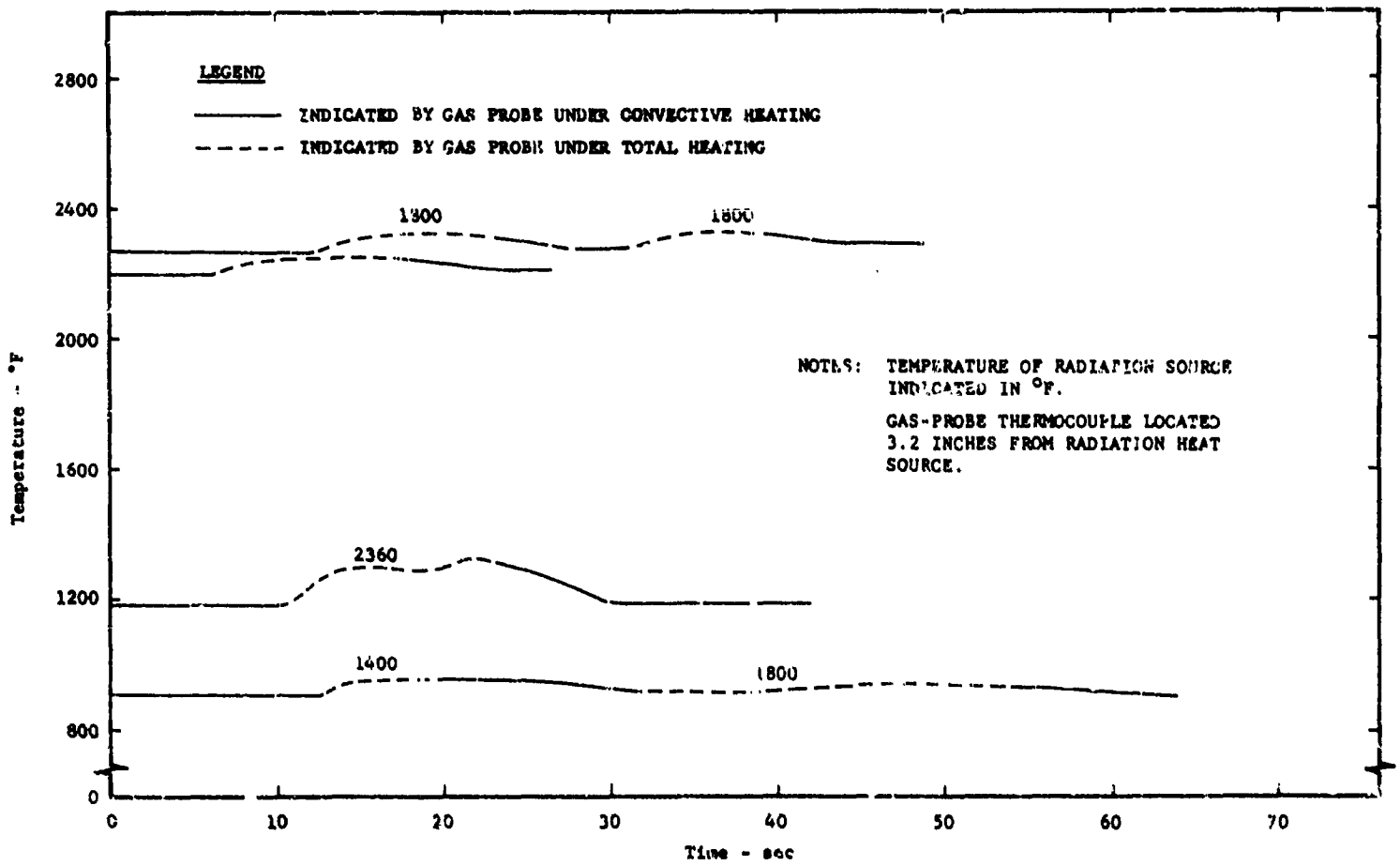

TEMPERATURE MEASURED BY GAS PROBE FOR THE INDICATED HEATING CONDITIONS

FIGURE 108

APPENDIX

TABULATED DATA AND RESULTS

TABLE I

DATA AND RESULTS FOR CONVECTIVE HEATING ON A C-111$ MEMBRANE TOTAL CALORIMETER MOUNTED IN AN M-31 HEAT-SHIELD PANEL AND LOCATED 6 INCHES DOWNSTREAM FROM BOUNDARY-LAYER INCEPTION POINT

Reference Heat Flux (Btu/ft^2-sec)	9.3	13.4	14.6	16.9	17.1	21.5	22.1	24.5
Free-Stream Gas Temperature (°F)	5000	1200	———	———	———	———	———	▶
Calorimeter Surface Temperature (°F)	154	150	145	148	150	135	130	136
Calorimeter Output for Isothermal-Surface Condition (Btu/ft^2-sec)	11.7	17.7	19.3	21.7	21.9	27.5	28.3	31.4
Structure-Surface Temperature (°F)	1150	———	———	———	———	———	———	▶
Surface-Temperature Discontinuity (°F)	996	1000	1005	1008	1000	1015	1020	1014
Calorimeter Output for Nonisothermal-Surface Condition (Btu/ft^2-sec)	14.2	23.0	25.0	26.0	27.2	33.7	34.0	34.0
$(\bar{h}/h)$ Experimental	1.21	1.30	1.29	1.20	1.24	1.23	1.20	1.08
$(\bar{h}/h)$ Calculated Using Rubesin's Results	1.22	———	———	———	———	———	———	▶
$(\bar{h}/h)$ Calculated Using Westkaemper's Results	1.12	———	———	———	———	———	———	▶
$(\bar{q}/q)_{isi}$ Experimental	1.46	1.62	1.6	1.46	1.50	1.49	1.46	1.31
$(\bar{q}/q)_{isi}$ Calculated Using Rubesin's Results	1.54	———	———	———	———	———	———	▶
$(\bar{q}/q)_{isi}$ Calculated Using Westkaemper's Results	1.41	———	———	———	———	———	———	▶

TABLE II

DATA AND RESULTS FOR CONVECTIVE HEATING ON A C-1118 MEMBRANE TOTAL CALORIMETER MOUNTED IN AN M-31 HEAT-SHIELD PANEL AND LOCATED 15 INCHES DOWNSTREAM FROM BOUNDARY-LAYER INCEPTION POINT

Reference Heat Flux (Btu/ft^2-sec)	5.1	6.0	7.2	7.8	12.6	13.5	14.0	16.5	17.0
Free-Stream Gas Temperature (°F)	3800	3800	3900	3950	4040	4070	4100	4150	4200
Calorimeter Surface Temperature (°F)	202	295	192	215	208	220	213	182	196
Calorimeter Output for Isothermal-Surface Condition (Btu/ft^2-sec)	6.3	7.5	9.1	10.0	16.3	17.2	17.8	21.4	22.0
Structure-Surface Temperature (°F)	1109	1132	1192	1212	1100	1222	1234	1196	1216
Surface-Temperature Discontinuity (°F)	907	837	1000	996	832	1002	1021	1014	1020
Calorimeter Output for Nonisothermal-Surface Condition (Btu/ft^2-sec)	8.0	11.3	11.5	12.7	20.8	21.3	19.0	23.7	27.0
$(\bar{h}/h)$ Experimental	1.27	1.51	1.26	1.27	1.28	1.24	1.07	1.11	1.23
$(\bar{h}/h)$ Calculated Using Rubesin's Results	1.33	1.30	1.35	1.35	1.30	1.34	1.37	1.30	1.33
$(\bar{h}/h)$ Calculated Using Westkaemper's Results	1.18	1.21	1.21	1.18	1.20	1.22	1.20	1.19	1.19
$(\bar{q}/q)_{isi}$ Experimental	1.64	1.71	2.06	1.72	1.54	1.73	1.69	1.44	1.48
$(\bar{q}/q)_{isi}$ Calculated Using Rubesin's Results	1.78	1.75	1.85	1.85	1.58	1.81	1.86	1.75	1.79
$(\bar{q}/q)_{isi}$ Calculated Using Westkaemper's Results	1.58	1.63	1.66	1.59	1.46	1.65	1.63	1.60	1.60

TABLE III

DATA AND RESULTS FOR CONVECTIVE HEATING ON A C-1118 MEMBRANE TOTAL CALORIMETER MOUNTED IN AN M-31 HEAT-SHIELD PANEL AND LOCATED 31.6 INCHES DOWNSTREAM FROM BOUNDARY-LAYER INCEPTION POINT

Reference Heat Flux (Btu/ft^2-sec)	2.5	2.7	5.0	5.0	6.0	7.7	7.8	8.0	8.3	8.7	10.2	10.7	10.8	10.9	11.2
Free-Stream Gas Temperature (°F)	2080	2100	2280	2300	2370	2670	2680	2720	2780	2860		3230	3260	3260	3310
Calorimeter Surface Temperature (°F)	105		171	290	235	230	186	247	247	202		155	190	150	190
Calorimeter Output for Isothermal-Surface Condition (Btu/ft^2-sec)	3.3	3.2	6.0	6.1	7.7	9.9	9.9	8.6	10.6	11.2	12.8	13.4	13.6	14.6	14.3
Structure-Surface Temperature (°F)	444		709	1110	354	1030	981	1050	1050	1001		947	1000	964	1000
Surface-Temperature Discontinuity (°F)	339		538	810	619	800	795	803	803	789		792	810	814	810
Calorimeter Output for Nonisothermal-Surface Conditions (Btu/ft^2-sec)	4.5	4.7	8.0	8.7	10.8	14.2	15.2	12.4	14.7	15.6	18.0	18.2	18.8	19.3	19.4
$(\bar{h}/h)$ Experimental	1.38	1.46	1.33	1.42	1.41	1.44	1.54	1.45	1.39	1.39	1.41	1.36	1.35	1.37	1.36
$(\bar{h}/h)$ Calculated Using Rubesin's Results	1.26		1.40	1.39	1.43	1.60	1.48	1.47	1.48	1.45		1.38	1.48	1.39	1.39
$(\bar{h}/h)$ Calculated Using Westkaemper's Results	1.17		1.25	1.25	1.28	1.39	1.31	1.31	1.32	1.29		1.25	1.32	1.25	1.26
$(\bar{q}/q)_{isi}$ Experimental	1.67		1.77	2.38	1.98	2.14	2.26	2.15	2.03	1.99		1.83	1.84	1.95	2.20
$(\bar{q}/q)_{isi}$ Calculated Using Rubesin's Results	1.52		1.88	1.89	2.02	2.68	2.17	2.15	2.19	2.07		1.86	2.21	2.25	1.89
$(\bar{q}/q)_{isi}$ Calculated Using Westkaemper's Results	1.41		1.68	1.70	1.80	2.33	1.92	1.93	1.95	1.85		1.66	1.97	2.02	1.71